Faculty of Natural Science and Technology
Department of Physics

NTNU
Innovation and Creativity

MASTER'S THESIS FOR

STUD. TECHN. NILS IVAR RINGDAL

Thesis started:	11.11.2007
Thesis submitted:	18.04.2008

DISCIPLINE: CONDENSED MATTER PHYSICS

Norsk tittel: *"Eksperimentell studie av Væskekrystallfase-Sjølvorganisering av Nano-Plateforma Leirepartiklar i Vassløysning: Dobbeltbryting og Struktur"*

English title: *"Experimental Studies of Self-Organized Liquid Crystalline Phases from Clay Nanoplatelets in Water: Birefringence and Structure"*

This work has been carried out at the Laboratory for Soft and Complex Matter Studies, Department of Physics, NTNU, under the supervision of Professor Jon Otto Fossum

---

Trondheim, 18 April 2008

Jon Otto Fossum

Responsible supervisor

Professor at Department of Physics

Abstract

Dispersions of anisotropic colloidal particles may have the interesting feature to exhibit phases of liquid crystalline order. Driven by the plate-like particle shape and high polydispersity, suspensions of the synthetic silicate clay Na-fluorohectorite (Na-Fht) is known to gravity separate into different strata, where a phase is of nematic order. The phase behaviour, particle orientation, density profiles, influence of sample geometry and magnetic fields are here experimentally studied for suspensions of different Na-Fht powder batches with various clay and NaCl concentration.

The principal experimental method is based on detection of birefringence, where optical microscopy and a cross polarized sample setup of a PC-controlled single-lens reflex camera are applied. Several thousand pictures have been taken at regular times from the samples were first poured with suspension until the final state. Photo series with time periods of a few minutes between each image, have been taken to compose videos showing in detail the process of sedimentation and phase development. Image processing scripts are used to analyse the particle settling behaviour for some selected samples. Permanent magnets of variable strengths until 1 Tesla are applied to investigate the influence of magnetic fields to the ordered phases. In addition, wide angle X-ray scattering experiments are carried out to provide further information about the structural orientation of the Na-fht particles.

The dynamical measurements of the phase behaviour have showed that the Na-Fht suspensions within a week separate into strata of different densities. Above the sediment, a nematic phase forms by birefringent fluctuations in a region with distinctive upper and lower boundaries. After several weeks of settling, a second nematic phase forms atop of the first nematic phase. This phase is found to be of sol character due to its fluidity and response by magnetic fields. Suspensions of one of the studied Na-Fht powder batches shows a striking dynamical behaviour when it beforehand has been crushed. The birefringent dynamic goes on for several months and can eventually end up exhibiting nematic Schlieren and threaded textures, where disclinations of strengths 1/2 and 1 have been identified.

During the first minutes of sedimentation, birefringent streaks are for many samples shown to appear in the vertical direction of settling. These findings may be caused from the combination of sedimentation flow and sample geometry. Horizontal bands of wave periodicity are observed to appear in some samples within the first days after sample preparation. The physical origin of the phenomena is either explained or been reasonably proposed.

A density profile is for two different Na-Fht powder batches found to give densities for the isotropic and nematic phase at 9 mg/ml and 32 mg/ml and 14 mg/ml and 30 mg/ml respectively. The values with the smallest gap, correspond to crushed powder, reflecting a lower polydispersity in particle size. Compared to theoretical simulation data of the Onsager entropy driven

isotropic-nematic phase transition, our values are less by a factor 5. This discrepancy may be attributed to particle morphology, polydispersity, gelation, electrostatic effects and unrealistic comparison to the simulation model. The relative proportion of nematic phase is found to increase linearly with total clay concentration, which may indicate the nematic ordering is of a thermodynamic nature. Even though gelation is present, it does not prevail isotropic-nematic separation at clay concentrations lower than 3 w/w%. However, when the Na-Fht powder is crushed, the gelation process is shifted towards lower clay concentrations.

At ionic strengths lower than 5×10^{-3} M, electrostatic repulsion is important to the phase behaviour. For ionic strengths above 5×10^{-3} M, van der Waals attractions come into play, where flocculation occurs at ionic strengths above 10^{-2}.

Wide angle X-ray scattering on the nematic phase of samples contained in flat 1 mm thick cells shows unexpected results of horizontal "lying" particle orientation. Measurements of the corresponding nematic phase in equal samples contained in round 2 mm capillaries, show at the other hand the previously observed orientation of vertically "standing" particles. These findings show in combination with additional birefringence observations, that sample geometry and wall-effects play an important role to the particle alignment and phase behaviour. From the Bragg peak position, calculation the lamellar d-spacing shows that birefringent regions formed by evaporation and air bubble shear contain 2 layers of intercalated water molecules. The nematic phases elsewhere are found to intercalate 1 water layer. Differences in salt concentration, particles size or other ordering processes may be attributing factors to this difference.

Long time observations reveal that particles settle from the upper isotropic phase and form a new layer of birefringence above the previously formed nematic phases. Depending of powder batch and clay concentration, this process can go on even a year after sample preparation. This slow particle settling may be of importance to the formation of a nematic domain structure, which develops in the nematic sol phase and takes the form as a zigzag pattern. The domains are observed to be composed of tangled thin birefringent threads with a typical individual width of 20 μm, giving a macroscopic size around 0.2 $\times$ 5 mm. From X-ray scattering results and birefringent considerations, the domains are argued to consist of particles stacked above one another. In some samples, the particles at the phase interfaces are found to show a strict lying orientation.

The application of magnetic fields to the nematic sol, yields changes in the birefringence after only few minutes, reflecting the particles reorientation behaviour. Several weeks and months of magnetic influence, have for some samples given rise to a visual change in optical phase retardation, from where the nematic order parameter can be concluded to have increased. An inhomogeneous transient Fréedericksz transition has been induced to the nematic sol in 2 mm capillaries, showing periodic stripe pattern with wavelength 0.7$\pm$0.1 mm.

The findings in this study have given new insight into the phase behaviour of suspensions of Na-Fht, in addition to have opened up new avenues for further studies.

Preface

This thesis reports the research work I have carried out in relation to the Master of Technology degree within the study programme of Technical Physics at the Norwegian University of Science and Technology (NTNU).

Performed at the Laboratory for Soft and Complex Matter Studies, the scope of the work has been to study the liquid crystalline phase behaviour in water dispersions of the synthetic nano-layered clay Na-fluorohectorite. The use of clay as a model system is interesting due its soft and complex structure of self-assembled nanoparticles. Developing new understanding of the basic physical properties and processes in soft and complex matter is of practical relevance to fields of actual importance to society, ranging from nanotechnology to environmental topics. Motivations for the research are to find relationship between nano-scale and macroscopic behaviour.

Although the first discoveries were done in the first decades of the last century, the research field concerning liquid crystalline ordering in dispersions of nanoparticles have in the last years seen a revived scientific era. This is reflected by noting that most of the cited articles in this thesis are published in the last ten years.

With emphasis on clays and related disk shaped particles, the thesis starts out by giving a general introduction to the most important aspects in the field of mineral liquid crystals. A compressed introduction with some additional references can also be found in a publication paper in the Appendix.

The most basic theoretical concepts concerning the physical principles of clay suspensions and its liquid crystalline phase formation is given in Chapter 1. Reading the chapter should be helpful in the understanding of many of the results presented in the thesis. Chapter 2 gives an explanation of the experimental procedure and methods of the exhibited work. Results, analysis and discussion of the obtained data are further presented in Chapter 3. The most important concluding remarks from the findings are outlined in Chapter 4.

A DVD is enclosed containing videos of the phase behaviour of some selected samples. Supplemented data that is left out of the document is also contained along with the PDF file of the thesis, where the presented pictures in the thesis can be viewed in full-scale resolution. This can be useful when it comes to get better insight into the detailed nature of the system.

Acknowledgements

First of all I express great gratitude to my supervisor Professor Jon Otto Fossum, for all his providing guidance and ideas of this interesting work.

I further want to acknowledge

Phd student Davi de Miranda Fonseca for the contribution of sample material, doing SAXS measurements and showing off his experience in sample preparations,

My fellow students

Henrik Hemmen for analysis of ESRF X-ray scattering measurements and his findings to the explanations of the results, Bård Martin Kjelling for proofreading the document, Elisabeth Lindbo Hansen for providing new interesting insight to the research subject, and coming up with helpful additional literature,

Arnolf Bjølstad and his crew at the workshop for creating the experimental setup and sample holders,

Dr. Bao-xiang Wang for help with SAXS experiments,

Professor Yves Méheust for suggestions of data analysis,

Phd student Yavuz Öztürk for his collaboration and hospitality during my experimental work in South-Korea, from where I also acknowledge the help from Phd student Yong Sam Kim, Dr. Jinwoo Kim and Professor Do Young Noh which made the experiments possible.

Trondheim, April, 2008 Nils Ivar Ringdal

Contents

General Introduction

Condensed matter that exhibit a phase intermediate between the crystalline solid and conventional liquid state are called liquid crystals or mesophases [1]. A liquid crystal may flow like a liquid and at the same time have its molecules or particles in the liquid arranged and/or oriented in a crystalline like way. Liquid crystalline phases were first discovered[1] in 1888 by the Austrian botanist Friedrich Reinitzer and later labelled by the German physicist Otto Lehmann.

With the combination of both being fluid and anisotropic, liquid crystals are usually based on anisotropic building block as molecules, polymers, micelles or aggregates. Liquid crystalline materials are extremely diverse, spanning from DNA to Kevlar, and from small organic molecules used in displays to self assembling amphiphilic soap molecules. A common feature of all these materials is that they are organic [2] or organometallic[2] and at this time there are more than 80 000 examples of organic liquid crystalline compounds [3]. When it comes to lyotropic[3] liquid crystals of colloidal suspension of mineral[4] nanoparticles, there are to date only a dozen substances known and characterized [4–8]. One reason is because there are only a few low-dimensional (one-dimensional or two-dimensional) purely-inorganic objects known to dissolve or to be dispersed in water or in other organic solvents. The solubility criteria of mineral moieties, their interactions with solvents, and the structures and physical properties of such fluids are currently a subject of intense research activity. In addition, organic synthesis techniques allow numerous structural variations of liquid crystalline molecules to be made whereas the solution chemistry of molecular mineral objects, i.e., prepared by high temperatures solid state reactions, is still under development [9].

The first comprehensive observations and analyses of the liquid crystallinity of suspensions of mineral particles was reported by the German scientist Von H. Zocher as early as 1925, where he observed isotropic-nematic behaviour

[1] Other scientists had earlier found phenomena in substances resembling of liquid crystals, but did not put their ideas together in a way that fully captured the significance of their work.

[2] Organometallic chemistry is the study of chemical compounds containing bonds between carbon and a metal and combines aspects of inorganic chemistry and organic chemistry.

[3] When the liquid crystal phase is dependent on the concentration of one component in another, the system is called a lyotropic liquid crystal.

[4] The term mineral to name this family of liquid crystals has been introduced by Gabriel et al. [4] to avoid any confusion by inorganic liquid crystals used for organometallic liquid crystals.

in aqueous suspensions of rod-like vanadium pentoxide (V_2O_5) [10]. He compared these suspensions with the newly discovered liquid crystal phases and concluded that these colloids had to be constituted from needle-like objects mutually oriented in the same direction. This behaviour is now known to arise from V_2O_5 ribbons forming a nematic phase.

In the next decade the American chemist and physicist Irving Langmuir examined suspensions of California bentonite clay platelets and manage to recognize their anisotropic and fluid-like properties [11]. In his paper from 1938 he showed at macroscopic level that test tubes of the clay suspension had phase separated into an isotropic phase and a birefringent gel after standing for several 100 hours. This separation was found to occur for sols containing between 2.0 and 2.2 w/w% clay particles. He also noted that this property of phase separation was gradually lost with time, something he tentatively explained by the incorporation of impurities diffusing from the glass tubes. He also compared this system to the days normal liquid crystals. However, all subsequent studies, even by himself, failed to reproduce this crucial observation and give evidence of a clear thermodynamic liquid-crystalline order but instead revealed a dominant gel formation [12]. The gel structure and its formation, which are responsible to many of the clays practical applications, have from its conflicting explanations in the 30-50s [13–17] until today been substantially debated [18–38]. Indeed, although some of the gel features indicate nematic ordering [39, 40], no true thermodynamic nematic order was ever clearly evidenced. In 2006 it was showed that aqueous suspensions of the natural clay nontronite exhibit a true isotropic-nematic transition, and that the nematic phase displays strong orientational order [41].

The first theoretical explanation of the spontaneous isotropic-nematic transition of mineral liquid crystal nanoparticles was given by Lars Onsager in 1949 [42]. He managed to give a quantitative despription of the phase transition of previously experimental observations of nematic ordering in suspensions Tobacco Mosaic Virus (TMV) rod particles [43, 44]. The thermodynamic stability of the nematic phase was explained to be arisen by the competition between the orientational entropy that favours disorder and the excluded volume (packing) entropy that favours order. This model has provided to be highly useful to understand and discribe the phase diagram in mineral and organic systems. The formalism applies in qualitative terms to any suspension of anisotropic rod-like or plate-like particles interacting solely through a hard-core potential and predicts that a nematic-isotropic first-order transition takes place at high enough particle concentrations.

The Onsager model has by later years undergone a series of theoretical and numerical simulations to predict the liquid crystal phase transitions in suspensions of disk-like particles [45–53]. Numerical simulations studies of model systems of infinitely thin hard platelets which have both an isotropic and a nematic phase was first presented in the 1980s by Rob Eppenga and Daan Frenkel [45, 46]. Later simulation studies of the phase behaviour of disk-like particles have predicted the existence of nematic and columnar phases [48]. Similar studies of rod-like particles also predicts the existence of nematic,

smectic and other exotic "rotator" phases [49]. From the work of Onsager to other statistical physics models, the theory of the phase behaviour of the nanoparticle liquid crystals can today be said to be very well understood [52].

In 1956 Emerson observed, by using optical microscopy, in swollen clay flakes a banded texture somewhat similar to that displayed by the tobacco mosaic virus [54]. The liquid-crystalline properties of colloidal suspensions of mineral nanoparticles were from these first observations more or less forgotten and got new research interest not much more than 15 years ago, where most new knowledge has been received in the 21th century. The reason for this very late interest in these systems can be attributed to two new trends. First there is the modern popularity around nano-science and nano-technology due to new fabrication and characterisation techniques that can provide control of materials and devices on the nanometric scale. Secondly, a new kind of solid-state chemistry ("chimie douce") has recently emerged, often based on inorganic polycondensation methods and sol-gel processes. This chemistry involves reactions in solvents and at much lower temperatures, in contrast with traditional solid-state chemistry. Consequently, it provides a wealth of new colloidal suspensions of anisotropic nanoparticles, often as a by-product of research on low-dimensional compounds [7].

A liquid crystalline phase can be identified by observing its texture when illuminated by white light between crossed polarisers. Unlike the isotropic phase, liquid crystalline phases can then be detected as birefringence when the fluid phase is at rest. The textures observed under polarized light are due to the existence of topological defects and their analysis gives information on the symmetry of the phase. For instance, the most common defects of the nematic phase are called disclination lines. These are one-dimensional singularities in the local average direction (director) of the anisotropic moieties. Thus, unless special caution is taken to remove these defects, nematic samples are usually random distributions of small nematic domains[5].

Nematic phases can often be aligned by the action of a magnetic field. The alignment is due to the anisotropy of the mesophase that reorients to minimize its free energy in the field. Therefore, the director is aligned along or perpendicular to the field direction, depending on the sign of the magnetic anisotropy of the building blocks. The alignment of the phase in an external field suppresses the topological defects and produces a single domain that is suitable for more detailed physical studies. Electric fields produce similar effects: this is the basis of most applications of nematic phases in display technology.

Small angle X-ray scattering (SAXS) is a useful technique to study the molecular organization of lyotropic nematic phases on a length scale ranging from 3 to 300 nm. In this range, the detailed atomic structure of the particles is irrelevant and the scattering is sensitive to only the particle shape and its electronic contrast with the solvent. In this respect, mineral liquid crystals are particularly convenient because their contrast is usually much larger than that of their organic counterparts. SAXS also allows a clear-cut demonstration of

[5] A nematic domain is defined as a region of the sample which shows ideal nematic orientational correlation.

the symmetry and structure of a complex fluid, avoiding possible and usual pitfalls that can come when one restricts itself to only a texture analysis. In contrast to organic liquid crystals,mineral liquid crystals can differ largely in size from one system to another. They actually range from molecular nanowires or nanotubes to anisotropic crystallites such as nanorods. Molecular nanowires can be considered as one-dimensional objects where the diameter is precisely defined by the molecular unit that makes up the chain (typically 5 to 25 Å). In contrast, molecular disks (nanosheets) are two-dimensional objects where the thickness of the disks is defined at the molecular scale, but the diameter is polydisperse (10 to 1000 nm). Finally, liquid crystalline suspensions may be formed from anisotropic crystallites whose dimensions are all in the colloidal range (10 to 1000 nm) so that these moieties are two to three orders of magnitude larger than usual organic liquid crystals.

The most common mesophases, the nematic, lamellar and columnar phases have now been found in colloidal mineral systems that consist of rod-like and disk-like particles. Much of the focus of the later research has been on the effect of gravity, gelation and polydispersity. Another research direction consists in trying to impart physical properties like magnetism to these liquid-crystalline phases. The systems and compounds that have had the most important research for mesogenic properties of mineral liquid crystals are based on molecular nanowires ($Li_2Mo_6Se_6$), nanotubes (imogolite and $NaNb_2PS_{10}$), molecular ribbons (V_2O_5), nanorods (Boehmite(γ-AlOOH), Akaganeite (β-FeOOH), Goethite (α-FeOOH), disks ($Ni(OH)_2$), platelets ($Al(OH)_3$) and exfoliated single sheets ($H_3Sb_3P_2O_14$ and smectic clays).

Clays of the montmorillonite family are lamellar 2:1 aluminosilicates [55] that have been used as building material, ceramics, rheology modification, paper filling oil well-drilling and -stability etc. [56]. All these application is made possible because of the swelling property the clay has when brought into contact with water due to the intercalation of water molecules between the sheets. Because of these reasons, a lot of studies have focused on the rheology of aqueous clay suspensions with the particular emphasis on yield stress, thixotropy, and ageing. Depending of the specific clay complete exfoliation can be induced leading to dispersions of disk-like particles of 10 Å thickness and $300-3000$ Å in diameter.

Because of the clay minerals anisotropic shape and high aspect ratio ranging from from 25 to 1000 these material will under the right circumstance form liquid crystalline phases. These clays have such a high electrical surface charge that electrostatic interactions between them have to be taken into account for the colloidal stability of these dispersions. The salt concentration of the suspension will together with the surface electrical charge have a mayor impact on the suspension since these properties vary considerably with its ionic strength.

From the first observations by Langmuir, the evidence of a liquid-crystalline phase of clays of the montmorillonite family was first presented in 1996 by Jean-Christophe P. Gabriel, Clément Sanchez and Patrick Davidson [39]. Natural bentonite and synthetic laponite B was studied under polarized light both on macroscopic scale and using optical microscopy. Concentrated gels of the

samples showed birefringence indicating liquid crystalline order over distances up to 1 cm. In the polarized light microscopy the gels showed textures like that of a nematic phase. An apparent feature that seems to be typical of these systems is that the nematic-isotropic phase separation is very unusually achieved. As the clay concentration is increased the suspension goes from first being an isotropic-liquid to next become isotropic-gel and finally birefringent-gel. Temperature seems to have no influence on the nematic organization as expected from the Onsager theory.

In the isotropic-gel phase the suspensions show very strong pretransitional effects such as flow and shock birefringence. If this birefringence is really intrinsic or is only due to freezing of some accidental flow birefringence is an open question. Some simple experimental observations have indicated the thermodynamic nature of the nematic ordering. First, the initially isotropic samples left to dry slowly over a few months finally showed birefringence though they hardly experienced any appreciable flow. Second, samples were occasionally obtained that showed both the isotropic and nematic phases separated by a sharp border which is just what is expected for a first order phase transition such as the nematic-isotropic transition. Third, freshly prepared concentrated birefringent gels show a large density of defects which decreases over a few weeks though the birefringence does not. Therefore these studies show that a nematic order reigns in the suspensions over a distance that can be as large as 1 cm. This discussion illustrates the difficulties of working with gels and that plain flow birefringence should not be confused with true nematic ordering.

In phase diagrams of bentonite and laponite gels, the liquid-gel and isotropic-nematic transitions can be changed by varying the NaCl and clay concentration. At high salt concentrations flocculation occur because the repulsive electrostatic interactions are screened so much that short-range attractive interactions are dominating. For bentonite an increase in the ionic strength induces both gelation and the isotropic-anisotropic phase transition to occur at lower clay concentration. Adding brine to an isotropic sample can make it birefringent though its clay particle concentration actually slightly decreases. This unexpected effect was in 1979 predicted by Forsyth et al. using a statistical physics model incorporating electrostatic interactions [53]. Furthermore, a similar phase diagram has been reported by Mourchild and Levitz on a closely related form of laponite [57]. The same authors have fully discussed the relation between gelation and nematic ordering in this system. They have also explored the phase diagram at very low ionic strength and found the existence of a soft phase, stabilized by long-range electrostatic repulsions [24]. In comparison, the nematic phase of laponite is not sensitive to NaCl concentration.

Later, the nematic order parameter for the laponite gels has been obtained using SAXS [40]. For those experiments, well-aligned samples were prepared by slowly concentrating isotropic sols directly in Lindemann glass capillaries. The SAXS patterns were found to be clearly anisotropic demonstrating nematic order over the whole sample. The positional correlations of laponite clay particles are known to be weak [18, 19, 24, 38, 58] which also was confirmed by the SAXS pattern. The nematic order parameter was obtained by

fitting the SAXS pattern against a simulated SAXS pattern calculated using the particle form factor and the Maier-Saupe orientational distribution [59]. The value, S = 0.55 ± 0.05, compares very well with the nematic order parameters of ordinary liquid crystals which range from 0.4-0.8. This experiment illustrate the magnitude of orientational correlations between clay particles in laponite gels, even in the absence of shear.

Today there are many experimental studies that directly or indirectly have documented the present of orientational order in clay gels, both from optical measurements [19, 39] that show visual nematic textures and neutron [60–62], X-ray scattering [40, 58, 63, 64] and MRI [65–70] which reveals structural correlations of the nematic order. None of these studies give the explanation of what is the interplay (if any) of the nematic-isotropic phase transition with the gelation of these suspension.

Today there are many studies which have investigated how the gravitational force influence the phase behaviour of colloidal systems [12, 71–81]. The balance between the gravitational force and the osmotic pressure gradient results in a sedimentation-diffusion equilibrium, i.e., a density profile varying with altitude [82–85].

Dimasi et al. [63] and Fossum et al. [64] have by using wide angle X-ray scattering and birefringence observations documented nematic order in gravity separated phases of suspensions of synthetic Na-fluorohectorite clay. The phase separation occurs because of high polydispersity in size of the Na-fluorohectorite particles. Precise characterization of the phase diagram of the samples as a function of salt concentration and vertical position in the sample tubes, have by de M. Fonseca et al. been obtained using small angle X-ray scattering [86]. De Azevedo et al. have by MRI studies of anisotropic water self-diffusion, investigated walls and magnetic fields effects of the particle ordering in suspensions of Na-fluorohectorite [70].

Chapter 1

Theory

1.1 Suspension of Colloidal Particles

Colloids or colloidal dispersions can be found almost everywhere around us in the world. The wide range of seemingly very different systems from shaving cream to paints and cosmetics, from shampoo to milk, from beer to agricultural soils, from mayonnaise to biological cells and from fog to clay all are the subject of colloidal science. What all these systems have in common is that they consist of small particles of one substance distributed more or less uniformly throughout another. The latter phase is continuous, whilst the particles are discontinuous.

For a general colloidal system the continuous phase may be a gas, a liquid or a solid while the discontinuous phase can also be a gas, liquid or solid. The system will be colloidal if the particles are small enough, which usually means less than about 1μm in at least one important dimension. When the disperse phase is solid and the dispersion medium is liquid the dispersion is said to be a sol, or colloidal sol, with the common name suspension. This is the case for a clay [87] mineral suspension in water, where the particles are dispersed throughout the solvent after being broken down from a much more insoluble substance. Such a system is regarded as colloidal if the size of the particles falls anywhere in the range 1-1000 nm. The reason for this rather arbitrary definition is that for smaller particles the systems show little or no difference from an ordinary solution. The upper limit is set by the fact that almost all of the special features of colloidal systems may be traced to their having a very large surface area in contact with the dispersion medium.

For particles larger than about 1 μm the surface or interfacial region becomes of rather less significance compared to the bulk properties. It is sufficient if one of the characteristic dimensions of the particle falls within the stated range, where the surface area is required to be large. The interaction of colloidal particles is determined by the following forces where the importance of each force depends on the specific systems and its conditions [88]:

Excluded Volume Repulsion refers to the impossibility of any overlap be-

tween hard particles.

Electrostatic interaction acts when colloidal particles carry an electrical charge and therefore attract or repel one another. The charge of both the continuous and the dispersed phase, as well as the mobility of the phases are factors affecting this interaction.

Van der Waals forces are due to interaction between two dipoles which are either permanent or induced. Even if the particles do not have a permanent dipole, fluctuations of the electron density gives rise to a temporary dipole in a particle. This temporary dipole induces a dipole in particles nearby. The temporary dipole and the induced dipoles are then attracted to each other. This is known as van der Waals force and is always present, is short range and is attractive.

Entropic forces are macroscopic forces whose properties are primarily determined not by the character of a particular underlying microscopic force, but by the statistical tendency of the whole system to increase its entropy. According to the second law of thermodynamics, a system progresses to a state in which entropy is maximized. Entropic forces generate the osmotic pressure of a dilute solution, and in colloidal suspensions they are for instance responsible for the crystallization of hard spheres.

Steric forces comes as repulsion whenever large molecules such as polymers, which may or may not be electrically charged, are adsorbed onto the surface of colloidal particles. The protective coating formed prevents the particles from approaching sufficiently closely for the Van der Waals forces of attraction to come into play. Therefore steric forces have a stabilizing effect on a colloidal system.

1.2 Stability and Instability in Lyopilic and Lyophobic Sols

Colloids are traditionally divided into two classes called lyophilic (solvent-loving) and lyophobic (solvent-hating) respectively, depending on the ease with which the system can be redispersed if once it is allowed to dry out.

Lyophilic colloids can be dispersed merely by adding a suitable solvent to the dry colloid which will first swell as it takes up the liquid and will finally form a homogeneous colloidal solution. A lyophobic colloid on the other hand can only be dispersed by vigorous mechanical agitation (or by the application of some other external source of energy.) Most biological colloids, like protein and polysaccharides, are lyophilic in character while larger structures like chloroplasts have some lyophobic character.

A sol in which the particles remain separated from one another for long periods of time, that is at least of the order of days, is said to be stable.

For lyophilic colloids the stability results from the fact that the solution is thermodynamically stable[1]. Such a sol can be stable indefinitely.

For lyophobic colloid there is always an attractive van der Waals force between the particles which will dominate and form aggregates if the particles get close enough together. The system can be made to appear stable for some time only of some other force is present which can reduce the chance of the particles closely approaching one another in the course of their Brownian motion. They are still thermodynamically unstable, but the barrier to coagulation is merely a kinetic one. Given enough time they will ultimately form aggregates. To say that a colloidal sol is stable then, is a relative notion: highly stable lyophobic colloids can appear homogeneous for weeks, even months, but coagulation is still going on all the time, although at a very slow rate.

As seen by the fact that the lyophobic sol does not disperse spontaneously suggests that solvation effects by itself are not sufficient to produce a stable sol. Other repulsive forces involved in a lyophobic system can either be electrostatic or steric[2] in origin. If the repulsive forces are not strong enough, the particles will clump together to form flocs (floccules), the system is then said to be unstable in the colloid sense.

Lyophilic colloids are not obviously affected by the salt concentration of the surrounding medium until it becomes quite high. Lyophobic colloidal sols on the other hand can be markedly affected and rendered unstable by quite low concentrations of salt ($< 10^{-2}$ M). There is a well developed theory to describe the interaction between particles of lyophilic colloids, but systems of lyophilic colloids are more difficult to describe theoretically. The reason for this is that all of the forces involved in lyophobic systems are again important for lyophilic systems but in addition there are very strong specific solvent effects which are difficult to predict.

1.3 Clays

Clay is a term used to describe a group of hydrous aluminium phyllosilicate[3] minerals, that are typically less than 2 μm in diameter. Clay consists of a variety of phyllosilicate minerals rich in silicon and aluminium oxides and hydroxides which include variable amounts of structural water. Clays are generally formed by the chemical weathering of silicate-bearing rocks by carbonic acid but some are formed by hydrothermal activity. Clays are distinguished from other small particles present in soils such as silt by their small size, flake or layered shape, affinity for water and tendency toward high plasticity.

Depending upon academic source, there are three or four main groups of

[1] A solution is thermodynamically stable when it has a lower Gibbs free energy than the separated components.

[2] Steric effects arise from the fact that each atom within a molecule occupies a certain amount of space. If atoms are brought too close together, there is an associated cost in energy due to overlapping electron clouds (Pauli or Born repulsion), and this may affect the molecule's preferred shape and reactivity.

[3] phyllosilicates being a subgroup of silicate minerals

clays: kaolinite[4], montmorillonite-smectite[5], illite[6], and chlorite[7]. There are about thirty different types of "pure" clays in these categories but most natural clays are mixtures of these different types, along with other weathered minerals.

Like all phyllosilicates, clay minerals are characterised by two-dimensional sheets of corner sharing SiO_4 and AlO_4 tetrahedra. Each tetrahedron shares 3 of its vertex oxygen atoms with other tetrahedral. The fourth vertex is not shared with another tetrahedron and all of the tetrahedra "point" in the same direction (i.e. all of the unshared vertices are on the same side of the sheet). These tetrahedral sheets have the chemical composition $(Al,Si)_3O_4$.

In clays the tetrahedral sheets are always bonded to octahedral sheets formed from small cations, such as aluminium or magnesium, coordinated by six oxygen atoms. The unshared vertex from the tetrahedral sheet also form part of one side of the octahedral sheet but an additional oxygen atom is located above the gap in the tetrahedral sheet at the centre of the six tetrahedral. This oxygen atom is bonded to a hydrogen atom forming an OH group in the clay structure. Clays can be categorized depending on the way that tetrahedral and octahedral sheets are packaged into layers. If there is only one tetrahedral and one octahedral group in each layer the clay is known as a 1:1 clay. The alternative, known as a 2:1 clay, has two tetrahedral sheets with the unshared vertex of each sheet pointing toward each other and forming each side of the octahedral sheet. Figure 1.1 shows the generic structure of the smectic clay group, where the individual clay particles are composed of one or more silicate lamellae that stack by sharing exchangeable cations between their faces.

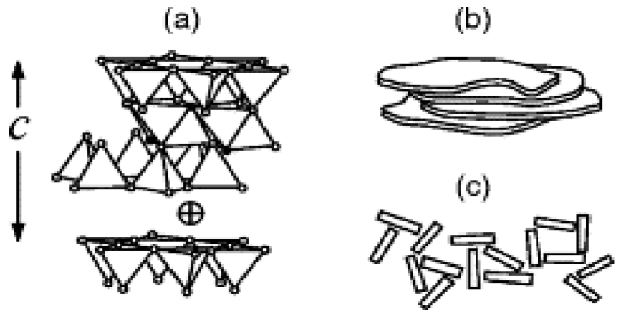

Figure 1.1: (a) A general sketch of the structure of the synthetic 2:1 swelling clay fluorohectorite. The structure are composed of oxygen (o), fluorine (•) and exchangeable cation (⊕) sites (b) Clay particle formed from stacked lamellae in the micron scale. (c) Face-to-edge and edge-to-edge aggregation of clay particles. The figure is taken from [89].

[4]Kaolinite group includes the minerals kaolinite, dickite, halloysite and nacrite.

[5]Smectite group includes pyrophyllite, talc, vermiculite, sauconite, saponite, nontronite and montmorillonite.

[6]Illite group includes the clay-micas. Illite is the only common mineral.

[7]the chlorite group is not always considered a part of the clays and is sometimes classified as a separate group within the phyllosilicates.

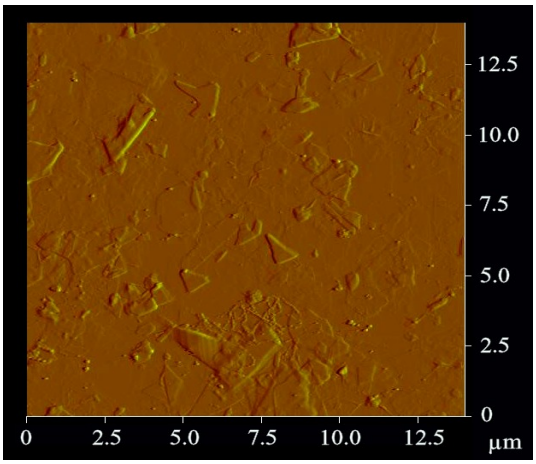

Figure 1.2: Atomic force microscope picture showing the Na-fluorohectorite particles from the nematic phase in a phase separated suspension.

In 1972 the AIPEA Nomenclature committee agreed upon usage of the terms "plane," "sheet," "layer," "unit structure," and their equivalents in other languages [90]. Recommended usage is as a single plane of atoms, a tetrahedral or octahedral sheet, and a 1:1 or 2:1 layer. Thus, plane, sheet, and layer refer to increasingly thicker arrangements. A sheet is a combination of planes and a layer is a combination of sheets. In addition, layers may be separated from one another by various interlayer materials, including cations, hydrated cations, organic molecules, and hydroxide octahedral groups and sheets. The total assembly of a layer plus interlayer material is referred to as a unit structure.

Depending on the composition of the tetrahedral and octahedral sheets, the layer will have no charge, or will have a net negative charge. If the layers are charged this charge is balanced by interlayer cations such as Na^+ or K^+. In each case the interlayer can also contain water. The crystal structure is formed from a stack of layers interspaced with the interlayers.

Clays sintered in fire were the first ceramic, and remain one of the cheapest to produce and most widely used materials even in the present day. Bricks, cooking pots, art objects, dishware and even musical instruments such as the ocarina are all made with clay. Common present day uses of 2:1 clays include building materials, ceramics, cement production, rheology modification, catalysis, paper making, oil well-drilling and other industrial processes.

1.3.1 Na-fluorohectorite

Na-fluorohectorite is a synthetic 2:1 smectite clay, which have the nominal chemical formula $Na_{0.6}Mg_{2.4}Li_{0.6}Si_4O_{10}F_2$. Like natural hectorite[8] Na-Fh is a swelling clay that incorporate a variable amount of water in the interlayer space, resulting in a change in lattice constant along the stacking direction.

[8] A clay mineral similar in structure to bentonite but with more negative charges on its surface.

Na-Fht has a rather large surface charge of 1.2 e^{-1}/unit cell, compared to for example laponite (0.4 e^{-1}/unit cell). The particle size of Na-Fht is quite large and varies up to 20 000 Å in diameter [91]. Compared to natural clays such as montmorillonite, Na-Fht might be expected to have a more homogeneous composition and charge distribution. The polydispersity in particle size makes the Na-Fht suspensions particularly interesting, because gravitational forces effectively sort the particles by size, stabilizing in some cases several strata of gels, sols and/or sediments within a single sample tube. Figure 1.2 shows an Atomic Force Microscope (AFM) picture of Na-Fht particles, where it can be seen that the shape of the particles is higly irregular. A detailed sketch of the lamellar and generic structure of Na-fluorohectorite can be found in Appendix F.

1.3.2 Cation Exchange

Cation exchange capacity measures two of the fundamental properties of clays, the surface area and the charge on this area. The exchange capacity is an estimate of both the number of ions absorbed between the layers of a clay structure and of those adsorbed on the outer surfaces.

Addition of a small concentration of salt to a clay suspension (where particles remain in the aqueous medium through Brownian motion) will tend to form particle aggregates. The process is called flocculation. The aggregates tend to become large and dense enough to settle and the clay water suspension is destroyed. This process is independent of the cation exchange by absorption (between the sheets of the clay particles).

The charge measured as being exchanged on sites between the layers of clays or within the structure varies between 40 and 120 meq. This value should be proportional to the charge on the layers induced by substitutions of ions which create an electrostatic charge imbalance on the silicate. One can distinguish two kinds of clay, those with low exchange capacities (10 meq) and those with high capacities (40-120 meq). The quantity of ions present is recorded as the charge, milliequivalents, which are found to be fixed on 100 g of dried clay. The cation exchange capacity is given in milliequivalents per 100 g of dried material (meq/100 g or simply meq).

From cation exchange selectivity the interlayer ions are loosely held, so much that they can be interchanged in aqueous solution which contains a high proportion of another ion. The exact ratio of ionic species in the solution will determine those in between the layers of the swelling clay. The proportion of one to another in each phase (aqueous and clay) determines the cation exchange isotherms of selectivity coefficients. The proportion of each site reflects the chemical activity of the ion in each substance.

By thermodynamic definition, when the solution and the clay come into chemical equilibrium, the activity of the ions in each phase is the same. However, some ions prefer the clay to the solution when in the presence of other ions. For example, calcium much prefers clay over sodium or potassium. In general, the divalent ions are preferred in swelling clay interlayer sites to mono-

valent ones. The reverse is true for micas (with high charges). If one changes the composition of the solution, for example, the clay interlayer ion composition will also change. For example, if the initial solution is at x, with 50% cation A, the clay composition will be 20%. If one changes the solution composition to y, with 75% A, then the clay will contain 50% A. Both will increase their A content but not in the same proportions. The concept of ion exchange and cation partioning is very important to studies which try to predict the chemical affinities and pathways during aqueous migrations.

1.4 DLVO-Theory

1.4.1 Attractive Van der Waals and Repulsive Double Layer Forces

Individual charged colloid particles dispersed in salt solution interact with one another according to what is commonly and formally known as the DLVO theory. It looks at the balance between two opposing forces, electrostatic repulsion screened by the ions present in the water solution and van der Waals attraction, to explain why some colloidal systems agglomerate while others do not.

A quantitative theoretical analysis of the problem of colloidal stability was independently published in the 1940s by two groups of scientists; Boris Derjaguin and the renowned physicist Lev Landau in the Sovjet Union, and Evert Verwey and Theo Overbeek in the Netherlands. This proposed theory became known by the initial letters of their names, DLVO. The Theory assumes that the more long-ranged interparticle interactions mainly control colloidal stability. Two types of forces are considered. A long range London van der Waals force operates irrespective of the chemical nature of the particles or the medium. If the particles are similar, this force is always attractive. Furthermore, most colloidal particles acquire a charge either from surface charge groups or by specific ion adsorption from the solution. For similar particles this charge leads to a repulsive double-layer force. From this the total interaction potential can be written as:

$$V(h) = V_A(h) + V_R(h) \tag{1.1}$$

and the corresponding force will then be

$$F = -\frac{dV}{dh} = -\frac{dV_A}{dh} - \frac{dV_R}{dh} \tag{1.2}$$

A stands for attractive and R repulsive. Depending on the relative strength of the attractive and repulsive terms, the interaction potential can be generated versus distance curves. The interaction potentials have the character of free energies and contain both energetic and entropic contributions.

To illustrate the typical properties of the interaction potentials and the force consider the interaction between two identical half-planes separated by a

distance h. The attractive van der Waals interaction V_A will here be

$$\frac{V_A(h)}{area} = -\frac{H_{121}}{12\pi h^2} \tag{1.3}$$

where H_{121} is the Hamaker constant for medium 1 separated by liquid 2. At large separations, the double-layer interaction force is

$$\frac{F}{area} \approx 32(kT)^2 \frac{\epsilon_r \epsilon_0}{z^2 e^2} \kappa^2 \Gamma_0^2 e^{-\kappa h} = 64 kT c_0^* e^{-\kappa h} \tag{1.4}$$

By integrating this equation, the potential is obtained as

$$\frac{V_R(h)}{area} = \frac{64 kT c_o^*}{\kappa} e^{-\kappa h} \tag{1.5}$$

Γ_0 is defined as $\tanh(ze\Phi_0/4kT)$ and depends on the potential at the surface, but distance dependence is solely determined by the Debye screening in the solution. From this, Equation (1.1) can be written

$$\frac{V(h)}{area} = -\frac{H_{121}}{12\pi h^2} + \frac{64 kT c_o^*}{\kappa} e^{-\kappa h} \tag{1.6}$$

and the force

$$\frac{F}{area} = -\frac{H_{121}}{6\pi h^2} + 64 kT c_0^* e^{-\kappa h} \tag{1.7}$$

The attractive term $V_A(h)$ dominates the repulsive term $V_R(h)$ when h is very small. At intermediate separations the double-layer force gives rise to a potential energy barrier if the surface is sufficiently charged and if the electrolyte ions do not screen too much.

When the low electrolyte concentration makes κ small, substantial energy barrier exists in the total *V(h)* and the colloidal system is typically stable. On the hand, for large κ and short screening length κ^{-1}, the barrier is small or non-existent and the colloidal system is unstable. To understand the approximate location of the barrier, consider the special case when the barrier is so small that the maximum value of $V(h)$ is zero. At the maximum

$$\frac{\delta V(h)}{\delta h} = \frac{\delta V_A}{dh} + \frac{\delta V_R}{dh} = 0 \tag{1.8}$$

differentiating Equation (1.6) gives

$$\frac{\delta V(h)}{\delta h} = -\kappa V_R - \frac{2}{h} V_A = 0 \tag{1.9}$$

Combined with the condition $V(h_0) = 0$, that is, V_R = -V_A, the separation h_0 at the top of the barrier is obtained as

$$h_0 = \frac{2}{\kappa} \tag{1.10}$$

The barrier moves to larger separations when $V(h_0) > 0$, but when the barrier is lower, the colloidal system coagulates rapidly. Thus, as the asymptotic

expressions in Equations (1.3) and (1.5) are valid for $h > \kappa^{-1}$, they are useful for predicting stability or instability.

The van der Waals idealized power-law form for parallel infinitely extended slabs of fixed thickness a and variable separation l can be written as

$$\frac{A_{Ham}}{12\pi}\left[\frac{1}{l^2} - \frac{2}{(l+a)^2} + \frac{1}{l+2a)^2}\right] \tag{1.11}$$

1.4.2 The Role of Salt Concentration and Aggregation

Debye Screening Length

Table 1.1: Roughly values of the Debye's screening lengths for the salt concentrations that are used in the experiment.

Concentration M	Debye's screening length nm
10^{-4}	30
2.5×10^{-4}	19
5×10^{-4}	13
7.5×10^{-4}	11
10^{-3}	9.6
2.5×10^{-3}	6
5×10^{-3}	4
10^{-2}	3
5×10^{-2}	1

The Debye screening length changes strongly with the salt concentration. For a 1-1 electrolyte (e.g NaCl) the screening length is

$$1/\kappa = \frac{0.304}{\sqrt{[NaCl]}} \tag{1.12}$$

Table 1.1 shows the screening length in aqueous solution for the salt concentrations that have been used in the experiment. Therefore, the competition between the repulsive and attractive interactions depends strongly on the added salt. At high salt concentrations the Debye length is smaller than the range of the attractions, and as a result, the suspension is unstable and shows irreversible flocculation. A suspension is therefore only stable, when λ is sufficiently large, meaning that the added salt content has to be sufficiently low. Then the range of the repulsive interactions can easily become larger than the separation between neighbouring colloidal particles so that the system becomes highly correlated, although the actual volume occupied by the particles is rather low. In totally pure water at pH 7, the Debye length is 960 nm, or about 1 μm.

Change from Stability to Instability

In the DLVO theory, colloidal stability is caused by a balance between double-layer repulsion and van der Waals attraction[9]. Therefore, the simplest means of controlling it is to change the nature and concentration of the electrolyte. Experimentally a rather abrupt change from stability to instability on changing the salt concentration will occur. Starting from the DLVO potential and viscosities of the solvent, the expected association rate for any electrolyte concentration can be calculated. A more qualitative approach is to specify a potential $V(h)$, which approximately represents the transition from stability to instability in practical terms. A mathematically convenient choice is to set $V(h)$ equal zero at the barrier maximum. In this case increasing the electrolyte concentration would give an unstable system, or slightly decreasing the electrolyte concentration would achieve long-term stability.

Depending on the electrolyte concentration and surface charge density or potential one of the following may occur:

a. For highly charged surfaces in dilute electrolyte (long Debye length), there is at the energy barrier a strong long-range repulsion that do a peak at some distance, usually between 1 and 4 nm.

b. For more concentrated salt solutions there is a secondary minimum (usually beyond 3nm) before the energy barrier. The potential energy minimum at contact is known as the primary minimum. For colloidal system, even though the thermodynamically equilibrium state may be with the particles in contact in the deep primary minimum, the energy barrier may be too high for the particles to overcome during any reasonable time period. When this happens, the particles will either sit in the weaker secondary minimum or remain totally dispersed in the solution. In the latter case the colloid is referred to as being kinetically stable (as opposed to thermodynamically stable).

c. For surfaces of low charge density or potential, the energy barrier[10] will always be much lower. This leads to slow aggregation, also known as coagulation or flocculation. Above some concentration of electrolyte, known as the critical coagulation concentration, the energy barrier falls below the $W = 0$ axis and the particles then coagulate rapidly. The colloid is now referred to as being unstable.

d. As the surface charge or potential approaches zero interaction curve goes to the pure van der Waals curve, and two surfaces now attract each other strongly at all separations (**e**).

[9] The van der Waals effective range typically extends to a few nanometres from the surface of the particles.

[10] If the barrier is cleared, then the net interaction is all attractive, and as a result the particles aggregates.

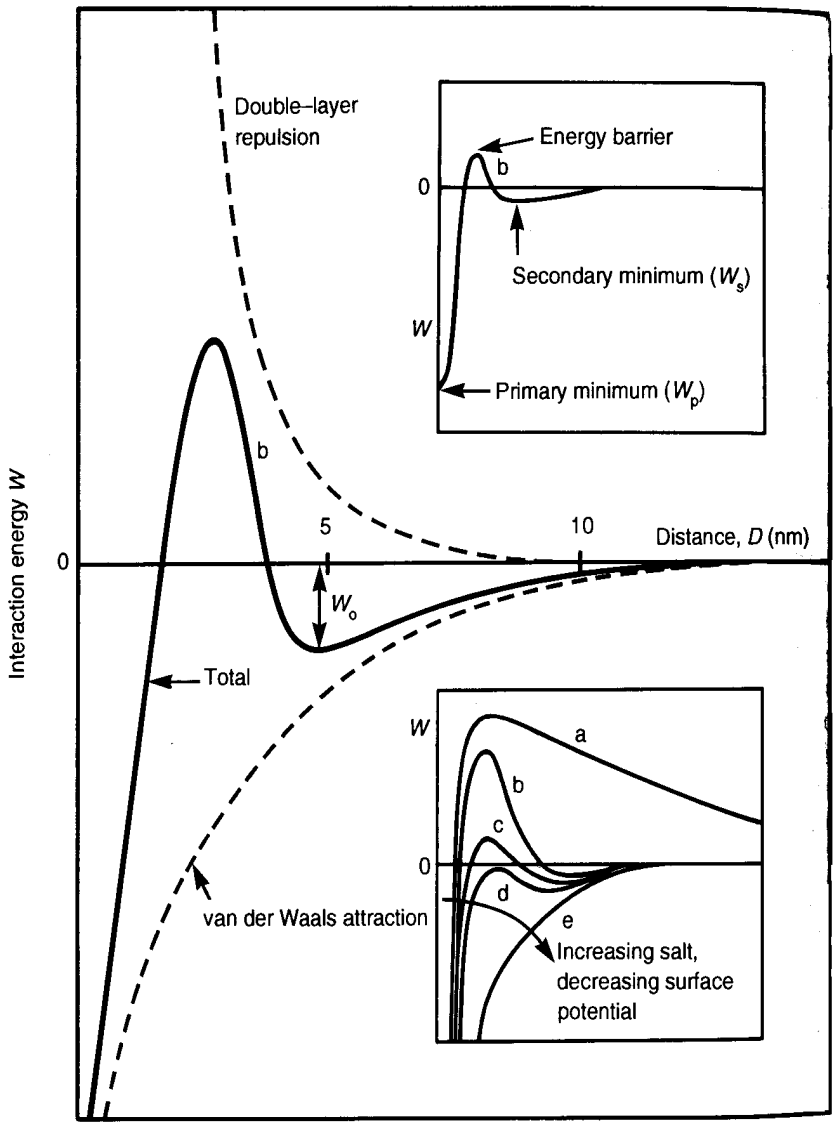

Figure 1.3: Energy versus distance profiles of DLVO interaction. **a**. Surfaces repel strongly; small particles remain stable. **b**. surfaces com into stable equilibrium at secondary minimum if it is deep enough (colloids remain kinetically stable). **c**. Surfaces come into secondary minimum: colloid aggregate slowly. **d**. The critical aggregation concentration. Surfaces may remain secondary minimum or adhere; colloid aggregate rapidly. **e**. Surfaces and colloids coalesce rapidly. Taken from [92].

1.5 Gels

Attracted particles may join to form extended networks, resulting in gels[11] [93]. In general the particles will have a negative surface charge partly made up for positive charge at the particle edges. This has made suggestions that the particles are connected in a face-to-edge configuration as illustrated in Figure 1.1 (c). The result from this is a suggested isotropic "house of cards" structure which has been treated under many theoretical studies.

From a work by Dijkstra et al. [31] the sol-gel transition in a suspension of monodisperse, charged, disklike platelets was examined within a simplified statistical model. The use of an initial primitive model of uniformly charged disks surrounded by microscopic co-ions and counterions was reduced to a model of nonintersecting disks carrying a rigid point quadrupole, resulting from the electric double layers around the disks. It was showed that the quadrupolar interactions favoured edge-to-face pair configurations which counteract the tendency of parallel nematic alignment of bare disks at high densities. The local structure and phase behavior of the quadrupolar disk model was studied over a broad range of clay concentrations and quadrupole moments which depend on the concentration of added salt by extensive Monte Carlo simulations. The model suspension was found to undergo a reversible sol-gel transition above a critical quadrupolar coupling. The gel phase lacks long-range order, and is reminiscent of a house-of-cards structure in which most of the particles are edge-to-face to each other. The critical concentration and quadrupolar coupling constant are not inconsistent with recent experimental data on the gelation of Laponite suspensions. Since most other recent experimental work has failed to verify the house of cards model, the structural correlations of liquid crystal phases is an alternative model that may be expected in these systems.

1.6 Liquid Crystalline Orientational and Positional Order

The two most common condensed matter phases, crystals and liquids, are fundamental states that differ in their microscopic structure and dynamics. The elements of a crystal are constrained to occupy only certain positions or sites in a lattice. This condition is described by saying that the crystal possesses positional order. The elements in these specific positions are also constrained in the way they are oriented with respect to one another, that their axes point in a specific direction. The crystal phase is in this way also said

[11] A gel (from the lat. gelufreezing, cold, ice or gelatusfrozen, immobile) is a colloidal system in which a porous network of interconnected nanoparticles spans the volume of a liquid medium. In general, gels are apparently solid, jelly-like materials. Both by weight and volume, gels are mostly liquid in composition and thus exhibit densities similar to liquids, however have the structural coherence of a solid. An example of a common gel is edible gelatin. Many gels display thixotropy - they become fluid when agitated, but resolidify when resting.

to possess orientational order. When a solid crystal melts to a liquid, both the positional and orientational order vanish and the molecules or particles diffuses randomly throughout the sample tube with their orientational axes freely tumbling around.

In nature there are phases that have more order than in liquids but less than what is typical in crystals. These are the liquid crystal phases, which share properties of both crystals and liquid. In liquid-crystalline order the particles are free to move around much like in a liquid, but they tend to remain oriented in a certain direction and sometimes also with some positional order. This orientational order is quite small compared to the order in a crystal. There is only a slight tendency for the particles or molecules to point more in one direction than others or to spend more time in various positions than others.

Liquid crystal phases are more similar to liquids than they are to crystals[12], something that is important in the understanding of their physical properties. Though the amount of order in liquid crystals is very small, it still have mechanical and electromagnetic properties typical of those in crystals.

1.6.1 Director and Order Parameter

Since the particles/molecules in the liquid-crystalline phase are not fixed, the amount of orientational order has to be described as some kind of average. When the entities undergo diffusion one of their common axes tends to be oriented along a preferred direction. This direction is called the director and is specified by means of a unit vector $\hat{n}$. Physically, $\hat{n}$ determines the direction of the optical axis. One way an average could be performed is to take a snapshot of a representative group of particles at a certain time.

Figure 1.4 shows how disk-like particles in such a group could be oriented at some angle relative to the director. A measure of the amount of orientational order could be described by taking the average of all the angles for the particles in the group. The more orientational order present, the closer the average angle would be to zero. In a liquid with no orientational order, such a snapshot would give values for the angle between 0° and 90° with angles representing all possible directions randomly distributed. When it is kept in mind that this random arrangement occurs in three dimensions,

[12]The fact that most of the order of a solid is lost if it transforms into a liquid crystal is revealed by the value of the latent heat, the amount of energy required to cause a phase transition for normal thermotropic liquid crystals. Values are around 250 Joule/gram, which is very close to the value of a direct crystal to liquid transition. When a liquid crystal transforms into a liquid, the value of the latent heat is much smaller being about 5 Joule/gram. The smallness of the latent heat of the liquid crystal to liquid transition is evidence that liquid crystals are more similar to liquids than they are to crystals.

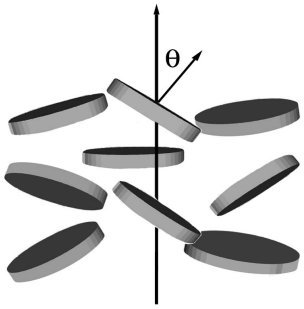

Figure 1.4: Disk-like particles orient with their normals at an angle θ to the director.

there will be much more particles distributed along 90° with the director than 0°. The average of these angles will therefore be greater than 45°. The exact value would be 57° and means no orientational order. Smaller angles would indicate the presence of orientational order, where complete alignment is obtained for an average angle of 0°. The degree of order is described in a suitable way by defining an order parameter where an orientational distribution function, f(θ, ϕ), covers the whole range of possible angles. The width of the distribution function determines the optical anisotropy and $\theta = 0$ corresponding to the direction of the director the fraction of particles with their symmetry axis which lies within the range of angles dθdϕ is

$$f(\theta, \phi) \sin\theta d\theta d\phi \tag{1.13}$$

Since all directions perpendicular to the director are equivalent in the most simple liquid crystal phase, the orientational distribution function does not depend on the azimuthal angle ϕ. Introduction of a second distribution function $f'(\theta)$ gives

$$f(\theta, \phi) = \frac{f'(\theta)}{2\pi} \tag{1.14}$$

Normalization of these equations

$$1 = \int_{\theta=0}^{\pi} \int_{\phi=0}^{2\pi} f(\theta) \sin\theta d\theta d\phi = \int_{\theta=0}^{\pi} f'(\theta) \sin\theta d\theta \tag{1.15}$$

$f'(\theta)$ can be expanded as a series of Legendre polynomials $\mathrm{P}_l(\cos\theta)$

$$f'(\theta) = \sum_{l=0}^{\infty} \frac{1}{2}(2l+1) S_l P_l(\cos\theta) \tag{1.16}$$

Mutual orthogonality of the polynomials give the expression

$$\int_{\theta=0}^{\pi} P_l P_k \sin\theta d\theta = \frac{2}{2l+1} \delta_{lk} \tag{1.17}$$

The coefficients S_l can be found by

$$S_l = \int_{\phi=0}^{\pi} P_l(\cos\theta) f'(\theta) \sin\theta d\theta = \langle P_l \rangle \tag{1.18}$$

where $S_0 = 1$ independent of $f'(\theta)$ and the first order series coefficient is zero[13].

$$S_1 = \langle \cos\theta \rangle = 0 \tag{1.19}$$

The second Legendre polynomial is from this the first non-zero contribution and gives a very useful formulation for the order parameter

$$S_2 = \langle P_2(\cos\theta) \rangle = \left\langle \frac{3\cos^2\theta - 1}{2} \right\rangle \tag{1.20}$$

The brackets can either denote an average over many particles at the same time or the average over time for a single particle.When all angles equal to 0° perfect orientational order causes this average to equal to 1. For an isotropic distribution with no orientational order the order parameter is equal to 0. For liquid-crystalline order typical values for the order parameter range between 0.3 and 0.8. If all particles in a small domain are aligned, the order parameter can be measured by scattering techniques (X-rays and neutrons) [94]. Usually a macroscopic property of the liquid crystal phase is measured, which then can be used to determine S_2 if the microscopic parameters that produce the macroscopic property are known. Diamagnetism, NMR and optical birefringence[14]

Other orientational order parameters can also be defined. An example is the average of the fourth Legendre polynomial

$$S_4 = \langle P_4(\cos\theta) \rangle = \left\langle \frac{1}{8}(35\cos^4\theta - 30\cos^2\theta + 3) \right\rangle \tag{1.21}$$

This order parameter is more difficult to find, but it is possible to measure it using Raman scattering, X-ray scattering, neutron scattering or electron spin resonance. Since the director can be defined in either of two opposite directions, there is no need to define order parameters based on the odd Legendre polynomials, because all of these averages are zero.

For liquid crystals that have positional order an order parameter can be described by considering the tendency for the particles centre of mass to spend more time in layers than between layers as they diffuse throughout the sample. When going from one layer to the next the density of the centres of mass will oscillate up and down along the normal to the layers. Denoting this normal the z-axis, the oscillation can be described by the sinusoidal function [95]

$$\rho(z) = \rho_0 \left(1 + \Psi \cos\left(\frac{2\pi z}{d}\right)\right) \tag{1.22}$$

where ρ_0 is the average density and d is the distance between the layers. Ψ is the positional order parameter and is complex. The modulus of Ψ, $|\Psi|$,

[13] This applies for non-polar systems, which is the case for the liquid-crystalline phases in this thesis.

[14] The difference in the refractive indexes that is responsible for birefringence is proportional to S_2

represents the amplitude of the density oscillation and have typical values much less than one.

In contrast to liquid crystals that always possess orientational order and sometimes have positional order, there is another phase of matter that possesses positional order but no orientational. Material in this phase are called plastic crystals and are said to exhibit rotator phases, because the molecules freely rotate along one or more of their axes, even though their centres of mass are fixed in a lattice. The existence of these exotic phases have been predicted to exist in colloidal systems of rod-like particles in a numerical simulations study by Bolhuis and Frenkel [96]

1.6.2 Anisotropy

In order that the particles in a colloidal suspension should form liquid-crystalline order it is necessary that they are anisotropic in shape[15]. The symmetry axis is significantly different from the other two. Rod-shaped nanoparticles and molecules where the axis along the director is much longer than the width are called calamitic liquid crystals and are the most common and well documented type. Disk-shaped nanoparticles and molecules having a rather small thickness compared to the diameter or length are called discotic liquid crystals and form a number of liquid crystal phases. A second condition for the formation of liquid-crystalline order is that the particles/molecules have some rigidity in its central region. An entity that flops around like a piece of cooked spaghetti is unlikely to have a liquid crystal phase. For molecules it also seems to be advantageous if the ends are somewhat flexible.

When the dissolved particles in a liquid get some small degree of order among one another, the formation to a liquid crystal destroys the isotropy and produces anisotropy. The directions for the elements in the liquid crystal are not equivalent, something that gives the fluid crystalline properties[16]. Elastic, electric, magnetic and optical properties all come from the liquid crystals anisotropy. Measurements of these physical quantities give different results for the elastic modulus, dielectric constant, magnetic susceptibility and the index of refraction depending on the direction along which it is measured. Since liquid crystals are fluids, there is also anisotropy in their flow behaviour. The viscosity will be direction dependent and give three different values, termed the Miesowicz viscosity coefficients, depending on the orientation of the director the measurement is arranged.

[15] For some molecules in normal liquid crystals the anisotropy can be that different parts of the molecules have very different solubility properties.

[16] Crystals can either be isotropic or anisotropic, depending on the molecules occupying lattice sites and the crystal lattice itself. Solids with cubic symmetry are isotropic, whereas solids with all the other possible symmetries are isotropic

1.6.3 Liquid Crystal Mesophases

The phrase mesophase is used for states of matter that occur between the isotropic liquid and crystalline state. Different mesophases that have liquid-crystalline order are various in its structure as different order exist between the particles/molecules. What kind of mesophase that can be formed in a compound, depends on the shape of the particles/molecules. Calamitic liquid crystals have more various mesophases than discotic liquid crystals, which by the other hand can have other phases.

In colloidal mineral systems comprised of rod-like and disk-like nanoparticles the most common mesophases, namely the nematic, columnar and lamellar phases have been found and documented. No liquid crystalline material exhibits all liquid crystal phase types but many compounds or systems do exhibit two or three different types of liquid crystalline phases. For the platelike fluorohectorite particles studied in this thesis, the nematic phase is the important one and is therefore the focus here.

Nematic Liquid Crystalline State

The nematic phase is the simplest and most common of the liquid crystal phases. In this phase the particles maintain a preferred orientational direction as they diffuse throughout the sample. There is no positional order in the nematic phase. The name comes from the Greek word for thread, $\upsilon\eta\mu$, because of many dark lines or brushes that are often visible when a sample with a nematic phase is viewed between crossed polarizers. This pattern is characteristic for nematic phases and is referred to as Schlieren texture. As will be described in more detail later, these threads are topological defects in the orientational order and are called disclinations. The preferred direction is undefined at these disclinations. The textures observed under the cross polarizers can give information on the symmetry of the phase.

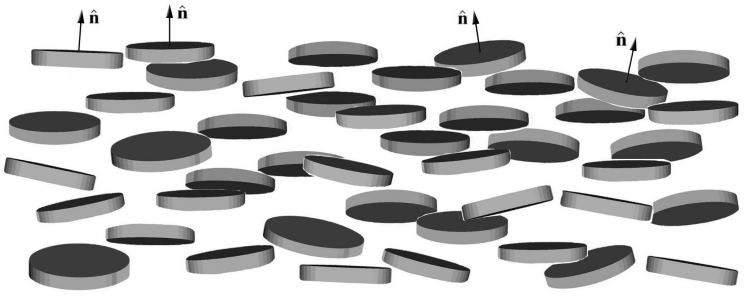

Figure 1.5: Nematic orientation of a system of platelets. The director is defined to point outwards of the face, which is along the optical axis. This organization is directly carried over to rods when the thickness of the platelets is increased to be larger than the diameter.

Nematic samples with defects will consist of random distributions (pow-

ders) of small regions that shows ideal nematic orientational correlation called nematic domains. Both rod-like and disk-like entities can form the nematic phase and will show an identical optical textures, even though the two phases are completely different and immiscible. While rod-like particles form nematic ordering by preferentially aligning their long axes along the director, disk-like particles preferentially orient their short axes along the director.

The phase is depicted in Figure 1.5, where it is clear that there is no positional order in this state. It is often a case to be able to remove the defects in a nematic sample and produce a single domain with all entities pointing in the same preferred direction. A single domain have homogeneous optical properties and are suitable for more detailed physical studies, among other things to find the nematic order parameter. The usual way to align a nematic phase is by the action of external magnetic and electric fields. The alignment is due to the anisotropy of the mesophase that reorients to minimize its free energy in the field. This property is the basic in the construction of liquid crystal displays since the reorientation changes the degree of transparency with respect to light. When it comes to clays, the nematic domain can be divided into a nematic sol and a nematic gel. The nematic sol phase readily displays Schlieren textures whereas the nematic gel often shows the so-called banded texture of sheared nematic polymers caused by filling the flat glass capillaries with gel samples. Nematic clay gels are not very likely to be magnetically orientated due to their strong elastic properties. Particles in an isotropic phase can also align in the action of a magnetic field, and the new phase is then called paranematic [97].

The chiral nematic state is a phase that arises if the molecules that form the nematic phase are chiral or if a quantity of another chiral material is added to the sample. In calamitic liquid crystals, the nematic phase is replaced by the chiral nematic phase, in which the director rotates in helical fashion about an axis perpendicular to the director. The pitch of a chiral nematic phase is the distance along the helix over which the director rotates by 360°. Because of the equivalence of the director direction, $\hat{n}$ = -$\hat{n}$, the structure of the chiral phase repeats itself every half pitch. The chiral nematic phase can also be formed in discotic nematic compounds, and the structure is identical to the chiral phase for rod-like molecules. A substance may possess either the nematic liquid phase or the chiral nematic liquid phase but not both. Due to lack of applications and expense, relatively few examples of discotic nematic compounds exist.

Mesophases with Positional Order

Liquid crystalline phases that in addition to the small amount of orientational order have a small amount of positional order constitute great many various phases. The molecules or particles are free to bounce around quite randomly, but they tend to point along the director and arrange themselves in layers. A snapshot in time would reveal that slightly more molecules tend to be positioned in regularly spaced planes with fewer molecules in between. Likewise, following a single molecule would reveal that is spent more time in these planes

than between them.

The smectic[17] liquid crystal state is a mesophases with such positional order that is generated by rod-like molecules or nanoparticles. There are many types of smectic phases, where the simplest have one-dimensional positional order. These are the smectic A and smectic C phases with its molecules randomly diffuse within each plane without having any positional order within each plane. Other smectic phases with order within each plane exist, and are called smectic hexatic phases. This type of order have become known as bond orientational order and the positional order these phases possess is in a sense three-dimensional.

Positional order found in thermotropic liquid crystal disk-like molecules displays itself by the tendency of the molecules to arrange themselves in columns. This is called the columnar phase and exhibits in several different types due to the way the columns are arranged relative to one another and whether the molecules within the columnar arrays are ordered or disordered. The columns form a two-dimensional lattice in a hexagonal, rectangular or oblique symmetry. In some of the columnar phases, the molecules are tilted with their short axes not parallel to the column. The tilt direction alternates from one column to the next.

For mineral systems the hexagonal columnar phase has been observed experimentally in suspensions of sterically stabilised [79] and charged [98] colloidal plates. Extensive structural investigations proved that the mineral phase observed for the first case are very similar to the hexagonal columnar mesophase of usual disk-like organic molecules.(thermotropic discotic mesogens) The observation of the columnar phase in a system consisting of polydispersed grafted gibbsite nanodisks, suggests that appreciable diameter polydispersities do not prevent columnar ordering. This system also organises in a lamellar phase instead of columnar ordering when the volume fraction increases. The detection of columnar phase for charged gibbsite plates showed that at low aspect ratio, a direct columnar/isotropic phase transition was observed whereas the nematic/isotropic phase transition was detected at large aspect ratio. This phase diagram of disk-like particles was predicted by numerical simulations by Verman and Frenkel in [46]. The columnar phase can be detected in natural white light by observation of small coloured bright spots due to Bragg reflections of light by the columnar lattice.

1.6.4 Magnetic Field Effects

As mentioned before the anisotropy of the liquid crystalline state manifests itself in many physical properties. When electric or magnetic external fields are applied to a liquid crystal, the phase responds differently depending on whether the field is applied along the director or at an angle to it. Nematic phases can often be aligned by the action of a magnetic field due to the anisotropic

[17] The name smectic comes from the Greek word of soap, $\sigma\mu\eta\gamma\mu$, since the early investigators noticed that these liquid crystal phases possessed mechanical properties reminiscent of soaps.

mesophase that reorients to minimize its free energy in the field. Therefore, the director is aligned along or perpendicular to the field direction, depending on the sign of the magnetic anisotropy of the building blocks. Topological defects in the nematic phase may be suppressed by the alignment and form a single domain.

The study of colloidal suspensions submitted to magnetic and electric fields dates back to the end of the 19th century, where John Kerr [99] discovered that certain liquids showed birefringence when applied to strong electric fields. This electro-optical effect is today known as the Kerr effect. The field of magnetic birefringence was developed by Kerr, Majorana [100–106] and Cotton and Mouton [107–112].

In the recent years may studies have been reported on the diamagnetic alignment of materials possessing magnetic anisotropy [70, 97, 113–115]. Lemaire et al. have reported some outstanding magnetic properties of nematic aqueous suspensions of goethite (α-FeOOH) nanorods [116, 117]. These nanorods align parallel to the field at magnetic fields lower than 0.35 T and reorient perpendicularly to the field at field strengths higher than 0.35 T. This unusual behaviour could be explained by the fact that the nanorods bear a small longitudinal remanent magnetic moment, and also have a negative anisotropy of magnetic susceptibility. Such a combination of dipolar and quadrupolar orders induces original symmetries somewhat hybrid between those of nematics and ferrofluids. Magnetic fields applied to a nematic phase in suspensions of these rods can also induce a 2 dimensional columnar mesophase of rectangular symmetry [118]. When the magnetic field is suppressed, this columnar ordering reverse back to the nematic phase.

Magnetic field induced orientational ordering in suspension of gibbsite ($Al(OH)_3$)) platelets have been studied by Lekkerkerker et al. [119]. Magnetic field strengths from 3-7 T applied to isotropic phases of the suspension show strong alignment of the particles.

Liquid crystals of organic molecules and mineral nanoparticles have two magnetic susceptibilities[18], one for magnetic fields applied parallel to the director and one for magnetic fields applied perpendicular to the director. A plate-like particle exposed to a magnetic field B will have different magnetic susceptibilities along different axes of the particle. Since the magnetization of the particle is the susceptibility multiplied by the external field the magnetization will have two coefficients for the normal and perpendicular direction. The total induced magnetization $\vec{m}$ of the particle can be written as

$$\vec{m} = \chi_{\parallel} B_{\parallel} \hat{e_{\parallel}} + \chi_{\perp} B_{\perp} \hat{e_{\perp}} \tag{1.23}$$

with $e_{\parallel}$ being the platelet normal and $e_{\perp}$ directed along the face of the particle. The magnetic energy per particle can be found by the general expression [120]

$$u_m = -\frac{1}{2}\vec{m} \cdot \vec{B} = -\left(\frac{1}{2}\chi_{\parallel} B_{\parallel}^2 + \frac{1}{2}\chi_{\perp} B_{\perp}^2\right) = -\frac{1}{2}\left(\chi_{\parallel} - \chi_{\perp}\right) B^2 \cos^2\theta - \frac{1}{2}\chi_{\perp} B^2 \tag{1.24}$$

[18] The magnetic susceptibility is the ratio of the magnetization to the strength of the applied magnetic field and is usually constant.

The anisotropy of the diamagnetic susceptibility $\Delta\chi$ is defined as

$$\Delta\chi = \chi_{\parallel} - \chi_{\perp} \tag{1.25}$$

Since the last term of Equation (1.24) is independent of orientation, the magnetic energy per particle can be written

$$u_m(\theta) = -\frac{1}{2}\Delta\chi B^2 \cos^2\theta \tag{1.26}$$

In a magnetic field the particles will reorient in the configuration that minimize the free energy of the mesophase. From the expression of the diamagnetic susceptibility it is clear that the sign decide whether the platelet are aligned with their faces parallel or perpendicular to the magnetic field. From measurements shown in Chapter 3.8 and reference [70], particles from exfoliated Na-fluorohectorite sheet align with their normals (directors) perpendicular to the field. This gives the lowest magnetic energy with a negative value of the magnetic susceptibility.

1.7 Boundary Effects

The surrounding elements on a liquid crystal have an important influence on how the director orients through the mesophase. Due to the competition between many effects, liquid crystals may behave in a very complex way when it is shut up between interfacial boundaries. In ordinary liquid crystals the response of the molecules are so delicate that any surface causes them to align in a specific direction near the surface. Treatment of a glass surface by rubbing it with a piece of cloth or paper[19] when a liquid crystal is placed against it may be enough to force the director to orient along the direction of rubbing.

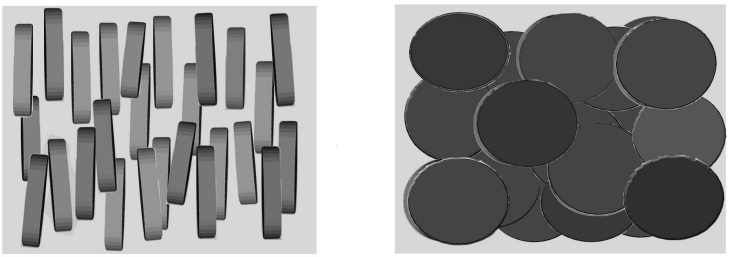

(a) **(b)**

Figure 1.6: Particle alignment with the walls lying in the plane of the paper. (a) Homeogeneous texture; the normals of the particles are parallel to the wall. (b) Homeotropic texture; the normals of the particles are perpendicular to the wall.

When the director of a liquid crystal that is trapped between two surfaces is oriented along the walls, it is called homogeneous (planar) alignment. An

[19] A thin film of a solid polymer coated on the glass substrate before rubbing increases the anisotropy of the surface.

opposite configuration where the director is oriented perpendicular to the walls is on the other hand called homeotropic alignment. This situation can be trigged by applying to the glass substrate a thin film of amphipilic molecules. The polar part of these molecules bonds to the glass and the non-polar part extends into the liquid crystal material. Figure 1.6 shows homogeneous and homeotropic anchoring of platelike entities. For rod-like entities the orientation of the axes of symmetry will be similar, that the long axes lies parallel to the wall in homogeneous alignment and perpendicular in homeotropic alignment. With different preparations of the glass surface, the director can be oriented in almost any direction. Other methods than using various chemicals can be to evaporate solid material onto the glass prior to using it with the liquid crystal.

In liquid crystals that is placed between surfaces that are not been treated to obtain any particular alignment, usually both homogeneous and homeotropic alignment occur at various positions. The thickness of the sample may have an influence on the alignment. Thin samples tend to generate homeotropic alignment whereas thicker samples tend to give some regions of homeotropic alignment and some regions of homogeneous alignment. Interfacial interaction between colloidal particles and hard walls may play an important role in the origin of nematic ordering. For purely repulsive forces between hard colloidal platelets and hard walls, density-functional theory calculations predict that the platelet faces must adopt, very close to the walls, a fully parallel alignment. However, at distances of approximately only one platelet radius a change in the order parameter to perpendicular alignment is expected.

In round sample tubes that have hydrophilic glass walls it has been shown that Na-fluorohectorite particles can form uniaxial nematic order where the platelets close to the wall are anchored with their faces parallel to the wall [70]. The significance of the polar walls[20] to give this effect have been demonstrated by the fact that the use of apolar walls[21] give considerably less face-to-wall anchoring of particles and a further disrupted nematic order in the whole sample. In other colloidal systems of hard platelets, such as gibbsite, the presence of non-adsorbing polymer is found to favour homeotropic face-to-wall anchoring of the platelets [121]. This can be due to a stronger depletion attraction in this configuration.

1.8 Deformation and Fréedericksz transition

The director in liquid crystalline order is generally free to point in any direction. A perfectly uniform director is usually obtained by treatment of the glass surfaces or the action of external fields. On a microscopic level the director varies with position with such a slight degree that the orientational order parameter can be considered to be constant through the whole phase.

[20] Hydrogen-bond-forming hydrophilic glass walls.

[21] In the experiment of ref [70] teflon walls were used to give apolar walls.

When a uniform director field loses its homogeneity due to an external deformation, elastic forces in the liquid crystal can be active and counteract the constraint. This elasticity is described in a continuum theory similar to mechanics where the account of the elastic energy is in analogy as that of a compressed spring. In the consideration all order parameters are assumed to be constant[22]. In a non-chiral system the director does not vary in its equilibrium state.

A deviation from the state are analogous to a deviation from the equilibrium length of a spring. Just as the elastic energy of a spring is proportional to the square of the deviation of its length from the equilibrium length, the free energy per unit volume of the liquid crystal can be expressed in terms of the square of the spatial derivative of the director. The difference for a liquid crystal compared to the case of a spring is that there are three directions in space and then three components of the director.

Figure 1.7: The three basic types of deformation of the director field: splay, twist and bend. The shapes represent disk-like particles that are viewed edge on with the face normal as the director. In all three cases, deformation is present in the plane of the page. There is no change in the director orientation in going into or out of the page. When disks are fully viewed edge on, they may look like rods oriented perpendicular to the director. For this representation the formation of the bend and splay distortion interchange.

In addition, there are other conditions the free energy must satisfy. For all terms, $\hat{n}$ and -$\hat{n}$ must give the same energy values. There can be no linear terms except in chiral systems. These terms change if the coordinate system is rotated about the director, if the director is reversed, or if the coordinate system is inverted. The last restriction is that $\hat{n}$ must not change its length since it is a unit vector. All of the terms that satisfy these criteria can be grouped together to a simple expression for the free energy density of a deformed nematic phase, which by theoretical analysis by Frank was found to be [122]

$$F_d = \frac{1}{2}K_1\left(\nabla\cdot\vec{n}\right)^2 + \frac{1}{2}K_2\left(\vec{n}\cdot\left(\nabla\times\vec{n}\right)\right)^2 + \frac{1}{2}K_3\left(\vec{n}\times\left(\nabla\times\vec{n}\right)\right)^2 \qquad (1.27)$$

The three terms in this expression correspond to three basic modes of distortion in nematic liquid crystalline order, which as illustrated in Figure 1.7 are

[22]This assumption does not count for regions with defects such as disclination points.

referred to the splay, twist and bend deformation. The three constants K_1, K_2 and K_3 are called the Frank moduli and describe how stiff the system is to distortions with respect to splaying, twisting and bending of the director. For chiral nematic liquid crystals, the twisted configuration is spontaneous, while a force is required to produce splay or bend or to change the amount of twist from its spontaneous value.

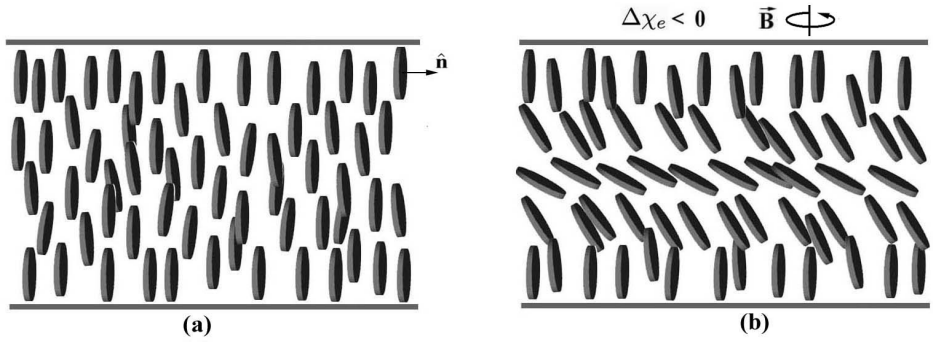

Figure 1.8: The homogeneous Fréedericksz transition in the splay and bend geometry. (a) Homogeneous texture, where the particles are oriented with their edges to two flat glass walls. (b) When the anisotropy of the magnetic susceptibility is negative, this splay-bend distortion can occur when a magnetic field above threshold is rotated in the plane parallel to the walls.

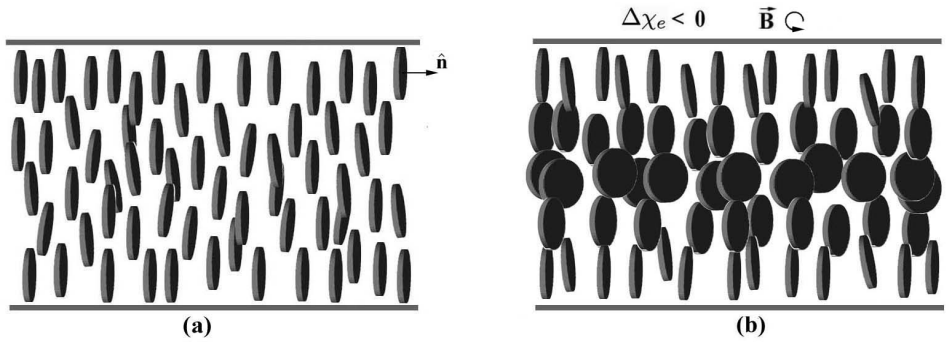

Figure 1.9: The homogeneous Fréedericksz transition in the twist geometry. (a) Homogeneous alignment. (b) For negative anisotropy of the magnetic susceptibility, twist deformation takes place when a magnetic field of strength above threshold is applied around the plane of the Figure.

The Frank elastic constants can be experimentally determined by applying an external field to a thin nematic layer placed between two surfaces that have been treated to produce alignment of the director either parallel or perpendicular to the surface. When the director is uniform through the sample, a director reorientation caused by an applied magnetic field will need to oppose the wall-imposed director orientation. The particles near the walls will not be

very free to orient with the field, but the particles in the middle are fairly free. The magnetic field will therefore cause the director to change its orientation the most in the middle and less and less closer to the walls. Depending on the wall-imposed director and the direction of the applied field, the nematic phase will be deformed as of a splay, twist or bend deformation. These three cases are shown in Figure 1.8, 1.9 and 1.10 for systems of initially aligned platelets.

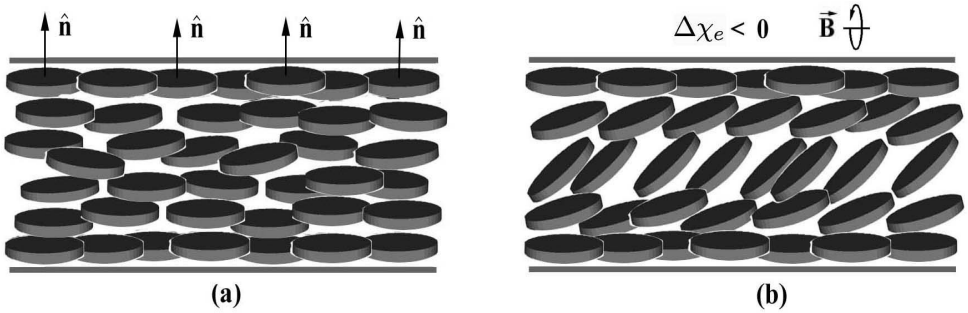

Figure 1.10: The homogeneous Fréedericksz transition in the bend geometry. (a) Homeotropic texture, where the particles are aligned with their faces towards the glass boundaries. (b) When the anisotropy of the magnetic susceptibility is negative, the shown bend distortion can occur when a magnetic field above threshold is rotated perpendicular to the boundaries.

If the particles are oriented with their director parallel to the surface in a homogeneous alignment, an applied magnetic field which tends to orient the director perpendicular to the walls, will give a deformation of the splay and bend geometry. If the magnetic field by the other hand are applied such as a free particle will orient with the director parallel to the walls but perpendicular to the initial director, the deformation will give a twist geometry. Are the director oriented perpendicular to the wall as in a homeotropic texture, a magnetic director reorientation parallel to the glass walls will form a bend deformation.

An important aspect of these deformations is that they do not occur gradually as the strength of the external field is gradually increased. For fields of strengths below a certain value, the liquid crystalline order remains in its undeformed shape without any change at all. Then at some threshold value of the field, the deformation begins to occur and increase as the field strength is increased.

This transition from an undeformed to a deformed texture at a certain value of the field is called the Fréedericksz transition after the Russian scientist who studied the phenomenon in the 1930s [123]. The Fréedericksz transition is not a phase transition, since the amount of order among the particles relative to one another remains the same. It is simply a transition from a uniform director configuration to a deformed configuration. To find the the threshold value the equilibrium director configuration needs to be considered. From Equation

(1.26) it follows that the magnetic energy density F_m is given by

$$F_m(\theta) = -\frac{1}{2}\rho\Delta\chi\left(\vec{n}\cdot\vec{B}\right)^2 \tag{1.28}$$

where ρ is the number density of the particles in the nematic phase. The sum of the distortion and the magnetic field energies give the total energy per density $F = F_d + F_m$. By minimising this energy integrated over the whole nematic phase, it can be shown that the threshold value is given by

$$B_c = \frac{\pi}{d}\sqrt{\frac{K_i}{\rho\Delta\chi}}(i = 1, 2, 3) \tag{1.29}$$

where d denotes the thickness of the nematic layer and K_i the Frank moduli of the deformation being applied. This expression is valid for nematic phases that are strongly anchored, in which the director right at the wall is not disturbed by the magnetic field.

1.8.1 Transient Periodic Structures

The director distribution of the Fréedericksz transition as described above, is uniform or homogeneous through the plane of the liquid crystal layer. However, under certain conditions the field-induced reorientation may result in a non-uniform transition consisting of spatially periodic distortions. This deformation can either be of a stationary steady-state or a transient instability. The periodic structures are dielectrically induced and in most cases appear as equidistant parallel stripes apparently similar to Williams[23] [124] domains and Rayleigh-Bénard instability [125]. Depending on the initial director direction and the applied field, the structure can also be oblique or two-dimensional [126–129].

The steady-state deformation give an equilibrium periodic structure where the relation of the elastic constants $K_1/K_2 > 3.3$ is found to be more favourable for the periodic splay-twist distortions than a uniform splay [130]. The physics behind this stationary structure are explained by free energy calculations and are different in origin than the transient structures. Since the liquid crystalline order of the clay suspensions undergoes the transient instability, the section will further focus on this process. The observation of periodic structures from this process in liquid crystals was first published by Carr in 1977 [131] and have later been found for all classes of nematics [126, 127, 129, 132–140].

For mineral liquid crystals, parallel stripe pattern have been studied in suspensions of vanadium pentoxide (V_2O_5) ribbons [141], gibbsite platelets [142] and nontronite swelling clay mineral [41].

[23] Williams domains is a regular pattern of bright and dark stripes, which can be formed in a cell of a nematic material with negative dielectric anisotropy when an electric voltage of sufficient magnitude is applied. The pattern is caused by a distortion of the initial director configuration due to a circulation of the liquid crystal molecules, which is caused by the motion of a small amount of charged impurities present in the sample.

The formation of transient periodic structures are not exceptionally for liquid crystals, but are often connected with processes in nature that take place far from its equilibrium state [143, 144]. In these phenomena, periodic order of dynamic behaviour emerges from a homogeneous state by spontaneous local symmetry breaking. When the magnetic field strength is much larger than the critical uniform threshold value, a field direction that reorients the director direction of a liquid crystal will suddenly place the system far from equilibrium. It responds by creating a distortion that maximizes the rate in where the liquid-crystalline order obtains the lowest total free energy. The response may be of periodic character, where the exact form of deformation depends on the viscous and elastic properties of the liquid crystal itself and outer conditions as magnetic field strength, geometry of the sample and boundary effects.

Since periodic patterns formed from this non-uniform Fréedericksz transition is a transient phenomena, the structure will disappear when it is subjected to the reorienting field for long enough time. The nematic phase will then reach a new equilibrium with the director oriented as preferred by the magnetic field. The dissipative structures arise short time after the reorientation is into stride, with a response speed which is faster than the uniform Fréedericksz transition.

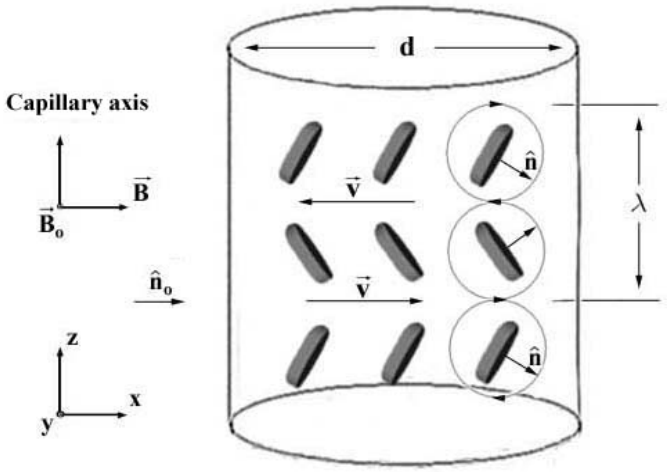

Figure 1.11: Geometry of the periodic instability in the capillary tube with diameter d. A magnetic field $\vec{B_0}$ is first applied along the y-axis, which orient the particles with an initial director $\hat{n}_0$ along the x-axis. A later magnetic field $\vec{B}$ applied transversely along the x-axis causes a periodic reorientation, which by oppositely rotating zones produces a fluid flow response with a macroscopic mass flux velocity $\vec{v}$. This flow is coupled to the periodically modulated rotation of the director $\hat{n}$ in the same plane, and the rate of the rotation of the director relative to the background fluid is lowered.

This occur because of a strong coupling between director rotation and fluid flow (the backflow effect) in addition to the large viscous and elastic anisotropy of the nematic phase. This coupling gives a considerably reduced effective viscosity which from a dynamic point of view is preferable for periodic structures, even though such structures are unstable with respect to free energy

considerations. An illustration of this is shown in Figure 1.11, where the observation of parallel stripes are revealed as being actually walls separated splayed microdomains with clockwise and counterclockwise rotations of the director. When an external field of high enough strength is exposed to the nematic phase, it becomes in unstable equilibrium and small fluctuations of the director field grow exponentially under the influence of the destabilizing field. A theoretical description of this was first carried out by Guyon, Meyer and Salan [145] in 1979, where a linear stability analysis of nematodynamic equations [125] was done with respect to the distortion angle.

The rate of reorientation or growth rate, s, is a function of a modulation wavelength, λ, and is inversely proportional to the effective viscosity of the particular distortion mode under consideration. The linear analysis assumes that all distortion modes are independent, and because of nonlinearities, the mode with the fastest growth rate suppresses all slower modes and is therefore the only mode which is macroscopically observable.

For disk-like systems (Kuzma [129]), an expression of the growth rate of this dominating mode is for the splay and bend geometry given as [146]

$$s(\lambda) = \frac{\Delta\chi_e B^2 - K_3 k_x^2 - K_1 k_z^2}{\gamma_1 - (\alpha_2 k_x^2 - \alpha_3 k_z^2)^2 / \left[\eta_b k_z^4 + N k_z^2 k_x^2 + \eta_c k_x^2\right]} \tag{1.30}$$

$\Delta\chi_e$ is the diamagnetic susceptibility anisotropy and B the magnetic field strength. γ_1 is the rotational viscosity, whereas η_b and η_c are the Miesowicz shear flow viscosities. α_2 and α_3 are the Leslie coefficients of the nematic viscosity in which the rotational and flow viscosities coefficients are coupled[24]. N is a particular combination of viscosity coefficients, while K_1 and K_3 are as before the Frank elastic constant for splay and bend respectively. For the bend geometry in Figure 1.11 the wave vector $k_x = \pi/d$, while the wave vector, $k_z = 2\pi/\lambda$, maximize the growth rate s for a certain wavelength λ for the stripes. In the splay geometry, the roles of k_z and k_x are interchanged.

The uniform Fréedericksz transition, for which the wavelength can be attributed to be infinity, depends effectively only on the rotational viscosity γ_1. In the transient periodic structures, the influence of the shear viscosities leads to a reduction of the overall effective viscosity, which consequently increases the speed of the reorientation process. However, as a result of larger director gradients, the elastic energy involved increases with decreasing wavelength. The reorientation process slows down with smaller wavelengths due to larger elastic forces. The distortion mode yielding the optimum balance between the viscous drag and elastic and magnetic forces is characterized by the maximum response speed. The relation between the magnetic field strength B, sample thickness d and fastest growing wavelength mode λ is from the linear stability theory given by a fourth-order equation in λ [142, 147]:

$$\left(\frac{B}{B_c}\right) = \frac{\eta\kappa}{\upsilon}\left(\frac{\eta}{\alpha\beta^2} - 1\right)\left(\frac{2d}{\lambda}\right)^4 + \left(\frac{2\eta\kappa}{\alpha\beta^2}\right)\left(\frac{2d}{\lambda}\right)^2 + \left(1 + \frac{\kappa\upsilon}{\alpha\beta^2}\right) \tag{1.31}$$

[24] $\gamma_1 = \alpha_3 - \alpha_2, \eta_a = \frac{1}{2}\alpha_4, \eta_c = \frac{1}{2}(\alpha_4 + \alpha_5 - \alpha_2)$

Here $\kappa = K_1/K_3$, $\alpha = \alpha_2^2/\gamma\eta_c$, $\eta = \eta_b/\eta_c$, $\beta = \alpha_3/\alpha_2$, $\upsilon = N/\eta_c$ and B_c is the critical threshold value for the uniform bend Fréedericksz transition given in Equation (1.29) with K_3. Equation (1.31) has finite roots for magnetic fields $B > B_s$ exceeding a second threshold field

$$B_s = \sqrt{\left(1 + \frac{\kappa\upsilon}{\alpha\beta^2}\right)} B_c \tag{1.32}$$

For magnetic field strengths $B_c < B < B_s$, the uniform Fréedericksz transition has maximum response speed and no structures are generated. Transient periodic patterns are formed at magnetic fields $B > B_s$ whose wavelength decreases with increasing field strength. The wavelength diverges when the magnetic field gets close to B_s. From Equation (1.31) it follows that the viscoelastic parameters of the nematic phase should be obtained by measuring the wavelength with the sample thickness dependence for the periodicity of the stripe pattern. Experiments with the application of the linear mode selection theory has shown to be successful in a qualitative sense by given reasonable estimates for the material parameters.

Using the analysis of periodic structures as a refined method to measure the elastic and viscous coefficients has for many experiments been inadequate. The drawback of the linear stability theory is that it is inappropriate to describe the actual evolution of the structures in time because it neglects the influence of thermal fluctuations and of inherent nonlinearities[25] of the system. Sagues, Arias and San Miquel [149] have developed a dynamic model which consistently includes these effects. The pattern formation is described by means of a time dependent structure factor related to the periodicity of the pattern. Whereas the wavelength of the pattern is time dependent, the value of the fastest growing mode predicted by the linearized stability theory is approached asymptotically in that model.

1.9 Light and Nematic Liquid Crystalline Order

In this thesis the main experimental method for detection of nematic liquid crystalline order in suspensions of Na-fluorohectorite is featured on the optical properties of the mesophase. The way liquid crystals are affected by light is very important when it both comes to experimental study and applications of liquid crystals. To get the best possible understanding of the results obtained from the experimental work, this section will contain some basic discussion of polarized light and birefringence in anisotropic media.

[25] Nonlinearities of the nematodynamics, that is coupling of the individual modes, might change the periodicity of the structure. As argued by Srajer, Fraden and Mayer [148], the observed wavelength is slightly shifted towards larger values during the evolution of the modes.

1.9.1 Polarized Light

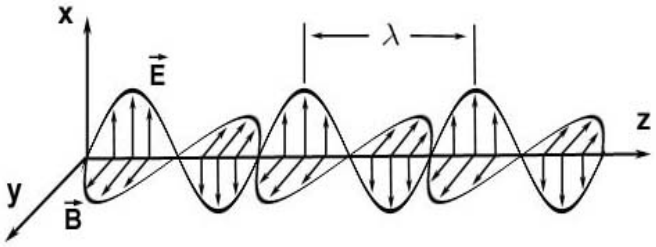

Figure 1.12: Electromagnetic wave with electric field in x-direction and magnetic field in y-direction, propagates with a wavelength λ along the z-direction.

Figure 1.12 shows the propagation of an electromagnetic wave and how it consists of oscillating electric and magnetic fields that are perpendicular to each other. Both the electric and magnetic fields point in a direction perpendicular to the direction of propagation. The wavelength, λ, is the distance it takes the fields to repeat themselves after a certain distance along the propagation direction. For the electromagnetic wave in Figure 1.12, the magnetic and electric field point for one another along a single direction in space. In this case, the wave is said to be linearly polarized. The electric field is normally chosen to define the direction of the polarization. The electromagnetic wave in Figure 1.12 is therefore linearly polarized along the x-axis. The polarization direction can be in any direction in the plane perpendicular to the propagation direction. The amplitude of the electric field can be given by the components; E_{0x} and E_{0y} along the x and y direction. The ratio of these two components can indicate the polarization property of the wave. A general expression of oscillating electromagnetic wave propagating in the z direction can with the two components be written as

$$E_x(z,t) = E_{0x}\cos(kz - \omega t) \tag{1.33}$$

$$E_y(z,t) = E_{0y}\cos(kz - \omega t + \delta) \tag{1.34}$$

where the parameter δ attends to a phase difference of the components. For linearly polarized light δ is either zero or $\pm\pi$. The amplitudes will then give the direction of the polarization by the angle

$$\theta = \tan^{-1}\left(\frac{E_{0y}}{E_{0x}}\right) \tag{1.35}$$

If $\delta = \pm\frac{\pi}{2}$, a 90° phase difference will make the electric field rotate around the z-axis in the xy plane. For the case of equal amplitudes, the wave is circularly polarized since the tip of the electric field vector maps out a circle during each period. If the amplitudes are different, the electromagnetic wave is elliptically polarized.

Even though the optical properties of liquid crystal are restricted to electromagnetic waves in the visible spectrum, much of what is described in the following section is also true for lower and higher wavelengths than for light.

1.9.2 Light Propagation in Anisotropic Matter

An electromagnetic wave that enters a material is affected in many important ways. The wavelength and velocity decrease by a factor n that is the index of refraction of the material. By this relation the velocity, v, and wavelength, λ, of the light in the material can be given as

$$v = \frac{c}{n} \tag{1.36}$$

$$\lambda = \frac{\lambda_0}{n} \tag{1.37}$$

where c is the velocity and λ_0 the wavelength of light in a vacuum. In general when light travels from one material to another, some of the light is reflected at the boundary while some is refracted through the other material with a change of direction. In most materials the index of refraction increases with increasing frequency, something that give various colours when white light is separated in a prism. In non-magnetic materials, which cover just about all organic and mineral liquid crystals, the index of refraction is equal to the square root of the relative permittivity or dielectric constant. Isotropic materials have a single index of refraction, because light polarized in any direction propagates at the same velocity in the material.

In anisotropic materials the relative permittivity is different for electric fields in different directions, which gives a different index of refraction for light polarized in different directions. This optical phenomenon is called birefringence or double refraction and is a property of all anisotropic materials, whether they are uniaxial or biaxial. The index of refraction for the light that is polarized in the direction which is different from the other two directions in uniaxial systems[26], is called the extraordinary index, n_e. The index of refraction for light polarized perpendicular to this direction is the ordinary index, n_o. In uniaxial nematic liquid crystalline order, the extraordinary index corresponds to light polarized parallel to the director and the ordinary to the light polarized perpendicular to the director. By labelling these indices $n_\parallel$ and $n_\perp$, the difference between them

$$\Delta n = n_\parallel - n_\perp \tag{1.38}$$

is called the optical anisotropy, or birefringence. It can be shown that Δn is proportional to the nematic order parameter [120]. For biaxial systems the optical anisotropy is usually defined as the difference between the largest and smallest indices. If the optical anisotropy is positive, $n_\parallel > n_\perp$, the liquid crystal phase is said to be positive uniaxial. For the opposite case, the mesophase is negative uniaxial.

[26] Nematic liquid crystals are normally uniaxial along with crystals of hexagonal, tetragonal and trigonal symmetry.

1.9.3 Optical Phase Retardation

A special property of birefringent materials, which is very important in liquid crystals, is an effect known as optical retardation. Consider polarized light, which contains components along both the x-axis and the y-axis, enters perpendicular to the surface of a birefringent material. In this case neither polarization is bent, so both polarized components propagate along the same direction in the material, but at different velocities. One of the polarizations therefore gets ahead of the other, causing the phase difference between the two polarizations to change as the light propagates through the material. If the two polarizations started out in phase, they will emerge with a phase difference that depends on the thickness of the material. For liquid crystals with a thickness d that have their director at an angle of 45° to the polarized light, will from Equations (1.33) and (1.34) have the following components propagating in the material

$$E_x(z,t) = E_0 \cos(n_\perp k_0 z - \omega t) \tag{1.39}$$

$$E_y(z,t) = E_0 \cos(n_\parallel k_0 z - \omega t) \tag{1.40}$$

In substituting z by the sample thickness d of the liquid crystal, the polarization state of the light as it emerges from the sample is given by

$$E_x(z,t) = E_0 \cos(n_\perp k_0 d - \omega t) \tag{1.41}$$

$$E_y(z,t) = E_0 \cos(n_\parallel k_0 d - \omega t) \tag{1.42}$$

If the director points along the y director, the equations can by using Equation (1.38) be written with a phase element

$$E_x(z,t) = E_0 \cos(n_\perp k_0 d - \omega t) \tag{1.43}$$

$$E_y(z,t) = E_0 \cos(n_\perp k_0 d\omega t + \Delta n k_0 d) \tag{1.44}$$

Thus the two components emerge out of phase by an angle $\delta_R = \Delta n k_0 d$. Since the argument of the cosine function grows more negative as time increases, δ_R represents the amount the x-component of the electric field is "retarded" over the y-component. Related to the two refractive indices of a uniaxial birefringnet material, the different electrical environment will affect the velocity at which the ordinary and extraordinary rays pass through the birefringent material. Because of the difference in refractive indices, one ray will pass through the crystal at a slower rate than the other ray. In other words, the velocity of the slower ray will be retarded with respect to the faster ray[27].

In general the emerging light is elliptically polarized with semi-major and semi-minor axes inclined at 45° to the x-axis and with a retardation between the components equal to

$$\delta_R = -k_0(n_\parallel - n_\perp)d = \frac{2\pi}{\lambda_0}(n_\perp - n_\parallel)d \tag{1.45}$$

[27]For positive uniaxial liquid crystals, the ordinary ray is the "fast" ray and the birefringence is positive. If the ordinary ray is "slower" than the extraordinary ray (negative uniaxial), the birefringence becomes negative.

As seen from this expression, the thickness d can give various possibilities for the polarization state of the emerging light. If d is such that δ_R = -$\pi/2$, then the linearly polarized light that entered the liquid crystal will emerge as left circularly polarized light. Such an optical component is called a quarter wave plate, since it retards one component by 90° relative to the other. If the liquid crystal is rotated by 90° about the z-axis, the indices of refraction in the x and y directions are switched and the light emerges right circularly polarized. If the thickness of the liquid crystal is such that $\delta_R = -\pi$, then the two components are out of phase by 180° when they emerge, producing light with a polarization direction perpendicular to the incident polarization direction. This optical component is called a half wave plate. Rotating the liquid crystal by 90° about the z-axis again switches the two indices of refraction, but the emerging light is again linearly polarized perpendicular to the incident light. Measuring the optical retardation of a liquid crystal with known thickness is a convenient method to measure the birefringence of the sample.

1.9.4 Birefringence in Nematic Phase between Crossed Polarizers

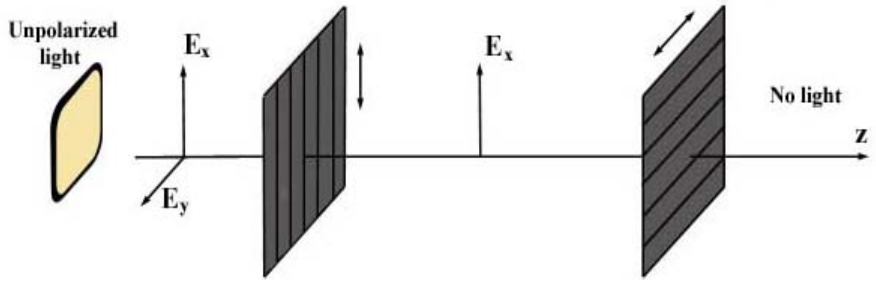

Figure 1.13: A setup of cross-polarizers, where the first polarizer produces light polarized along the x-direction. The second polarizer, the analyzers, only lets pass light polarized along the y-direction. Unpolarized light is therefore extinguished by the two polarizers. A corresponding Figure with an anisotropic sample placed between the polarizers is shown in Appendix F.

As stated above, the anisotropy of nematic phases causes light polarized along the director to propagate at a different velocity than light polarized perpendicular to the director. The birefringence in a sample with nematic order can be seen by placing the sample between two perpendicular oriented linearly polarizers[28]. Figure 1.13 shows such a setup of crossed polarizers where the first polarizer produces linearly polarized light along the vertical axis when it is illuminated by unpolarized light. The second polarizer, which is usually referred to as the analyzer, allows only light polarized along the horizontal axis to pass. Normally no light will emerges from crossed polarizers, since the

[28] A polarizer is a fabricated material that absorb one polarization nearly completely while allowing most of the other polarization to pass through.

light emerging from the first polarizer is completely absorbed by the analyzer. Insertion of an isotropic material does not change this because the polarization of the light is unchanged as it propagates through an isotropic material. The field of view will therefore generally appear black for an isotropic phase that is viewed between crossed polarizers.

For a nematic phase that has its director oriented at an angle to both polarizers, the light will consists of both a component parallel and perpendicular to the director. As described previously, these two components will travel with their own index of refraction. The polarizations get out of phase and will in general emerge as elliptically polarized light. Since some of this light will pass through the analyzer, the introduction of a liquid crystal between crossed polarizers will normally cause the field of view to appear bright.

There are two conditions a liquid crystal will continue to appear dark when viewed between crossed polarizers. If the director in some part of the liquid crystal is parallel to either polarizer, the incident light propagates according to a single index of refraction and suffers no change in polarization. This light is therefore extinguished by the analyzer and the liquid crystal appears dark. The other case the liquid crystal will appear black, is when the incident light propagates along the director itself, as in homeotropic alignment. Since the index of refraction for light polarized in all directions perpendicular to the director is the same, there is no optical retardation and the liquid crystal will appear dark.

1.9.5 Interference Colours

When white light is illuminated to an anisotropic sample between cross polarizers, the retardation of the ordinary and extraordinary waves makes the two waves interfere as they pass through the analyzer. This interference, which can either be constructive or destructive, gives unequal transmission by the analyzer of the various components of the white light. This may for some birefringent samples result in various colours when the samples are viewed between cross polarizers. These observed colours are known as interference colours, and are dependent on the retardation in the birefringent material for each of the wavelengths.

To the understanding of the colour appearance, it may be useful to consider the light transmittance of a uniaxial anisotropic material between cross polarizers. This is basically described as

$$I = \frac{I_0}{2} \sin^2(2\vartheta) \sin^2\left(\frac{\pi \Delta n(\lambda) d}{\lambda}\right) \tag{1.46}$$

where ϑ is the angle between the optical axis of the birefringent material and the cross polarizers, d the sample thickness and $\Delta(\lambda)$ is the materials effective birefringence which is dependent of the wavelength λ (Equation (1.37)). The product $\Delta n(\lambda)d$ is the relative retardation. The relative transmission of light through the cross polarizers becomes maximum when the orientation of the optical axis is 45°. With $\vartheta = 45°$, Equation (1.46) gives the relative transmitted

intensity as

$$T(\lambda) = \sin^2\left(\frac{\pi\Delta n(\lambda)d}{\lambda}\right) \tag{1.47}$$

This equation shows that for a given retardation, the analyzer transmits a curve of different wavelengths. If the retardation is zero, which for instance is the case for isotropic media and in the direction of an anisotropic materials optical axis, the transmittance is zero and the region will appear black. As the retardation increases from zero, the relative transmission varies with wavelengths. For retardations right over zero, the transmission curve does not have any extrema, but decreases in the visible spectrum of wavelengths. An anisotropic sample of retardation 200 nm will generate a interference colour of first-order bluish-white. This results from transmission of all wavelengths, but less of the colours at the end of the visible spectrum. This means less orange and red colours are transmitted, but more of violet, blue and green.

Table 1.2: The range of retardation that gives colour orders with different properties.

Retardation (nm)	Order	Colours	Notes
0	Zero	Black	
0-550	First	Gray, white, yellow, red	Neutral colours are cold, yellows dull
550-1100	Second	Violet through spectrum to red	Purest colours, though not totally pure
1100-1650	Third	Violet through spectrum to red	Have a "fluorescent" appearance
1650 and up	Fourth and higher	Mostly greens and pinks	Colours become more washed out with increasing retardation

At higher retardations, the transmission curve is minimum or maximum at specific wavelengths. A retardation of 550 nm will have a minimum when the wavelength is 550 nm, which corresponds to green. The analyzer therefore absorbs green, but transmits red and violet. The interference colour will therefore appear as magenta. Each multiple of 550 nm will result in a magenta hue, and the sequence of colours from one magenta to the next is termed an order. For very large retardations, several wavelengths are blocked, while others are transmitted. As more and more windows in the spectrum appear, the colours

become progressively more pale. Finally they approach white, but a warmer off-white rather than the cold neutral white of low retardation [150]. Table 1.2 shows the description of the interference colours for the order of retardation range.

1.9.6 Defects in the Nematic Phase

In a normal unaligned nematic phase the director usually points in different directions at different points within the sample. Since the places where the director orients parallel, perpendicular or along the normal of the polarizer appear dark and all other directions appear bright when viewed between crossed polarizers, a nematic phase often consists of both bright and dark areas. In many nematic textures the brightness often changes abruptly, which indicate that the director also changes abruptly at those places. It is impossible to define the direction of the director at the point of an abrupt change, so such a point represents a defect in the liquid crystalline order. Theoretically, these defects could be points, lines or sheets where the director discontinuously changes in passing through one of the defects. Point defects tend to occur in restricted geometries and at surfaces[29].

Sheet defects tend to spread out such that the change in orientational order is continuous over a slab containing the sheet rather than discontinuous at a set of two-dimensional points defining a sheet. Such structures are called walls. Line defects are the most common in liquid crystals and have been given the special name disclinations[30]. Viewed between crossed polarizers, a nematic phase with disclinations are often visible as a characteristic pattern with dark threads converging at right angles. These dark branches are usually named brushes and the pattern is referred to as a Schlieren texture. Many different disclinations are possible, and can be specified of a description of the change in the director direction around the point where the director field is not defined. A mathematical description of this is done by defining a polar angle, ϕ, and the director direction, Ψ, in the director configuration in the plane perpendicular to the direction of the line:

$$\Psi = m\phi + \phi_0 = \pi/2 \tag{1.48}$$

The parameter m is referred to as the strength of the disclination and equals a multiple of $\pm 1/2$. For negative strengths, the director rotates clockwise in traversing along the same counter-clockwise path of ϕ. For positive strengths it rotates counter-clockwise. The strength is a measure of how much the director is rotated when ϕ is increased by 2ϕ. If the strength is $\pm 1/2$, the director rotates 180° for one full loop around the disclination point. For a disclination of strength ± 1, the director rotates 360° for a similar full loop.

[29] Point defects sometimes occur in spherical droplets of liquid crystals, around droplets of isotropic liquid in a liquid crystal, and in thin capillary tubes [151].

[30] The name disclination stems from the fact that the line represents a "discontinuity" in the "inclination" of the director.

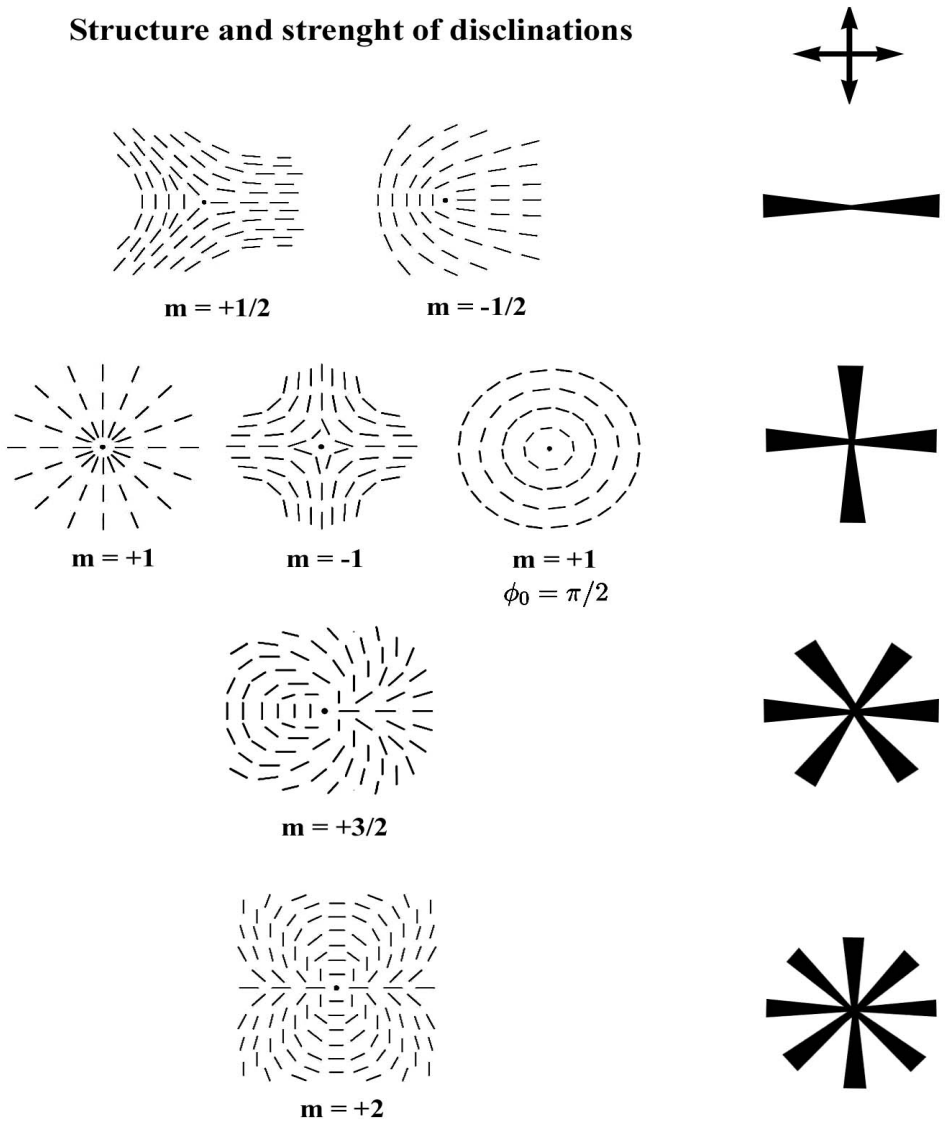

Figure 1.14: The structure and strengths of seven disclinations as described by Equation (1.48). The appearance of the structures when viewed between crossed-polarizers is shown to the right. Except the last four-brush Schlieren structure, all cases have intitial director direction $\phi_0 = 0$.

Figure 1.14 shows the director structure of different disclinations with various strengths and constant ϕ_0. The corresponding appearance of Schlieren brushes when the nematic distortion is viewed between crossed polarizers are illustrated to the right. These brushes appear black, since the director in these places is either parallel or perpendicular to one of the crossed polarizer axes. The rest of the liquid crystal is bright. Thus there will be two dark band emanating from opposite sites of disclinations of strength $\pm 1/2$, and four dark bands emanating from disclinations of strength ± 1. The sign of the strength

can be determined by a simultaneous rotation of the two polarizers. If they are rotated counter-clockwise, the dark bands will rotate clockwise for disclinations of negative strengths and counter-clockwise for disclinations of positive strengths. By combining the number of brushes with rotation of the crossed polarizers, the type of disclination can easily be identified.

Defects in chiral nematic and smectic liquid crystals differ from those in nematics due to either the twisted or the layered structure. Since the director twist in chiral nematic phases, an entirely new class of disclinations form in these phases. In a twist disclination, the rotation axis is perpendicular to the disclination.

1.10 Isotropic-Nematic Phase Transition, Onsager Theory

For ordinary liquid crystals there are several theoretical explanations for the formation of liquid-crystalline order among its elongated shaped molecules. To the description of an isotropic-nematic phase transition there is the established Maier-Saupe theory, a mean-field description which never considers the effect of harsh repulsive forces on the liquid structure explicitly [59]. In the Maier-Saupe theory the onset of nematic ordering is attributed to the effect of relatively long-ranged anisotropic intermolecular interactions (e.g. the anisotropic dispersion forces which decay as r^{-6}). When it comes to the description of the nematic phase formation by anisotropic colloids, a theoretical explanation was first proposed by Lars Onsager in 1949 [42] inspired by the experiments of Langmuir in 1938 on clay particles.

As opposed to the Maier-Saupe theory, the Onsager theory starts out from the assumption that the effect of the anisotropic repulsive forces on the liquid structure is of crucial importance for the transition to the nematic phase. Onsager claimed that the spontaneous isotropic-nematic phase transition were primarily driven by the shape anisotropy of the particles. He based his explanation on purely entropic grounds by considering the competition between packing (excluded or free volume[31]) entropy and orientational entropy of the colloidal system. Whilst the packing entropy favours nematic ordering among the particles, the orientational entropy favours isotropic ordering. As the packing entropy becomes more important at higher volume fractions, the particles tend to order in parallel alignment and a first order phase transition from isotropic to nematic is expected to occur when the particle concentration is sufficiently high enough.

In a dilute system of hard rods or disks, it should be clear that the particles will experience a loss in entropy when the concentration is increased since they are no longer completely free to rotate. But for particles that become oriented

[31] The excluded volume is the volume which is denied to particle "A" by the condition that it must not intersect particle "B". For a pair of spheres of radius r, the excluded volume is a sphere of radius 2r, i.e. the volume that is not allowed for the centre of sphere A when sphere B is fixed at the origin.

in a common direction, they will be more efficiently packed than particles of random orientation. Thus the ordered particles will form a dense phase. The remaining particles will then have a greater freedom, and hence the disordered phase will gain in entropy. At some point the gain of entropy in the disordered phase will outweigh the loss of entropy in the ordered phase, and the system will spontaneously separate into two phases. Onsager explained this behaviour quantitatively for a system of thin hard rods, but his theory is restricted to a qualitatively description for concentrated suspensions of plate-like particles. He showed that particle shape alone is enough to induce isotropic-nematic phase transition, and hard rods or plates without any interaction and independent of temperature may thus form a nematic phase. Onsager formulated the statistical mechanics of the system within the second virial approximation[32], shown to be valid for highly anisotropic particles with large aspect ratios. In the discussion he made the assumption that the only forces of importance correspond to steric repulsion; that the particles cannot interpenetrate each other.

For the approach to systems with a number concentration c of hard rods with a length L being much larger than the diameter D the volume fraction $\Phi = c\frac{1}{4}\pi LD^2$ is assumed to be much smaller than unity. That the aspect ratio of the particles is required to be high for this condition, comes into view since the interesting values of Φ near the isotropic-nematic phase transition in practice turn out to be such that $\Phi L/D \sim 4$.

To deal with anisotropic particles, an angular distribution of the particles is specified by the number of particles per unit volume with directors oriented in a small solid angle $\mathrm{d}\Omega$ around a unit vector $\mathbf{a}$. By the probability distribution function $f(\mathbf{a})$ this can be expressed as

$$\Delta N_p/V = cf(\mathbf{a})d\Omega \tag{1.50}$$

The sum of all these solid angles gives the total concentration c, with the distribution function satisfies the normalization condition

$$\int f(\mathbf{a})d\Omega = 1 \tag{1.51}$$

In the isotropic phase all orientations are equally probable which gives $\mathrm{f}_{iso}(\mathbf{a}) = 1/4\pi$. Phase transitions in a fluid of hard rods or hard disks is appropriatly

[32]The virial expansion, introduced by Kamerlingh Onnes in 1901, is an empirical systematic correction to the pressure P of an ideal gas at higher number densities

$$P/kT = c + B_2c^2 + B_3c^3 + \cdots \tag{1.49}$$

B_2 is the second virial coefficient and contains interactions between two particles. The third virial coefficient B_3 involves all clusters with simultaneous interactions between three particles. Neglection of all coefficients higher than B_2 may be satisfactory to low density dispersions where three-and-higher particle overlap is much less probable than two-particle collision. For very thin rods ($L/D \to \infty$) Onsagers theory within the second virial approximation becomes exact, because in that limit all higher virial coefficients of the hard rod fluid vanishes.

described by using the distribution function in a virial expansion of the free energy of the solute ΔF[33]

$$\begin{aligned}\frac{\Delta F}{NkT} &= \frac{\mu_0(T)}{kT} - 1 + \log c \\ &+ \int f(\mathbf{a}) \log(4\pi f(\mathbf{a})) d\Omega \\ &- \frac{c}{2} \int\int \beta_1(\mathbf{a}, \mathbf{a}') f(\mathbf{a}) f(\mathbf{a}') d\Omega d\Omega' \\ &- \frac{c^2}{3} \int\int\int \beta_2(\Omega, \Omega', \Omega'') f(\mathbf{a}) f(\mathbf{a}') f(\mathbf{a}'') d\Omega d\Omega' d\Omega'' \\ &+ \cdots \end{aligned} \tag{1.52}$$

μ_o is the chemical potential of the colloidal particles and represents their kinetic energy. The integral terms, that are due to the finite size of the anisotropic particles, are corrections to the first terms, which represents the free energy of an ideal gas. The first integral gives the orientational and translational entropy, which is minimized by random orientation. The other integrals are the entropy of packing related to the excluded volume of the system and is minimized by perfect ordering [152]. $\beta_1(\mathbf{a}, \mathbf{a}")$ is the excluded volume of two particles, which respectively are oriented in direction **a** and **a'**. Similarly, $\beta_2(\mathbf{a}, \mathbf{a'}, \mathbf{a}")$ represents the probability that three particles of orientation **a**, **a'** and **a"** will overlap simultaneously. Onsager calculated the excluded volume for two cylindrical particles of diameter D and thickness (length) L to be

$$-\beta_1(\gamma) = \frac{\pi}{2} D^3 \sin\gamma + \frac{\pi}{2} L D^2 + \frac{\pi}{2} L D^2 |\cos\gamma| + 2 L D^2 E(\sin\gamma) + 2 L^2 D \sin\gamma \tag{1.53}$$

with γ being the angle between the directors of the particles and $E(\sin\gamma)$ denotes the complete elliptic integral of the second kind. This expression for β_1 is general for all cylindrical particles, both rods ($L > D$) and disks ($D > L$). For the case of long thin rods ($L/D \to \infty$) only the last term of Equation (1.53) remains, and all higher virial coefficients become vanishingly small, reflecting the infinitesimal probability that three rods will simultaneously intersect. For infinitely thin disks, where $L \to 0$, the excluded volume is confined to the first term of Equation (1.53). However, for thin disks the chance that one disk has contact with two or more disks simultaneously is more significant, and the higher virial coefficients do not vanish[34]. The Onsager second virial approximated equation of state is therefore not an exact description for a fluid of hard disks.

Compared to Monte Carlo simulations [45], the Onsager approximation ($P/kT = c + B_2 c^2$) to hard-disks yields pressures that are consistently too

[33] ΔF is the difference between the free energy of the solution and solvent, where the solution contains colloidal particles in dialytic equilibrium across an osmometer membran with a solvent of constant composition.

[34] Eppenga and Frenkel [45] numerically obtained the virial coefficients 3-5 with $B_3/B_2^2 = 0.445$ and negative value for the fifth coefficient.

low in the isotropic region at higher densities. These deviations are still not very large due to the strong degree of cancellation of higher order virial terms. In fact an equation of state which includes both the exact B_2 and B_3 would do much worse than the Onsager theory. Still, the Onsager theory yields a very poor estimate of the isotropic-nematic phase transition and the theory, which was stated by Onsager, is only qualitatively correct for suspensions of disk-like particles. To investigate the role of orientational order, Onsager used a variational method by setting the distribution function to a trial function[35] of the form

$$f(\mathbf{a}) = f(\cos\theta) = (\alpha/4\pi \sinh\alpha)\cosh(\alpha\cos\theta) \tag{1.54}$$

which satisfies the constraint (1.51) and is equal $1/4\pi$ for the isotropic phase ($\alpha = 1$). θ is the angle between the director to a particle and a preferred orientation direction. α is a variational parameter used to minimize the free energy. For large values of $\alpha(\sim 20)$, the distribution is strongly peaked around $\theta = 0$ and $\theta = \pi$. The particles are then close to be parallel oriented and the system is nematic. On the other hand for low values of α the angular distribution is spread out and the system may be said to be isotropic. In the same way, the excluded volume of Equation (1.53) has a minimum for parallel orientation and a maximum when the particles are perpendicular oriented. The nematic order parameter, Equation (1.20), is in terms of α expressed as

$$S_2 = 1 + \frac{3}{\alpha^2} - \frac{3\coth\alpha}{\alpha} \tag{1.55}$$

By substituting the expression for the distribution function, Equation (1.54), into Equation (1.52), the free energy will depend on the number density and the Onsager α parameter. Minimizing the free energy with respect to α, one may use the value of α to calculate an order parameter using Equation (1.55). A function $F(\alpha)$ of the free energy is to show a first-order phase-transition from isotropic to nematic when the number concentration c is sufficiently high. From theoretical studies on monodisperse systems uncharged laponite disks, Rowan and Hansen have by using coefficients from the PRISM equation of state [153, 154] in the excluded term, found that an isotropic-nematic phase transition is predicted to occur at the density $\rho D^3 \approx 3.2$ [155].

The theory can also be applied to charged particles, in where it by later efforts [52, 156, 157] have been extended to incorporate electrostatic effects by the inclusion of the particles electric double layers. The particles aspect ratio will by this undergo a significant modification, and the dimensions are then described by an effective diameter and effective length[36]. The electrical double layer, which is roughly proportional to the Debye screening length λ_D, will contribute to the effective diameter D_{eff} by being added to the bare diameter. At very low salt concentrations D_{eff} can differ from the bare diameter by 2 orders of magnitude, and the second virial coefficient $B_2 = \pi L^2 D_{eff}/4$ is thus

[35] The choice of trial function is not absolute, and many different trial orientational functions give essentially the same result.

[36] This notion goes back to Onsager himself.

greatly increased, leading to a much reduced critical concentration of rods at the isotropic-nematic transition.

Chapter 2

Experimental

2.1 Na-Fluorohectorite Powder Preparations

The Na-fluorohectorite used for the experiments is ion exchanged through dialysis from synthetic fluorohectorite clay powder purchased from Corning Inc. in New York. Three dialysis were carried out at different times, and Na-fluorohectorite powders were produced finished in April, August and November 2006[1]. The behaviour of these three various Na-fluorohectorite powders have proved to be different when dissolved in water. In this thesis the three batches are referred to as April, August and November powder. All these three powder types are used in the experiments without any further treatment, but the April and August powders are also hand crushed by mortar (Haldenwanger) to obtain a very fine crushed powder. Extensive use of the milling machine was carried out on the August powder, where the total crushing time was around 100 seconds[2].

2.2 Sample Tubes

Most of the samples are initially prepared in 5 ml vials, where the Na-fluorohectorite is directly weighed and dissolved in the NaCl solution by hand or machine shaking. When the clay is visually dissolved in the vial, a preferred amount is poured into a specific sample tube for experimental study. Three kinds have been used depending on the intention of the experiment. Photograph of the sample tubes can be found in Appendix F.

[1] The April and August powders were made by postdoc Ahmed Gmira, while the November powder was prepared by Phd student Davi d. M. Fonseca. A detailed description of the procedure is given in Appendix F. All the powders were treated by a milling machine crusher (IKA A11 basic, Guangzhou, China) after it had dried up.

[2] To avoid overheating, the crushing was carried out in 10 seconds interval with some minutes break to cool down the machine and powder.

2.2.1 Vitrotubes

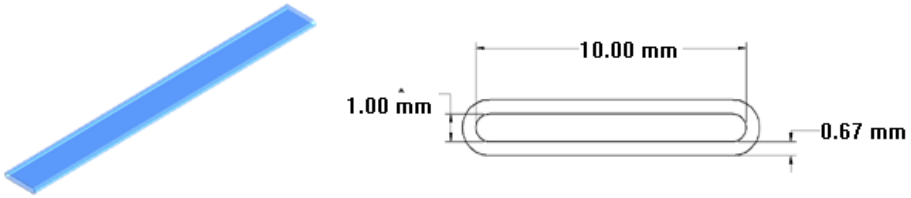

Figure 2.1: The Vitrotube with inner dimension of 1.00 x 10.00 mm and wall thickness of 0.67 mm.

The sample tube that is used for the main optical study is of type Vitrotube 4410-100 from VitroCom [158] (formerly known as VitroDynamics, USA). This Vitrotube has a length of 10 cm high, inner dimensions of 1x10 mm and wall thickness of 0.67 mm. Vitrotube 4410-100 is made of Borosilicate glass, which is the standard material for all the sample tubes for our experiments. The tubes have open ends that need to be sealed before and after they are filled with clay suspension. The glass tubes could not be usable retained by fusing, since this affects the polarizing abilities to the glass. Alternative retaining was done by using silicon rubber of type ELASTOSIL A33. This glue will by proper use manage to seal the tube, but should not be used since some of the silicone at the bottom seems to interact with the liquid sample. By some early samples, Capillary Wax (Hampton Research HR4-328) was used to seal the upper part of the tube. This method was hardly used since the wax could have a bad habit to "pop out" of the tubes[3]. Preferably, the sample tubes have been sealed at both ends by Parafilm (PM-992), a laboratory film from SPI Supplies and Structure Probe, Inc. This film does not seem to do any harm to the sample, but if it is not carefully put on the tube air bobbles may very easily penetrate from the bottom of the sample. Insufficient sealing will also expose the sample to evaporation.

2.2.2 Davi Cells

A flat sample container is made for the purpose of being suited for X-ray experiments. Two 0.2 mm thick borosilicate glass plates (microscopeslides) with dimensions 24×60 mm makes up the front walls of the cell. Those are glued on a 1 mm thick POM plastic (polyoxymethylene) plate[4] cut with a inner rectangular shape of 8×52 mm. When the tube has been filled with clay suspension the top is sealed with elastosil silicone glue.

[3]This might not necessary be any problem, and by proper use, wax is a very effective material to seal the sample tubes.

[4]Since any metal would corrode with the salt solution, POM is found to be of the better suited plastic material for this purpose. Drawing of the POM cell can be found in Appendix C.

2.2.3 Capillaries

With the purpose of doing X-ray scattering experiments, samples are prepared in capillaries of thin walls. Bought from Hilgenberg GmbH, Mark tubes with inner diameter of 1 mm (code-no.: 4007610) and 2 mm (code-no.: 4007620) are used. These Mark tubes are made of borosilicate glass with a wall thickness of 0.01 mm. The Mark tubes are sealed with capillary wax after injection of suspension.

2.3 Sample Stage Setup

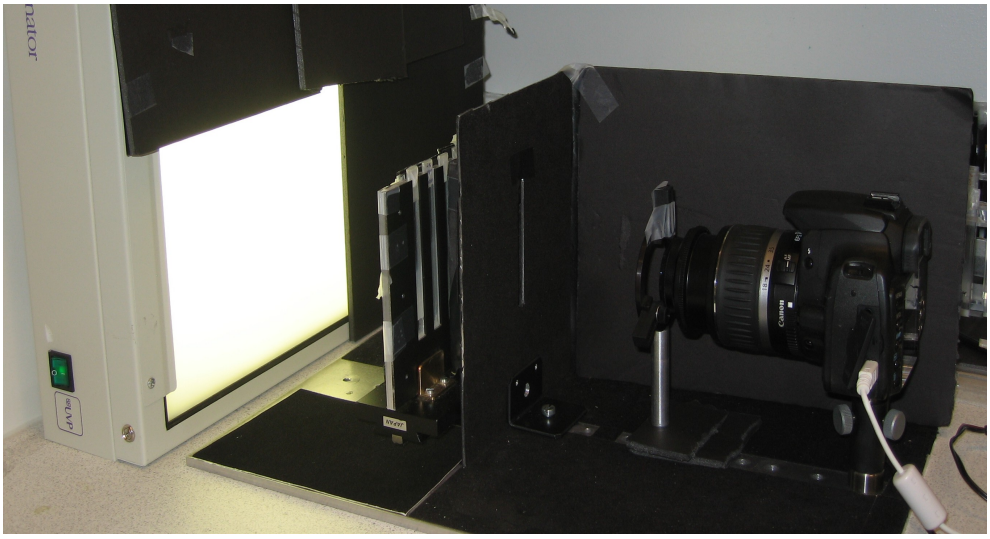

Figure 2.2: The cross polarized sample stage setup. A polarizer film is attached behind the sample rack and a glass polarizer is placed in front of the camera. During photography, black sheets of cardboard are placed as complete cover to prevent external light from disturbing the image.

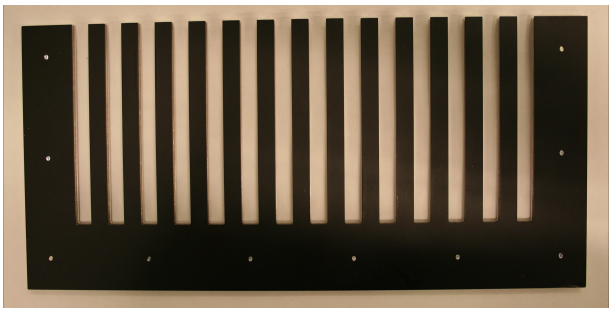

Figure 2.3: The rack can hold up to 14 samples. It is designed for the purpose to use Vitrotubes with parafilm attached around the ends.

Figure 2.2 shows the experimental cross polarized setup used for birefringent observations of the samples.

To make a stable system that could hold several samples for fast recording, a stage setup with a metal holder was worked out. A metric long travel linear translation stage and track from Edmund Optics makes up the foundation of the breadboard travelling. The track is made from extruded aluminium into a low-profile dovetail design to fit against the mating dovetail of the mounting stage. Helical movement on brass rack allows for precision and smooth travel along the entire length of track. Each track includes a scale that is aligned with the stage vernier. The coarse movement of the stage can be aligned within 0.1 mm. Combination of stage and track has total height of 40 mm; knobs do not exceed stage height. The total length of the stage is 250 mm and is put upside down for the experimental purpose.

On top of the stage, sample tube racks (Figure 2.3) are placed between to double pillars. The rack is designed with the Vitrotube 4410-100 in mind. It is composed of 3 parts, where a middle part is surrounded on both sides with two equal fronts. The first rack that was made has a slightly smaller slit width than the later version. The tube width were made larger because is should make a better fit for Vitrotubes sealed with parafilm. The racks can hold a number of 12 and 14 samples for the two versions respectively. The part of the rack heading towards the camera is painted black to reduce reflection. The three parts of the rack is fastened with even distributed screws across the the middle line of the outer parts. Additional racks are made for capillaries and Davi cells. Drawings of the racks can be found in Appendix C.

In addition to this birefringence observation setup, an optical microscope (Zeiss Stemi 2000C Stereomicroscope) with polarizer and analyzer is used to view small details in the samples.

2.3.1 Polarizers

For the sample stage setup, two types of polarizers from Edmund Optics are used. The polarizer that is behind the samples is a commercial-quality film polarizers with 22% transmission (Figure 2.4). The polarization efficiency[5] is over 99%. The film is coated with a peel-off protective layer for safe, easy handling.

[5]Polarization Efficiency is the percentage of how efficiently one polarizer polarizes incident light over the total amount of polarized light. With 99% efficiency the polarizer transmits 99% of the incident light in the intended polarization (p-polarization state) and 1% in the opposite polarization (s-polarization state). Polarization Efficiency = P.E. (%) = $[(H_0\text{-}H_{90})/(H_0\text{-}H_{90})]^{1/2} \times 100$, where H_0 is the average transmittance (unpolarized incident light) of parallel polarizers, and H_{90} is the average transmittance of crossed polarizers, over 400-700nm [159].

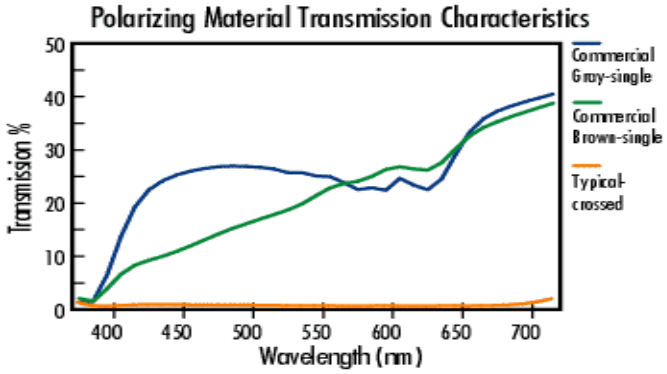

Figure 2.4: Polarizing material transmission characteristics for the film polarizer. Taken from EdmundOptics.

The polarizer (analyzer) used before the camera is a mounted linear glass standard 42 mm threaded polarizing filter. Mounted clear aperture is mount diameter less 5mm and mounted maximum outer diameter is mount diameter plus 2 mm. The thickness of the filter includes 2 mm male thread. The filter has a polarization efficiency of 95%, single transmission of 30% and 0.15% average transmission when crossed. The transmission characteristics for crossed glass polarizers are given in Figure 2.5.

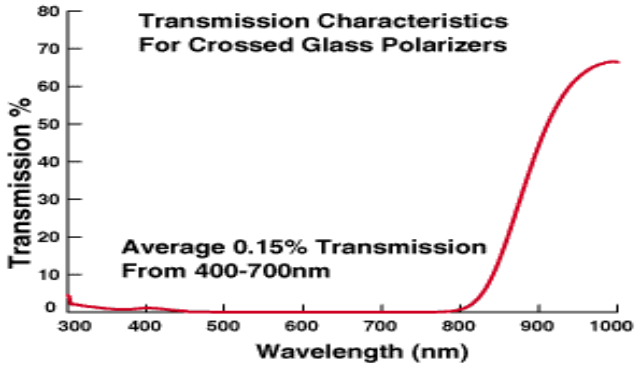

Figure 2.5: Polarizing material transmission characteristics for the linear glass filter polarizer. Taken from EdmundOptics.

2.3.2 Canon EOS 350D

The camera used for sample photography, is a Canon EOS 350D single-lens reflex camera. The camera is connected to a PC from where it is operated. By using timer mode, the camera can be set to automatically take pictures with intervals from 5 seconds to 90 minutes. The camera can be put into a lot of different modes, depending of the use. For pictures taken in the experiments,

the Tv[6] shutter-priority AE mode has been used. In this mode the shutter speed can be manually adjusted, and the camera will automatically set the aperture value to suit the brightness of the object. This is called shutter-priority AE.

Even though automatic focusing is possible, manual focus has shown to provide optimal focus. A lot of patience is needed to get the right focus, since just the smallest adjustments may give considerable differences in image quality. A trick to set the focus can be to compare zoomed in pictures taken after each other, and adjust the focus accordingly.

2.3.3 Light Source

The light source that is being used for illumination is a white light transilluminator (UVP, Inc. Upland, CA USA) model TW-43, fuse: 2 x T2 ampere. The illumination is highly uniform, which give very good results for all sample tubes[7]. Since the light can be very intense, parts of the light are blocked by cardboard.

2.4 Magnet

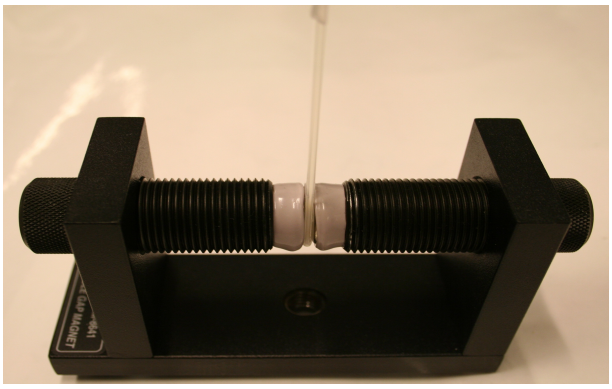

Figure 2.6: Variable Gap Lab Magnet from Pasco scientific. The magnetic field strength is at maximum 1 Tesla when the gaps are screwed this much together.

For studies of magnetic field effects of the Na-Fht suspensions, a variable gap lab magnet from Pasco scientific is used. The magnet consists of two 19 mm diameter neodymium magnets on an iron base, that are plastic-coated to prevent chipping. The magnets heavy-duty iron base is stable in four different freestanding positions and also mounts on standard 12.7 mm rods. The magnet will not have a great effect on its surroundings because the field drops off

[6] Tv stands for time value

[7] When it comes to capillaries, almost every ordinary light sources have difficulties to give satisfied illumination at the edges.

to about 30 Gauss at the outside edges of the magnet. The maximum magnetic field strength is from the manufacture given to be 0.75 Tesla, however, by "overscrewing" to a minimum gap of 2.2 mm, a magnetic field strength of nearly 1 Tesla can be achieved. With this gap, the inserted samples will, at least in the central part, experience a magnetic field of this strength.

2.5 Computer Softwares

When taking pictures, the Canon software ZoomBrowser EX is used for direct view of the pictures. Canon's PhotoStudio 5.5 is used for further treatment of the pictures. Videos made from the jpg pictures, have been created by the audio/video editing, converter program Blaze Media (Mystik Media). By this program it is possible to make videos of MPEG-1, MPEG-2, AVI, WMV, ASF, MOV formats. For further video editing, as putting on the time frame on the videos, Ulead MediaStudio Pro 8.0 is for instance used. To automatically cut and resize series of images, the amazing software ImageMagick® is used.

2.6 Synchrotron X-ray Scattering Methods

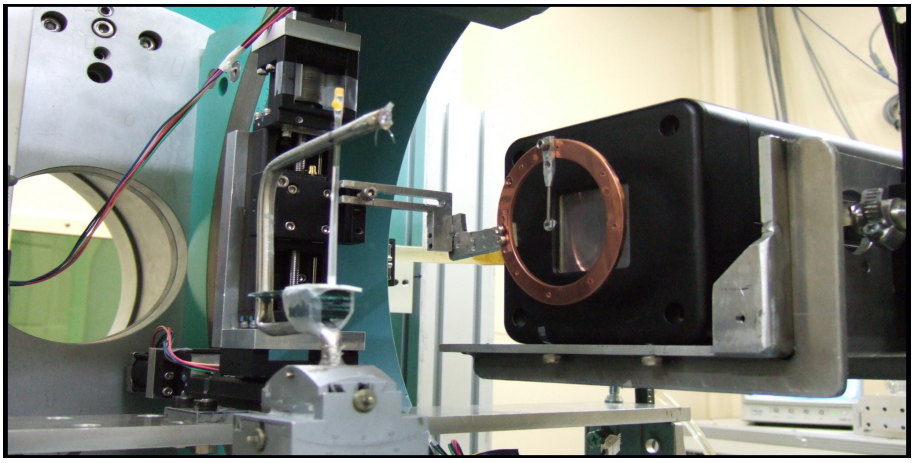

Figure 2.7: Experimental hutch. Photo showing the sample, beam stop and detector as them were positioned for the final measurements. For rotation of the sample, around 20° will be covered by the sample holder.

Synchrotron wide angle X-ray scattering were carried out on beamline KJIST-II at the Pohang Light Source (PLS), South-Korea. The incident X-rays had a wave energy of 10 keV, which corresponds to a wavelength of 1.24 Å. The beam size at the sample position was at final measurements sat to be 0.3 mm vertical and 2 mm horizontal. This way the beam could easier hit the desired position in the vertical capillary axis, since the different phases in some samples can be of very small size. The 2-dimensional WAXS Bragg patterns were acquired using

a beryllium CCD detector model 1300 from Princeton Instruments[8]. The pixel array size of the detector is 1300 × 1340 where the pixel size is 20 × 20 μm. This gives a CCD size of 26 × 26.8 mm and the sample-to-detector distance was 12 cm for the measurements[9]. The sample holder for the capillaries is made as a stand were the sample is hanged from the top. This makes the whole sample from the sediment to the top liquid-air interface uncovered for X-rays.

[8]Technical specification: CCD type: 100 kHz/1 Mhz or 50 kHz/1 Mhz, Spectral range(typical): 400-1100nm, cooling: air, liquid or LN, output amplifiers: low-noise (2250,000e^-) and high-capacity ($\geq$500,000e^-), camera dimensions: PI-LCX: 400/1300 LN head; 15.56 cm width, 22.86 cm length, 36.98 cm height and 4.2 kg weight, PI-LCX: 400/1300 NTE head: 11.8 cm width, 11.8 cm height, 22.15 length and 4.54 kg weight.

[9]Because of technical issues the detector was in the beginning placed a distance longer from the sample that could only cover 1/4 of the Bragg ring.

Chapter 3

Results and Discussion

This chapter presents results from how liquid crystalline order forms in suspensions of Na-fluorohectorite by various clay concentration and ionic strengths. Three different batches of Na-flurohectorite powders are used, where the effect of crushing before dissolving has been examined. Identification of nematic phases is done by optical and X-ray scattering methods. Extensive photography has recorded the slow gravity induced phase separation, where the composition of pictures to video has both revealed how the phase formation occur in addition to other dynamics of the system. Even though many samples seem to be similar when just looking at the pictures, the dynamics of the sedimentation or phase settling process could be completely different when the corresponding videos are studied. The influence of a magnetic field to particle orientation is found to have a great impact in specific parts of the nematic phase.

3.1 Samples

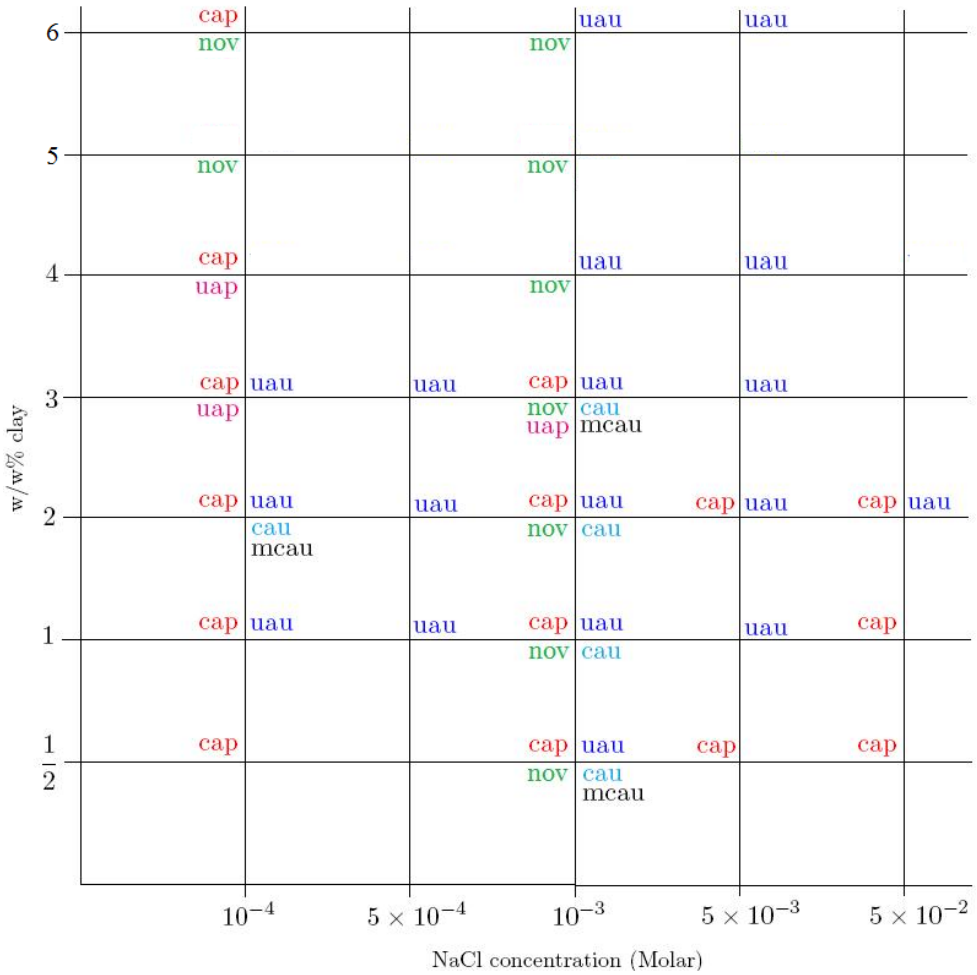

Figure 3.1: The various samples how they have been made by different weight % in salt solutions ranging from 10^{-4} to $5{\times}10^{-2}$ Molar. cap is crushed April powder, uau is uncrushed August powder, cau is crushed August powder, nov is November powder, uap is uncrushed April powder and mcau is August powder that has been extra crushed with a milling machine crusher.

Figure 3.1 shows the extent of samples prepared by varying the w/w% clay concentration from 1/2 % to 6 % in 5 different ionic strengths ranging from 10^{-4} to $5{\times}10^{-2}$ M. Most of the combinations in Figure 3.1 are represented by only one sample, something that may not give complete reliable results when it comes to some special data analysis and reproducibility. Impurities in both the sample holder and powder, shaking length for dissolving the suspension, evaporation, air bubbles and other irregularities in the sample tubes are factors that could have some impact on the individual sample. Some of the combinations are though equally prepared for more than one sample and some also for

different sample holders.

The best studied combination are samples with 3 w/w% clay dissolved in 10^{-3} M salt concentration. As much as 8 samples in the same kind of sample holder have been made for just the crushed April powder for this concentration. Two of them differ by the fact that the sample tubes are filled some months after the sample preparation itself. The sedimentation and dynamics are a great deal different than the others, where the behaviour is more or less similar.

Most of the samples have aged well when it comes to outer disturbances as evaporation, air bubble penetration and other external influences. Some samples have been halfway or completely damaged before they reached their final level where no further phase separation or dynamics are observed. Since pictures are taken on a weekly basis for all samples, the results from earlier time are presented for some of these samples. A lot of samples are prepared for the purpose of doing X-ray scattering experiments. Since most of these samples are prepared in highly breakable glass capillaries, many of these samples are made of the same kind. Comparison of those samples have given some uncertainty information concerning reproducibility.

3.2 Sedimentation and Phase Separation

Immediately after the sample tubes are filled with suspension, sedimentation starts due to gravity acting on the clay particles. This process can be very different for each sample, depending on powder type, crushing method, ionic strength, clay concentration and if the suspension has already phase separated in the preparation vial before injection to the final sample tube. All samples except those with very high salt or clay concentration get sediments at the bottom. The sedimentation rate is highest at the first minutes and hours after preparation. Flocs of clay that is large enough to be seen directly from the camera pictures, sediment to the bottom in a great number and form a white bottom layer even in crossed polarizers. The speed can differ much from each floc, but typically varies from 10-50 mm per minute.

Suspensions of uncrushed powder sediment more rapidly and form more sediment than suspensions of crushed powder. Uncrushed August sediments most rapidly followed by milling machine crushed August, November, uncrushed April, mortar crushed August and (mortar) crushed April. For uncrushed August the unsuspended particles settle and make up the main sediment in less than 10 hours. In the following time, a more transparent sediment layer forms above. This layer can be regarded to consist of smaller clay particles, and takes about twice the time to settle. These two layers have about an equal height, but have a different mass density.

From density measurements (Section 3.7) the bottom sediment is about twice as dense as the strata above. From X-ray scattering and birefringence experiments these layers are shown to be isotropic at large scale, but not necessary completely isotropic. When the main sedimentation process has reached the end, further settling is going on much slower. In the next weeks

a new phase that possess nematic liquid crystalline order forms atop of the isotropic phase. This phase may form as slowly settling occurs in rest of the suspension above the sediment. This part of the suspension can be considered to be isotropic, and a transition to a nematic phase takes place due to an increase in the density.

During or after the formation of the nematic phase, extensive dynamics could go on in the phase in form of small fluctuating nematic domains. After long enough time, this dynamic relaxes and the nematic phase can be considered to be of gel character. The part of the sample above these phases, has a much lower mass density and are completely isotropic. The gravitational force is still acting on the particles that are in this part, and in a time period of several months a new nematic phase slowly forms above the nematic gel. This phase is very easily affected by magnetic fields and any small shaking of the sample tube. It can therefore be characterized to be of sol structure. The phase is much more visually complex than the nematic gel phase by having a texture of separated domains. From a macroscopic point of view, these nematic domains can be considered to have positional order among one another.

The remaining part over the nematic sol, consists of a low dense isotropic distribution of clay particles. As is shown by Figure 3.2, suspensions of uncrushed August Na-flurorohectorite clay can with long enough time principally consist of 4 gravity-dispersed phases. Depending on the sample conditions, other phases within these main phases can also be separated.

Suspensions of milling machine crushed August and November powder show a similar sedimentation process and phase separation as suspensions of uncrushed August powder. Suspensions of April powder, by the other hand, show a bit different behaviour during sedimentation and phase separation. For uncrushed April this behaviour may not be unpredicted for a colloidal suspension in the gravitational field. For most of the time, particles or flocs of particles can be seen to first settle as heavy sediment for then to later show birefringence higher up in the sample. Suspensions of crushed April show a not too different behaviour during the first hours of sedimentation, but starts after some days to get birefringent fluctuations it apparently is difficult to explain by the gravitational force alone. An example on how these fluctuations occur for the first 50 days is shown in Figure 3.3.

By studying videos of these suspensions, it can be seen that the speed of the fluctuations vary in smaller time sequences, but is on average more or less constant. However, the dynamics in the suspensions slow down as time elapses and reaches an equilibrium state with birefringence covered nearly over the whole sample. At this time, a new nematic phase with sol structure may have been formed above the fluctuating part. Depending on the sample conditions, this phase can have stratum with different particle orientations. Unless the clay concentration is not too high, an isotropic phase with low particle density remains at the top when the settling process is at the end. In total, 5 phases can be induced by gravity in suspensions of the April powder.

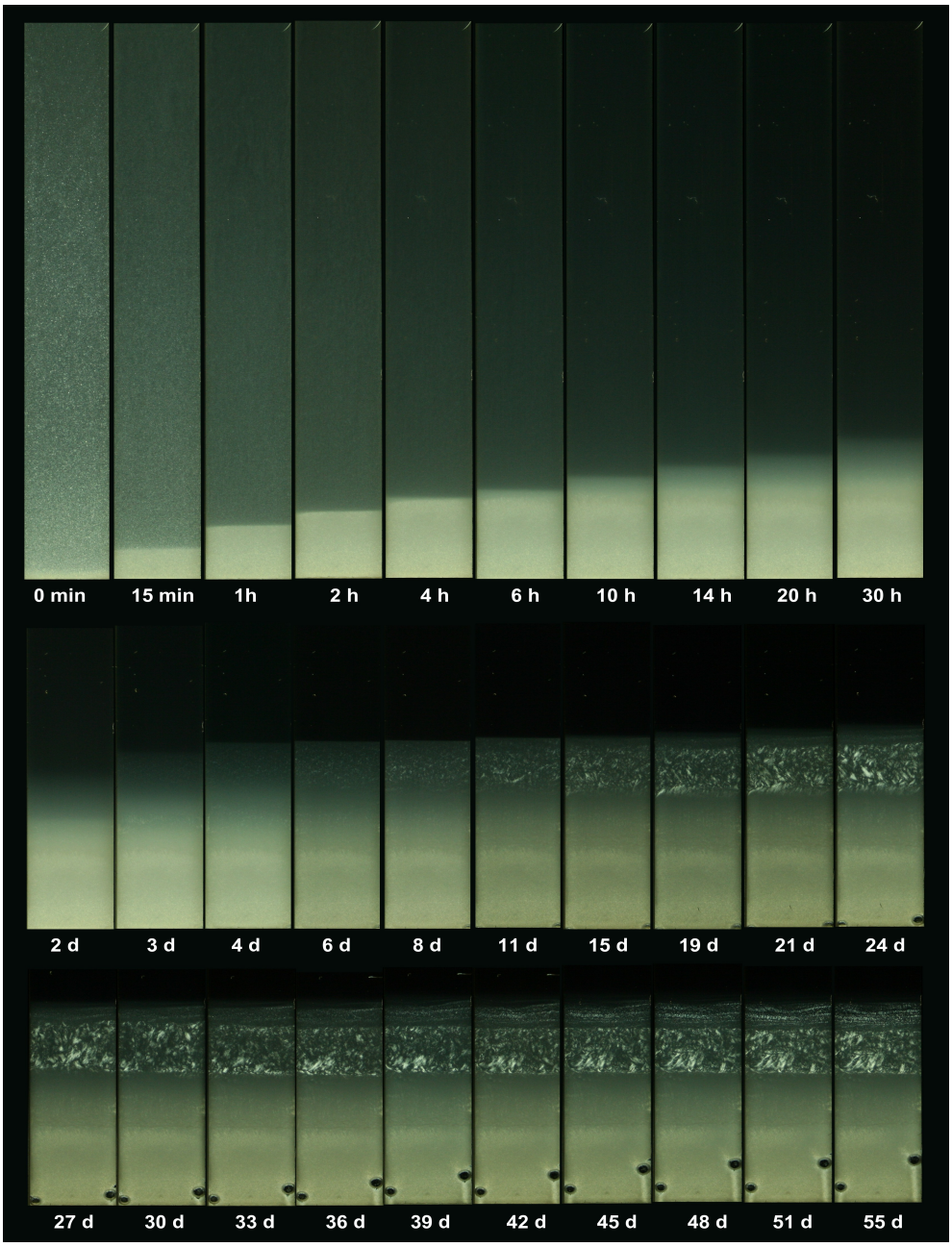

Figure 3.2: 55 days time progress of 2 w/w% uncrushed August at 10^{-3} M salt concentration. As can be seen from the first row, the uncrushed August sediments very rapidly the first hours after preparation. A second sedimentation layer, consisting of lighter particles and flocs, forms above the first sediment in a 2 days settling process. From the second to the fourth day a new layer has settled above the sediment. This layer can be considered to consist of homogeneous refined particles and be more or less isotropic in all directions. After 6 days some birefringence starts to appear in this isotropic phase. Over the next following days a transition to a nematic phase takes place by the formation of nematic domains. After around 21 days the amount of birefringence has reached a flagging level. Instead some very active dynamics find place in the nematic phase. As can be better seen from the video of this sample, the nematic domains are constantly changing direction. After 27 days a new nematic phase is forming over the first nematic phase.

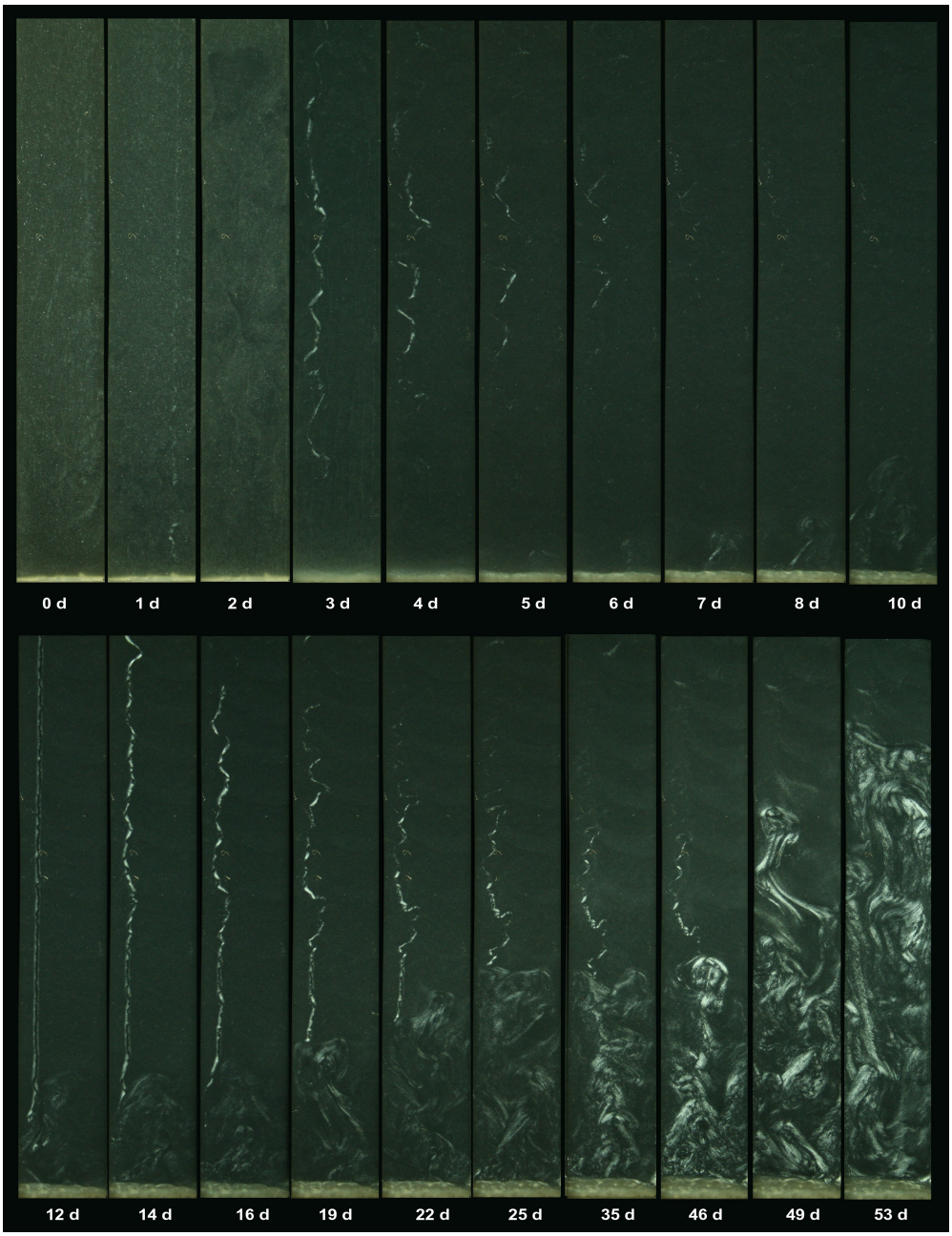

Figure 3.3: The 53 first days of a suspension of mortar crushed April in 10^{-3} M salt solution. The birefringent coil that appears in the left part of the samples is caused by air bubble buoyancy. After about 5 days, fluctuations set in right above the sediment and continue its way to the top. This coil appears on the right side already in the beginning, but in a very hazy way. A new coil appear after 3 days for then to disappear after 6-7 days. The strongest coil appears after some 12 days. This coil is in some way being slowly devoured by active dynamics.

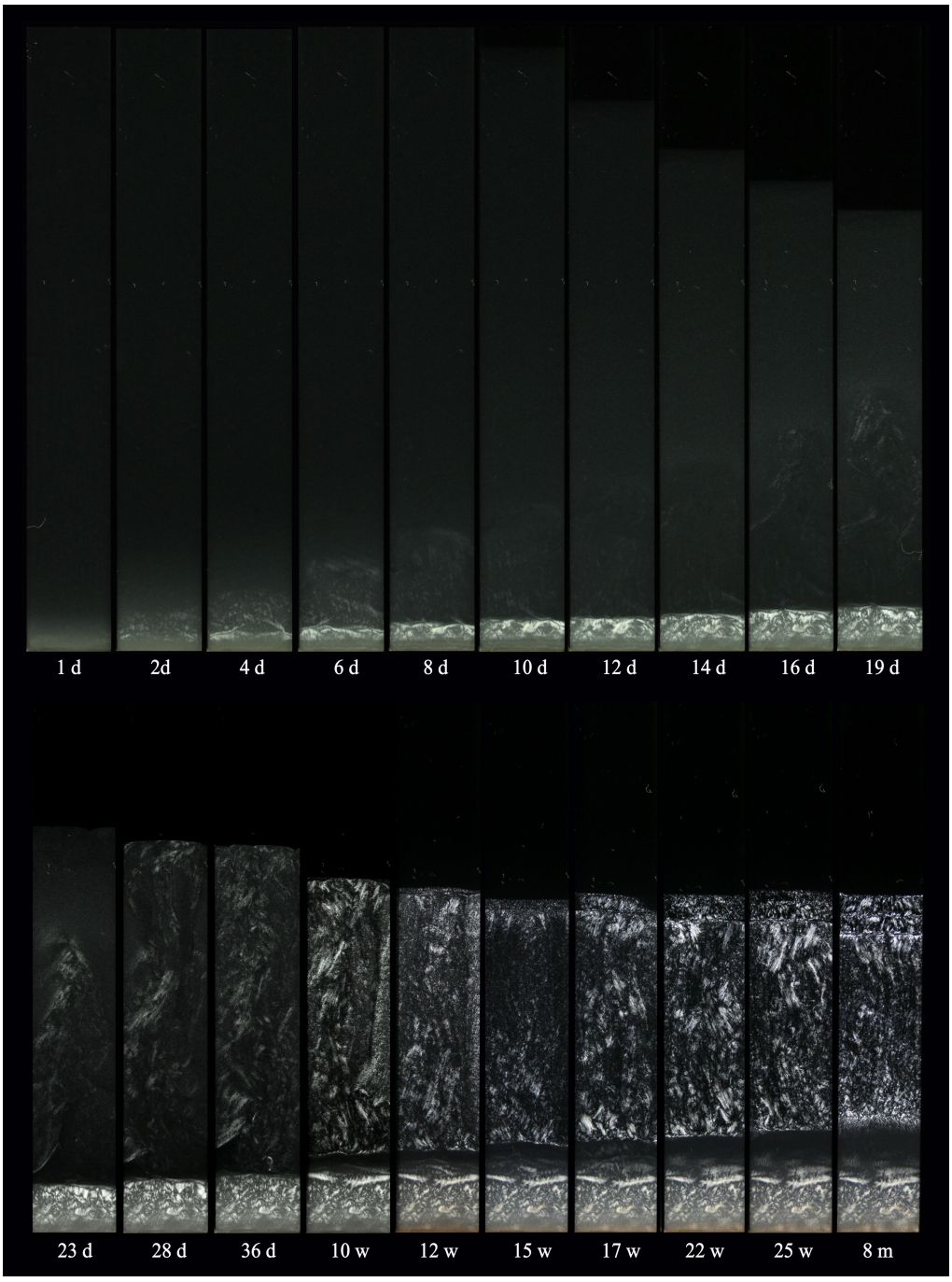

Figure 3.4: The time evolution for the 8 first months of a sample with 2 w/w% April at ionic strength 10^{-3} M.

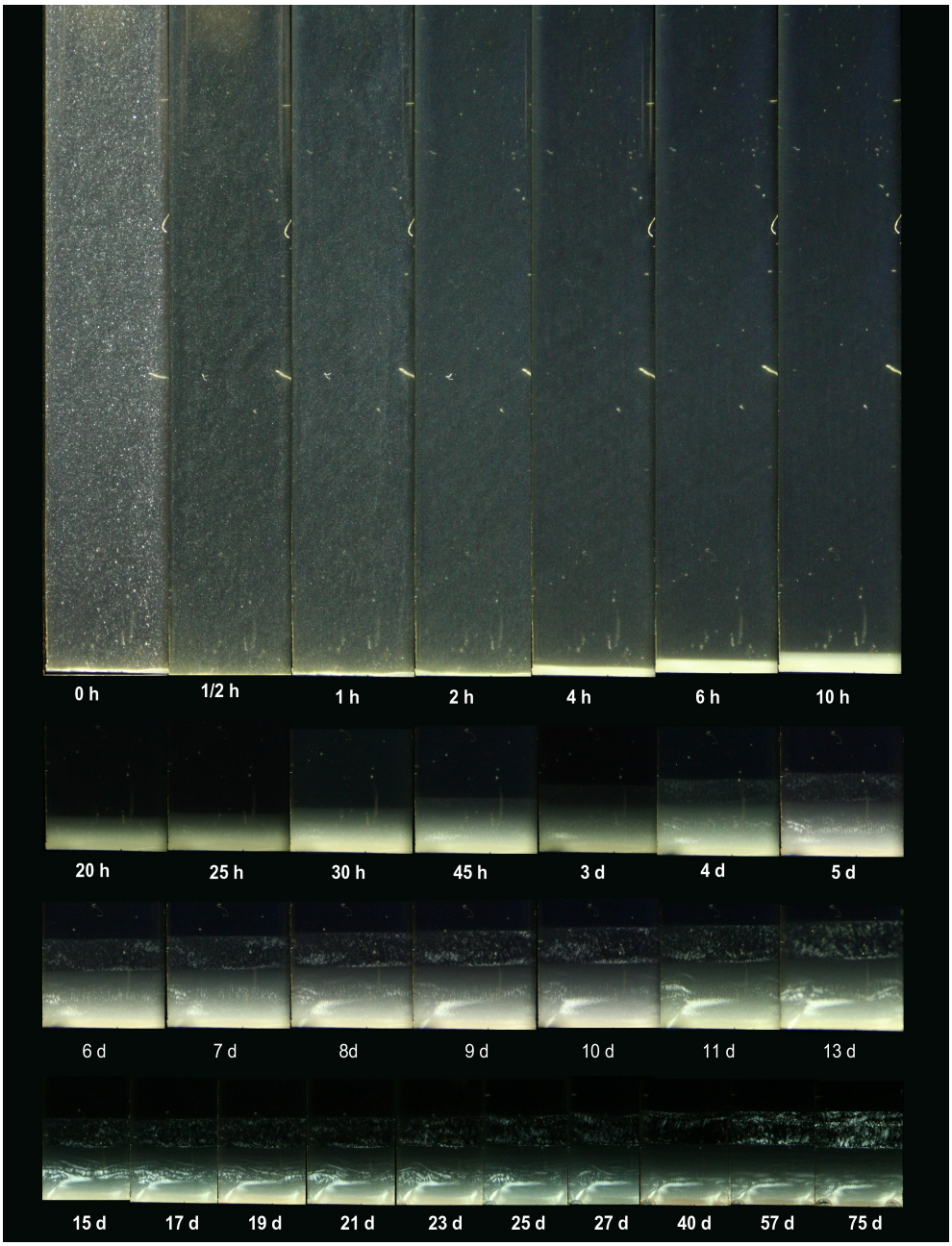

Figure 3.5: Time progress for 10^{-4} M concentrated April solution with 0.5 w/w% clay. The light sensitivity of the pictures in the first row have an ISO number of 1600. The rest of the pictures have ISO 800, which is used as standard for this sample. The use of this high ISO number might give a wrong impression for the lower phase since it appears much brighter than it should. The reason for the high light sensitivity is to better be able to spot the birefringence in the upper phase. Even after 75 days this upper phase is constantly fluctuating.

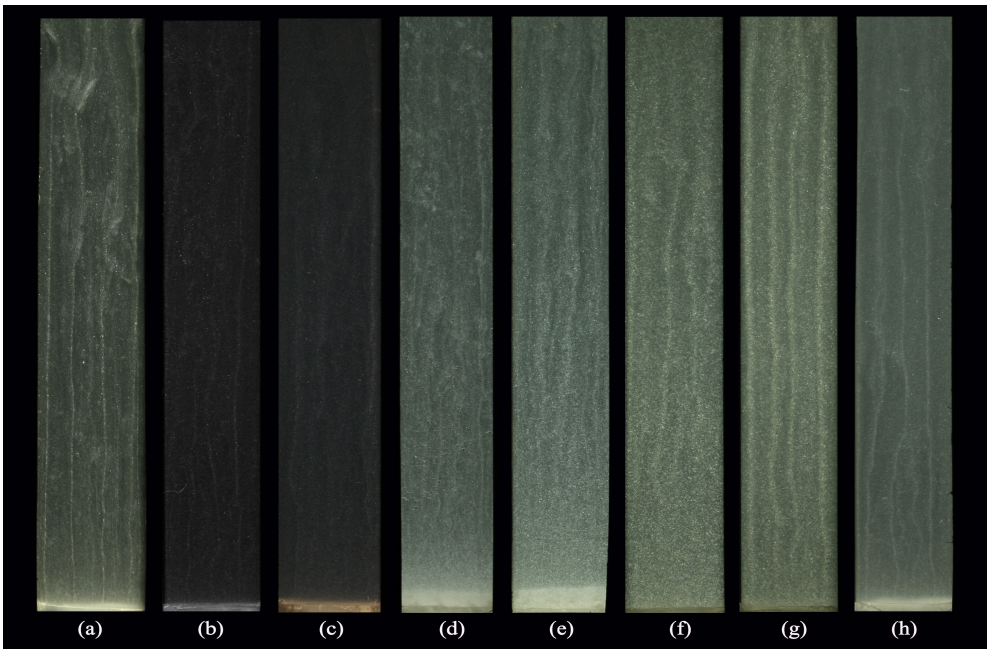

Figure 3.6: Photographes of some samples that show a streak pattern in their sedimentation infancy. The streaks can start to appear already after some very few minutes and last up to 2 days. The times for the pictures are when the streaks are most dominant. (a) 2 w/w% crushed April in 10^{-4} M salt solution four hours after injection. (b) 2 w/w% crushed April in 10^{-3} M salt solution 30 minutes after injection. (c) 2 w/w% crushed April in 5×10^{-3} M salt solution 30 minutes after injection. (d) 3 w/w% uncrushed April in 10^{-3} M salt solution 17.5 hours after injection. (e) 2 w/w% uncrushed August in 10^{-4} M salt solution 15 minutes after injection. (f) 3 w/w% uncrushed August in 5×10^{-4} M salt solution 6 minutes after injection. (g) 4 w/w% uncrushed August in 10^{-3} M salt solution 10 minutes after injection. (h) 3 w/w% crushed August in 10^{-3} M salt solution 20 minutes after injection.

When the August powder is crushed by mortar, the sedimentation and phase behaviour get some pronounced changes. Compared to suspensions of Uncrushed August, the sedimentation of mortar crushed August could be described to consist of a stream of smaller particles or flocs. In the cases of high clay concentration, an appearance of vertical white streaks can take place very short time after the beginning of the sedimentation. Filled in Vitrotubes, a number around four of these stream lines appear with a more or less equal distance between one another. Such streaks can also appear during sedimentation in suspensions of any of the other powder batches, but they become much more distinct and narrow when the powder is crushed.

Figure 3.6 shows a selection of the samples where the appearance of sedimentation lines is found to be most pronounced. Since the whole sedimentation process is not covered for every samples, it can be difficult to draw a conclusion about the conditions as regard the mass concentration or ionic strength that promote the streaks. For the lowest clay concentration, 0.5 w/w% and 1 w/w%, the streaks seem to be absent or have a very short diffuse appearance.

With a small amount of clay, each particle is surrounded with much more free space and do not as easily interact with other particles to form streaming lines. By observing suspensions of uncrushed August in 10^{-3} M salt solution, the samples with 0.5 w/w%, 1 w/w% and 2 w/w% clay do not show any descent sign of streaks, but the increase to 3 w/w% show some line shapes, and the 4 w/w% clearly have long lasting streaks.

When it comes to ionic strength, there can be an indication that low salt concentration better gives streaks. From the experiments that consider crushed April and uncrushed August, the samples with salt concentration of 10^{-4} M and 5×10^{-4} M for 2 w/w% and 3 w/w% clay show a much more pronounced streak pattern than those of higher ionic strength. Since the repulsion between the particles is higher for low ionic strength, it will as for high clay concentration give tighter circumstances in the sample tube during sedimentation. As a consequence of this, the suspension sediments slower and can therefore give better time for the streaks to form. A higher pressure during flow is resisted by the formation of narrow streaks. Since the lines appear white between crossed polarizers, it can be expected that there is an increase in orientational order between homogeneous sedimentation channels. This flow birefringence could be advantageous since oriented particles may perhaps better sediment through the suspension without being disturbed by slow flow. Since sedimentation processes are only studied for suspensions in Vitrotubes, it is unclear if the walls have any influence on the formation of the streaks.

By studying the sedimentation and phase separations of various samples, other striking behaviours can be observed. One special phenomenon that occurs in some few samples is the appearance of horizontal bands. Viewed between crossed polarizers, as much as 10 birefringent bands with equal distance between one another can be visible. Figure 3.7 shows an example for this in a suspension of crushed April. The bands start to appear after 4 days, a time when the gravitational force has already dispersed different strata within the sample. Most of the sedimentation process is finished, and an isotropic phase in a small layer is formed between two layers with birefringence. The first birefringent layer is of steady gel, while the birefringence in the second layer is slowly formed by fluctuations. The bands appear in the second layer before it is formed into a birefringent phase. They last until they get disrupted by the fluctuations or confined by sedimentation of the particles in the top. The bands of the sample in Figure 3.7 is visible distinct and have a constant distance of 5 mm between one another.

Another example of horizontal bands is shown in Figure 3.3, where they can be observed clearly from the top to the middle after 10 days. The bands show a common appearance by being curve shaped and having equal length. They make a small angle to the polarizer axes and get common changes as the time elapses. The fact that the bands are separated by equal distances, could indicate there are some kind of interaction between them. Since observations with the cross polarizers at different angles is not carried out, it is impossible to tell if there is some shift in orientational order between the bands. A proposed explanation is that these bands are backward-propagating waves [160], which

perhaps are caused by a conflict between particle settling and gelation due to the different height density.

Figure 3.7: The appearance of horizontal bands in a suspension of 2 w/w% mortar crushed April in 10^{-4} M salt solution. The picture to the left is taken 13 days after preparation, and the one to the right 3 days later. A total of 10 bands can be spotted with more or less equal distance between one another.

3.3 Phase Behaviour of Different w/w% Concentrations

The Na-fluorohectorite concentrations of the suspensions used for the experiments are of either 0.5, 1, 2, 3, 4, 5 or 6 weight% clay. Irrespective of powder type or ionic strength, the phase behaviour is very much similar for most of the different clay concentrations. The main difference is the height level and relative fraction of the separated phases in the sample tube. For the samples with the lowest clay concentration, the relative amount of birefringence is in general lower for the same induced phase than for those of higher concentration.

Figure 3.8 shows photographs of August 10^{-3} M samples aligned with increasing clay concentration. All the samples from 0.5 to 4 w/w% can be said to have phase separated in the same way. A total of 5 common strata are induced without regard to the clay concentration; sediment at the bottom, an isotropic gel phase, a nematic gel phase, a nematic sol phase and an isotropic liquid upper phase.

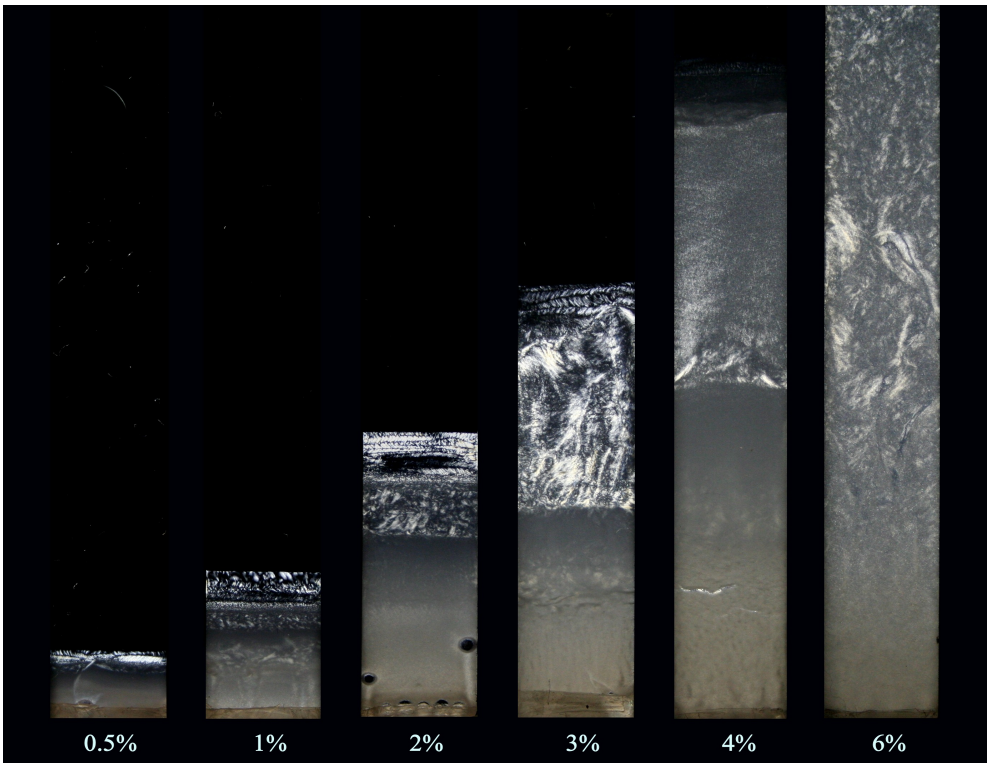

Figure 3.8: 0.5 - 6 w/w% August at ionic strength 10^{-3} M. The time after preparation for the photographs are 3 months for 0.5 %, 4 months for 3% and 6% and 8 months for 1%, 2% and 4%.

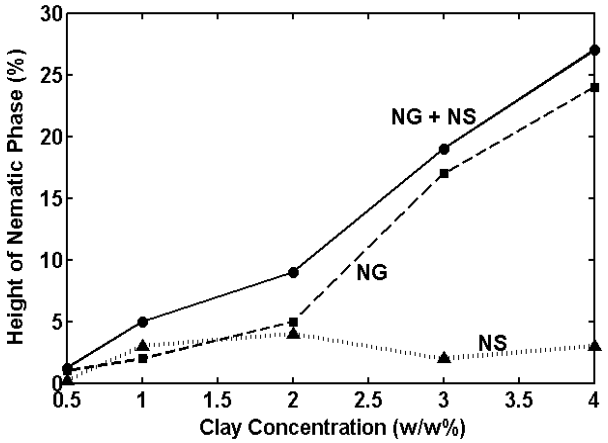

Figure 3.9: The height (volume) fraction of the nematic phase of the August powder at ionic strength 10^{-3} M as the clay concentration is increased from 0.5 to 4 w/w%. NG is the main nematic gel, while NS is the nematic sol formed atop of the nematic gel. Since the sample tube is filled to almost 10 cm, the fraction % is equal to the height of the nematic phase in centimetres.

The contribution of the sediment to the sample height increases as what could be expected when the clay concentration is increased. Above the sediment, a density profile is induced where the formation of an interface between the isotropic gel and nematic gel takes place. This behaviour is common for all of the samples in this concentration range, but there is a difference in the way the nematic gel is formed. For the samples with 0.5, 1 and 2 weight% clay, the nematic gel is formed by a homogeneous appearance of nematic domains. By continuous inspection of this formation, the nematic domains are seen to undergo fluctuations in a period of several weeks.

When the dynamics leave off, the final nematic gel consists of birefringent spots uniformly scattered over the phase. This nematic phase is formed in a slightly different manner for the suspension of 3 w/w% clay. Like in the case of the lower concentrations, birefringent spots appear in the middle gravity dispersed part of the suspension. But instead of the formation of fluctuating nematic domains, the birefringent spots sediment down to the interface to the isotropic gel. As new spots continuously appear in the whole part, there is a steady increase in birefringence from the bottom to the top of the nematic phase. At the final gelation state, there can often be a region with less birefringence in the top middle part of the phase.

By following the time progress, it can seem that these dark regions could be isotropic fields that remain after the sedimentation of the nematic spots. Closer inspection reveals that these field appear dark due to homeotropic anchoring[1] of the particles. The reason for this alignment in the upper part of the phase is not fully clear. An explanation can be that the particles during the formation of the nematic phase initially prefer to align with their faces towards the glass walls. This orientation is then further on disturbed by gravity and the nematic domains undergo a director change as they sediment through the phase. As the particles at the lowest part have travelled the longest path, the disturbance of the director can be expected to be more profound there. With less particle interactions, the particles in the upper part manage to remain some of their orientation unchanged before gelation.

The effect of polydispersity should also be taken into consideration for possible explanations of this orientation difference. Gravity may fractionate the particles by their size or aspect ratio, and the separations in these qualities may interact differently to the sample wall.

For the suspension of 4 w/w% clay, the formation of the nematic phase occur in the same way as for 3 w/w%. However, for the samples of higher clay concentrations, gelation takes place before the nematic phase becomes as birefringent as the lower concentrated samples. When looking at the finished settling state of the nematic gel, the most pronounced difference across the concentrations is the height of the stratum. For 0.5 w/w% the first nematic phase just slightly appear. In 1 w/w% the height has increased more than twice. For 2 w/w% the height is about the double as for 1 w/w%, but by

[1] A region with homeotropic anchoring becomes birefringent when the sample tube is tilted an angle with respect to its height. In this alignment there will be no change in birefringence when the crossed polarizers is simultaneously rotated.

increasing the clay concentration one and a half time to 3 w/w%, makes the nematic gel to triple in height. This can be explained by an increased density in the upper suspension that remains after the first settling of the sediment and isotropic gel. The further increase in clay concentration to 4 w/w%, the ratio of the heights of the nematic gels is the same as the increase in added clay. Figure 3.9 shows a graphical representation of the relative height of the nematic phases as the clay concentration is increased from 0.5 w/w% to 4 w/w%.

For the formation of the second nematic phase (nematic sol) atop of the first nematic gel, there are both similarities and differences for the various clay concentrations. The common characteristic is the ordering of macroscopic nematic domains, that start to form when the first nematic phase are close to its equilibrium state. This typically occur between one and two months after preparation, and further formation can then go on for several months. The domains seem to look the same for all clay concentrations, having an elongated shape that twines from the interface of the nematic gel to the isotropic liquid phase at the top. The difference from each clay concentration is the size of the domains. From 0.5 w/w% to 2 w/w% the height roughly double as the clay concentration is increased.

On the other hand, for higher concentrations there seems to be a decline as more clay is dissolved in the sample tube. At the same time of settlement, the height of the phase for 3 w/w% can typically be around 1/3 smaller than for 2 w/w%. The formation of the domains for 3 w/w% also takes place around 4-6 weeks later than for lower concentrations, for then to use longer time in the further development. At 4 w/w% and higher concentrations, the formation of nematic domains seems to be more or less absent for the August powder. A reason for this retreat of the nematic domains as the clay concentration is increased, can be because the isotropic liquid upper phase constitutes a much less part of the sample tube.

By the assumption that the second nematic phase is formed by slow settlement of particles from the isotropic phase, less particles makes it impossible to get an increase in the relative size of the phase. However, when less volume of suspension is poured into the sample tube, it is observed that the second nematic phase over time constitutes a greater part of the total sample height. The actual phase height itself can also be higher than for samples with more volume. In addition, the relative height of the first nematic phase is lower than what should be expected for a decrease in injected volume of the sample tube. This behaviour is not observed for the sediment and the isotropic gel beneath the nematic phase, where the height of the strata is what could be expected. On the other hand, the relative height of the isotropic upper phase increases as the volume in the sample tube is decreased. By decreasing the volume down to some specific amount, the isotropic sol is seen to increase in actual height. This could indicate that the effect of gravitational settling is of importance for the explanation of the increased contribution of the nematic sol phase when less volume is filled into the sample tube. A more detailed discussion of the domain structure is treated in Section 3.12.

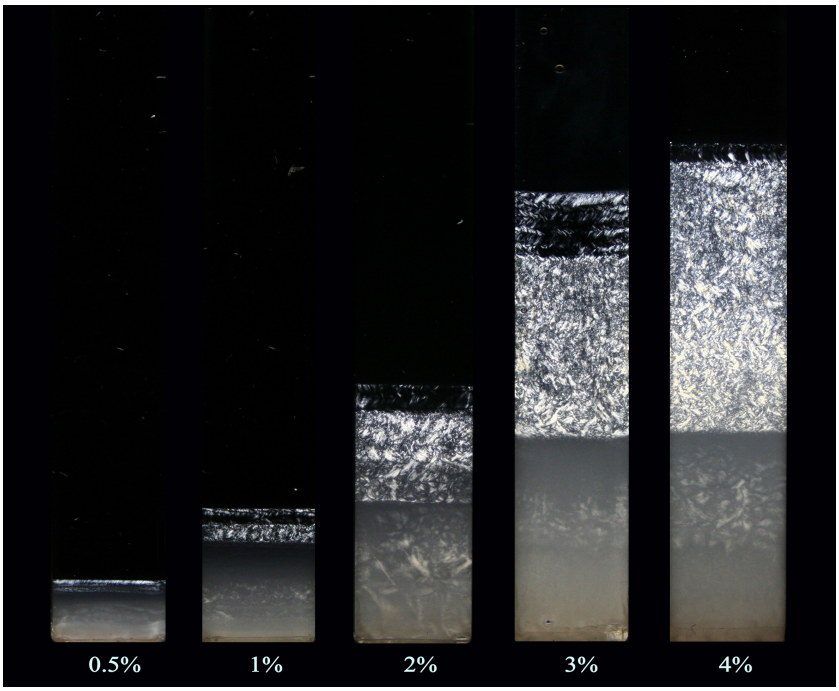

Figure 3.10: 0.5 - 4 w/w% November at ionic strength 10^{-3} M NaCl. The time after preparation for the photographs are 1 months for 0.5 %, 2.5 months for 1%, 3 months for 3% and 4.5 months for 2% and 4%. The picture of the 3% sample represents the stabilized settling state, where no further dynamics or changes of the phases are observed. The sample therefore looks the same after 4.5 months, and can be directly compared to the 2% and 4% samples.

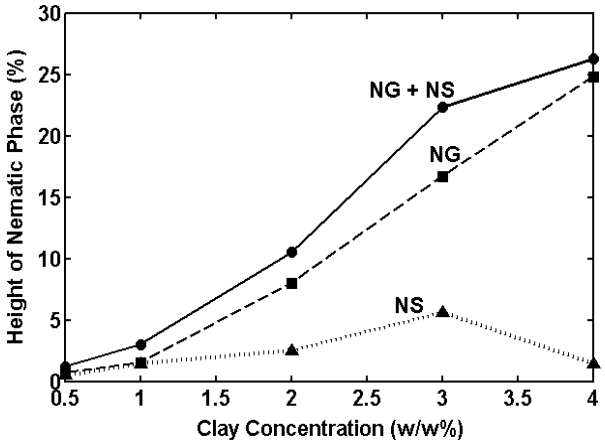

Figure 3.11: The height (volume) fraction of the nematic phase of the November powder at ionic strength 10^{-3} M as the clay concentration is increased from 0.5 to 4 w/w%. Since the top height of the sample is almost 10 cm, the fraction % is equal to the relative height of the nematic phase in centimetres.

The 6 w/w% sample has not phase separated into different phases similar to the others. After the suspension is poured into the sample tube, slow sedimentation occur for about a week for then to stop due to gelation. Some birefringence get formed in the suspension above the sediment, but there is no clear distinction between separate phases.

Figure 3.10 shows suspensions of the November powder at ionic strength 10^{-3} M with clay concentration ranging from 0.5 w/w% to 4 w/w%. The pictures show the near finished form of the suspensions, where no drastic change or further settlement are to be expected. The phase separation is very similar to the suspensions of the August powder, but differ in some specific behaviour qualities. Of the most pronounced alteration compared to the August samples, is the more refined and homogeneous appearance of the birefringence in the nematic gel of all the concentrations. This can be reasonable due to the more extensive crushing process of the November powder, and therefore giving rise to a smoother (or denser) phase profile. Figure 3.11 shows a graphical representation of the relative height of the nematic gel and nematic sol of the samples in Figure 3.10. In contrast to the suspensions of the August powder (Figure 3.9, the November suspensions show a strict linear increase of the nematic gel as the clay concentration is increased.

By studying the phase settlement from the video of the 3 w/w% sample, birefringent spots look to be influenced by gravity in that they fall towards the interface of the isotropic gel. As the process is going on, the nematic-isotropic crossing is slowly lowered[2] as the nematic phase becomes more compressed. Like the suspension of August powder, the intensity of the birefringence is greatest in the lower part of the nematic phase. However, this is not the case for the 2 w/w%, where the nematic phase can be divided into two regions with an upper part being more birefringent than the lower part. It is not clear why this special difference occur for the 2 w/w% sample, but it could probably be due to earlier gelation of the lower part.

In all the samples there are some birefringent spots with low intensity that can be seen in the stratum between the sediment and the isotropic gel. As the boarder to the nematic phase is lowered, a slight increase in this birefringence is observed. This may be due to a density increase, as greater pressure is induced by the weight of the nematic phase and the isotropic gel itself. From the comparison to the August samples, it can seem that the gelation process for the November powder is displaced towards larger clay concentrations. At the time no further settling occur in the sample with 4 w/w% August clay, the 4 w/w% November suspension continues the phase separation in the same progress as the lower concentrated samples. A similar displacement are also seen for the formation of the second nematic phase, where the extent of the phase is largest for the 3 w/w% sample[3].

[2]Over a period of 1 months the isotropic-nematic interface may be lowered by around 2 mm in the Vitrotube.

[3]The large height of the second nematic phase in the 3 w/w% sample shown in Figure 3.10 is not fully reproducible or representative for this clay concentration, since the phase has shown to be of less height in other equally prepared samples.

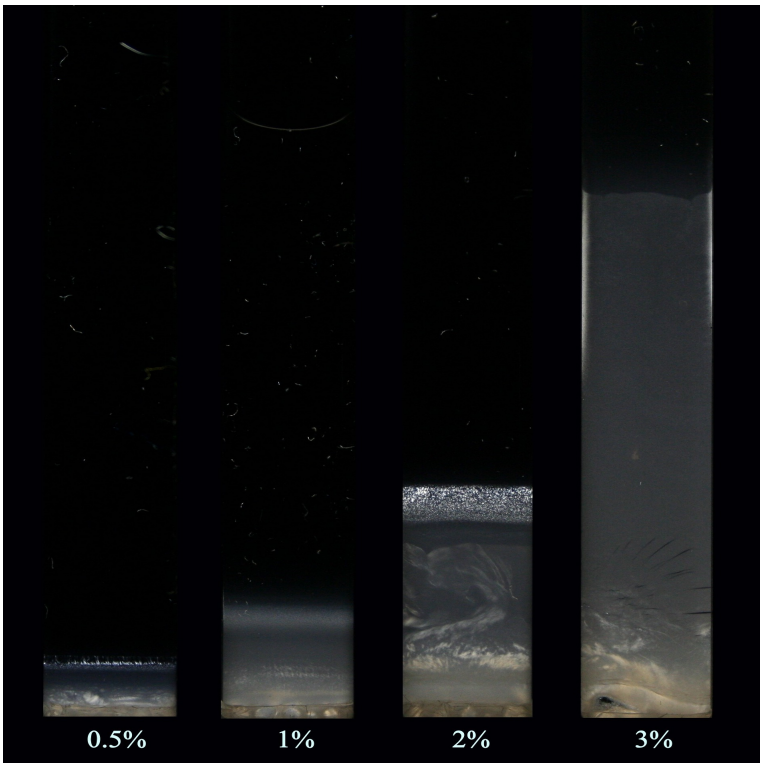

Figure 3.12: Pictures of 0.5 - 4 w/w% mortar crushed August at ionic strength 10^{-3} M NaCl taken 8 months after preparation. The 1% sample has vaporized some from the top, something that seems to be of minor effect.

Figure 3.12 shows 4 samples of mortar crushed August at ionic strength 10^{-3} M with various clay concentrations being 0.5, 1, 2 and 3 w/w%. The phase behaviour of these samples may look less interesting than their uncrushed counterpart. Still there are some distinctive features across the different clay concentrations that stand out to be peculiar for this powder.

All the concentrations have some birefringence just over the sediment, but it does not seem to be any relative increase in the amount when going from low to high clay concentration. The 0.5 w/w% sample can be said to have more birefringence than the 1 w/w% sample and the 2 w/w% sample definitely has more birefringence than the 3 w/w% sample. The suspensions of the 0.5 and 2 w/w% concentrations are the only of these samples where a clear second nematic phase has formed at the top of the first main settlement. The formation of this phase is for the 0.5 w/w% very similar to the cases for the uncrushed August and November powder, by consisting of small nematic domains. However, the nematic domains in this case are less pronounced by being fewer and smaller in size.

The nematic phase of the 2 w/w% differ completely from the structure of ordered elongated nematic domains. Between crossed polarizers, the phase consists of randomly distributed birefringent spots separated with dark fields

representing a director change. The phase starts after about 2 months to appear in the middle of an isotropic phase that has already formed over the first strata. From Figure 3.12 some of this isotropic phase is still intact under the nematic phase in the 2 w/w% sample, and for the 3 w/w% sample such a layer are seen to be totally unchanged. The reason a nematic phase is absent for the 3 w/w% sample is probably due to early gelation, but it is more difficult to explain why it has not clearly formed for the 1 w/w% sample.

When it comes to suspensions of the April powder, samples with various clay concentrations share a great deal of the same phase behaviour in addition to having their own dissimilarities. Figure 3.13 shows 0.5, 1, 2 and 3 weight% samples of mortar crushed April with a NaCl concentration of 10^{-3} M. The pictures resemble a near final stabilized form of the phase separation, but some slow fluctuations are still going on at most of the samples.

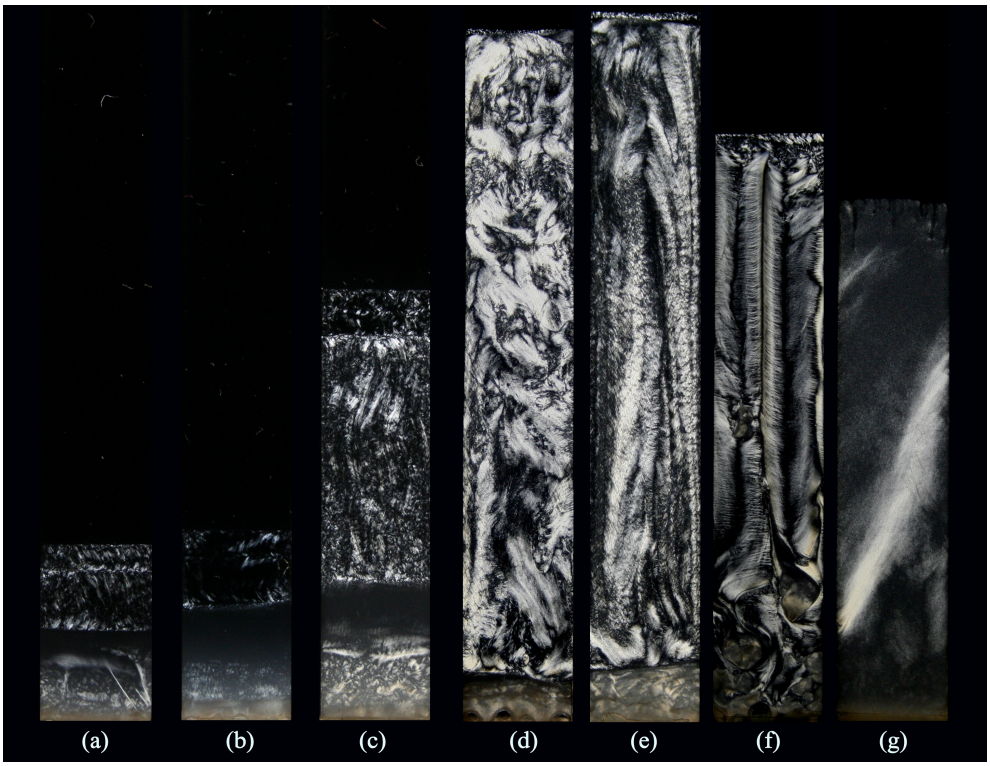

Figure 3.13: Crushed April samples of salt concentration 10^{-3} M. (a) 0.5 w/w% 2.5 months after preparation. (b) 1 w/w% 3 months after preparation. (c) 2 w/w% 8 months after preparation. Samples (d)-(g) contains all 3 w/w% clay where (d) is 8.5 months, (e) and (f) are 4 months and (g) is 2 months from tube injection. Sample (d) and (g) are made from the same initial clay suspension, but the last tube is as the sample in Figure 3.89 filled first 6.5 months after tube (d).

To demonstrate how fluctuations and slightly different preparations may form different structures of the same concentration, Figure 3.13 includes three additional samples with 3 w/w% clay. When the special case of the last sample

is not taken into account, all the samples have a similar basic phase separation after the sedimentation. From the settling processes of the 0.5 w/w% 2 w/w% and 3 w/w% samples shown in Figures 3.5, 3.4 and 3.3, a birefringent layer is during the first weeks formed above the sediment. This layer is scattered with a relative high height for the lowest clay concentrations, but seems to be denser for higher concentrations. This is most likely due to slower settling occuring as the clay concentration is increased and approaches the gel transition. For the 3 w/w% suspensions, a lower height of particles may be accessible to the formation of a nematic phase, and with a higher particle concentration the phase becomes more dense and exhibits a stronger birefringence[4].

When looking at the final form of the samples shown in Figure 3.13, the three lowest concentrations differ from the 3 w/w% by having a broad isotropic phase above the lowest nematic phase. For the 0.5 w/w% and 1 w/w% suspensions this isotropic stratum is formed faster and more directly than for the 2 w/w% sample. By studying the separation progress it is seen that the isotropic phase appears as a new nematic phase is being formed above. In the two lowest concentrations the isotropic and nematic phase are formed in a simultaneous process, where the isotropic phase is getting higher and the nematic phase becomes more birefringent. For the 2 w/w% sample, the isotropic stratum first appears as a small slit after 2 months, for then becoming broader as the nematic phase is slowly being "lifted" during the next months. The isotropic stratum seems to be missing for the 3 w/w% suspensions, but a close inspection will reveal a very small isotropic slit between the two nematic phases. The reason for its modest appearance may be due to the density and dominance of the fluctuating nematic phase.

For the 2 w/w% sample 3 different birefringent regions can clearly be separated, where the top phase could further be divided into two sub-regions. It can apparently be difficult to tell which of these regions that should correspond to the top nematic phases of the 0.5 and 1 w/w% samples, where two strata can be observed. As shown in Figure 3.32 and Figure 3.29 from the discussion of magnetic field effects, the upper stratum can be characterized to be a nematic sol since it is easily being affected by magnetic fields. The lower stratum is like the largest birefringent region of the 2 w/w% and 3 w/w% samples unaffected by magnetic fields[5] and can therefore be said to be a nematic gel. For the 2 w/w% sample the nematic sol starts to form about 3 months after preparation, whilst it is around 1.5 and 2 months for 0.5 w/w% and 1 w/w% respectively. The further twofold separation of the nematic sol in the 2 w/w% sample starts to occur when 2 more months have elapsed. Detailed microscope pictures of this phase showing the particle orientation when a magnetic field is applied, is shown in Figure 3.36. A very small nematic stratum also forms as an upper phase in the 3 w/w% samples after 3 months from preparation.

When it comes to how the different phases extend as the clay concentration is increased, the April powder are very similar to the August and November

[4]It could be possible to imagine that a denser birefringent phase at the bottom occurs because of pressure from the suspension from above.

[5]At least up to 1 Tesla.

powders. The same explanation that the higher clay concentrations have a lower upper nematic phase in the August and November suspensions, probably also counts for the April suspensions.

3.4 The Effect of Salt Concentration

The salt concentration is expected to play a major role of the phase behaviour of the aqueous Na-fluorohectorite solutions, because of the particles high surface charge. Since the theoretical understanding of the salt-induced ordering of charged colloidal particles of large particle size is not yet fully established, the phase behaviour present in this section are qualitatively discussed within electrostatic, DLVO and also Onsager theory.

Figures 3.14, 3.15 and 3.16 show respectively a sample series of 3 w/w% November, 2 w/w% August and 0.5 w/w% April with an increasing salt concentration from 10^{-4} M to 5×10^{-2} M. These three examples show the same trend, irrespectively of powder type and clay concentration. At low salt concentrations, the phase separation is the same with the formation of nematic phases between an isotropic gel and an upper dilute isotropic sol. As the ionic strength is increased, the relative height of nematic phase decreases along with an increase of the upper isotropic sol.

For the cases of the August and April suspensions, the relative height of the isotropic gel also clearly decreases with ionic strength from 10^{-4} M to 10^{-3} M. This is not as pronounced for the November powder, where just a very slight decrease can be seen over the same salt concentration range. But as the ionic strength is further increased, the height of the isotropic gel and the nematic phase suddenly get a larger drop when the salt concentration is increased from 2.5×10^{-3} M to 5×10^{-3} M. A further increase to 7.5×10^{-3} M makes very little change to any of these heights, but the next increase to 1×10^{-2} M gets a new pronounced drop for both the nematic and isotropic gel.

For the cases of the August and April suspensions, the relative height of the isotropic gel also clearly decreases with ionic strength from 10^{-4} M to 10^{-3} M. This is not as pronounced for the November powder, where just a very slight decrease can be seen over the same salt concentration range. But as the ionic strength is further increased, the height of the isotropic gel and the nematic phase suddenly get a larger drop when the salt concentration is increased from 2.5×10^{-3} M to 5×10^{-3} M. A further increase to 7.5×10^{-3} M makes very little change to any of these heights, but the next increase to 1×10^{-2} M gets a new pronounced drop for both the nematic and isotropic gel.

The August and April suspensions have a rather different phase behaviour at the salt concentration 5×10^{-3} M by having no clear phase separation of an isotropic and birefringent layer.

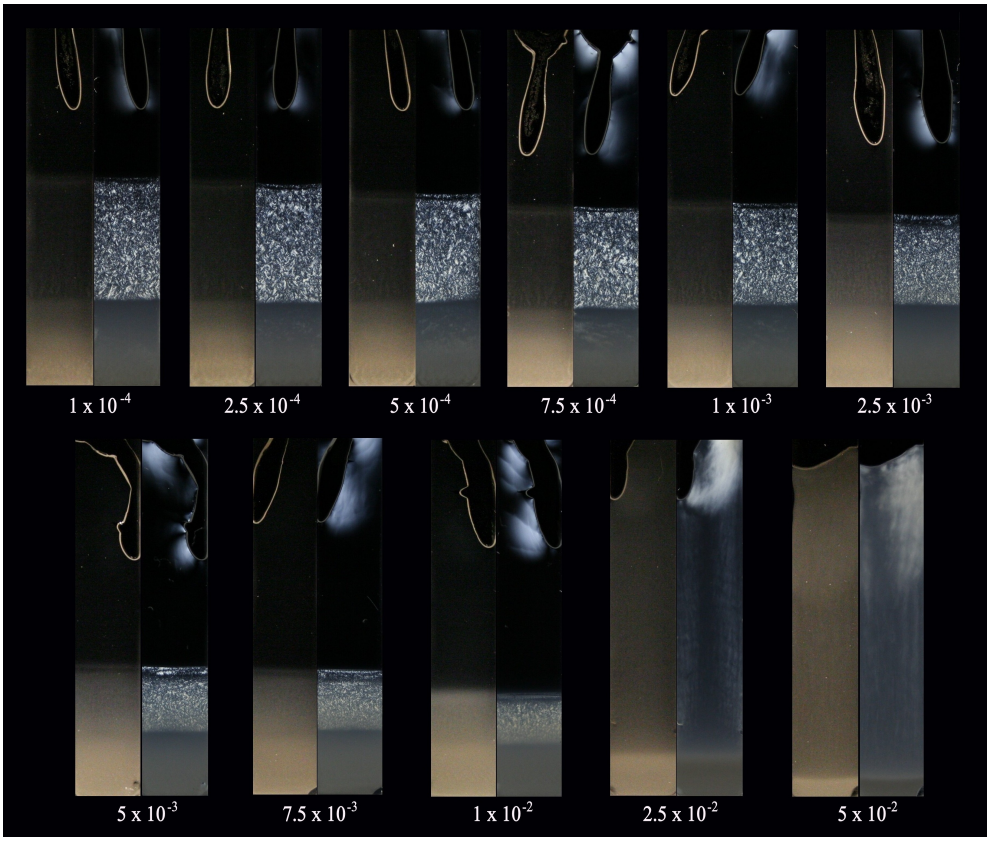

Figure 3.14: 3 w/w% November samples at salt concentration ranging from 10^{-4} M to 2.5×10^{-2} M. The samples are prepared in Davi cells, where the formations at the top part is due to defective damage. For each salt concentration; the picture to the right is taken between crossed polarizers, while the picture to the left is taken without. There is very little change in the phase separation for each increase from 10^{-4} M to 2.5×10^{-3} M. The relative height of the nematic phase decreases with ionic strength as the electrostatic interaction is more effectively screened. The transition between the repulsive and attractive forces, happens at a ionic strength between 10^{-2} M and 2.5×10^{-2} M. All of these concentrations are initially reproduced, where pictures of a second sample show no major deviation from the samples shown above. See Appendix F for figure showing only the cross polarized pictures.

Instead there seems to be a gravity settled equilibrium distribution of the particles above the largest sediment. By following this settling in a time frame of several months, a very slow increase of the sediment height can be seen to take place. Some very thin strata of birefringence may be observed, but it is nowhere close to the nematic appearance as of the 3 w/w% November 10^{-3} M sample. However, for 3 w/w% August suspension at the same ionic strength 5×10^{-3} M, a 1 cm high birefringent layer do form above the sediment. The phase behaviour is still different from the November powder, since the total height of the sediment and isotropic gel beneath the nematic phase is almost the same as for the lower salt concentrations. In addition, the phase separation

process of the August sample seems to have been prevented from the same dense settling as in the November sample due to gelation. Since the November suspensions is contained in another sample holder, and the steps is not as small for the August series, explanations of the different phase behaviour of these two powder types may not be charitable from these pictures alone.

From the pictures of the samples between the crossed polarizers, it can be difficult to decide whether the relative decrease of the nematic phase with ionic strength is due to a decrease in the amount of the nematic phase itself. By studying the pictures of the samples without polarizers in Figure 3.14, it can be seen that the density of the upper isotropic sol increases with the ionic strength. Since this phase also increases in volume as the salt concentration is increased, the actual amount of nematic phase must decrease with ionic strength. This can of course be contradicted if the sediment and the lower isotropic gel increase enough in density as the ionic strength is increased. From the pictures, there seems to be a density increase in all the phases which is expected due to less repulsion. Anyway, quantitative measurements must be carried out to give any clear statement about the density profile throughout the height of the sample.

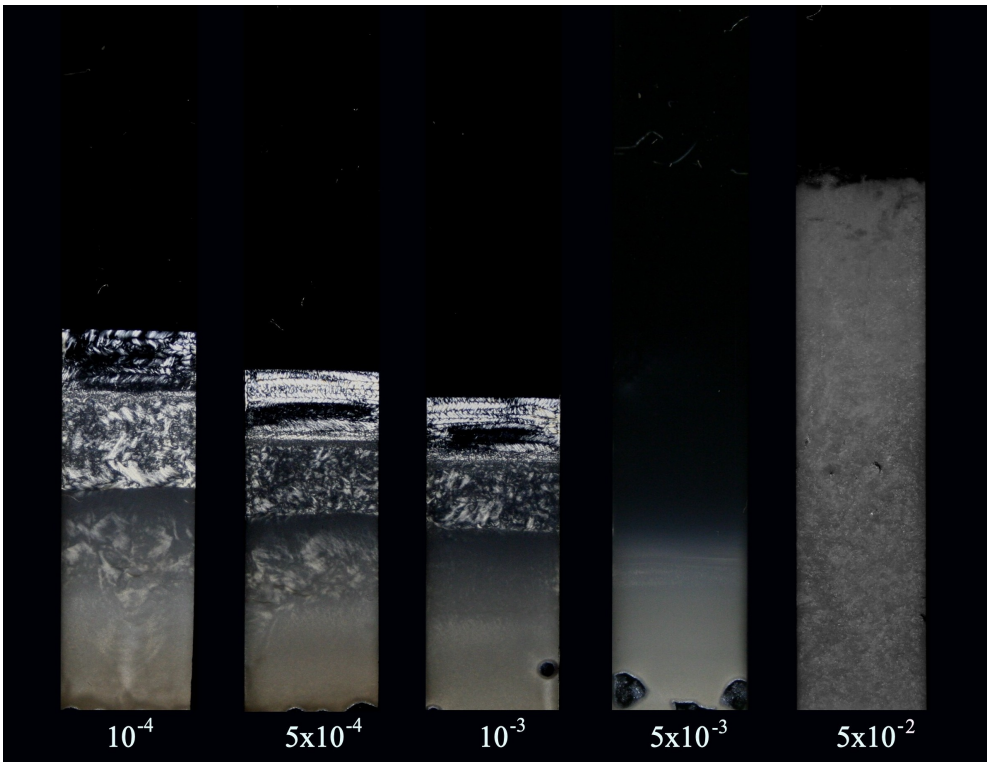

Figure 3.15: 2 w/w% August where all samples are 8 months from preparation except the 5×10^{-2} sample which is just 4 days old. .

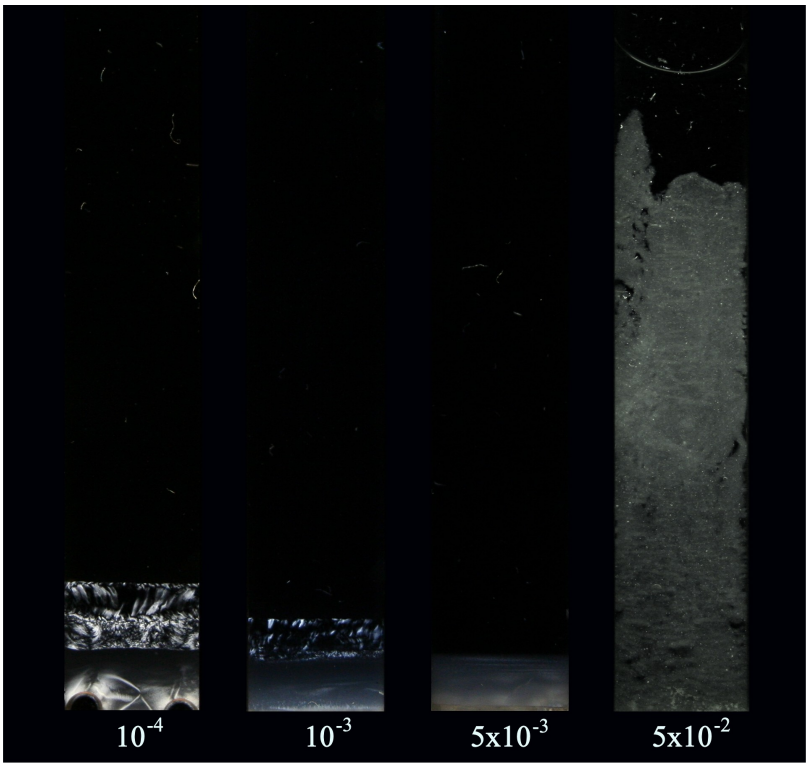

Figure 3.16: Phase behavior of 0.5 w/w% April by increasing salt concentration. The shots of the 10^{-4} and 10^{-3} samples are taken 7 and 6 months from preparation. 5×10^{-3} is 1 months from preparation. The picture of the 5×10^{-2} sample is taken 3 months from the preparation, but it looks more or less the same as it did after 1 day of settling or aggregation.

For any clay concentration or powder type, the Na-fluorohectorite suspensions coagulate at a salt concentration of 5×10^{-2} M. In Figure 3.14 a more exact flocculation transition is found to take place between an ionic strength of 1×10^{-2} M and 2.5×10^{-2} M, at least for 3 w/w% November suspensions. At two times higher salt concentration, the suspension undergoes a perceptible faster coagulation and very little sediments catch to settle at the bottom. For the 0.5 w/w% April suspension shown in Figure 3.16, no sediment at all settle at the bottom. This is also the case for higher April clay concentrations, where the suspension flocculate almost immediately after the sample tube is filled.

The behaviour is slightly different for the 2 w/w% August suspension, where some ordinary sedimentation occur the first minutes until larger aggregates collapse and divide the sample into a uniform distribution of floc at the lower part and an upper part containing just water. Since the August suspension undergoes a more rapid coagulation than the April samples, the final flocs is more dense and occupy a smaller volume. For the April suspension, the flocs almost fill the whole available volume and they hardly settle at all even for small clay concentrations. The whole structure is very tenuous, and contains a great deal of entrapped water. Since the high ionic strength very

effectively screen the repulsive forces between the particles, they attract one another at all separations. The more compact flocculation of the August powder, may correspond to a more well aligned arrangement caused by a optimum orientation of the particles that increase the attractive forces. No experiments have been carried out to get a description of the aggregate structure, and some possible fractal dimensions is therefore not known for this system.

A flocculation transition between 2.5×10^{-2} M and 5×10^{-2} M is similar to data found for Wyoming montmorillonite, published by Abend and Lagaly [161][6]. The transition line for these data shows a negative slope as the clay concentration is increased, which is also probably the case for Na-fluorohectorite since slightly slower coagulation occur for the lowest clay concentration. Experiments carried out by Michot et.al on sodium nontronite [41], also show a flocculation transition at ionic strength 10^{-2} M. However, the phase diagram of this clay type has a positive flocculation slope at low volume fractions, for then to show a negative sol-gel transition as the volume fraction is further increased. Compared to other clay minerals, the flocculation transition for Na-fluorohectorite is lower than for bentonite but higher than for laponite [39].

Table 1.1 shows the values of the Debye screening length for the samples different NaCl concentrations. When these values are taken with the total potential energy curve of the DLVO interaction given in Figure 3.63, a comparison of the behaviour across the salt concentration of the samples in Figures 3.14, 3.15 and 3.16 closely resembles the given curve. The secondary minimum at a screening length of 5 nm, may corresponds to the sudden behaviour change that take place for the November suspensions at 2.5×10^{-3} M. The flocculation transition at 2.5×10^{-2} M gives a screening length of 2 nm, in which the interaction curve in Figure 1.1 is dominated by van der Waals attraction. The energy barrier is then surmounted, and the colloidal clay suspension is referred to as being unstable.

From salt concentration 10^{-4} M to 10^{-3} M, the Debye screening length decreases from about 30 to 10 nanometer. As the screening length is roughly proportional to the electric double layer, the effective particles dimensions increase as the salt concentration is decreased. In aqueous salt solution, the thickness of the particles is increased by an extra height of two times the screening length. From the Onsager theory of the interplay between excluded volume entropy and orientational entropy, a change in the particle dimensions should reduce the critical concentration of particles at the isotropic-nematic transition[7]. It is difficult to tell how much influence this grow in effective particle size has for the observations of the increased nematic ordering with decreasing ionic strength in the Na-fluorohectorite suspensions.

From simulation experiments by Rowan and Hansen [155], it is suggested that the swelling effect is negligible for large particles, and the phase behaviour

[6] An exact comparison between these data and our experiments, show that a transition at 2.5×10^{-2} M for the 3 w/w% November suspension is slightly below the corresponding value for Wyoming montmorillonite.

[7] Provided that the volume is being constant, and no extension has taken place.

may be explained solely on electrostatic grounds. In suspensions of very large Na-fluorohectorite particles, the phase diagram is then dominated by long-range electrostatics, which disfavour nematic ordering. However, the strong influence of polydispersity in the size of the Na-fluorohectorite particles must be taken into account in the explanation of the phase behaviour. Since the smallest particles remain in the upper isotropic sol after gravity has been acting on the suspension, the significance of the double layer expansion in particle size must be of most influence for this phase.

The increase in the relative amount of nematic phase for the low salt concentrations, could come from particles in the upper isotropic sol where nematic orientation has become favourable. The extra height of the nematic phase for low salt concentration, can also be thought of being extension driven by repulsion alone. When it comes to the formation of the second nematic layer, there does not seem to be any significant differences as the ionic strength is varied.

Complementary samples, shown in Figure 3.17 and Figure 3.18, exhibit an idea for expected phase behaviour when the repulsive interaction is tuned by ionic strength. Combination of the final gravity settled visual state of the various samples, may give a sensible qualitatively account of the slope of phase transition lines.

From the phase settling behaviour of the samples, it is clearly seen that the different powder suspensions give different results in a phase diagram. For the low salt concentration 10^{-4} M, the second and third pictures of Figure 3.17 show the near final state of 3 w/w% and 4 w/w% clay concentration of crushed April suspensions. For the equal salt and clay concentrations, the two first pictures of Figure 3.18 show how the suspension have settled for April powder that is not crushed. By comparing these two cases, it is obvious from these pictures alone that the particles for the uncrushed suspensions have undergone a much greater gravity settling than the suspensions of the crushed powder. This behaviour difference is further confirmed by looking at pictures taken for regular time periods between the preparation and the state shown in the mentioned pictures.

3.5 Phase Diagram

The visual observations of the various samples covered in Figure 3.1 are insufficient to give a precise phase diagram of clay concentration with ionic strength. The different and complex phase behaviour from the various Na-fluorohectorite powder preparations complicates a liquid crystal phase diagram behind the ubiquitous sol-gel transition lines. The results present in the above sections adequately describe the phase behaviour in suspensions of Na-fluorohectorite for a specific clay and salt concentration range, but is incomplete to provide accurate determination of the associated phase transitions.

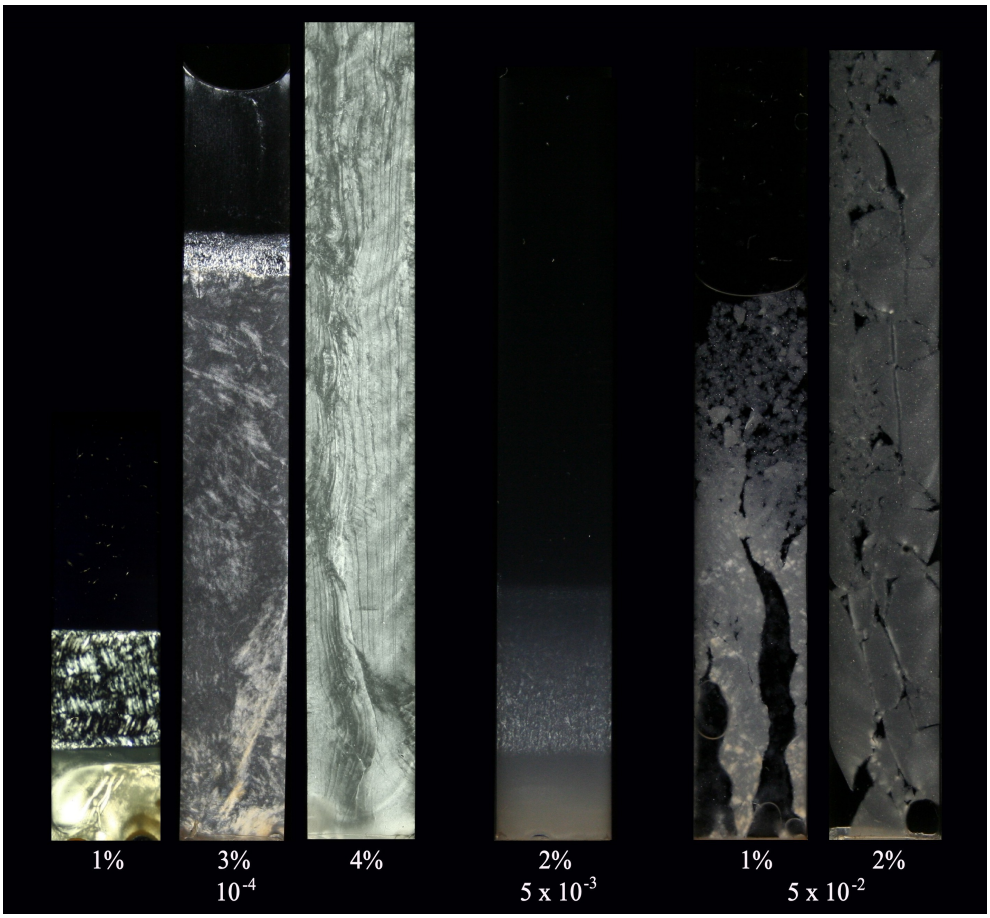

Figure 3.17: Samples of crushed April powder at some specific clay and salt concentrations. The three first samples, show how the phase behaviour changes by increasing the mass concentration from 1 to 4 w/w% when the salt concentration is kept constant at 10^{-4} M. The picture of the 1 w/w% sample is taken one and a half month after preparation, and four separate phases have formed (sediment/birefringent gel, an isotropic gel of height 1-2 mm, nematic sol/gel and black isotropic sol). For this picture, the polarizers are not completely crossed, which have given rise to a slightly bluish brightness and some reduced contrast. The pictures of the next two samples of 3 and 4 w/w%, are taken 6 months and 3 weeks from preparation respectively. The curved separation in the top of the 3 w/w% sample, is due to evaporation. The picture of the 2 w/w% sample with salt concentration 5×10^{-3} M is taken 8 months after preparation, but the sample looks nearly identical to what it did one month after the sample tube was filled with suspension. The last two pictures are 1 and 2 w/w% samples with the high salt concentration 5×10^{-2} M. The attractive gel or floc structure is formed short time after preparation. At the time the pictures are taken (7 and 5 months after preparation), a lot of air has penetrated and "cracked" the samples.

For both the 3 w/w% and 4 w/w% samples for the crushed powder the settling process is very stationary, where there for the first weeks are only a very small visible change each day. The 3 w/w% sample has as expected a bit

more dynamics than the 4 w/w% sample. The phase behaviour is similar to the 3 w/w% suspensions with salt concentration 10^{-3} M. Compared to those samples with 10 times higher ionic strength, the 10^{-4} M sample fluctuates much slower and reaches the final steady state much earlier. For the 4 w/w% 10^{-4} M sample, the behaviour is very different from the 3 w/w% samples. Here none of the upward or downward fluctuations occur. Instead strong gelation takes place in the suspension, and some larger aggregates slowly settle towards the bottom.

The 4 w/w% uncrushed April 10^{-4} M sample in Figure 3.18 may with its scattered birefringent spots look like the 6 w/w% November samples in the same figure and the 6 w/w% 10^{-3} M August sample in Figure 3.8. However, the time evolution reveals that particle fluctuations take place with a much greater effort for the uncrushed April sample than for the others. Suspensions of 4 w/w% uncrushed April with ionic strength 10^{-4} M are close to the complete gelation state of the 4 w/w% crushed April suspensions.

It may seem that crushing the powder moves the transition for vibrant fluctuation and settling to static gelation towards lower mass concentration. This is also the case for suspensions of August powders, where a stratum of nematic phase is not observed for clay concentrations above 2 w/w% [8] for mortar crushed August suspensions.

This trend where a more refined clay powder forms gels at lower mass concentrations is displayed in Figure 3.19. In this phase diagram the lines illustrate for each powder a transition from a solution where nematic and isotropic phases have formed by settling and fluctuation to a state where the whole suspension pretty soon "freeze" to a solid gel. This transition does not, as it may seem from the phase diagram, happen suddenly at a specific clay concentration, but occurs more gradually. The lines are deduced by visual observations from the pictures shown in this report and additional pictures showing the settling evolution of the suspensions. The position and slope of all the transition lines should not be considered to be absolute or very accurate.

The phase diagram is made for samples that are filled completely in Vitrotubes. Other sample holders and different preparation methods may give a different diagram, at least quantitatively. For the clay and salt concentrations to the left of a line, the suspension have some parts which are more sol-like. This could be a small nematic stratum which is susceptible to be influenced by an external magnetic field or have a large fluid isotropic phase. To the right of the transition line, no important phase separation occur and the suspension becomes very soon static. Gelation is still present in the phase separated samples to the left, both as an isotropic gel and nematic gel very soon after the first sedimentation and as nearly complete gelation of the whole sample has

[8] This is correct for suspensions that are filled in Vitrotubes, which are the kind of sample tubes these measurements are compared to. Figure 3.12 of crushed August samples shows that there are some birefringence at the bottom of the 3 w/w%, but there are no major nematic phases elsewhere in the sample. By the other hand, Figure 3.53 clearly shows that nematic orientation has formed in 3 w/w% mortar crushed August suspensions filled in Davi cells.

taken place after long enough time of settling.

The transition lines in the diagram are drawn with a slightly positive slope for salt concentrations ranging from around 10^{-4} M to 10^{-3} M. Since the visual observations of the samples is not very accurate to draw this kind of phase diagrams, the slope just give a qualitative sense of how the phase behaviour change when the ionic strength is varied. The gradient of the slope may look different for the different powder batches. For the crushed April powder, there is a clear difference between the 3 w/w% 10^{-4} M suspension and the 3 w/w% 10^{-3} M shown in Figures 3.3, 3.13, 3.24, 3.26 and 3.89. From the observations, the slope seems to be larger for suspensions of the April powder compared the November powder, where the samples behaves almost identical for 10^{-4} M and 10^{-3} M. For 60-70 % of the height of the sample, gelation seems to be more present for very low salt concentrations. The around 4 mm thick upper nematic phase in the 3 w/w% 10^{-4} M sample in Figure 3.17 is formed by slowly settling from the isotropic upper part. The first birefringence of this phase started to appear around one month after preparation, and received the end height after further two months of settling.

The dotted upper line, represents the flocculation transition where aggregation takes place and no phase separation occur. The line is not accurately measured (except for November powder in Davi cells, Figure 3.14) and is likely to be slightly different for the different powders.

When it comes to the 4 November samples in Figure 3.18, the difference between the 10^{-4} M and 10^{-3} M salt concentration is not as strict as for the April powder. The clay concentration where the suspension no longer separates into two strata of an isotropic and birefringent gel is found between 5 and 6 w/w%. For the 5 w/w% samples, the transition from the isotropic bottom phase to the birefringent part is less divided in the 10^{-4} M sample than in the 10^{-3} M sample. This is also the case for the 6 w/w% samples, where there for the 10^{-3} M suspension is a clear separation between an isotropic gel from the sediment up to the remaining part consisting of non-regularly birefringent spots. From these observations it may seem that particle settlement is less rapid for lower ionic strength, and the gelation process happens at a faster rate than at higher salt concentrations. An explanation for the less difference for the 10^{-4} M and 10^{-3} M samples for the November powder, could be because it has a higher threshold salt concentration for flocculation compared to the April powder.

When the suspension of the November powder with salt concentration 5×10^{-2} M (Figure 3.14) is compared to the 5×10^{-2} M April samples (Figure 3.17 and 3.16), the structure formed for the April powder has a much more floc like look than the November sample, which should be considered to be an attractive gel. It might be possible to imagine that the clear transition across the ionic strength for a specific mass concentration observed for the April powder, can be found at higher salt concentrations than 10^{-3} M for the November powder. The transition line can also just simply have a less slope in any range of ionic strength for the November suspensions than for the April suspensions.

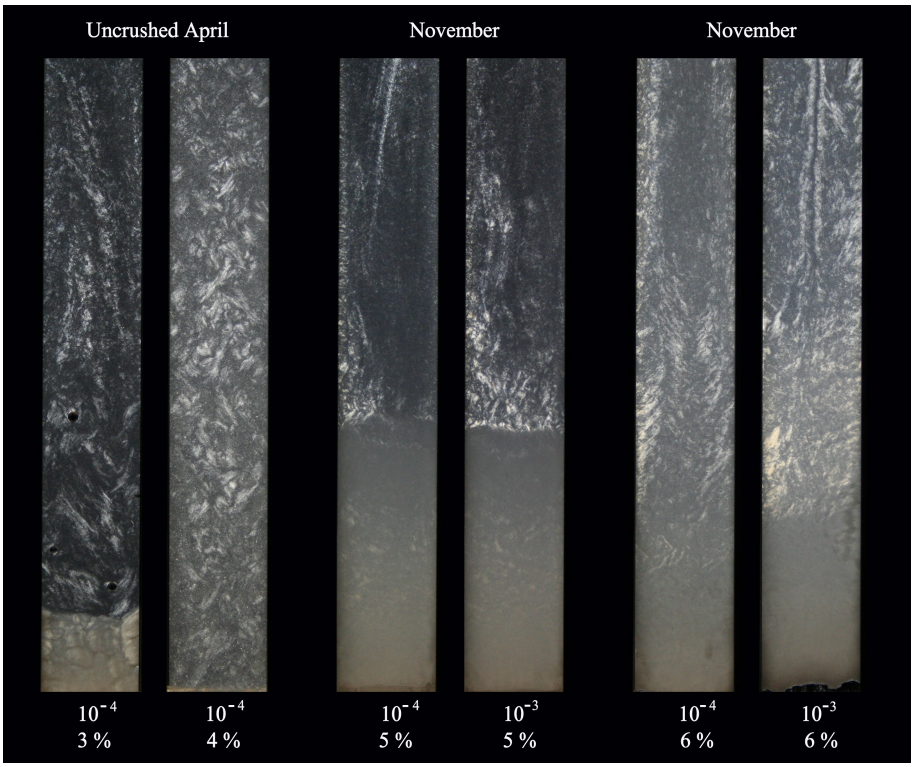

Figure 3.18: Samples of uncrushed April and November powder at salt concentration 10^{-3} M and 10^{-4} M. The two first samples show how the settling behaviour changes when the clay concentration is incresed from 3 to 4 w/w% at ionic strength 10^{-4} M. The settling process for the 3 w/w% sample at ionic strength 10^{-4} M is very similar to how this suspension behaves at ionic strength 10^{-3} M (Figure 3.23). Both pictures of these samples are together with the next two 5 w/w% samples taken 3 months from preparation. The last samples with 6 w/w% clay concentration are at the time of the photographs 5 months from preparation.

As indicated in the previous sections, the November powder is most similar to the August powder. In the phase diagram (Figure 3.19), the transition line for the August suspensions is drawn about 1 mass concentration to the left of the November powder. This is seen by observing that the phase behaviour of the 4 w/w% August sample (Figure 3.8) is similar to the 5 w/w% November suspensions. The 6 w/w% August sample in Figure 3.8 apparently looks similar to the 6 w/w% November samples in Figure 3.18. However, when the settling process of the samples is viewed, it is revealed that the birefringent pattern seen in the August sample already formed after one week. The structure seen in the November samples, has not even 4 months after preparation reached its stationary state. From these results, a "sol-gel" transition should takes place at lower mass concentration for suspensions of August powder than for November powder.

The indication that gelation seems to occur at lower clay concentrations for suspensions of crushed powder and hence smaller particle size, is in accordance

with experiments carried out on size fractionated Wyoming montmorillonite clay [15, 33]. From the rheological phase diagram derived by Michot et al. [33] it is found that suspensions of smaller particles exhibit a sol-gel transition at lower solid concentration than larger particles[9].

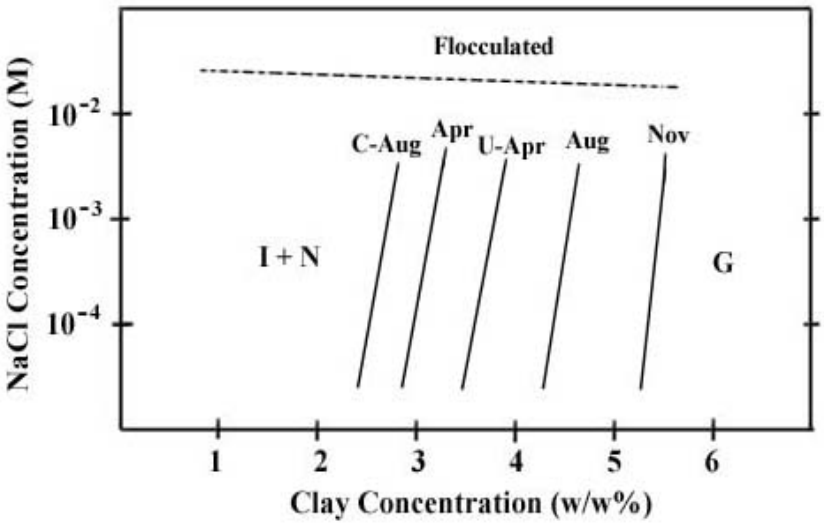

Figure 3.19: Phase diagram which gives a schematic representation of where the suspensions go from having a separation of isotropic and nematic phases to becoming a complete gel with no major settling or fluctuations after the very first time of sedimentation. Transition lines are drawn for the different powder types, where C-Aug means mortar crushed August, Apr is mortar crushed April, U-Apr is uncrushed April, Aug is uncrushed August and Nov is November.

3.6 Effect of Different Sample Holders

The geometry of the different sample tubes, which are described in Section 2.2, give three specific contributions to how the shape of the sample holder effects the phase behaviour. The largest sample tubes, Vitrotubes with dimensions 1×10×100 mm, are for the most cases nearly completely filled with 1 ml clay solution. The smaller flat Davi cells with dimensions 1×8×52 mm are filled about 1 cm below the top and are therefore contained with 0.35 ml suspension. The round capillaries used, are supposed to have a uniform thickness of 2 mm, but show considerably individual variations.

All of the capillaries are initially filled to an equal height level of about 7 cm, but evaporation and thickness differences vary the final suspension volume from 0.15 to 0.3 ml. Since all of the sample holders consist of walls made from borosilicate, direct walls effects should therefore not contribute to different phase behaviour across the various sample holders. Figures 3.20-3.25 show how

[9]They found that the concentration corresponding to the sol-gel transition increased linearly with particle anisotropy, which is opposite to the same evolution of the isotropic-nematic transition.

suspensions of the five different powder preparations have phase separated in the three sample holders. To see if any irregularities in the sample preparation may have affected the phase behaviour, three equal samples of every kind are made.

For the Davi cells, pictures without polarizers are also taken. Every picture are taken at the same time, 6 weeks after they were carefully prepared with same procedure.

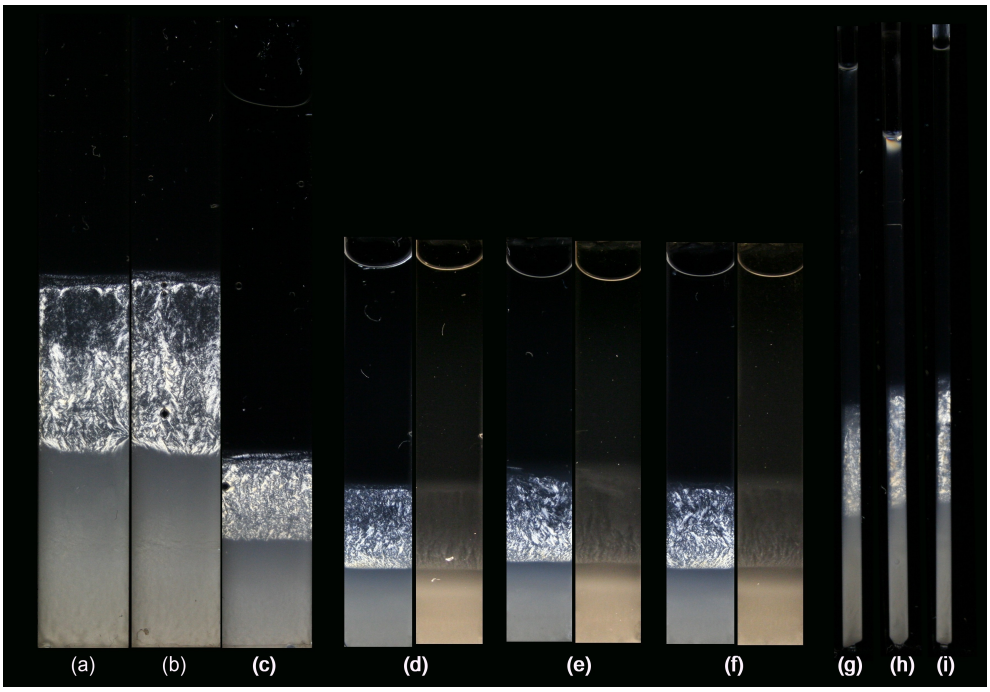

Figure 3.20: 3 w/w% August at 10^{-3} M NaCl concentration. All pictures are taken 6 weeks after preparation. Sample (c) is filled to a lower level than (a) and (b). For (d)-(f) the pictures to the right are without polarizers. (g)-(i) are fabricated 2 mm round capillaries, but each capillary have a different non-uniform size.

For all powder types, there are appreciable differences in the phase behaviour for the different sample holders. Figures 3.20 and 3.21 show the August and milling machine crushed August samples, where the main phase dispersion is the same for each sample. The most noticeable difference for the various sample holders, may be the even transition line between the nematic and isotropic phase in the davi cells. For the Vitrotubes and probably also the capillaries, this transition is more rough and indistinct. From Figure 3.20, an exception for this is seen for sample (c), where much less solution is filled in the Vitrotube. The settling height therefore seems to be of decisive importance for a clear separation between the isotropic and nematic phase. When it comes to the formation of a second nematic phase, it is evident that there is a slight dependence of sample holders.

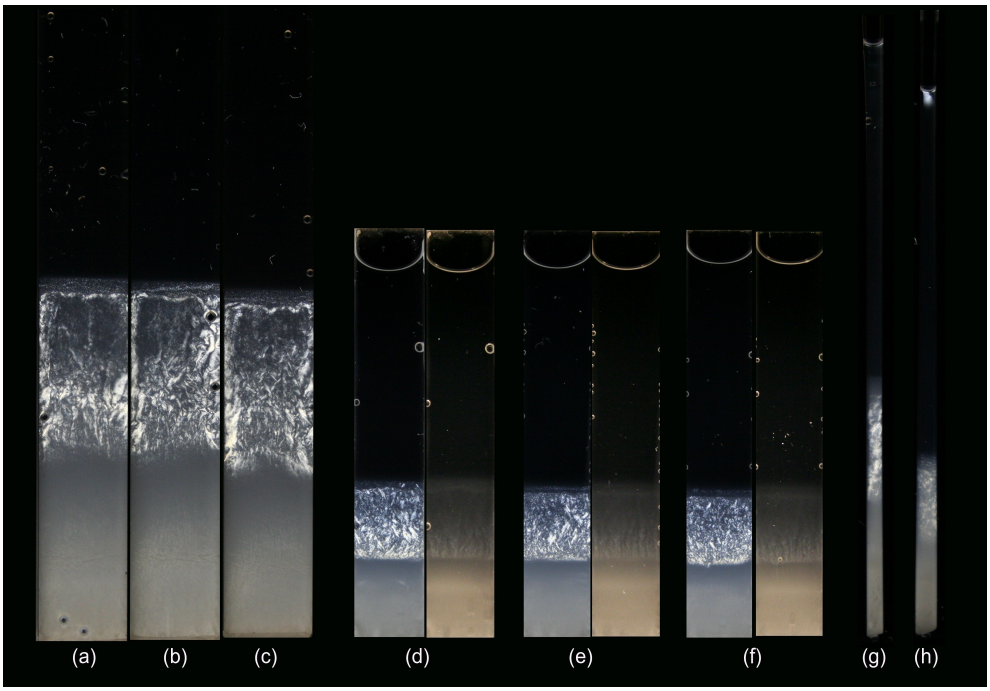

Figure 3.21: 3 w/w% milling machine crushed August at 10^{-3} M NaCl concentration. (a)-(c) There is a small decrease of the top of the nematic phase in the Vitrotubes, but the height and form of the layer are the same for the three samples. (d)-(f) The pictures taken without polarizers show a structure of the nematic phase where a vertical particle alignment looks engaging. In sample (h) the bottom phases have settled to a lower level than sample (i), since this capillary has a broader thickness.

For the uncrushed August samples there is a separate stratum for all the samples, but the formation of nematic domains is much more pronounced in the three Vitrotubes. When the phase behaviour evolves behind the 6 weeks in the figure, nematic domains also become visible in the Davi cells and capillaries. After the same time period, the domains in the Vitrotubes are far more developed than in the other sample holders. This phase behaviour difference is not as obvious in the three different sample holders for the case of the milling machine crushed August suspensions. Here the nematic sol has a very similar evolution for the Vitrotube and Davi cell, but does not seem to fully develop in the capillaries. In contrast to the uncrushed August suspensions, the nematic domains may at later settling time even be more profound in the Davi cells than in the Vitrotubes.

Figures 3.55-3.57 show one of the milling machine crushed August Davi cell samples at 4 weeks later settling than in Figure 3.21. The domains in the nematic sol are very closely packed, and are easily disturbed by some small disturbance involving movement of the sample.

A last difference to mention for these samples, might be that the particle alignment in the upper part of the nematic gel is more homeotropic in the Vitrotubes than in the Davi cells. As indicated by the half-filled sample tube

in Figure 3.20, this tendency is probably related to the gravitational length of the sedimenting particles.

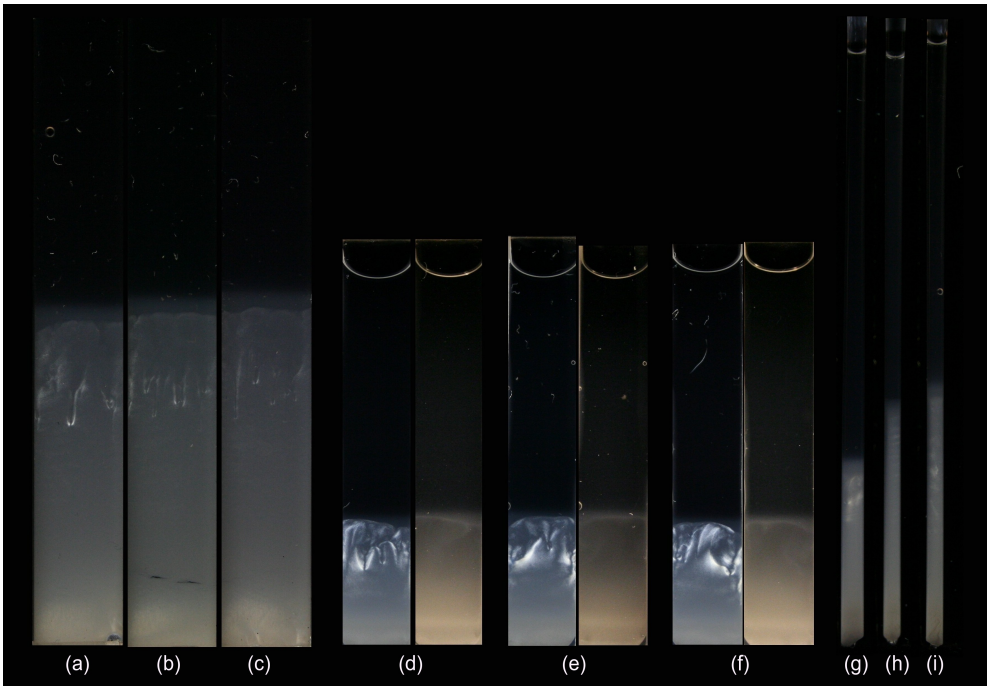

Figure 3.22: 3 w/w% mortar crushed August at 10^{-3} M NaCl concentration.

For the suspensions of the mortar crushed August powder, shown in Figure 3.22, there is simply one appreciable change when the suspension is injected to the alternative sample holders. The samples of the Davi cells stand out from both the Vitrotubes and capillaries by having a much stronger birefringence in the part expected to be nematic. For the Davi cells this part makes up almost half of the total settling height, while it for the Vitrotubes and capillaries there are just small spots of birefringence scattered above the isotropic gel. An adequate explanation for this difference is currently not proposed, but a conspicuous observation of a lower settling height in the Davi cell compared to the Vitrotube may indicate that the birefringence difference is due to density considerations.

Samples of the April suspensions, uncrushed powder in Figure 3.23 and crushed powder in Figure 3.24, show a similar trend in variation for the sample holders. For both powders, there is a marked difference in phase behaviour for the Davi cells compared to the Vitrotubes and capillaries. As seen from the photographs, a dominating birefringent layer has for all the Davi cells been formed under the curved air-liquid interface. It might be possible to imagine that the narrow environment and the POM side walls in combination with the surface tension have suspended a great deal of the injected clay solution from gravitational settling. The size of this phase is a bit less for the samples of the

crushed powder than the suspensions of the uncrushed April powder, which also have a more grainy appearance.

When it comes to the formation of a birefringent gel phase right over the first sediment, this apparently seems to be exclusive to the Vitrotubes. The capillaries may have some weak birefringence in the bottom, but it is almost totally absent in the Davi cells. The main covering nematic phase, where the formation in the Vitrotubes seems to be fluctuating driven for the crushed April powder and gravity settled for the uncrushed powder, have a much more systematic and equal structure for the Davi cells. For both powders there is in these cells no smooth separation boarder for either the start atop of the sediment or at the transition end to the isotropic phase. The nematic phase is separated from the sediment by an isotropic curved layer and the top consists of arbitrary bulges.

For the crushed April samples, there are for all three Davi cells an almost equal non-birefringent area over the nematic birefringence. This region is for sample (d) in Figure 3.23 a bit larger than the other two, which may come from a smaller top birefringent layer in this sample.

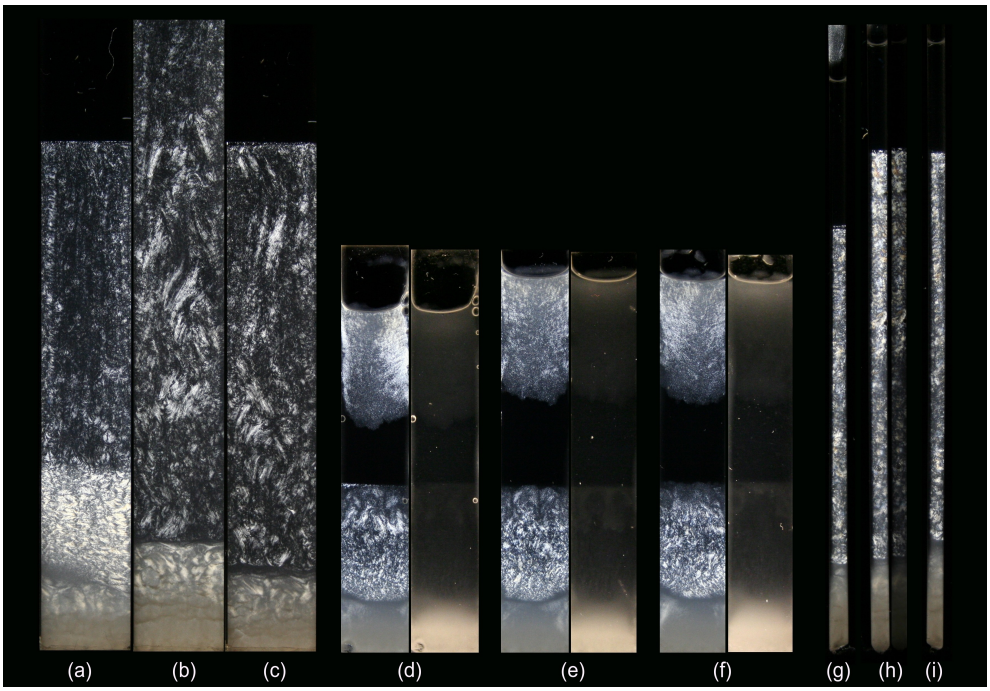

Figure 3.23: 3 w/w% uncrushed April at 10^{-3} M NaCl concentration. Sample (c) is filled to a lower level than sample (a) and (b). Some evaporation has taken place in sample (d), and the birefringent top layer has sunk to remain just a small region of transparent solution. (g) The start of the formation of a nematic sol phase may be spotted on the top of the birefringent mid-part. (h) The intensity is reduced for the picture to the right.

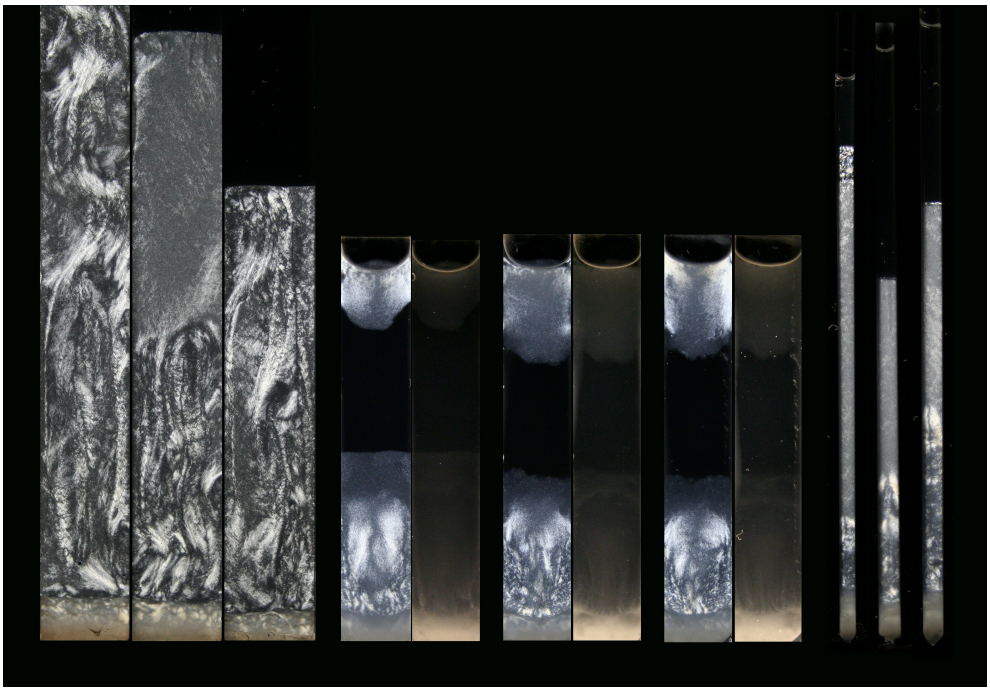

Figure 3.24: 3 w/w% crushed April at 10^{-3} M NaCl concentration. The last of the Vitrotubes is initially half-filled. A nematic sol phase is formed in the first capillary sample, which may have been trigged by a pronounced evaporation for this sample.

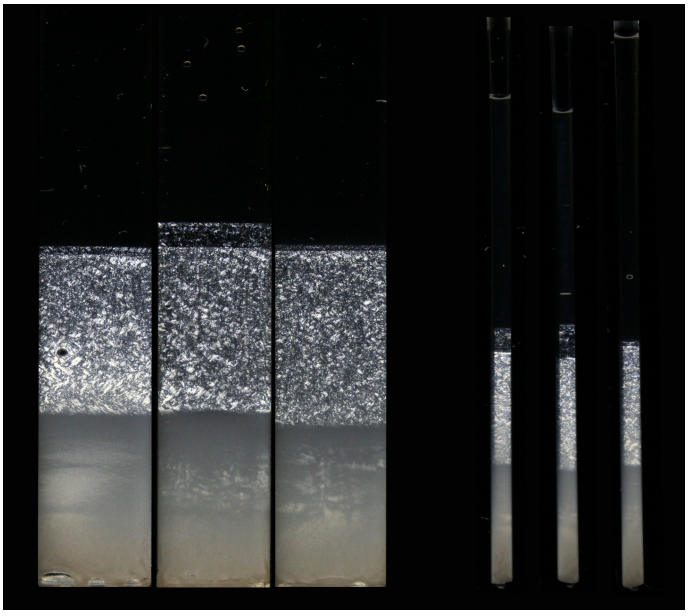

Figure 3.25: 3 w/w% November at 10^{-3} M NaCl concentration. Vitrotubes to the left, and capillaries to the right.

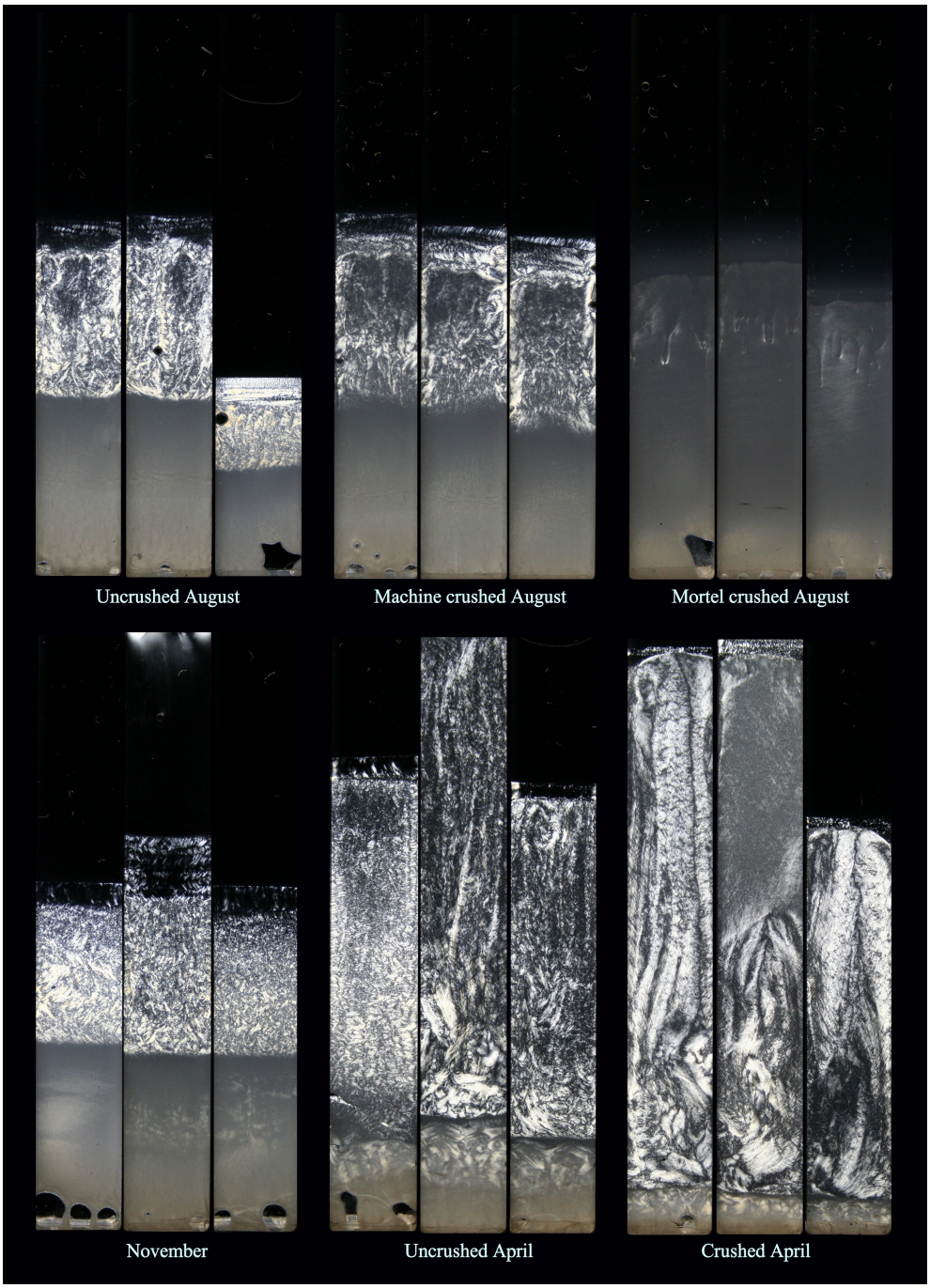

Figure 3.26: Pictures of the 6 different 3 w/w% Na-fluorohectorite powders at 10^{-3} M NaCl concentration 5 months after preparation.

Figure 3.25 shows November samples in Vitrotubes and capillaries, the same clay and salt concentration for Davi cells is shown in Figures 3.14 and 3.54. The pictures taken after 6 weeks show there is no difference in exterior phase behaviour between the Vitrotube and the capillary, but the formation

of a second nematic phase seems to be fortuitous for each individual sample. As the suspensions continue to settle, this top nematic sol phase do after long enough time form and evolve in all November samples. Even though this phase should be thought as having the same structure for both the Vitrotube and capillaries, the application of external magnetic field has only showed changes for the capillaries.

Since the Vitrotube is half the thickness of the capillaries, the magnetic threshold field is higher for the Vitrotubes. This may be of importance for this difference, but can not solely explain it since the nematic sol phase in the capillaries has showed to be influenced by magnetic field strengths that are 10 times lower than for strengths which give no affect for the Vitrotubes. The geometry of the sample holder may be of direct importance, or indirect influence on gelation of the sol phase which seems to have happened in the Vitrotube.

It should also be noted that the nematic sol in capillary samples of 4 w/w% November powder also show no sign of reorientation by influence of magnetic field strengths up to 1 Tesla. The process of the formation of the nematic phases in these samples is far from uncovered, and alternative methods should be carried out to give complete understanding.

Figure 3.26 shows a comparison of all the Vitrotube samples for the 6 Na-Fht powder types/batches above, as they look five months after preparation. All of the samples look more or less the same. The most pronounced difference is the development of the nematic sol phase above the first nematic phase. In Section 3.11 it is showed how this phase forms by slow particle settlement from the upper isotropic phase.

3.7 Mass Density Distribution

To get knowledge of density differences between the various phases and how much the density varies within each phase, the clay concentration is for two similar samples of 3 w/w% August and April at 10^{-3} M measured from the liquid top to the sediment at the bottom. The suspensions were made in holders[10] of 50 ml, which the height was 7.5 cm and diameter 2.9 cm. The samples were left to settle for 2 months (August) and 2.5 months (April) before the measurements. At this time the samples have separated into 5 main different strata from top to bottom: liquid top layer, isotropic phase, nematic sol, nematic gel and sediment[11]. Figure 3.27 shows two equal reference samples in 50 ml glasses. The measurements were carried out by pipetting out 250 μLitres

[10] The suspensions were made in two 50 ml plastic syringes where the top had been cut. The initial idea was to measure the clay concentration for a few height levels in the suspension, i.e. use the syringe to push out and get to each phase.

[11] The nematic sol corresponds to the layer between the isotropic and nematic phase. This layer may be a possible coexisting region of with both isotropic and nematic phases. Any isotropic phases between the nematic gel and sediment are not possible to characterize by visual considerations or from the density measurements and are therefore not mentioned here.

from the top to the sediment. In total; 177 measurements were done for April and 163 for August. Since it was too difficult to suck up the sediment into the pipette, the remaining sediment was dried and weighed to be 0.285 gram for April (8.5 mm) and 0.561 gram for August (14 mm).

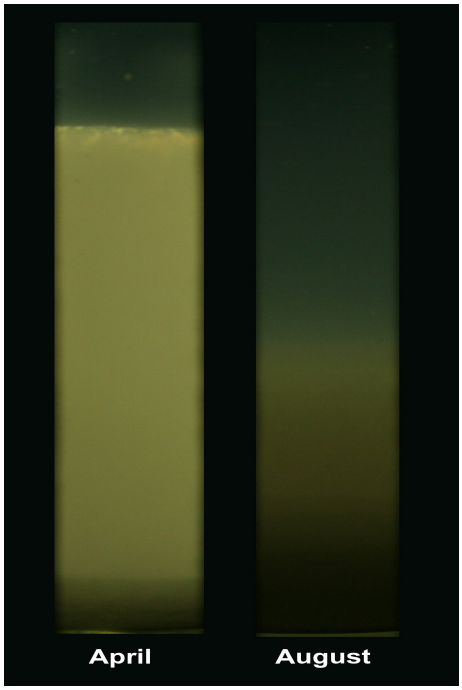

Figure 3.27: 3 w/w% April and August samples of 10^{-3} M concentration in 50 ml glasses placed between crossed polarizers.

Figure 3.28 shows the clay concentration as function of relative height, where zero is set at the end of the nematic phase. The volume fraction is found by dividing the clay concentration by the mass density of Na-Fht, which is 2.0 g/cm^3 when it is taken into account that two water layers are incorporated in between the clay platelets [162]. The difference between the clay concentration at the nematic and isotropic phase is slightly different for the April and August suspensions. The clay densities at the phase boundaries are for August about 0.031 g/cm^3 for the nematic phase and 0.010 g/cm^3 at the isotropic phase. For April it is 0.029 g/cm^3 and 0.015 at the nematic and isotropic phase respectively. This difference between the two batches may be explained by the fact that the April powder is crushed and might therefore have a lower polydispersity. The gap between the nematic and isotropic phase ranges over a height of about 4 mm. This is about equal to the height of the nematic sol for the 3 w/w% concentration in Figure 3.9, when the height difference between the two different sample holders is taken into consideration.

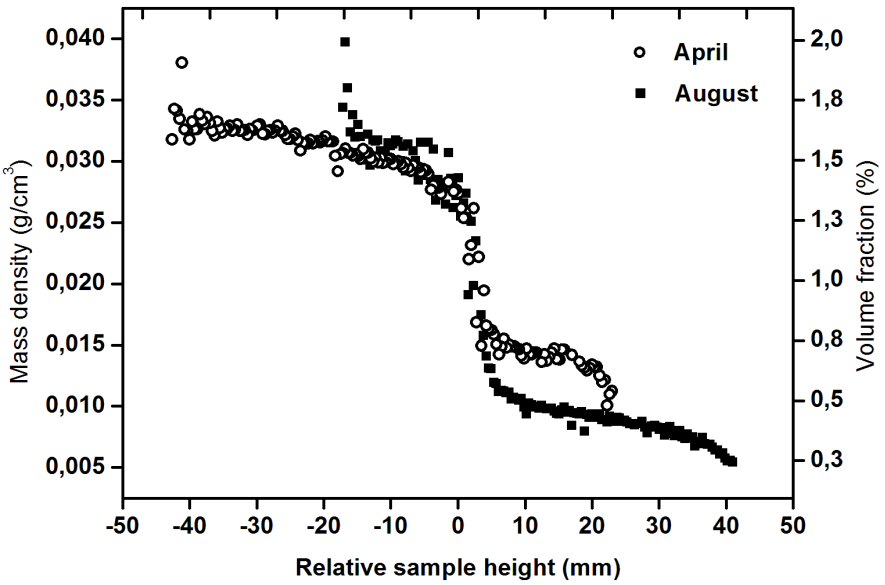

Figure 3.28: The mass density as function of relative sample height for the two August and April samples shown in Figure 3.27.

Because of sedimentation and gelation it is not possible from the very Na-fluorohectorite powders to obtain samples where isotropic or nematic phase constitute the whole volume of the sample[12]. Figure 3.11 shows that the relative amount of the nematic gel increases linearly from 1 to 5 w/w% before gelation strongly takes place from 6 w/w%. Such a linear increase is similar to systems of gibbiste [121] and nontronite [41, 163] when the volume fraction is gradually increased. These systems have proved to undergo a true thermodynamic isotropic-nematic phase transition, where any attractive forces are not of importance for the nematic ordering. Their experimental values for the densities of the coexisting isotropic and nematic phases are in reasonable agreement to theoretical computer simulations [50][13], where dimensionless number densities, that is the number density $n = N/V$ multiplied by three times the diameter D, at zero polydispersity are found to be $n_{iso}D^3 \approx 3.7$ and $n_{nem}D^3 \approx 4.0$. If the polydispersity is 25%, which is least to be expected for our system, the densities are $n_{iso}D^3 \approx 3.5$ and $n_{nem}D^3 \approx 5.0$.

Since the sedimentation process in our Na-fluorohectorite suspensions may fractionate the particles samples, the size (or shape) of the particles in the

[12]When the suspension has phase separated, the isotropic or nematic phase may be extracted and dried. New suspensions of this powder might tell how the proportion of the nematic phase increases with increasing total clay volume fraction.

[13]This simulation is done for infinitely thin platelets, but platelets with a finite thickness do not give any major difference; $n_{iso}D^3 \approx 3.8$ and $n_{nem}D^3 \approx 3.9$ when the diameter thickness ratio is 10 [48].

isotropic phase may be different from the particles in the nematic phase. The values in Figure 3.28 for the volume fractions at the isotropic and nematic phase might still be used to give an estimate for number densities to compare to theoretical and other experimental [98, 121] results. The relation between volume fraction ϕ and nD^3 is for round platelets of diameter D and thickness t

$$\phi = n\frac{\pi}{4}D^2t = \frac{\pi}{4}\frac{t}{D}nD^3 \tag{3.1}$$

When polydispersity in taken into account, this can be expanded to [121]

$$\phi = \frac{1+\sigma_D^2}{1+3\sigma_D^2}\frac{\pi}{4}\frac{\langle t\rangle}{\langle D\rangle}n\left\langle D^3\right\rangle \tag{3.2}$$

where σ_D is the polydispersity of the diameter[14]. Rewriting gives

$$n\left\langle D^3\right\rangle = \phi\frac{4}{\pi}\frac{1+3\sigma_D^2}{1+\sigma_D^2}\frac{\langle D\rangle}{\langle t\rangle} \tag{3.3}$$

An exact value for the polydispersity of our suspensions of Na-fluorohectorite is not known, but AFM pictures have revealed that the polydispersity is quite high. To get estimated quantities, the use of an approximated average particle diameter of 2μm, which corresponds to a circle of same facial area, give the coexisting densities $n_{iso}D^3 \approx 0.4$ and $n_{nem}D^3 \approx 0.8$, when the polydispersity is set as high as possible and the thickness of the particles is 100 nm. The large difference between the isotropic and nematic densities, may be indicative of large polydispersity. These estimated values are at least a factor 10 smaller, when they are compared to predicted values of the accessible computer simulations. Since the Na-Fht particles are very irregular in shape, both Equation (3.3) and the theoretical calculations are far too ideal for our system too except a realistic agreement. Further computer simulations by Bates [51] has showed that the coexisting densities for the nematic-isotropic transition is dependent on the shape of the particles. The study showed that the transition densities for triangular particles, which may be a better approximated shape for Na-Fht than a round object, are almost one order of magnitude lower than particles of circular shape. The simulation data does not account for lath-shape biaxial particles with large differences between the facial dimensions, something which is representative for a great deal of the Na-Fht particles.

It is difficult to propose how much the large discrepancy to the existing theoretical calculations, must be attributed to unrealistic comparison of the simulation models or the incorrect calculations of the densities for the irregular Na-Fht particles. It is therefore difficult to be sure how much influence attractive and repulsive forces might have for the ordering of nematic and isotropic orientation in our Na-Fht suspensions. The high particle charge of the Na-Fht particles, do not make them hard-body. The use of effective diameter and effective thickness from the Debye screening length do not yield better agreement to the predicted data.

[14] The polydispersity corresponds to the standard deviation of the diameter distribution of the particles: $\sigma = \sqrt{\langle D^2\rangle - \langle D\rangle^2}/\langle D\rangle$

The different Na-Fht particles within the suspension may interact and behave differently from each other. Particles of large size (3-10 μm), may form nematic ordering in coexistence with an isotropic phase of smaller particles ($<$ 1 μm). The different strata of different nematic textures which form in many of our samples, could be due to the various Na-Fht particle shapes within the single suspension. Particles that are fairly lath-shaped, may form a different nematic ordering than particles which are for instance more round. This could be compared to the different nematic phases that form in mixtures of rod and plate-like particles [164].

3.8 Influence of Magnetic Field

Application of strong magnetic fields to the nematic phase of Na-fluorohectorite suspensions has with the use of diffusion-weighted magnetic resonance imaging of water [70], showed that the clay particles orient with their normals perpendicular to the direction of the magnetic field. The anisotropy of the diamagnetic susceptibility, defined in Equation (1.25) as the difference between the diamagnetic susceptibility parallel and perpendicular to the normals of the particles, is therefore negative. This is what has been found for other layered silicates such as bentonite [165], talc, kaolite, sericite [166–169] and Na-montmorillonite [170]. From this, the principal axis of the diamagnetic susceptibility can be said to lie parallel to the basal face of the silicate sheets. Since the shape of the faces of the Na-Fht particles may be considerable anisotropic, the magnetic susceptibility should be different along different directions of the particle face. Since the silicate sheet is homogeneous through the basal plane, it would be reasonable to believe the susceptibility is largest along the longest of the face directions. The influence of magnetic field to a nematic phase of a Na-Fht suspension might therefore to some extent give biaxial nematic particle order. This could change the optical properties of the nematic phase, since biaxial nematic order has an extra index of refraction and exhibit extended trirefringence.

In this thesis, the influence of magnetic field to suspensions of Na-Fht have been carried out by far lower magnetic field strengths than in the previous NMR experiments [70]. For our experiments the maximum field strength has with the use of permanent magnets been 1 Tesla, which is half of the 2 Tesla magnetic field used in the NMR study. Since the gel structure is highly reluctant to be affected by magnetic fields, the effect by applying a magnetic field of only 1 Tesla to our samples was beforehand expected to give restricted results. Magnetic field has been applied to all batches of samples with different Na-Fht powder types. Some samples have been examined for visual changes as the magnetic field is applied during sedimentation. This has not proved to have any noticeable effect in appearance of birefringence or at the phase behaviour otherwise in the sample.

For almost all samples which have phase separated into isotropic and nematic phases, the effect of magnetic fields is examined to all separated parts

of the suspension. The study provide that a phase separated suspension of Na-Fht for the most parts, that is the sediment, nematic gel or any isotropic phase, is unaffected by magnetic fields up to strengths of 1 T. The only part which has turned out to be affected by magnetic fields of 1 T and lower, is the nematic phase formed between the upper isotropic phase and middle nematic gel. This phase has also shown to be very apt to being disturbed by easy shaking or movement of the sample. From these observations, this phase could be characterized as a nematic sol. Depending on powder type, ionic strength and clay concentration, this phase forms from some few weeks to several months after sample preparation. The appearance of the phase is apparently different for the three Na-Fht batches. For the August powder, the phase is more birefringent and consists of more structured nematic domains than the suspensions of the April powder, which has a far greater tendency to be homeotropic. The November powder is most similar to the August powder, but the domain structure is usually less ordered and regions of homeotropic alignment are also more frequent.

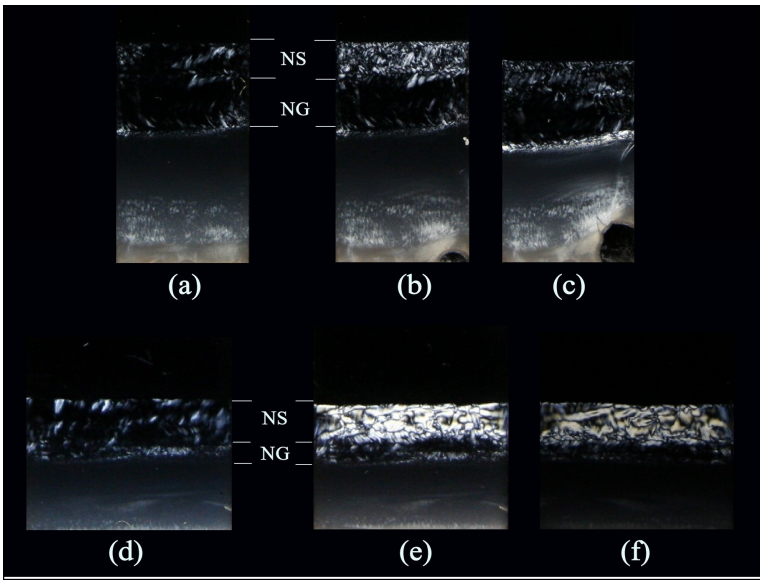

Figure 3.29: The effect of a 1T magnetic field applied perpendicular to two of the samples previously presented in Figures 3.13 and 3.16. (a) 1 w/w% April at ionic strength 10^{-3} M 3 months after preparation. (b) Nearly 2 hours in the magnetic field. (c) The sample has been standing undisturbed 1 day after it was taken out of the magnet. The birefringent slit right above the isotropic interface has arisen as effect of the air bobble at the bottom is penetrating the sediment. The dynamics can be inspected closely in Video 6 (see Appendix A). (d) 0.5 w/w% April at ionic strength 10^{-3} M before it was exposed to the magnet. The sample is 4.5 months from preparation and still have dynamics in the upper phase, but without any change in intensity of the birefringence. (e) Picture taken after the sample has been standing continuously 12 days in the magnet. (f) Picture taken with reduced light sensitivity after the magnetic field has been applied for 1 month. Some colour changes can be seen at the edges.

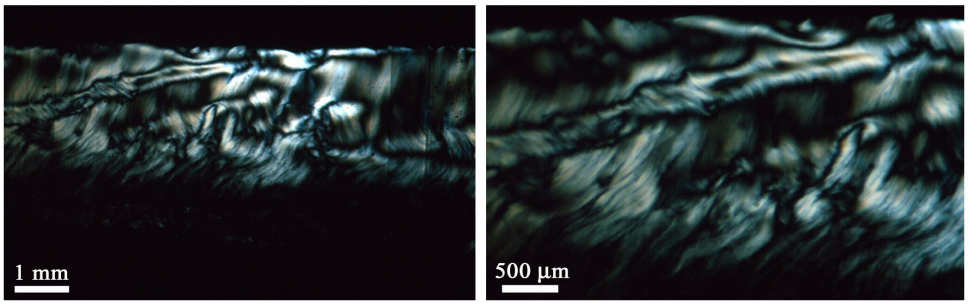

Figure 3.30: Optical microscope pictures of the nematic phase of the 0.5 w/w% April sample in Figure 3.29.

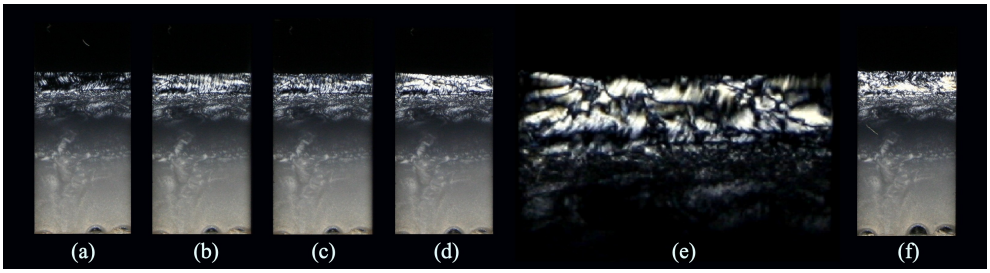

Figure 3.31: The upper region of a 1 w/w% August 10^{-4} M sample exposed to a perpendicular 1T magnetic field. (a) The sample is 4 months from preparation before it was placed in the magnet. (b) After 12 days in the magnetic field the sample has an increase in birefringence for the upper nematic phase, while the lower nematic phase is being unchanged. (c) Just one minute later some of the birefringence in the very upper part has decreased. This happen very fast right after the sample is taken out of the magnet, but slows down very fast after some few minutes. (d) After one further week in the magnet the birefringence has increased to larger domains. (e) A close up picture of the nematic phase after the magnetic field has been applied for 1 month. (f) This picture is taken after the sample has been standing undisturbed without magnetic field for one month.

The appearance of the nematic sol as it changes after the magnetic field is applied, is very similar for all the powder batches. Figures 3.29, 3.30 and 3.31 show the changes of the nematic sol for samples of April and August as the magnetic field is applied perpendicular to the sample walls. The effect of the magnetic field is observed as steady increase in birefringence all over the nematic sol. The first evident sign of increased birefringence can be seen already after the first minutes the sample has been standing in the magnet. The nematic sol of the April samples in Figure 3.29 has shown to undergo a faster change than what is observed in the August samples in Figures 3.31 and 3.32. The birefringence induced by the magnetic field, also retires faster for the suspension of the April powder. This may indicate the nematic sol of the April samples is more a true sol than the nematic sol in the August samples,

where the structure might be more gel-like.

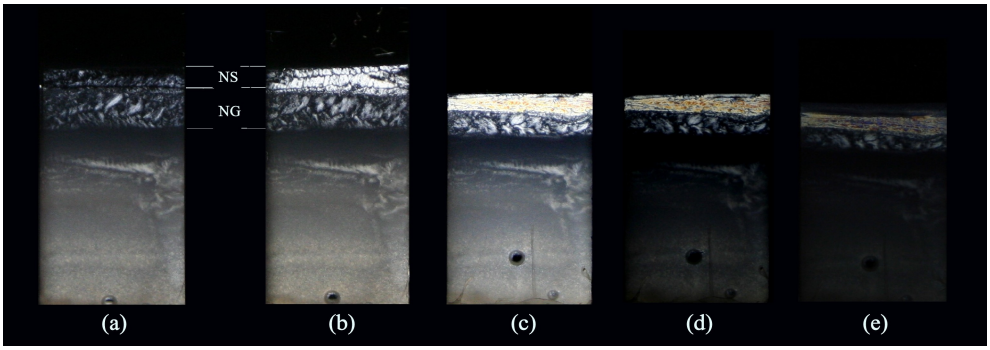

Figure 3.32: Detection of birefringence of a 1 w/w% August 10^{-4} M sample where a magnetic field has been applied perpendicular to the flat sample wall. (a) The sample how it looked before it was exposed to the magnet. Time from preparation is 8 weeks, and the upper birefringent part has separated into two phases distincted by a small dark boundary. (b) The changes in birefringence after the magnetic field has been applied for 5 days. (c) 12 further days in the magnet. The centre of the magnet was now moved a bit lower down, something that could have exposed the upper phase to a higher magnetic field strength. (d) With reducing the brightness of the picture one can better see some yellow colours in the birefringence. (e) After 10 more days in the magnet, other colours have arisen in the upper nematic phase.

Figure 3.30 and Figure 3.31 (e) show the nematic sol as it looks after the magnetic field is applied for 12 days to two samples of 0.5 w/w% April and 1 w/w% August respectively. Birefringent threads are prominently seen together with dark regions which to a great deal appear as distinct stripes both crosswise and between the birefringent threads. As clearly seen from the right micrograph in Figure 3.30, the birefringent threads are visible since they make an angle to the axes of the cross-polarizers. Extinction occurs when the threads twine into parallel or perpendicular alignment with the polarizer axis. This means the threads consist of particles oriented either parallel or perpendicular to the direction the threads go. Since the nematic sol is initially fairly homeotropic, it could be impulsive to believe the threads are similar to the transient stripes which arise in the non-uniform Fréedericksz transition as studied in the next section. However, the birefringent threads as appeared in Figure 3.30 differ from these stripes in many aspects. Either the faces or normals of the particles in the non-uniform Fréedericksz stripes lie along the horizontal direction of the stripe pattern. This could be irrelevant since rotation of the polarizers will change the black stripes to become the birefringent ones. But then the black stripes would be dominantly wider than the white stripes, something which does not take place in the pattern of the twining birefringent threads. The time of formation of the structure is also very different for the two cases. In the non-uniform Fréedericksz transition, the stripe pattern appear and disappear within some hours, while the birefringent thread structure is fully developed after several days. The threads in Figure 3.30, with

a thickness of around 60 μm, are much thinner than the hydrodynamic stripes, which are typical around 300 μm for the 2 mm thick capillaries. The smaller sample thickness of the 1 mm thick Vitrotubes is not enough to make up this difference alone.

The appearance of the nematic thread pattern after the magnetic field is applied perpendicular to the flat sample tubes, is most likely enhancement of the self-assembly formation of the nematic domain structure that takes place without external magnetic fields. Since the anisotropy of the diamagnetic susceptibility is negative, the normals of the clay particles may align in any direction perpendicular to the magnetic field lines. The pattern is therefore a mixture of bright birefringence and black areas with the presence of texture defects. A nematic single domain with director pointing in any particular direction along the front walls, is therefore not possible to attain by applying a static magnetic field perpendicular to the walls. A single domain with homeotropic alignment, should at the other hand be possible to achieve by placing the sample with the front walls parallel to the magnetic field, since this would prefer face-to-wall alignment of the platelets. However, when the sample is placed in this direction in the magnet, the field strength has been too low to successfully manage to obtain a complete homeotropic single domain. Since this is not an issue with 2 mm capillaries, the nematic sol can become fully dark in the direction perpendicular to the magnetic field. This is demonstrated in Figure 3.42, where it is seen that a time of hours is needed before the magnetic reorientation is stabilized.

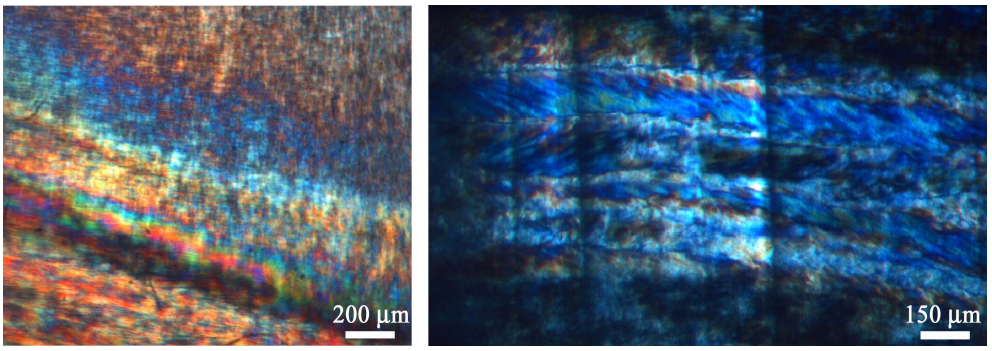

Figure 3.33: The nematic colour region in Figure 3.31 magnified using an optical microscope with crossed polarizers.

In some samples where the magnetic field is applied for a longer period of time, parts of the nematic sol have shown to become quite coloured. The appearance of colours in nematic phases is generally explained by the fact that the amount of optical retardation is a function of wavelength. Some colours may therefore pass through the analyzer with more intensity than others. This effect is prominently seen in Figure 3.33, which shows two micrographs of the magnetically changed nematic phase of the sample in Figure 3.32. It may be important to note that the decrease in height of the nematic phase that

has occurred after the 12 and 22 days action of the magnetic field, shown in pictures (c) and (e) respectively, might be the direct cause of the colour change. Some evaporation of the sample was shown to have taken place at some later time, from where it could be predicted that about 1 cm might have evaporated during the given time above.

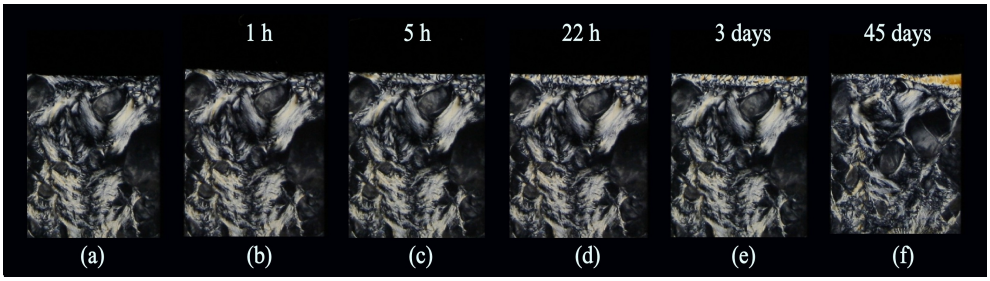

Figure 3.34: The upper region of a 1 w/w% April 10^{-4} M sample exposed to a perpendicular 1T magnetic field. (a) The sample is 9 months from preparation before it was placed in the magnet. (b) After one hour in the magnetic field the sample has a small increase in birefringence in the very upper nematic phase, while the rest of the sample is unchanged. The first minutes with the magnetic field of this layer show some dynamics where the complete layer moves to the edge. (c) 4 more hours in the magnetic field there is further increase in the birefringence of the top layer. Compared to the previous measurement, the dynamics in the top is now absent. (d) After 22 hours in the magnetic field a more profound effect can be observed. (e) After 3 days a brown-yellow colour has arisen in the magnetic affected part. (f) After the magnetic field has been applied for 45 days, the yellow colour has increased to a size visible to the naked eye.

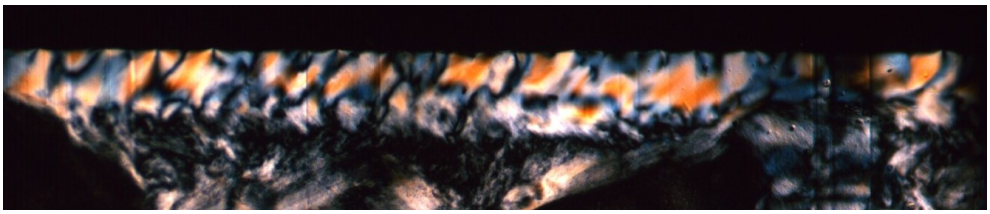

Figure 3.35: A micrograph of the upper region of picture (e) in Figure 3.34.

An example where the appearance of colours are certainly induced by the magnetic field alone, is shown in Figure 3.34. For this sample, the nematic sol is suppressed to a very thin layer above the nematic gel. The figure shows that a dark yellow colour has after 45 days of applied magnetic field arisen close to the right edge of the sample. When microscope is used, it can also be seen that the same yellow colour is weakly developed already after the first days. This is shown in Figure 3.35, where the appearance of the whole nematic sol is regarded after 3 days in magnetic field. By using a standard

interference colour chart [171], it is found that the yellow colours[15] correspond to retardation values from 300-400 nm. Using that the retardation is equal to the product of the birefringence and the sample thickness, Δnd, a value of the birefringence is found to be $3.5 \pm 0.5 \times 10^{-4}$. Since the birefringence is proportional to the nematic order parameter, it can be concluded that the application of magnetic fields to the sample slowly increase the order of the nematic phase.

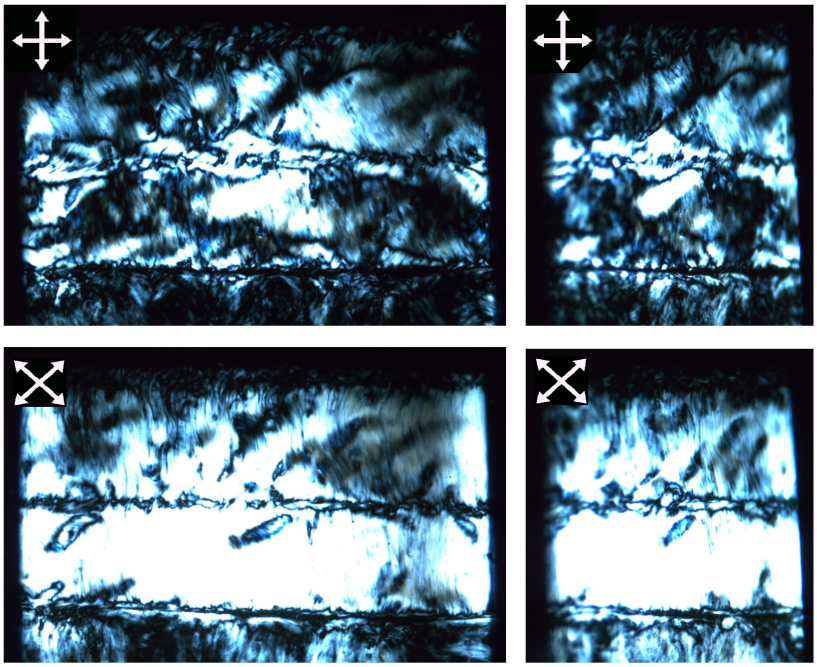

Figure 3.36: A magnetic field of 0.8 T is for 18 hours applied perpendicular to the nematic sol of the 2 w/w% April 10^{-3} M sample presented in Figure 3.4. The two pictures to the right are projections of the sample vertically rotated 45°. The sample is 8 months from preparation.

As presented in Figure 3.4, the settling and phase development of a sample of 2 w/w% April 10^{-3} M are carefully looked at for the first 8 months under the action of gravity only. For the picture representing the sample 8 months from preparation, a nematic sol of height 5 mm is seen to be very well-developed atop of the nematic gel. This phase is very fluid and is very easily affected by magnetic fields. Magnetic field strengths as low as 0.1 T has shown to yield slight distortion to the phase. Close-up micrographs of this phase is given in Figure 3.88 in Section 3.12.2. Figure 3.36 shows the changes of the phase after a magnetic field of 0.8 Tesla is applied perpendicular to the phase for 18 hours. The most conspicuous change is the rise to greater birefringence at any angle of the cross-polarizers. This indicates the magnetic field has increased the

[15]The yellow colours are of first order, which have the general description found in Table 1.2. A detailed colour nomination for the first-order colours can be found in reference [150].

overall orientational order of the phase. Figure 3.37 shows how the 45° crossed polarizers picture in Figure 3.36 looks when the light exposure is decreased. Concealed behind the bright birefringence, a texture of vertically streaming threads is clearly revealed across the whole nematic phase.

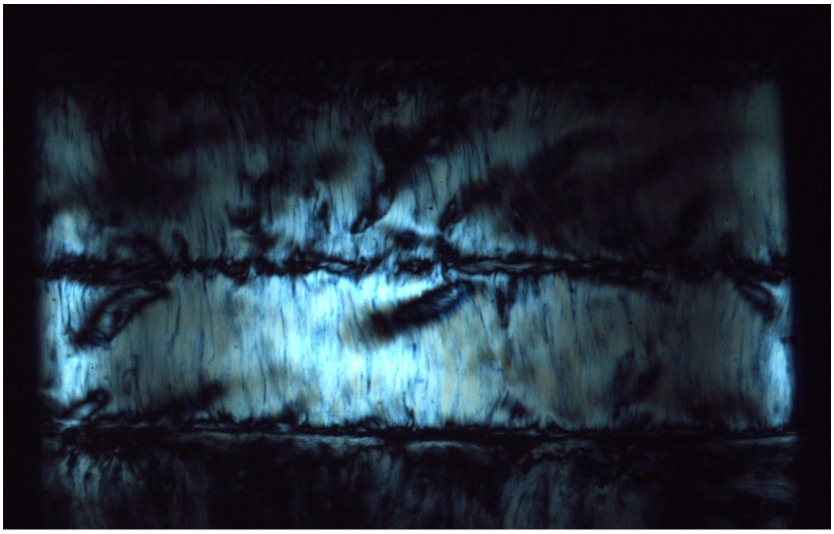

Figure 3.37: Reduced light exposure of the lowest left picture of Figure 3.36.

As discussed in Section 3.12.2, a peculiarity of the nematic sol for this sample, is its dividing into two equal parts. Two respective dark horizontal lines separate both these two parts and the lower part from the nematic gel. A proposal to explain the origin and cause behind the separation is for now not assigned, but optical considerations of the sample may give an idea about the orientational order in the boarders. As particularly seen for the black boarder between the nematic gel and nematic sol in Figure 3.36, the dark line does not vanish or change position during either rotation of the polarizers or sample. This may indicate that the two nematic phases are separated by a small slit of isotropic stratum, which eventually could be proposed as being a disclination line.

The long-time effect of magnetic field applied continuously to the nematic sol is studied and presented for the first 6 months in Figures 3.38,3.39 and 3.40. The experiment was started two months later than the first magnetic study in Figure 3.36. At this time, the amount of birefringence and structure of the nematic sol are at the state with regard to the absence of external magnetic fields. The nematic sol could now be characterized to consists of three strata, where a larger region is sandwiched between two smaller regions with less birefringence. With an exerted magnetic strength of ~0.85 T[16], the first changes are observed already after the first minutes. In one hour, the

[16]The inhomogeneity of the permanent magnets used in the experiments, may vary in field strengths of 0.1-0.2 T from edge to centre of the magnetic faces.

phase has become considerable more birefringent and the pattern of nematic domains in the middle part is enhanced to a more visible complex structure.

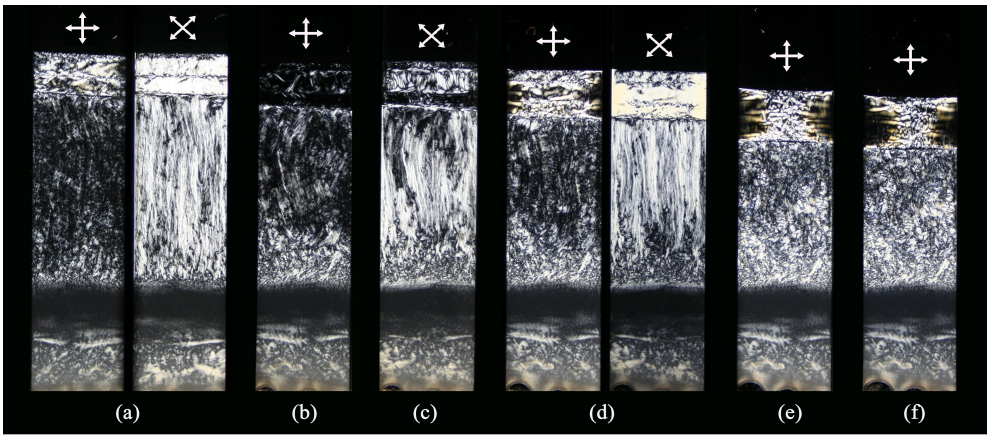

Figure 3.38: Continuation of the photo series in Figure 3.4 of 2 w/w% April 10^{-3} M. Now magnetic field is applied to the upper part, covering the whole nematic sol. (a) A magnetic field of 0.8 T is applied for 18 hours. The sample is 8 months from preparation and the appearance of the sample before it was subjected to the magnet is given in Figure 3.4. (b) 10 months from preparation and the sample has been standing without magnetic field in 2 months. The picture shows the initial zero field appearance of the sample in the magnetic long-time effect study, which results follows in the next pictures. (c) 1 hour in the magnetic field. (d) 1 month in the magnetic field. (e) 3 months in the magnetic field. (f) 4 months in the magnetic field.

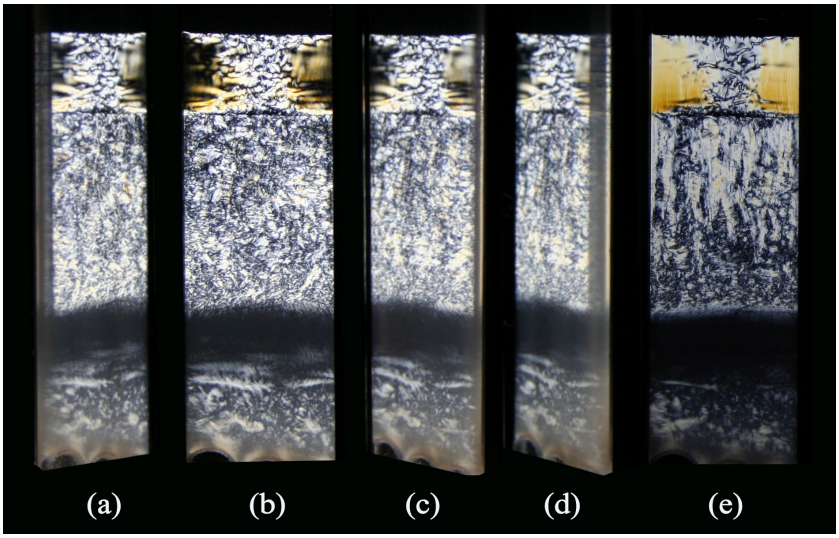

Figure 3.39: The appearance of the nematic sol when the magnetic field has been applied for 6 months. (a) Projection image of the sample rotated 45° between the two polarizers. (b) Viewed from the front. (c) Rotated 45° the other way around. (d) 60° rotation. (e) 45° rotation of the cross-polarizers.

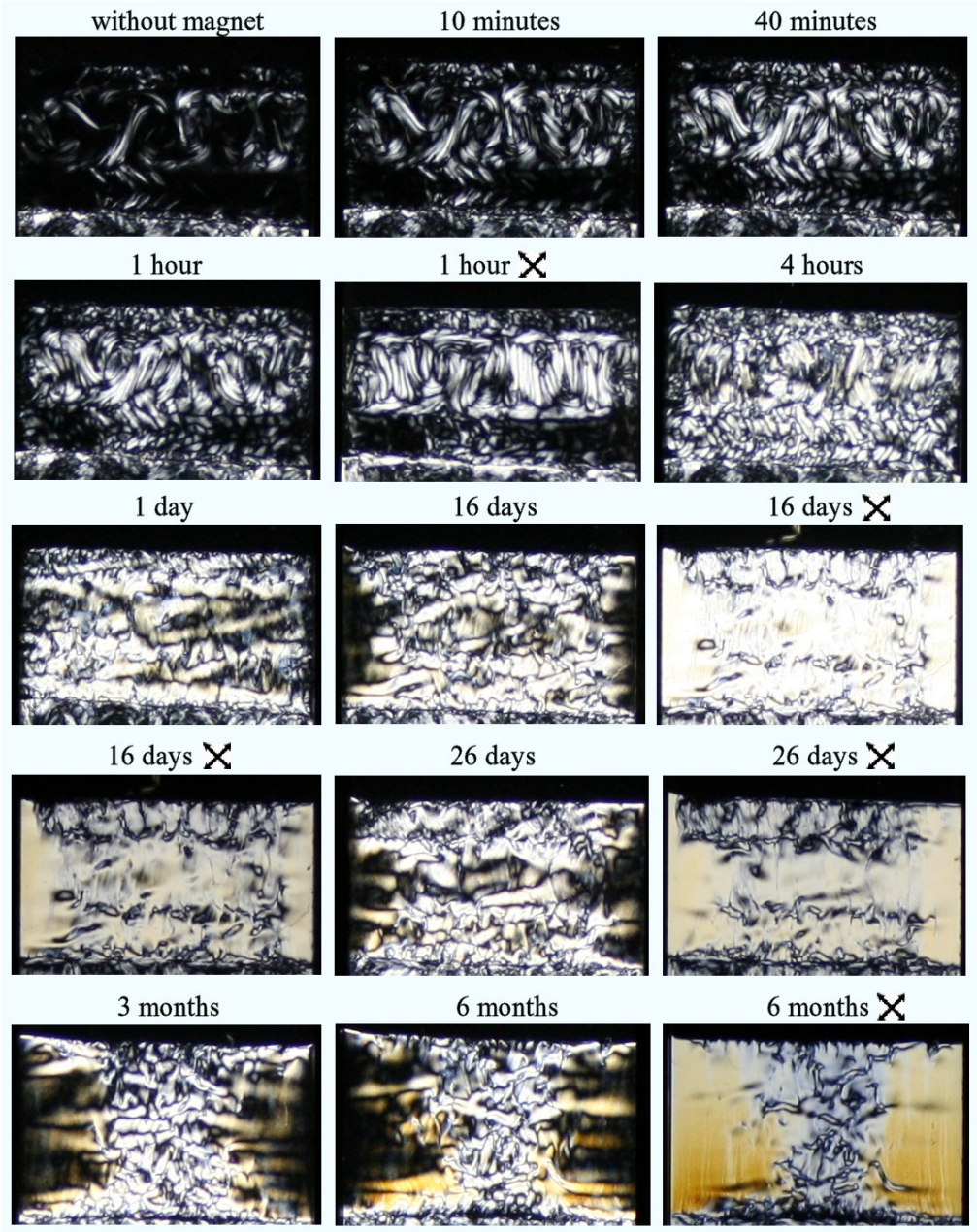

Figure 3.40: The nematic sol of 2 w/w% April 10^{-3} M continuously subjected to a magnetic field of 0.8 T over a period of 6 months. The polarizers are oriented vertical and horizontal for the pictures where the direction is not marked as 45°. The third picture representing 16 days, is taken with reduced light exposure to better be able to see the underlying structure of the phase.

For the two nearly homeotropic regions below and over the middle part, a square (rectangular) lattice structure of birefringence is greatly formed from 40 minutes to 5 hours. This structure may be explained in relation to the

inhomogeneous Fréedericksz transition discussed in the next section.

After one day, the birefringence is further increased and are much more regular (larger domains) and equally divided over the whole nematic sol. It is at this time no longer possible to distinguish the phase into separate strata when the axes of the polarizers are parallel and perpendicular to the sample edges. As the sample continues to be exposed to the magnetic field, changes of the texture are minimal for each day. During the next weeks and months a very slow reorientation process takes place in the phase. What can be seen for the pictures representing 16 days of employed magnetic field in Figure 3.40, is an increased order vaulted from the right and left edges. When the polarizers are parallel or perpendicular to the edges, these regions appear quite dark. When the cross polarizers are rotated 45°, the same regions become almost completely monodomain white. Figure 3.39 shows that the regions continue to appear dark when the sample is rotated 45°. This may indicate that the magnetic field tend to orient the particles with their normals directed vertically close to the edges.

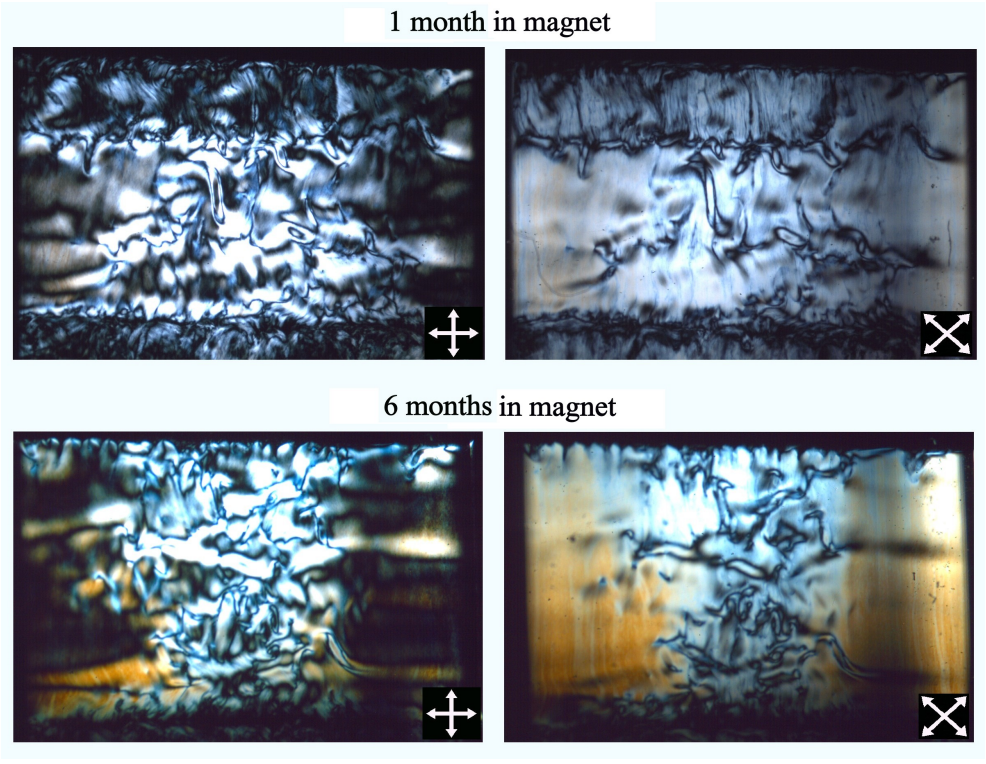

Figure 3.41: Micrographs of the nematic sol when the magnetic field has been applied for one and six months respectively. The pictures cover the whole nematic sol, which means there is one centimetre from left to right of the pictures.

The three different strata the nematic sol might be divided into in the initial state, are still apparent when the axes of the polarizers are at 45°. After one month, the upper stratum has reappeared for the vertical/horizontal

direction of the cross-polarizers. A close-up view of the structure is presented in Figure 3.41, where the formation of the upper part is similar to what is previously seen in Figure 3.36. When the sample continues to be subjected to magnetic field, the ordered edge regions not only further grow in size, but also undergo a striking colour change. The birefringence of the edge regions has after 6 months become considerable yellow. Because of the variable light conditions of the microscope and the birefringent camera setup, it is difficult to give a precise desription of the colour. Compared to the 1 w/w% April 10^{-4} M sample in Figures 3.34 and 3.35, the yellow colour for the 2 w/w% April sample may be slightly more pale. When it is taken into consideration that the birefringence of edge regions is considerable white, the birfringence for these regions is estimated to be $3.0 \pm 0.5 \times 10^{-4}$.

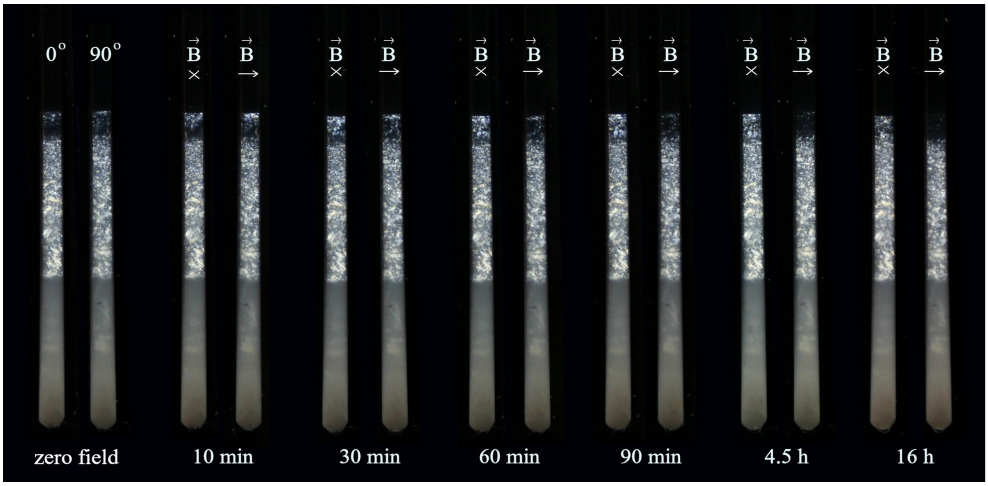

Figure 3.42: 3 w/w% November powder at 10^{-3} M salt concentration that has been settling for 2.5 months in a 2 mm capillary. The magnetic field of 0.9 T covers the upper part of the sample, but just the nematic sol phase on the top is being affected by the field.

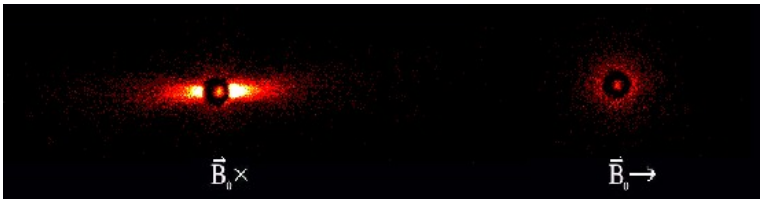

Figure 3.43: SAXS measurement of the nematic sol for a magnetically aligned November sample, which represents the orientation of the last two pictures in Figure 3.42.

3.9 Inhomogeneous Fréedericksz Transition

This section presents transient periodic structures in the Fréedericksz transition of nematic sol phase with uniform alignment. Periodic stripe patterns, which arise from an opposite director reorientation of particles with a distance $\lambda/2$, appear prominently in our samples of 2 mm round capillaries. Samples used for the experiment were well separated suspensions of the November powder with 3 w/w% clay and 10^{-3} M salt concentration. The samples had a settling time of 4-5 months before they were placed into a magnetic field. At this time sufficient height of nematic phase with low enough viscosity to give stripe pattern for magnetic fields below 1 Tesla is formed above the nematic gel. Before the measurement of the Fréedericksz transition, a magnetic field of about 1 Tesla was applied to the nematic phase until the particles reached an initial alignment as shown in Figures 3.42 and 3.44.

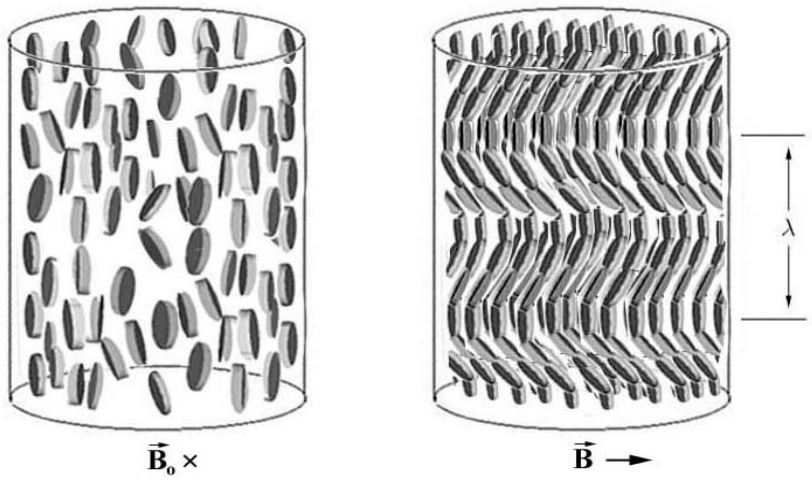

Figure 3.44: Orientational representation of how the particles may tend to align under the initial and reorienting magnetic field in the capillary.

Even though the nematic phase shows birefringence when the particles are viewed edge on, the phase may from wall-face alignment [70] be considered to consists of particles with normals mainly pointing in the same orientation. With this particle configuration, the samples were inserted into a magnetic field directed parallel to the initial director n_0 as shown in Figure 3.45.

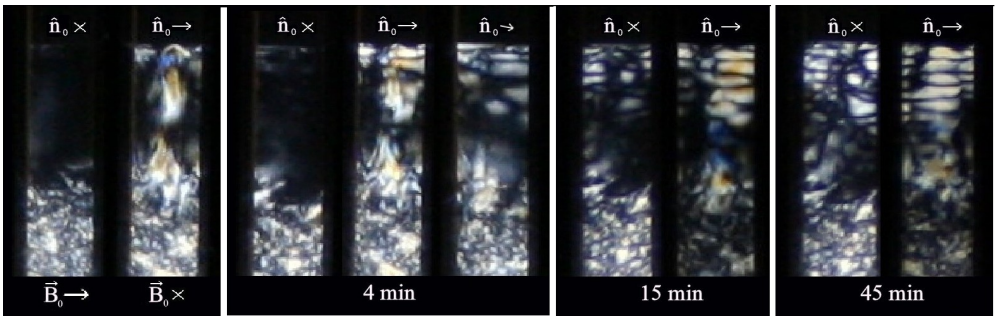

Figure 3.45: Pictures showing the development of a stripe pattern as viewed in different directions of the reoriented magnetic field. The sample has been standing untouched in a magnetic field B_0 of 0.9 T for about a week before the sample was rotated 90° in the same field. The first two pictures show how the nematic sol phase looked right before the reorientation of the magnetic field. The first picture show almost complete homeotropic alignment where most of the particles are oriented with their normals out of the paper. In the second picture, where the sample is rotated 90° to the former picture, the nematic sol phase is birefringent in the middle but dark close to the edges due to a stronger face-wall alignment there. For rest of the pictures, a magnetic field is applied in the same direction as the initial director n_0. Already after the first minutes, stripe patterns can be spotted in every direction of the phase. As shown by the last four pictures, the stripe pattern appears clearest when the phase is viewed in the direction where the magnetic field points in the same direction as the initial director.

Pictures with polarizer in the same direction as the magnetic field are then continuously taken with some minutes interval. As the magnetic field reorients the particles, transient periodic stripes gradually appear and disappear in the hours-long process of reorientation. In the pattern, the white stripes correspond to places where the particles are oriented with the director making an angle to the polarizing axis and the magnetic field direction. For the case of 1 Tesla magnetic field, the complete progress from start to end is by small reorientations at the time shown in Figure 3.46. From the photographs it is not possible to give an exact description of how the reorientation occurs for each particle and their interaction within the periodic assembly. In all the pictures it is possible to see the appearance of some roughly 0.1 mm thick domains that is slanted crosswise of the white stripes. These domains may look like large rods that in two adjacent white stripes are oppositely rotated towards the intermediate black stripe, as would be the case in a splay-Fréedericksz transition for rod-like entities.

When the sides of the capillary with homeotropic anchoring are considered as the boundary-walls, the initial magnetic field oriented platelet particles may viewed edge on look like rods oriented perpendicular to the director. This will for disk-like particles correspond to the bend geometry. With the homogeneous direction in the capillary, the induced Fréedericksz transition in the clay-capillary system is of the bend-splay geometry. The observation of periodic horizontal stripes in the suspensions of Na-fluorohectorite by using the

procedure in these experiments, is surprising and not understood.

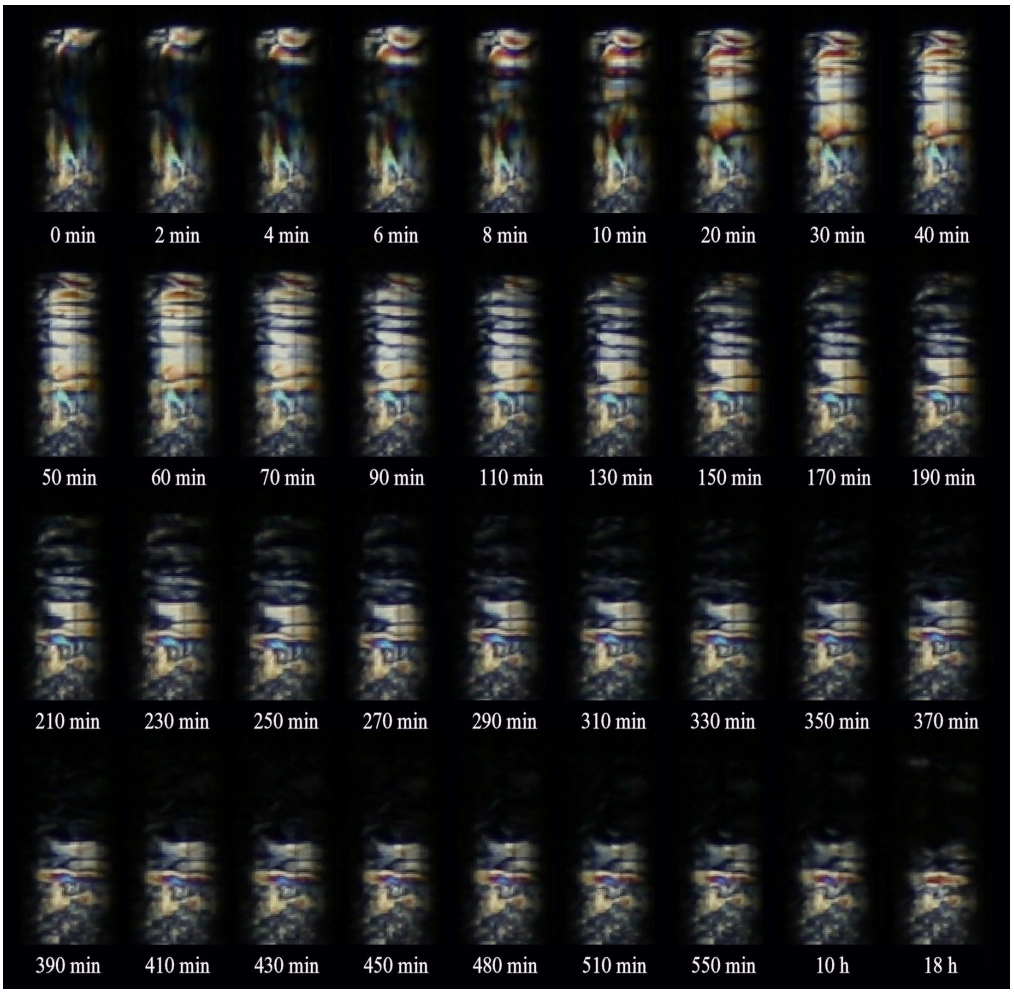

Figure 3.46: Photo series of the whole reorientation process of a nematic phase standing in a 1 T magnetic field. The particles are initially aligned with a magnetic field applied normal to the plane of the figure. A reorientation is then triggered by applying a magnetic field in the same direction as the director field orientation before the transition, that is in the horizontal direction. The first sign of stripes appears already after the first minutes, being best visible in the upper part. This might be explained by a slightly stronger magnetic field in the middle of the magnet. For 1 Tesla, the stripes appear at their best from 45 minutes to 2 hours. After about 8 hours, the most of the particles are reoriented to give a homeotropic alignment as viewed from the same angle. The vertical black stripes in the pictures are reflections from the magnet.

In systems of platelets with negative diamagnetic susceptibility anisotropy, the non-uniform Fréedericksz transition is different from systems with positive diamagnetic susceptibility anisotropy in that the first case possesses a degeneracy in tilt-angles directions perpendicular to the director axis. For a round flat

particle with negative anisotropy of the magnetic susceptibility, there is no way a magnetic field by itself can decide which orientation the final director will obtain. In other experiments on systems of disks with this behaviour [129, 142], the degeneracy is removed by rotating the magnetic field in the plane normal to the final director orientation. Since Na-fluorohectorite platelets suspended in water orient the normals of their faces perpendicular to an applied magnetic field, the same tilt degeneracy should be preconceived to occur in this system as well.

Since most Na-fluorohectorite particles are not round in shape, but have a different length and width, there is a possibility the magnetic field might align the particles in a biaxial nematic orientation. This additional length anisotropy should be able to break the tilt degeneracy. However, the tilt degeneracy might by apprehensive considerations anyway not be of concern, since the preferred wall-face alignment of the system would give a single orientation of the final director. The magnetic distortion should basically by such a perpendicular director change, resulted in vertical stripes along the capillary axis when the sample is viewed in the direction of the magnetic field. In the initial homogeneous direction, no periodic structures should appear. As opposed to this, the measurements of the Fréedericksz transition reveals that the periodic structures results in pretty obvious horizontal stripes along the direction of the magnetic field.

Figure 3.47: A region of homeotropic alignment in a 1 mm thick vitrotube where a magnetic field of 1 Tesla has been applied perpendicular to the plane of the figure. In the upper middle part of the left picture, a square lattice reorientation pattern can be observed. The picture to the right is the same experiment, reproduced one month later. This time elongated slanted domains appear with periodic distance.

In Figure 3.45, the photographs of the initial homeotropic orientation show a structure containing vague stripes with the same periodicity as those from the perpendicular direction. This structure is still different by having white spots surrounded with black extinction. The left 45 minutes measurement picture in Figure 3.45 shows a clear optically extinct brush along the middle of the capillary axis and two smaller lines with a half wavelength distance to the left and right. By being viewed from an initial hometropic particle alignment, this reorientation pattern gives a close resemblance of a two-dimensional square lattice pattern as observed by Kuzma [129] using static field on samples with negative anisotropy of the magnetic susceptibility. The appearance

of this structure is further been examined by applying a magnetic field along the director orientation of a sample that contains a complete homeotropic region. The results shown in Figure 3.47, give for a first measurement a pattern with birefringent squares, but in a later experiment the birefringent spots are elongated and adjacent as a slanted stripe pattern. Since this structure is considerable different than the stripe pattern observed in the round capillaries, it may not be a periodic formation due to the inhomogeneous Fréedericksz transition.

If it is to be taken for granted that Na-fluorohectorite behaves as ideally disk-shaped particles in suspension, a periodic stripe pattern should be formed in the initial homeotropic view by rotating a magnetic field in the plane perpendicular to the capillary or vitrotube axis. The observed horizontal stripes in the 90° particle reorientation in the static magnetic field applied along the stripe direction, is in contradiction to the formation of vertical stripes predicted by the fluctuation of the fluid flow and director rotation. To give an accurate description of the reorientation, it would be necessary to fully know about the viscous and elastic anisotropy of the nematic phase. The influence of gelation and other colloidal interactions and properties, makes the nematic phase in the clay suspension different from ordinary liquid crystals. From the pictures of the evolution of the periodic pattern, Figure 3.46, it can be seen that the first stripes form at the top near the upper isotropic phase. This could come from a viscosity distribution along the capillary axis which is lowest near the isotropic interface and highest in the overlap to the nematic gel.

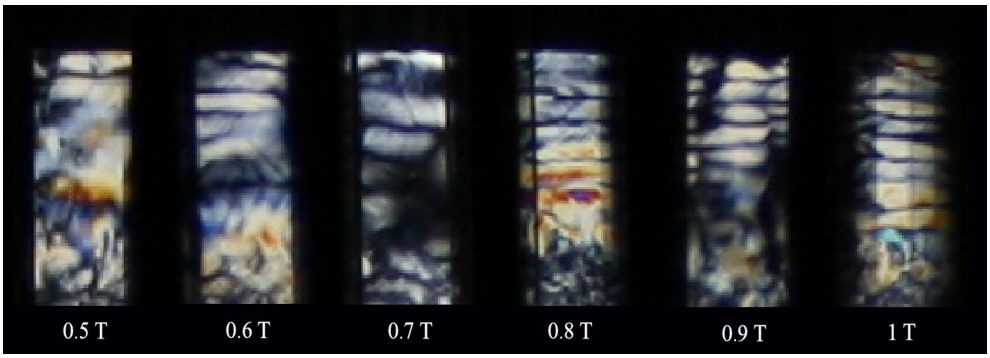

Figure 3.48: Stripe patterns for magnetic fields from 0.5 to 1 Tesla in the same sample. The pictures are when the stripes are at their best appearance. From the start of the reorientation, that is 2.4 hours for 0.5 T, 2 hours for 0.6 T, 30 minutes for 0.7 T, 2 hours for 0.8 T, 45 minutes for 0.9 T and 1.5 hours for 1 T.

A suggestion to explain the instability in the experiments, could be that the domains seen in the white stripes themselves undergo fluctuated rotation. At the disintegration of the stripes, the domains break up and the magnetic field and walls then reoreint the particles in the preferred new orientation. Contribution to the anisotropy of the elasticity and viscosity can come from a possible biaxial alignment which are due to elongated particle face shape. The

Fréedericksz transition is dependent on the geometry of the sample holder and its glass boundaries.

Table 3.1: Approximately values of the wavelength as measured out from the pictures of Figure 3.48. Except for 0.5 Tesla, the values represent the same position in the nematic sol.

$B(Tesla)$	0.5	0.6	0.7	0.8	0.9	1.0
$\lambda(mm)$	0.7	0.7	0.8	0.78	0.65	0.61

Figure 3.48 shows measurements of the periodic instability for different magnetic fields from 0.5 to 1 Tesla. The threshold value for the inhomogeneous Fréedericksz transition in the capillary system is found to be right bellow 0.5 Tesla. From the linear stability analysis, the wavelength and magnetic field are from Equation (1.31) supposed to follow a quadratic dependence, where the wavelength should decrease with increasing magnetic field. Because of irregularities in the structure, accurate and reproducible values of the wavelength for a specific magnetic field strength have not been obtained. From Figure 3.48 it is obvious there is a decrease in wavelength when the magnetic field is increased near 1 Tesla. Close to 0.5 Tesla, the wavelength looks to diverge, as is expected.

Some qualitative values of the wavelengths for the measurements in Figure 3.48 are for about the same position given in Table 3.1. For all the measurements the wavelength shows a tendency to be greater close to the nematic gel, something which could be due to higher viscosity there. The duration of the instability decreases with increasing field strengths, where the whole structure formation can last for over 3 hours for fields close to threshold and under 2 hours for fields of 1 Tesla. For low field strengths, the first sign of stripe formation appears after 10 minutes, while it for the highest strengths can take less than five minutes. The periodic structures are clearly transient phenomena, and are seen to decay soon after the magnet is removed. The lifetime is around 2 hours after which there is no longer is any pattern with systematic structure.

3.10 Wide Angle X-ray Scattering

This section contains results from the wide-angle X-ray scattering measurements carried out at Pohang Light Source (PLS). The Figures below show the CCD pattern together with a crossed polarized picture of the sample where the position and shape of the beam is marked. With a CCD size of 26 $\times$ 26.8 mm, (001) Bragg peaks from the lamellar clay stacks were achieved at a sample to detector distance of 12 cm with the beam wavelength being 1,24 Å.

The shape of the Bragg peak reveals information about particle orientation, where an anisotropic pattern indicates nematic ordering. The amount of anisotropy of the scattering tells something about the overall alignment of the

particles in the nematic phase. Scattering on a region where the particles are fairly well-oriented as in a nematic single domain, an order parameter could be derived from the length of the anisotropic Bragg arc. Scattering from a region of perfect orientation would give two opposite spots as from a single crystallite. Since the nematic orientation in most of the samples consists of a rather large director distribution, the WAXS pattern may from scattering of a nematic part the size of the beam, show a large part of the Bragg ring. If the nematic phase locally consists of a large random director distribution, the scattering pattern could almost be isotropic. The position of the Bragg ring gives information about the number of intercalated water layers that are contained in the clay stacks.

For the experiments two kinds of sample holders were used, 2 millimetres round capillaries and the 24×60×1 mm flat Davi cells. The settling time of samples before measurements varied from 1.5 to 3 months. Within this time the samples had clearly phase separated and at least one nematic phase was formed in all the samples. However, a nematic sol phase, which is crucial to study the magnetic reorientation of the nematic phase, were only fully formed in a few samples. The nematic sol phase in samples of November powder, which has shown to be very easily influenced by magnetic fields (Figures 3.42 and 3.43), was not developed with a height suitable to obtain successive results.

In most cases, the flat samples with 0.2 mm thick walls turned out to give good scattering patterns showing clear anisotropic Bragg rings[17]. Figure 3.49-3.58 show 14 scans for 7 different flat samples where anisotropic semi-circles are located with vertical emphasis, which means the particles tend to be oriented with the faces parallel to the bottom of the sample cell. This is contrary to what is seen for the round capillaries, Figures 3.64-3.67, where the scattering pattern shows horizontal anisotropy. The result that the particles are mainly oriented with their faces towards the walls in the capillaries, is as expected and is in accordance with previous experiments [63, 64, 70]. The reasons behind the difference in particle alignment for flat and round sample tubes, which show the same phase behaviour, is not clear. It is most likely due to the sample tubes geometrical difference, since both have glass walls made of borosilicate. The POM side and bottom walls of the Davi cell should not have major influence of the total particle orientation.

Figures 3.49-3.58 show the measurements on flat tubes, carried out on birefringent regions of samples with 1 w/w% August 10^{-4} M, 2 w/w% August 10^{-3} M, 2 w/w% milling machine crushed August 10^{-4} M, 3 w/w% crushed August 10^{-3} M, 3 w/w% November 10^{-3} M, 3% milling machine crushed August 10^{-3} M and 3 w/w% crushed April 10^{-3} M. Except the sample with April powder (3.58), all of these samples had clear prevalence of Bragg semi-rings. The August powder proved to probably be the most useful powder, and gave good results almost anywhere in the nematic phase. Measurements on the nematic gel for 3 w/w% milled August (Figure 3.57) show a very wide

[17] The key to obtain a good diffraction pattern in the nematic phase was to slightly move the sample (using the smallest steps) until the beam hit a part with well-aligned particle orientation.

distribution of (001) Bragg scattering, which tells that there is a rather spread order in this phase. On the other hand, for the domain structured nematic sol shown in Figures 3.55 and 3.56, the pattern is slightly more anisotropic than for the lower nematic gel. This makes sense, since the order should be expected to be greater in the domain structure. Because of the large size of the beam, it was not possible to do accurate measurements on the individual domain. By comparing these X-ray results to the close-up pictures in Figure 3.73, it seems that the domains consist of lying particles stacked upright on each other. The origin of why the particles prefer to align in this manner is though not understood.

The appearance of the birefringence in the samples used for these experiments can be divided into two kinds; the common "grainy" nematic phases that form by undisturbed gravity settling and "smooth" birefringence formed due to evaporation or any direct disturbances like shaking or air-bubble penetrations. Examples of the last type is shown in Figures 3.49 and 3.50, where it can be seen that the (001) Bragg peaks appear at 0.42 $Å^{-1}$, corresponding to a platelet separation of 15 Å[18]. For this position of the Bragg peak, 2 water layers are intercalated in the lamellar clay stacks [172, 173]. As observed from the results, this differ from the other nematic phase where the d-spacing is calculated to be 12.4 Å, which corresponds to the intercalation of 1 water layer. This findings have not previously been documented, and the physical explanation still remain to be stated. For the 2 w/w% August 10^{-3} M sample in Figure 3.50, it could be proposed that the reason the upper vivid birefringent region have two water-layer is due to change in salt concentration, which have occurred beacause of the evaporation. This can still not explain the same observation for the 1 w/w% August 10^{-4} M sample in Figure 3.49. Another explanation could be that the particles in the top are smaller and therefore better intercalate water. This could also account for the 1 w/w% sample if size segregation have taken place with smaller particles located above the sediment. The close interface to the air, which may give rise to a different particle orientation [174], could also be of importance. As can be seen from the figures, the birefringence for the 15 Å peaks are brighter than the birefringence elsewhere, which indicate a greater amount of order. It might be possible to imagine this somehow is related to the intercalation of water.

The diffractogram in Figure 3.51 for a sample of 2 w/w% milled August, shows there is anisotropy in a small region close to the bottom sediment where some weak birefringence can be observed in the cross polarized picture to the right. Since the anisotropic Bragg semi-ring is greatly vertical and has a short length, the birefringence should appear clearer by rotation of the polarizers. This measurement shows that orientational order may form in denser parts of the clay suspension. The position of the Bragg peak for this part is also different from the other nematic phases by appearing at 0.48 $Å^{-1}$ (d_{001} = 13.1

[18] Calculated from Bragg's law

$$2d_{001}\sin\Theta = n\lambda \tag{3.4}$$

with a scattering angle of 2Θ to the positions of the Bragg ring.

Å), which will correspond to HendricksTeller states of mixed intercalation.

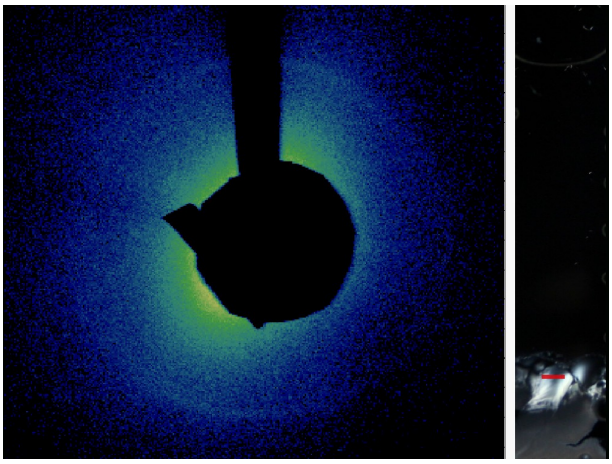

Figure 3.49: The nematic phase of a 1 w/w% August 10^{-4} M sample, where the director at the beam spot is about 25° from a vertical center line. The nematic phase is for the most a single-domain, but a four-brush schlieren texture can be seen to the left. The position of the peak appears at 0.42 $Å^{-1}$.

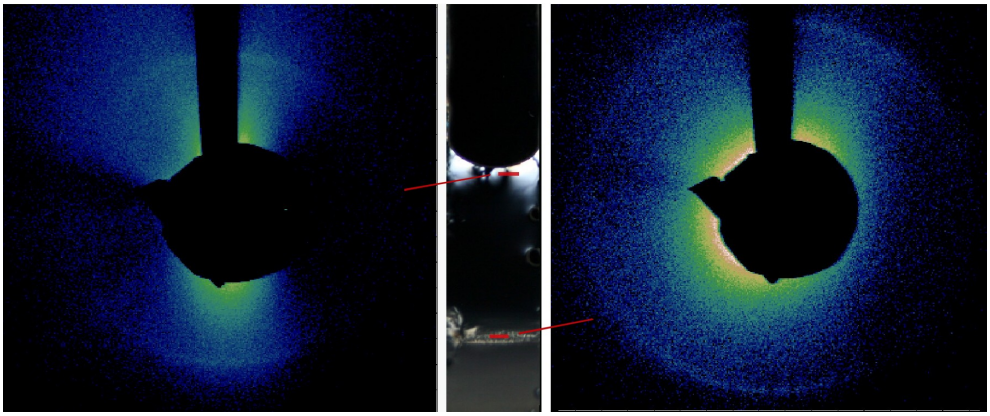

Figure 3.50: Measurements of two birefringent regions of a 2 w/w% August 10^{-3} M sample. The left is a scan of a birefringent region which has formed right under the air-liquid interface. The beam hits a dark region of the nematic phase, where most of the particles are aligned with the director pointing up. For this region Bragg peaks are at the two-water layered 15 Å position. The right scan is of a lower nematic phase that consists of vertically domain structure. The WAXS pattern shows that the clay particles of the domains are aligned with their faces laying. In the picture of the sample viewed between crossed polarizers, the domains are seen to point in different angles with a vertical curvature. This is the emphasis that gives the rather broad semi-rings of the WAXS pattern. The d-spacing of this phase is calculated to be 12,4 Å, corresponding to one water layer.

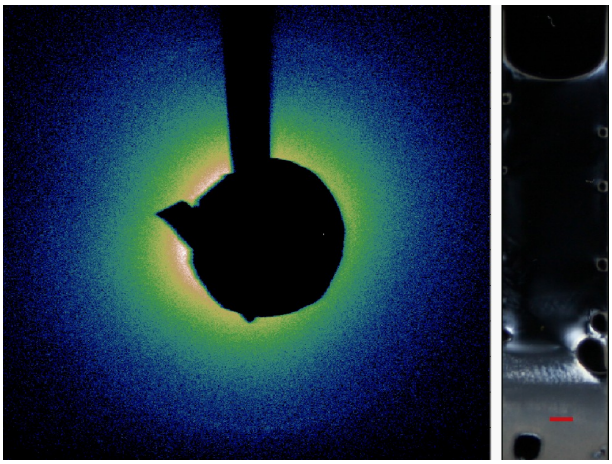

Figure 3.51: 2 w/w% milling machine crushed August 10^{-4} M. The beam hits a weak birefringent region situated between the sediment and isotropic gel. The appearance of a weak Bragg peak shows that there is anisotropy in the lower part of this suspension.

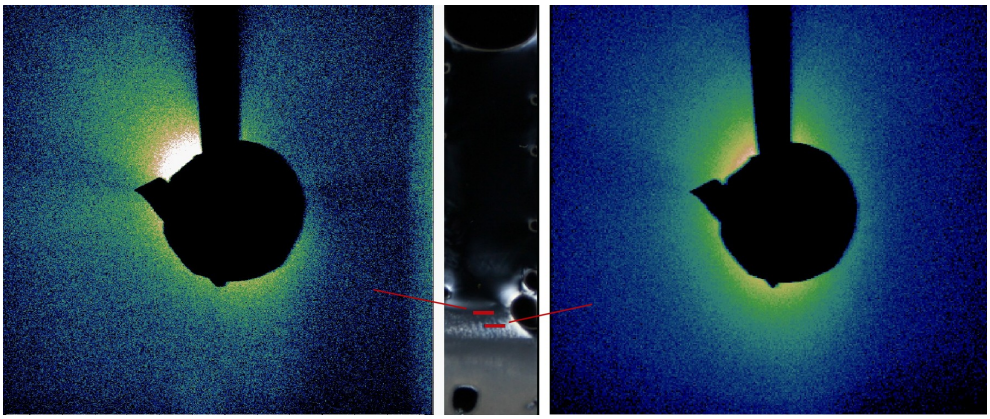

Figure 3.52: 2 w/w% milling machine crushed August 10^{-4} M. A magnetic field of 1 Tesla has been applied to the nematic phase for some days before the x-ray scan. No Bragg peak was achieved for the desired scan region, indicating the magnetic field did not give any reorientation on the phase. There were also no visible texture change anywhere in the sample. The boarder to the right is probably the air bubble seen just beside the beam.

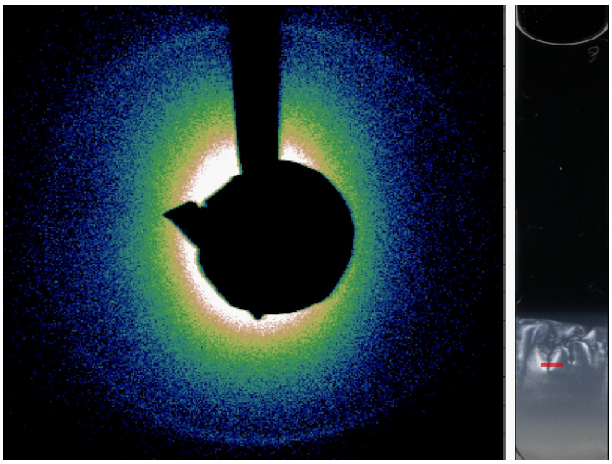

Figure 3.53: 3 w/w% crushed August 10^{-3} M. The beam hits a part of the nematic phase where the particles are ordered in a u-shaped manner. Scattering from the lower part gives rise to a rather broad and clear anisotropic Bragg peaks. This pattern proved to be restricted to a small fraction of the sample, and it was necessary to move the beam in small steps through whole of the nematic phase to finally hit a well oriented domain.

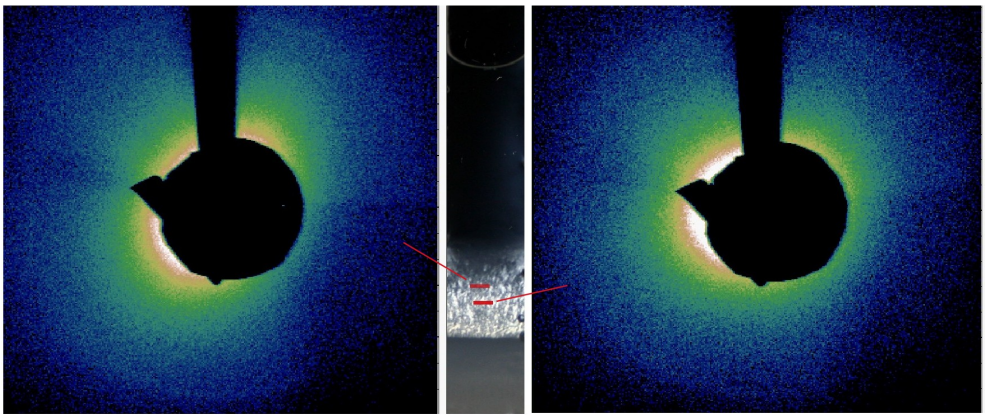

Figure 3.54: A sample of 3 w/w% November 10^{-3} M depicts Bragg peaks in the CCD image, without constituting a clear and well-defined anisotropic pattern. This is as expected since the nematic phase structure as viewed between crossed polarizers for this sample is typically of powders (random distributions) of small nematic domains. For this sample, scanning higher up than most intense birefringence did not results in any ring pattern.

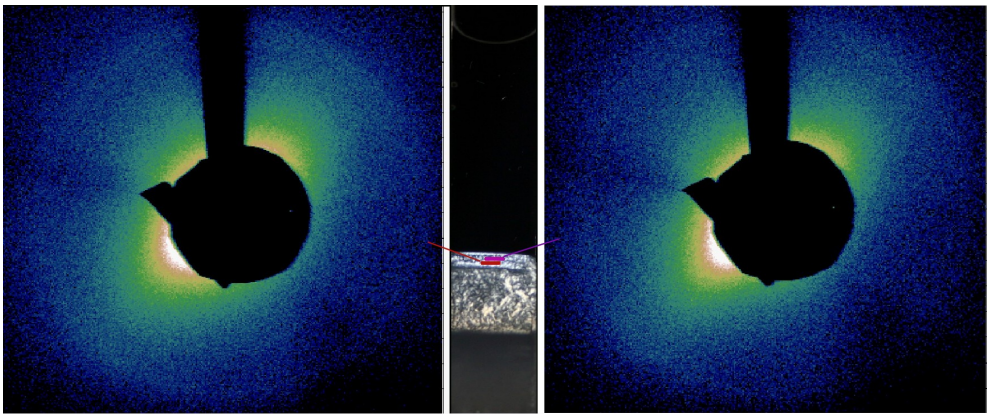

Figure 3.55: Two measurements of the domain ordering in the upper nematic phase of a 3 w/w% milling machine crushed August 10^{-3} M sample. The CCD image to the left is from a sample scan positioned around 1 mm lower than the one to the right. Both show a similar anisotropic pattern with Bragg peaks and strong small angle scattering showing a slanting particle orientation. A close inspection of the cross polarizer picture, reveals distinctive domains that are oriented in the same direction as the anisotropy in the CCD images. Compared to the right image scan, the anisotropy of the Bragg peak is less for the left lower scan which has an almost complete ring. Stronger birefringence for the same part in the sample picture coheres that there is a wider orientation distribution for this case.

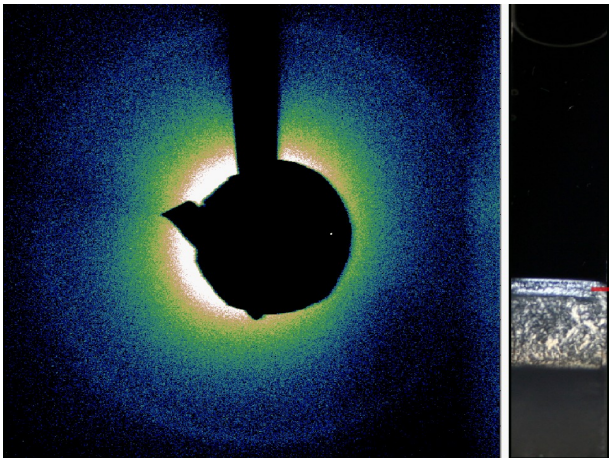

Figure 3.56: Another scan of the nematic domains in the sol of the 3 w/w% milling machine crushed August 10^{-3} M sample. The beam very closely skirts the right brink of the sample, and the appearance of a nearly whole intensity ring shows there is a pretty random distribution of the nematic domains in the area covered by the beam size.

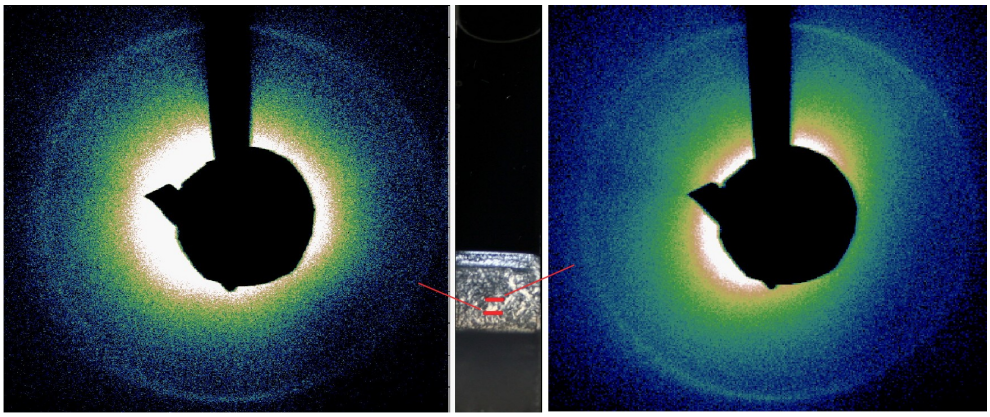

Figure 3.57: 3 w/w% milling machine crushed August 10^{-3} M. The extensive rings from X-ray measurements of two arbitrary positions of the nematic gel shown in the sample picture, show that this phase consists of nematic domains with directors steadily represented in every directions.

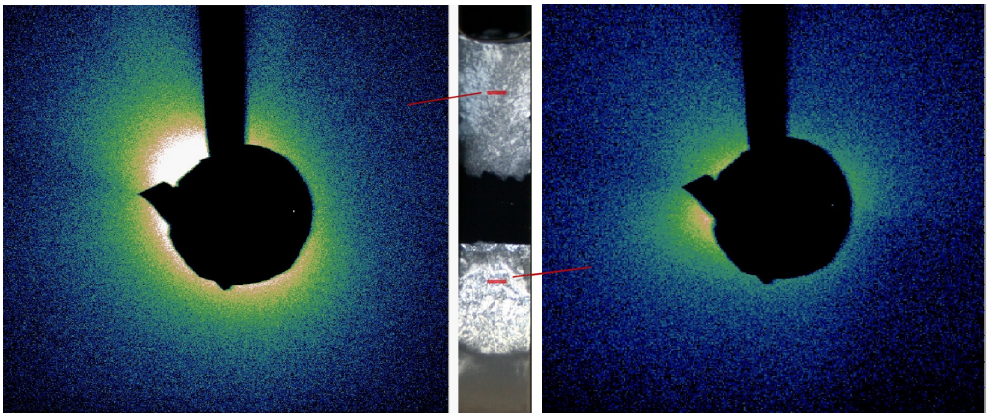

Figure 3.58: Measurements on the suspended birefringent region of the 3 w/w% crushed April 10^{-3} M sample did not results in any Bragg peak, but some anisotropic small angle scattering may indicate orientational order.

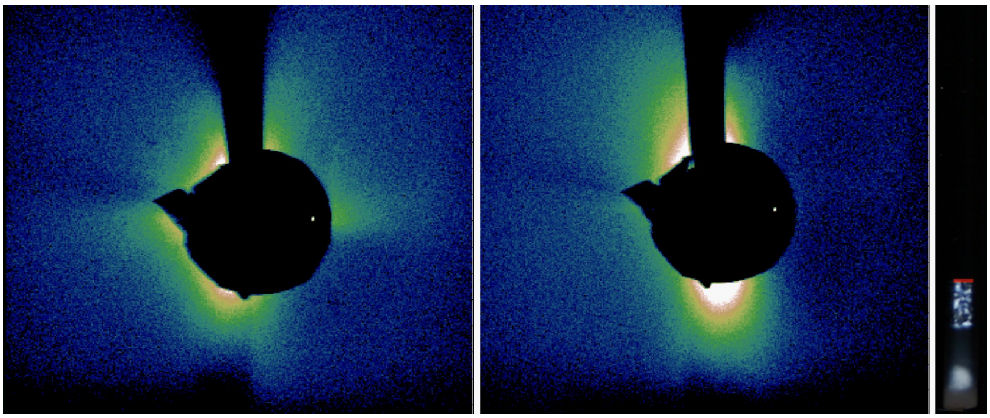

Figure 3.59: 0.5 w/w% crushed April 10^{-3} M. The beam hits at the water-liquid interface, which gives some very pronounced small angle scattering. For the image to the left, the sample is rotated 90 degrees.

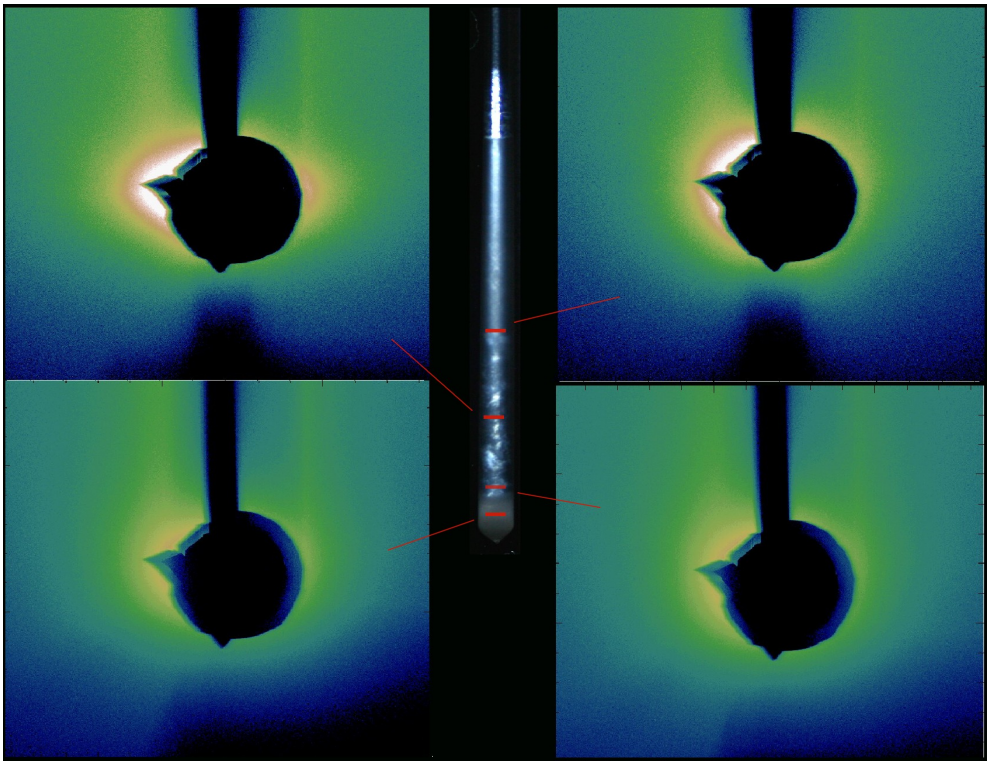

Figure 3.60: Four selected positions of a 3 w/w% crushed April 10^{-3} M sample, which has undergone settling for three months. Even though there are some areas with birefringence in the lower part, there is mainly isotropic ordering among the particles in this sample.

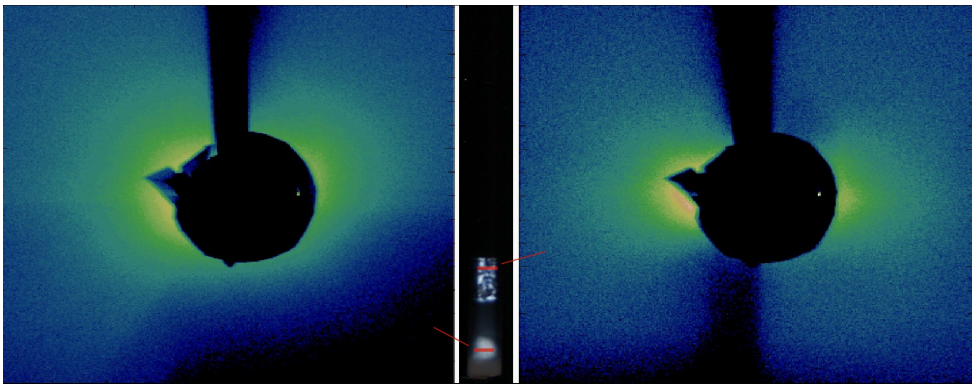

Figure 3.61: 0.5 w/w% crushed April 10^{-3} M. The same sample as above, but the beam is now lowered 1 mm down in the nematic sol for the right image and further 6 mm for the left scan. None of the birefringent regions of this sample gave Bragg peaks.

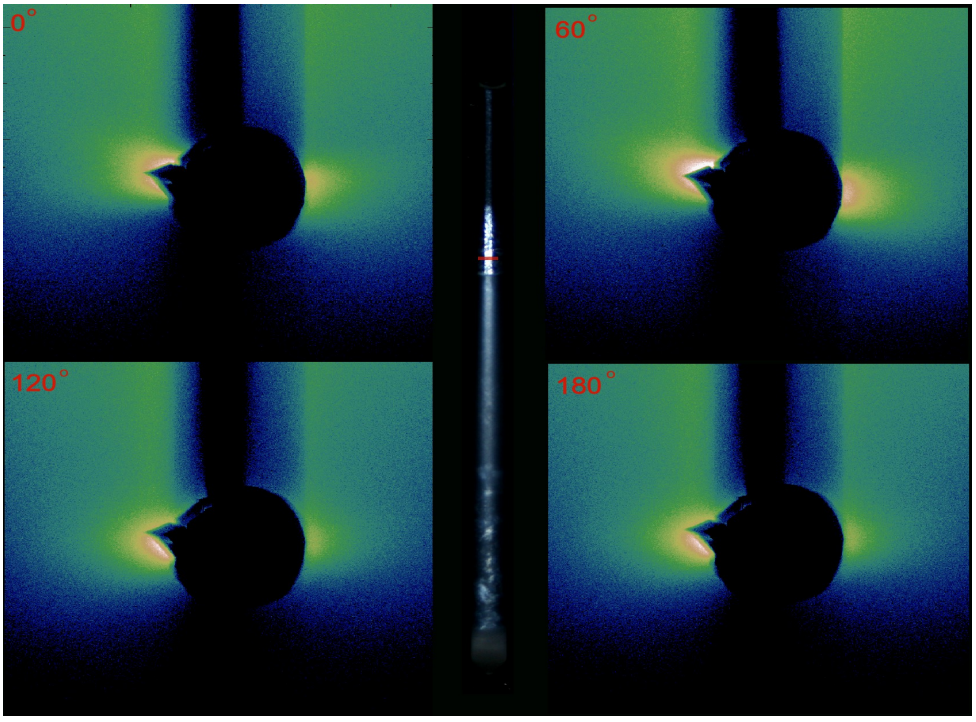

Figure 3.62: Scattering from the nematic upper phase of 3 w/w% crushed April 10^{-3} M for four different rotation angles. The horizontally oriented scattering without any change under rotation, shows the platelet faces are oriented parallel to the walls with the normals being isotropically distributed in the plane of rotation. The tilt variations of a present small inclination are in good accordance with the rotation angles. Small removals of the beam upwards the nematic phase give small random angles of the scattering direction. This reveals the nematic domains are profoundly large.

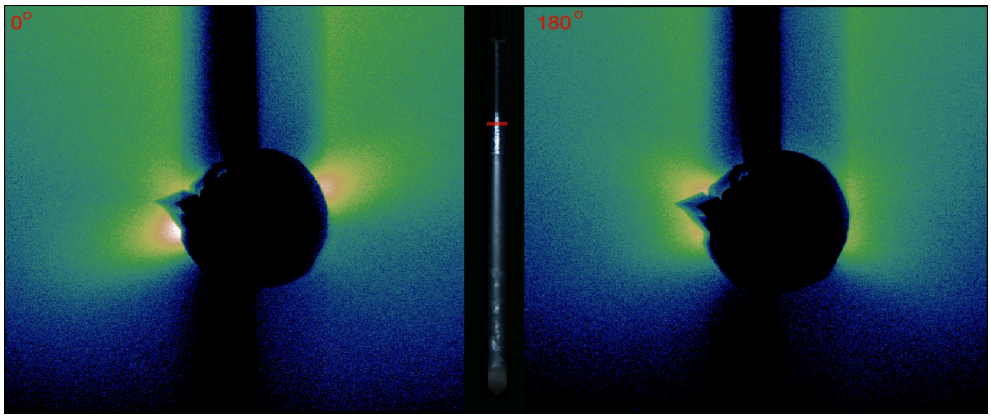

Figure 3.63: 3 w/w% crushed April 10^{-3} M

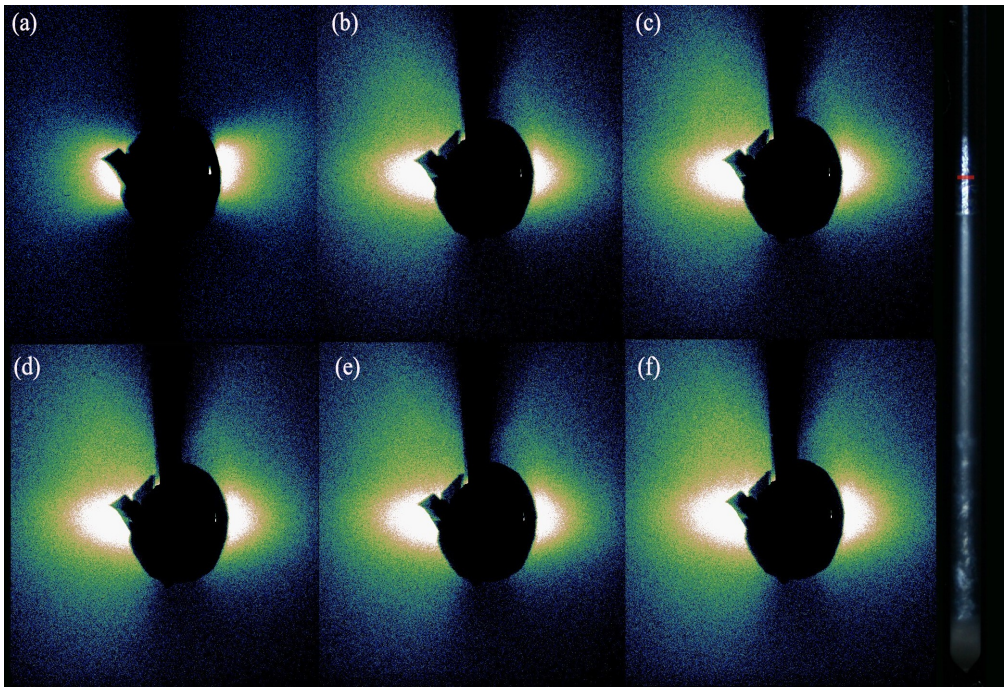

Figure 3.64: A scanning series of the nematic sol phase in 3 w/w% crushed April 10^{-3} M, where a magnetic field of 0.05 T is applied in the same direction as the beam. (a) Before the magnetic field was applied to the phase. (b)-(f) The time between each scan is around 25 minutes. It can apparently look like the nematic phase becomes more anisotropic in the direction of the magnetic field, but this is most likely due to the extraction variations of the original CCD data files.

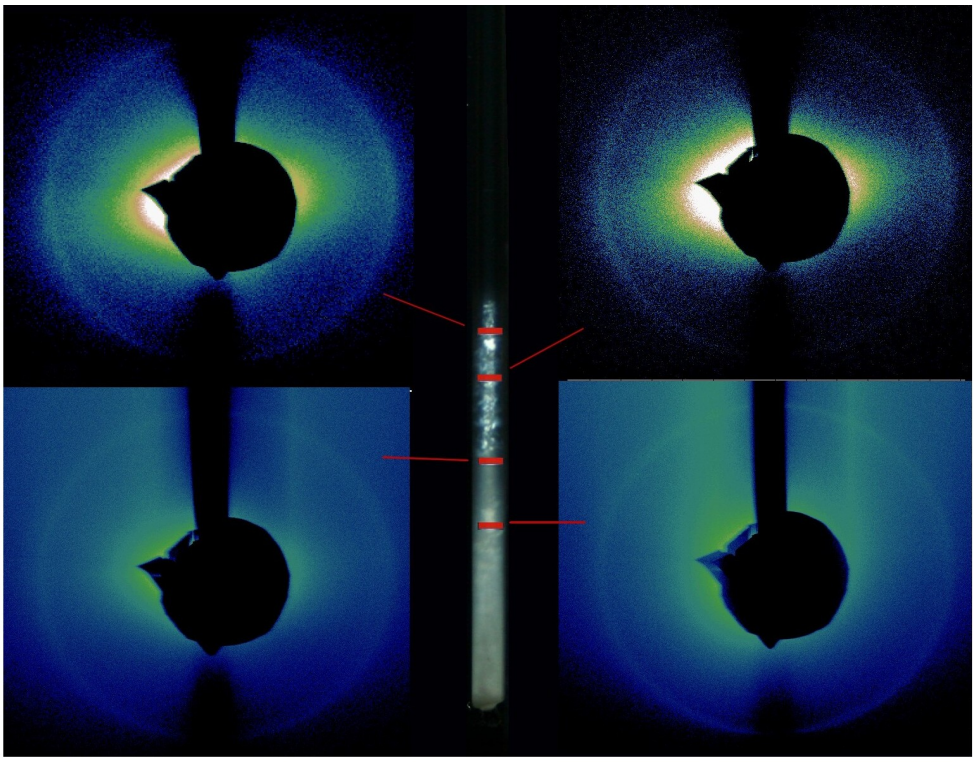

Figure 3.65: 2 w/w% milled August 10^{-3} M. The upper scans are from the nematic phase and prove that the particles tend to be oriented with their normals towards the glass walls. The lower left scan is a measurement in the transition region to the isotropic gel. The lower right scan shows an isotropic pattern for a low part 10 mm from the bottom of the sample. Even though some birefringence can be seen in this height, it is not expected the pattern would turn out being anisotropic. Since orientational order in this part of the sample is restricted to very small regions, the beam is most likely to not scatter from this particle order. The distribution of nematic order that could make up this birefringence, can also be highly random.

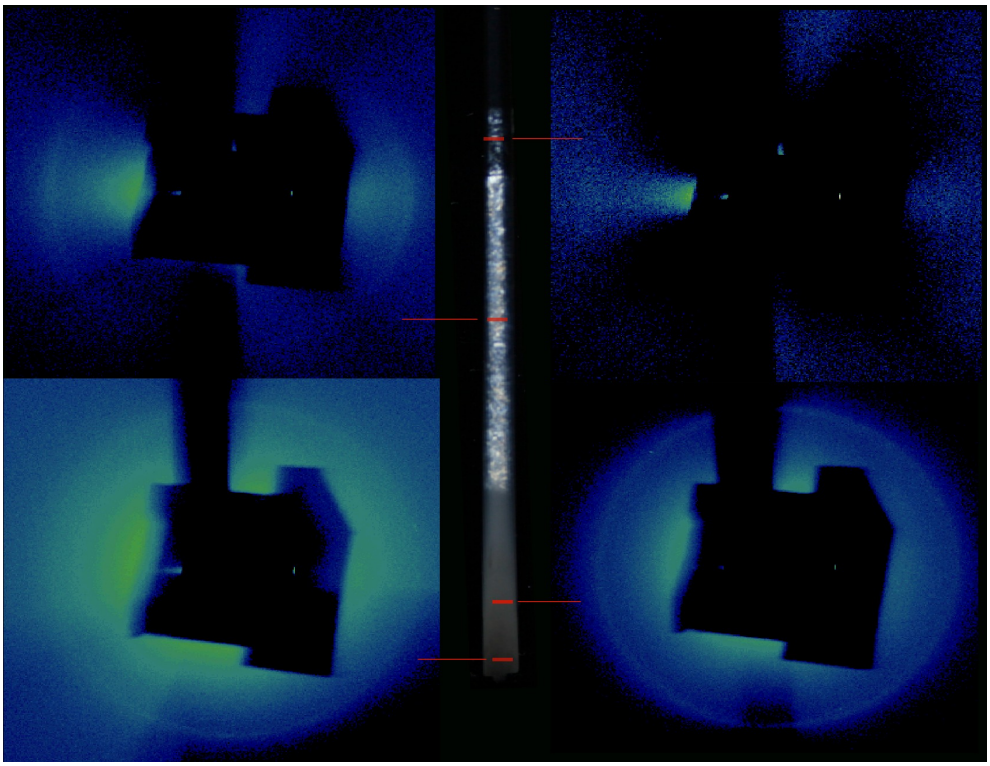

Figure 3.66: Measurements for four different parts of a 3 w/w% August 10^{-3} M sample. The upper scans show that the particles of the nematic phases are mainly oriented with their faces parallel to the glass walls. The signal is a bit weaker for the nematic sol, which makes it difficult to compare the degree of ordering against the nematic gel. The lower scans show that the sediment and suspension beneath the nematic gel can be considered being isotropic.

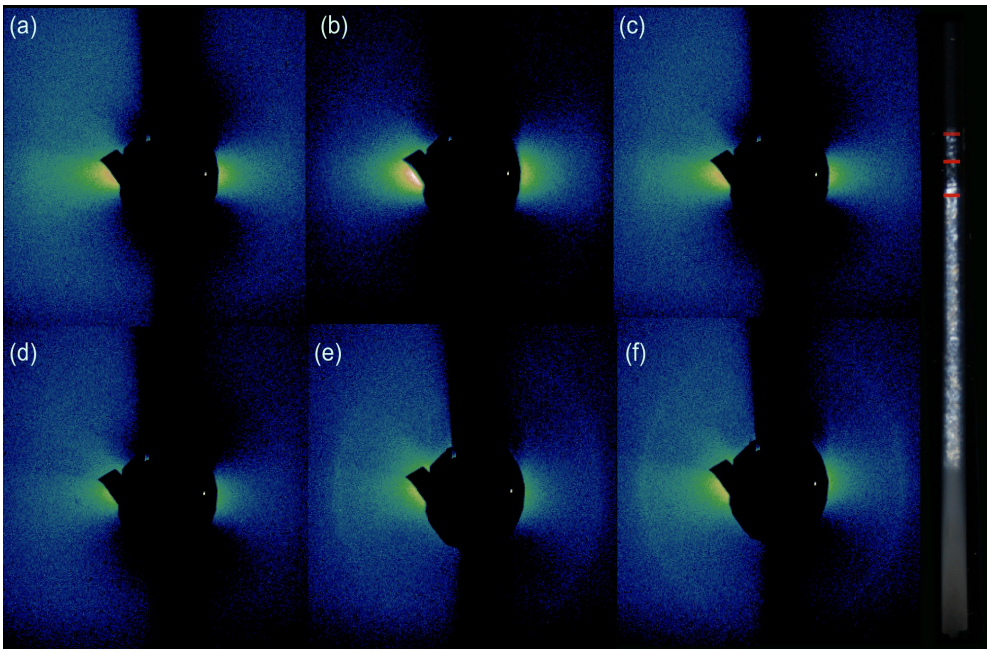

Figure 3.67: 3 w/w% August 10^{-3} M. A magnetic field has for two days been applied to the upper part of the sample, covering the whole nematic sol and about 5 mm of the top of the nematic gel. The three upper scan images are for the middle part of the nematic sol, where (a) is the measurement of the sample right after it was taken out of the magnet, (b) the sample is rotated 90° and (c) is original position after 30 minutes. (d) A scan 2 mm higher up, right beneath the water-liquid interface. (e) A measurements of the upper part of the nematic gel. (f) The original position after 1 hour[19].

3.11 Settling from Isotropic Sol

As shown in the previous sections, the upper nematic phases for samples in the final state can be said to have been formed in two different ways. The most pronounced nematic formation occurs short time after sample preparation, where a specific area gradually becomes more and more birefringent. This formation is on a time-scale of days very dynamic, where birefringent spots can be seen to fluctuate in undefined directions. When this dynamic has slowed down and a transparent isotropic phase remains at the top after the first weeks of settling, the nematic phase continues to grow in height several months after the preparation.

To shed more light on how this increase occur, an intensity profile of the upper isotropic phase has been extracted and compared at different times of some selected samples.

[19]We are not sure if this is really true, it is possible this measurement is actually quite another position.

The analysis is performed by image processing of the isotropic phase which to the eye appears completely black in the crossed polarized pictures. Since the efficiency of the cross polarizers is not 100%, some light transmits to the CCD of the camera. This results in some slightly different values for the pixels that construct the black parts of the digital picture.

Since the values of these pixels are very close or equal to zero, the image part of the isotropic phase is very sensitive to small changes in the surrounding light conditions. In addition, the analyzer and polarizer are not either totally equal crossed for every picture. Because of these experimental irregularities, it is not possible to directly use the variations of the pixel values themselves in comparison of different images. Instead, the changes that take place over time in the intensity height distribution of the isotropic phase may give some information about the particle settling process of the phase. If the intensity difference between the top and bottom of the isotropic phase decreases as time elapses, it reveals that particles must have settled towards the nematic phase.

Figure 3.68 shows an intensity profile for 4 different events of a sample of crushed August powder within a settling period of 10 months. The corresponding cross-polarized picture is shown to the right, where zero of the distance axis starts from top of the image. Since the picture does not show the whole sample, the upper part of the isotropic phase is not represented in the graph. The figure shows that one month after preparation, the intensity distribution of the isotropic phase increases comparatively much from top to bottom. At this time no birefringence in the transition region to the isotropic phase is observed. Two months later a small layer of nematic phase is formed atop of what was the previous separation boundary to the black isotropic phase. For this time, the slope of the intensity curve can be seen to be less than two months earlier.

When the sample is left standing for further seven months, the same tendency is observed to take place as the time elapses. At the time of six months after preparation, the nematic phase has increased in height and the slope of the intensity curve has undergone a considerable decrease. When the time of total settling has reached 10 months, the nematic phase has increased to a final height of around 4 mm. No further increase or any changes in the phase behaviour is observed after this time. As seen in the corresponding graph, the intensity is about the same in any height of the isotropic phase.

These results show that the nematic phase in suspensions of crushed August forms from very slow particle settlement from the upper isotropic phase. When the particles reach the bottom of the isotropic phase, the density increases and it becomes favourable for the particles to order in nematic orientation.

In the representation of the intensity profile, the transition from the black isotropic phase to the birefringent phase does not occur with a sudden inflection. By considering the graph and picture of the last 10 months event in Figure 3.68, it is seen that the intensity starts to increase considerable at a distance where the cross-polarized picture is still completely black to the eye. By taking a closer look at the full-sized original picture (Figure 3.71), it is revealed that the area close to the birefringence is slightly brighter than the rest of the isotropic phase. The most reasonable explanation for this observation,

would be that the birefringence reflects light into the dark isotropic phase.

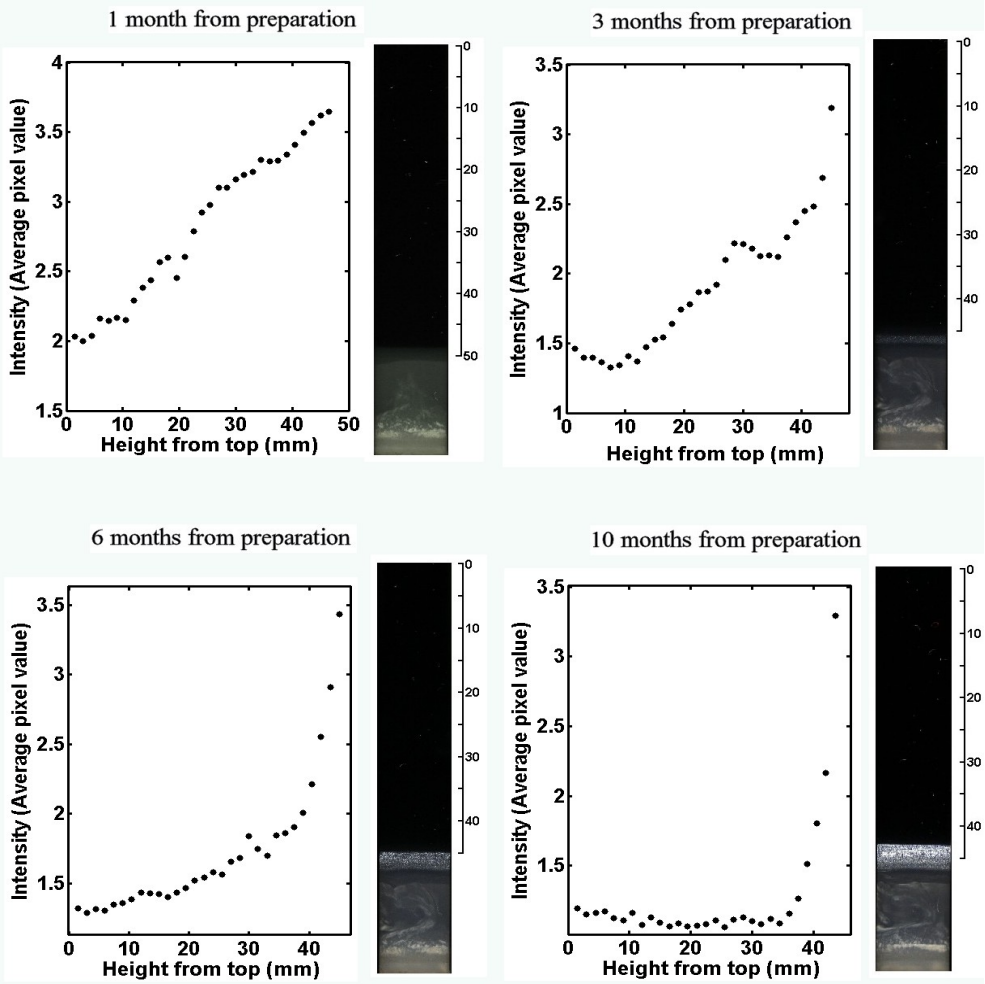

Figure 3.68: 10 months settling process of a sample of 2 w/w% mortar crushed August 10^{-3} M. The interface that is located at distance 50 mm from the top, starts to appear after 10 days of settling. This intermediate isotropic stratum continues to increase for about 6 weeks and reaches a final height of 0.4 mm. In the 3 months old picture, a small slit of birefringence is formed in the middle of the isotropic stratum. This birefringence starts to appear after 1.5 months of settling and continues to increase for 8-9 months. The birefringence that is located below the upper nematic phase, is formed in the first 1.5 months by fluctuations above the first sediment. After this time no further dynamics occur in this part. In the last picture the lower part looks a bit different because the axis of the cross polarizers is rotated 45° to the edge of the figure. This gives a slightly brighter appearance of the nematic phase, but it does not change the position of the boundaries.

Figure 3.69 illustrates the settling process and the formation of a nematic sol phase of a sample of 3 w/w% November 10^{-3} M during a period of 9 weeks. After this time no further changes occurred, and the last picture therefore

represents the final state of this suspension. By height considerations, it is revealed that the nematic sol forms both by settling of the nematic gel below and from settling of the isotropic phase above. From the intensity profiles it may seem that particle settling from the isotropic phase is of least influence of the formation of this nematic stratum.

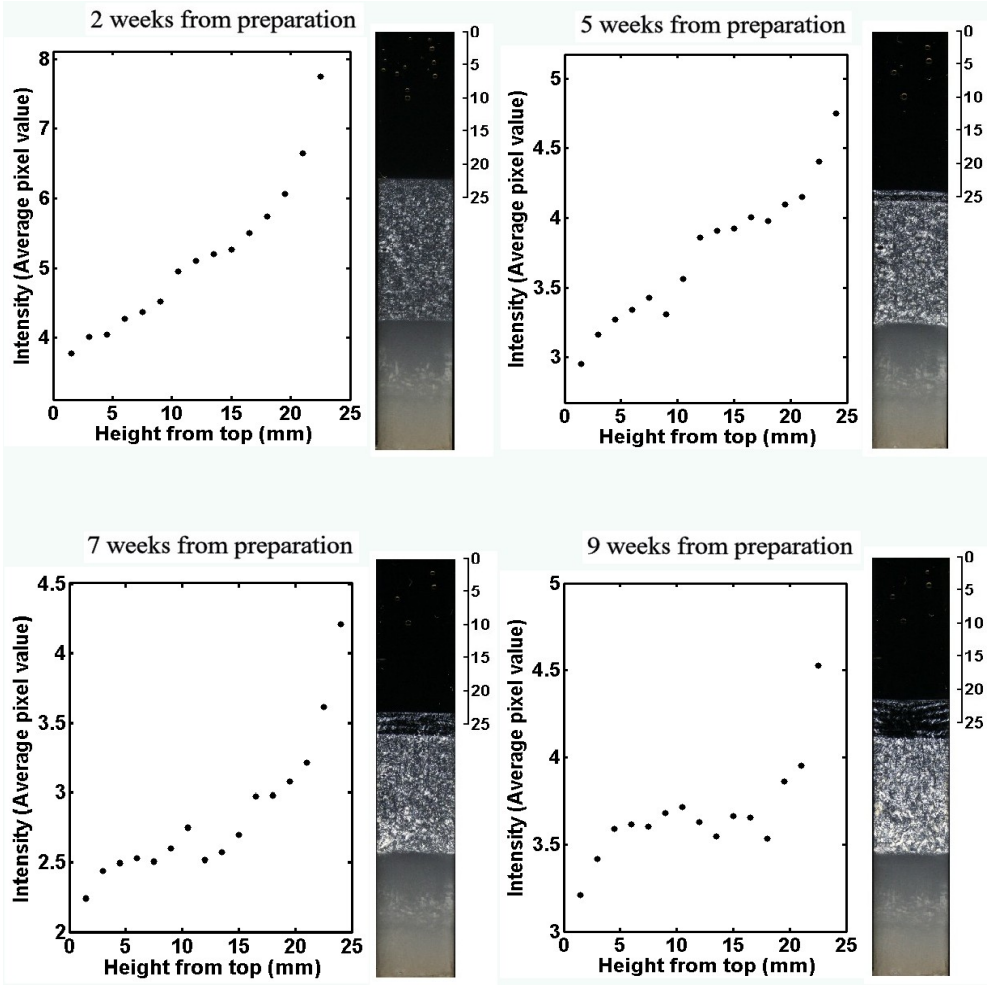

Figure 3.69: The settling process of a suspension of 3 w/w% November 10^{-3} M. The first upper graph shows the pixel intensity distribution of the upper isotropic phase when a clear boundary to the nematic phase is developed. The sample has then been settling for two weeks, and the intensity in the isotropic phase has a steady increase over the considered distance of 20 mm. At the next event, a second nematic phase is started to develop over the first nematic phase. The first sight of this phase, appeared after one month. The last two pictures, show how the phase has developed after 7 and 9 weeks of total settling. The corresponding intensity profiles show that particle settling from the upper isotropic phase is at the end. After 9 weeks, no further increase of the phase is observed.

Figure 3.70 shows a sample of 3 w/w% August $5{\times}10^{-4}$ M with a total

settling time of 13 months. From 4 to 7 months, the nematic phase does not grow considerably in size. The intensity distribution of the isotropic phase also does not undergo any major changes. From 7 to 13 months an extra height of birefringence has built up on the nematic phase. Since the intensity at the top and bottom of the isotropic phase is almost the same already for the 7 months sample, the last graph does not give any further information about the settling in the phase.

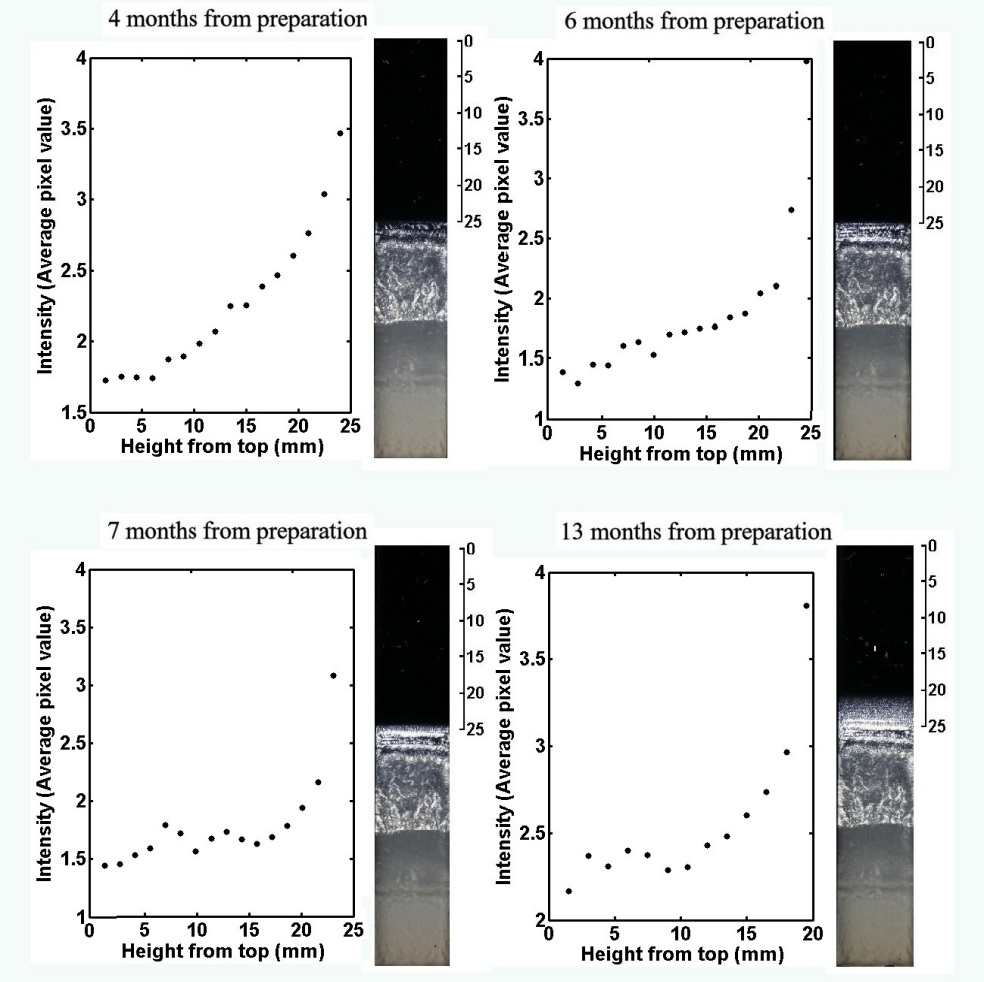

Figure 3.70: The pixel intensity distributions of the dark isotropic phase in the cross-polarized pictures of a sample of 3 w/w% August 5×10^{-4} M. For the first graph and picture, the sample has already been settling for 4 months and the suspension has separated into all of its final phases. From this time, only the upper nematic phase undergoes further development. The intensity profile at 6 months from preparation, show that there is not a very large intensity difference between the upper and lower part in the isotropic phase. One month later, the nematic sol has increased about 0.1 mm in height and the birefringence has become slightly brighter. The 13 months picture shows an extra height of birefringence, which in structure is similar to the nematic phase formed for crushed August powder. At this time about 10 mm of evaporation has taken place in the sample.

It is possible that an eventual height distribution is too small to be detected in the image, but it could simply be more or less equal through the whole phase and the particles are still settling. In a close-up picture of this upper nematic phase, shown in Figure 3.72, the latest nematic layer has a texture that is similar to the nematic phase seen for the crushed August sample (Figure 3.68). This may indicate that the particles that remain in the isotropic phase after

7 months, is of a size comparable to the particles in the nematic phase of the crushed powder. From Figures 3.68 and 3.70 it is seen that the formation of this "fine-corned" nematic phase slowly forms in a process of several months for the suspension of both crushed and not crushed powder.

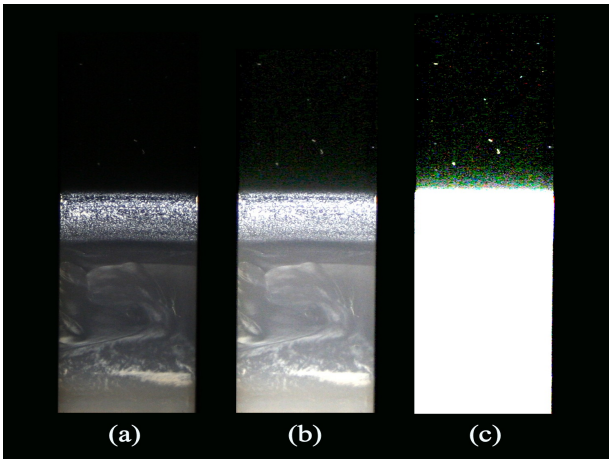

Figure 3.71: Image adjustments of a sample of 2 w/w% crushed August 10^{-3} M to be able to see invisible intensity variations. (a) By very close inspection of the original picture, it can be seen that the black area right above the birefringence is slightly brighter than the rest of the isotropic phase. By enhancing the brightness and contrast, (b), and further tone adjustment, (c), this variation becomes very clear.

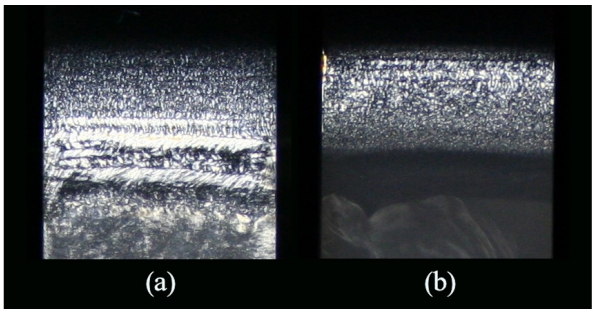

Figure 3.72: Close-up images of the nematic phases of suspensions of 3 w/w% August 5×10^{-4} M (a) and 2 w/w% crushed August 10^{-3} M (b). The suspension of the not crushed sample can be considered to have 3 nematic phases, where the texture of the upper nematic phase is similar to the one observed for crushed powder.

3.12 Nematic Phase Particle Alignment

The orientational order of the particles in the nematic phase of a sample is usually random distributions of small regions with well-oriented nematic order. The texture throughout the phase appears as patches of birefringence scattered

randomly around the phase. Over a large area of the phase, the total nematic particle distribution can be almost isotropic (Figure 3.57). Even though an arbitrary particle in the nematic phase can be oriented in any direction, there is for most samples a tendency of particle alignment along a specific direction. In long round capillaries, the particles in a nematic phase of random birefringence tend to be oriented with their faces along the walls. For flat sample tubes, the particles have on the other hand showed to have a tendency to be oriented with their faces lying towards to the bottom. The average particle orientation of a visible disordered nematic phase is best found by the use of X-ray scattering. When there is order on a macroscopic scale in the nematic phase, different optical considerations of the sample is useful to determine the orientation of the particles.

The orientation of the particles of a nematic single domain is easily detected by rotating the axes of the polarizers. If the particles are oriented with their normals in the plane of rotation, extinction of light occurs when the normals become parallel or perpendicular to the axes of the polarizers. The nematic phase also appears dark when the particles are oriented with their faces against the plane of the polarizers (homeotropic alignment). In this particle correlation, the nematic phase continues to appear dark in any direction of the cross polarizers. It becomes birefringent if the nematic sample is rotated between the polarizer and analyzer.

In almost all of our samples of Na-fluorohectorite suspensions studied, there are nematic textures which show a more complex structure than the dominating textures of random birefringence. Depending on powder type, crushing property and settling time before sample preparation, this nematic order forms in separate strata or may appear throughout the whole sample. The formation occurs gradually over a long period of time, usually several months.

This section gives some examples of the structures, where the use of cross polarizers in combination with X-ray scattering show how the particles in these regions have to be oriented.

3.12.1 Nematic Domain Structures

Figure 3.73 shows a peculiar domain filament structure which has developed in the second nematic phase of a suspension of 3 w/w% August Na-Fht. This structure forms in all samples of August and November powder with clay concentrations from 0.5 to 3 weight% at ionic strength 10^{-4} or 10^{-3} M. The structure forms for powder that is not crushed or crushed by the milling machine. For powder crushed by mortar and pestle, the structure is only observed for clay concentrations at 0.5 w/w%. The domains then appear in less amount and have a smaller size than compared to 0.5 w/w% samples of uncrushed powder. The macroscopic order and appearance of the structure vary from each individual sample. Some samples may just show a tendency of domain formation, while there at others can be observed highly developed individual domains.

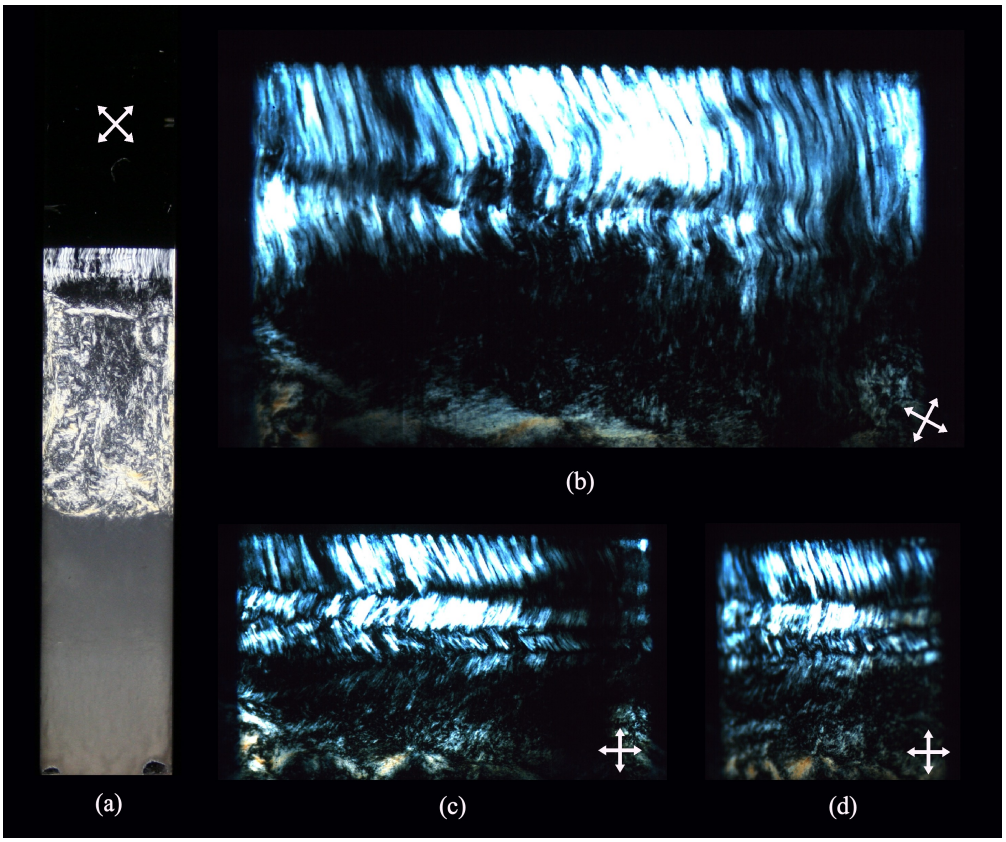

Figure 3.73: Domain structure in a 3 w/w% August 10^{-3} M sample, five and a half months after preparation. (a) A picture showing the whole sample, where the upper nematic sol phase consists of a black homeotropic region beneath a structure of birefringent domains. (b) Microscope picture of the nematic sol phase between crossed polarizers with 30° rotation from the edge of the figure. (c) The axes of the polarizer and analyzer are vertically and horizontally aligned, which give extinction for the vertical parts of the domains. (d) The sample is rotated 45°.

Suspensions of low clay concentrations form nematic domain filaments faster than in suspensions of higher clay concentrations. Figure 3.74 shows the development of nematic domains in a suspension of 0.5 w/w% November. For this sample the first sign of the structure appears in less than three weeks, and becomes fully visible in only a period of two weeks. The domain structure of the 3 w/w% sample in Figure 3.73 starts to appear first 4 months after preparation where it takes further one month until it has formed the order in the pictures. After this time the domains continue to exist in the phase, but after 8 months from preparation the structure slowly disintegrates into smaller birefringent domains[20]. Figure 3.76 shows the domain structure as it appears 9 months after preparation for the 0.5 w/w% milled August sample shown in Figure 3.75.

[20] A figure showing the time evolution of the phase over a time period of 8 months can be found in the supporting content of the enclosed DVD.

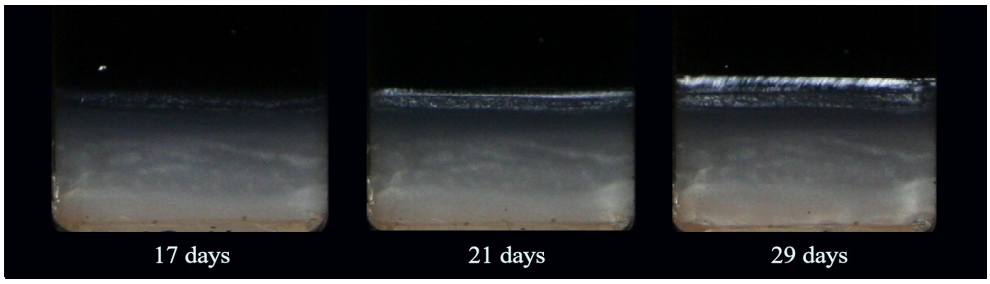

Figure 3.74: The formation of the nematic domain phase of 0.5 w/w% November 10^{-3} M during a settling period of 12 days.

Figure 3.75: Zigzag pattern of the nematic phase formed in a sample of 0.5 w/w% milled August 10^{-3} M. Time from preparation is 5 months. Since the axes of the cross polarizers are parallel to the edges of the sample tubes, a dark line appears in the middle of the zigzag pattern where the domains are vertical.

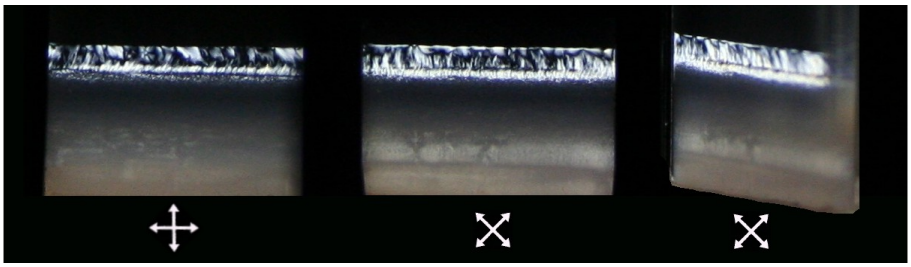

Figure 3.76: The appearance of the nematic phase of the same sample as in Figure 3.75 as it looked 9 months from preparation. The domains structure has now changed and look less ordered. 45° rotation of the polarizers and sample shows an increase in birefringence at both boundaries of the nematic phase, indicating a high tendency of lying particles.

A characteristic feature of the nematic domain structure is how the domains form in a zigzag pattern. This is shown prominently in Figure 3.77, where it is revealed that the birefringent domains become dark when they are oriented along the axes of the cross polarizers.

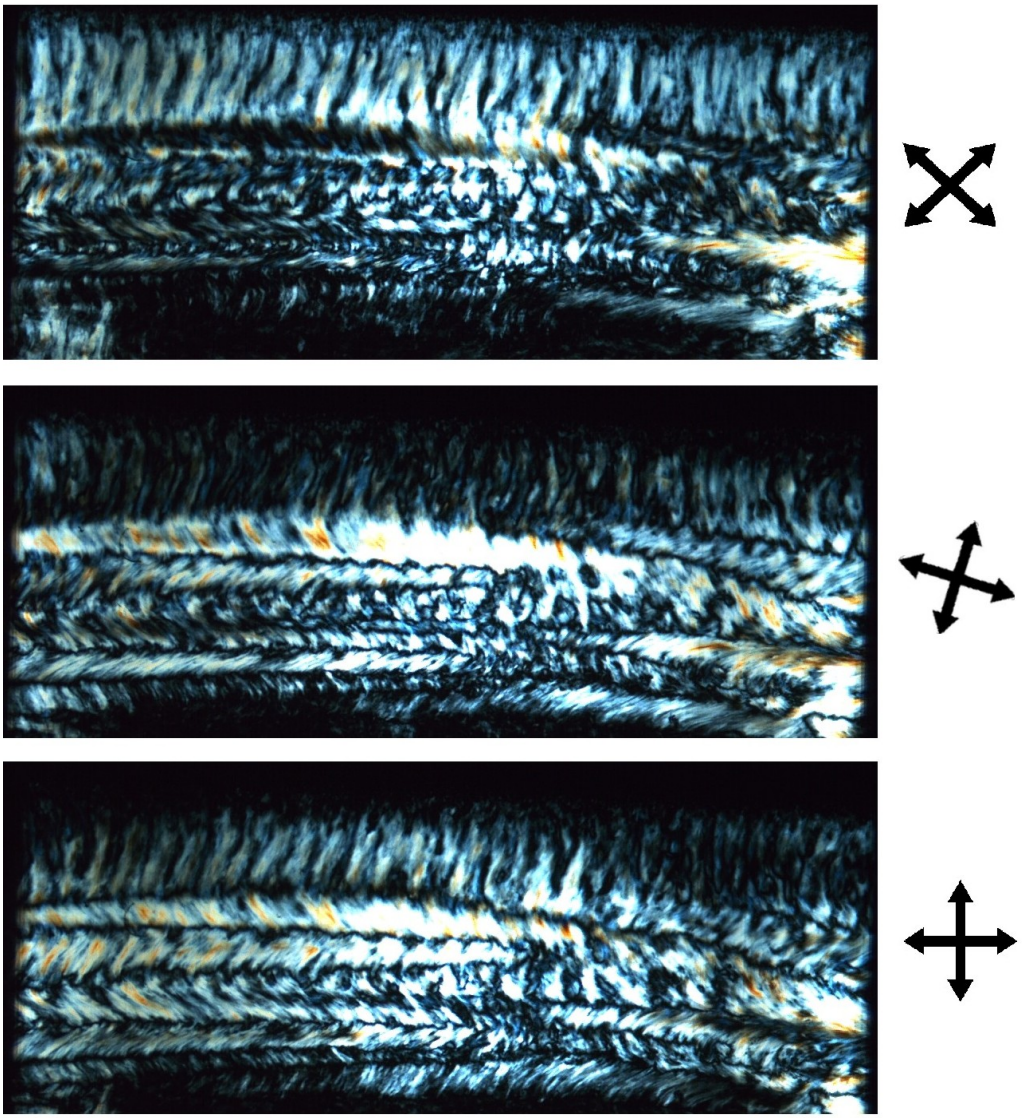

Figure 3.77: Three cross-polarized microscope pictures of the upper nematic phase of 2 w/w% August 10^{-3} M, where the polarizer is oriented at 45°, 75° and 90°. Time from preparation is 9 months. The places where the nematic domains are parallel to the axis of either the polarizer or analyzer appear dark. This shows the domain structure is continuous through the phase.

Wide angle X-ray scattering on the domains (Figures 3.55 and 3.56) gives Bragg semi-rings oriented vertically. This shows that the domains consist of lying clay particles stacked upon each other. The black lines between the domains do not change either when the cross polarizers or the sample is rotated. This indicates that the dark parts of the domain pattern is isotropic, which means this intermediate stratum is a coexisting region of both a nematic and an isotropic phase. It is not clear why the domains form in a zigzag pattern, but a

possible explanation could be that the domains have been squeezed downward and bended due to pressure from the above suspension. This would make sense since the zigzag pattern is most pronounced for the domains situated closest to the bottom. The domains are much more straight for suspensions of 3 w/w% clay than for 2 w/w% or 0.5 w/w% which have more volume above the upper nematic phase.

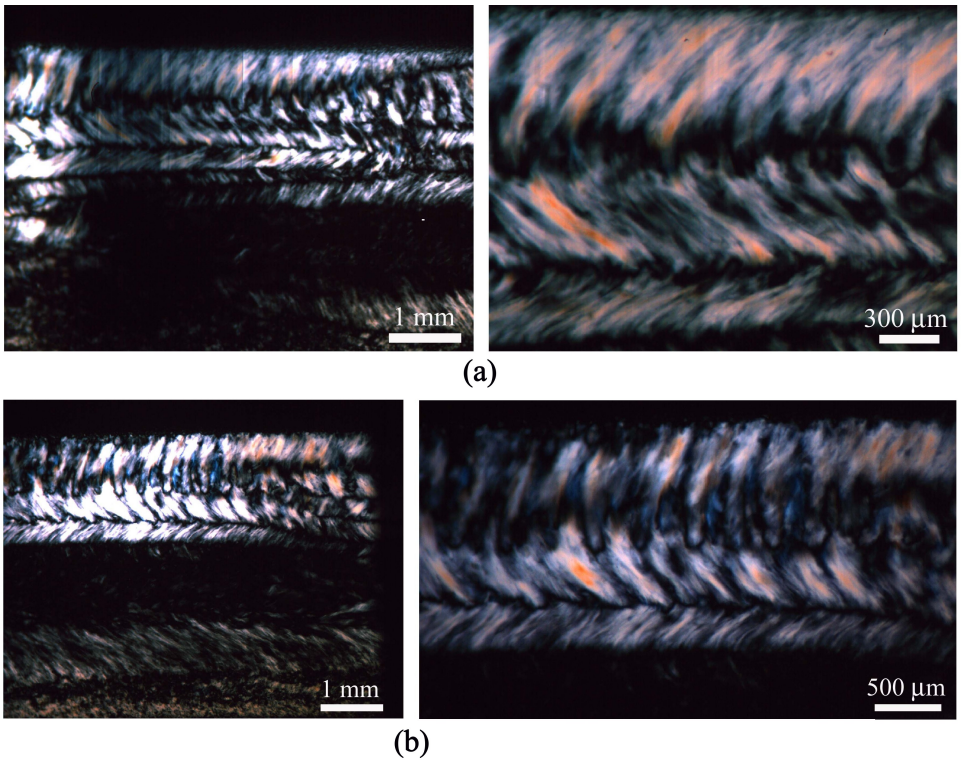

Figure 3.78: Nematic zigzag pattern of the upper nematic phase of 2 w/w% August viewed by optical microscope between cross polarizers. Thin birefringent threads appear when the light sensitivity is reduced, otherwise the brightness of the birefringence will make the phase apparently just consist of large white domains. (a) Salt concentration 10^{-3} M. (b) Salt concentration $5{\times}10^{-4}$ M.

The width of the birefringent domains seen in Figures 3.73, 3.75 and 3.77 is around 0.2 mm. The height depends on the clay concentration, where it for 2 and 3 w/w% clay typically varies from 3-5 mm. Since it is not useful to view the samples from their side, it is from visual considerations not possible to decide the thickness of the domains. The thickness of the sample tubes are 1 mm, which would correspond to the width of 4 domains when the black stripes are added. The fact that the domains are clearly separated by black lines when viewed from the front, must mean that the domain formation is ordered crosswise of the sample tube thickness. The birefringent domains may be fully continuous through the thickness or consist of two or more thinner domains surrounded by a black region.

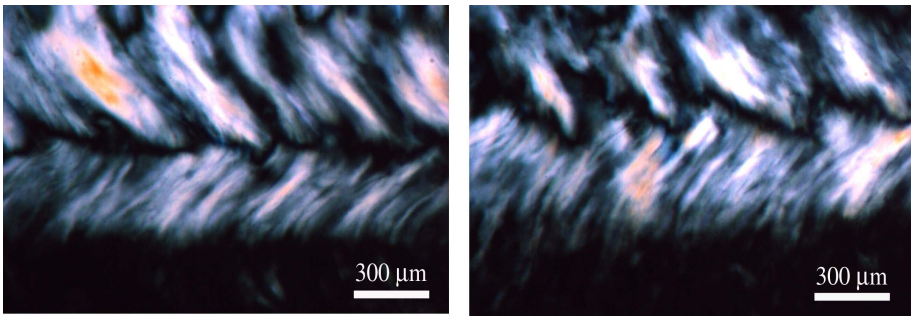

Figure 3.79: Microscope pictures of the upper nematic phase of 2 w/w% August 5×10^{-4} M. With this magnification, the separate nematic domains seen in the Canon camera pictures, are revealed to consist of thin threads.

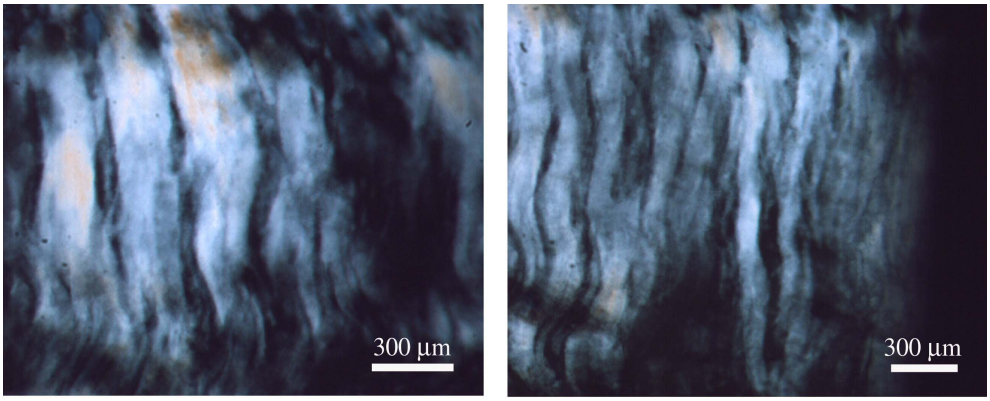

Figure 3.80: Micrographs of the vertical oriented nematic domains in the upper nematic phase of the sample in Figure 3.73.

When the 0.2 mm wide birefringent domains from the standard camera pictures are closer inspected by microscope, Figures 3.78 , 3.79, 3.80 and 3.81, it is revealed that the domains are composed of thin threads. A single thread is typically around 10 times thinner than the larger domains. This gives a thickness of 20 μm, which corresponds to the length of the Na-fluorohectorite particles of largest size.

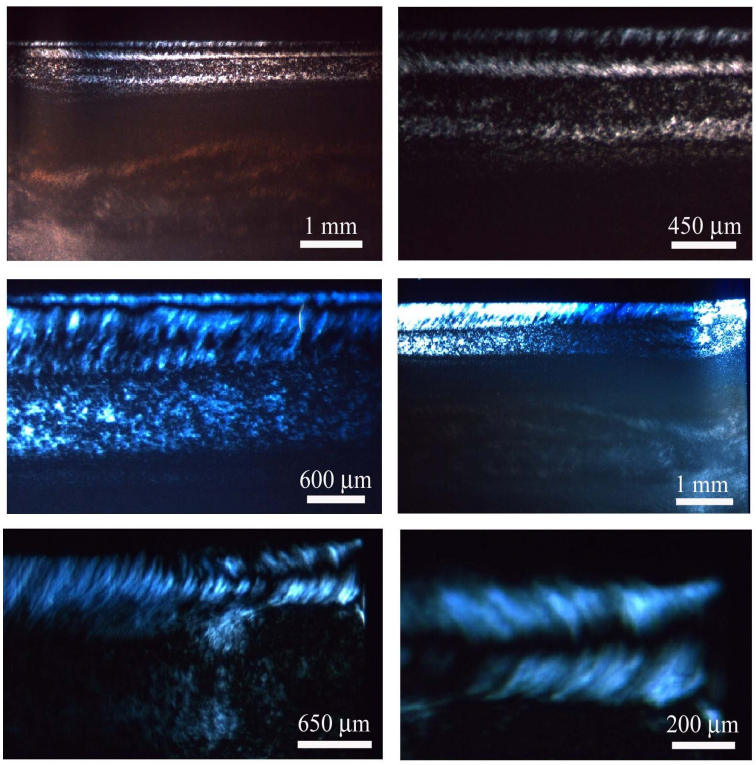

Figure 3.81: The 0.5 w/w% November sample from Figure 3.74 viewed in optical microscope between cross polarizers. The two upper pictures are taken 21 days from preparation, while the rest are 1 week later. The two lowest pictures show the right side of the upper phase of the the sample.

3.12.2 Interfaces

In many of our samples of phase separated Na-fluorohectorite, there has been observations of a different particle orientation at the interfaces between two phases. Figures 3.82 and 3.83 show the results from an X-ray synchrotron experiment on a sample of 3 w/w% August 10^{-3} M which had been settling for 5 weeks in a 2 mm capillary. Over the whole height of the nematic phase, the particles tend to be oriented with their faces towards the walls except at a very thin region at the bottom of the phase, where they are oriented with their normals parallel with the capillary axis.

This observation that the particles are lying at the boundary between the lower isotropic phase and middle nematic phase is also proved to be the case for flat sample tubes, as shown in Figures 3.84 and 3.85. Van der Beek et al. have by simulations and experiments reported the same interfacial orientations in systems of gibbsite platelets [174], showing consistence to the Zwanzig model of interfacial properties of rectangular platelets [175–177].

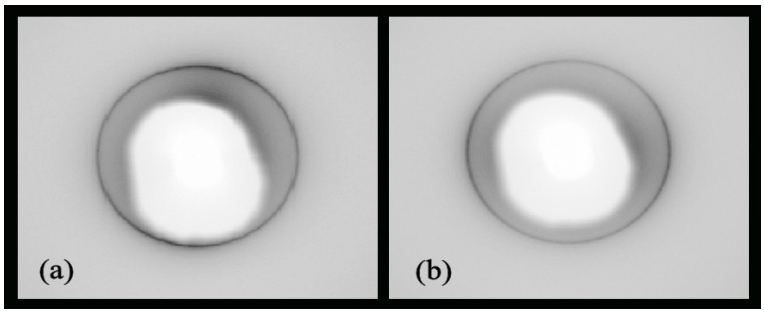

Figure 3.82: Detector image of X-ray scattering measurements on a 3 w/w% August 10^{-3} M capillary sample carried out a ESRF. (a) Scan right at the boundary between the lower isotropic and middle nematic phase gave anisotropic (001) Bragg peak with most intensity vertically. (b) All over the rest of the nematic phase, the Bragg peak is anisotropic with most intensity horizontally. The distance from sample to detector is 390 mm, the wavelength is 0.8089 Å and the beam size is 0.3×0.3 mm. Experiments and analyses by Henrik Hemmen (NTNU).

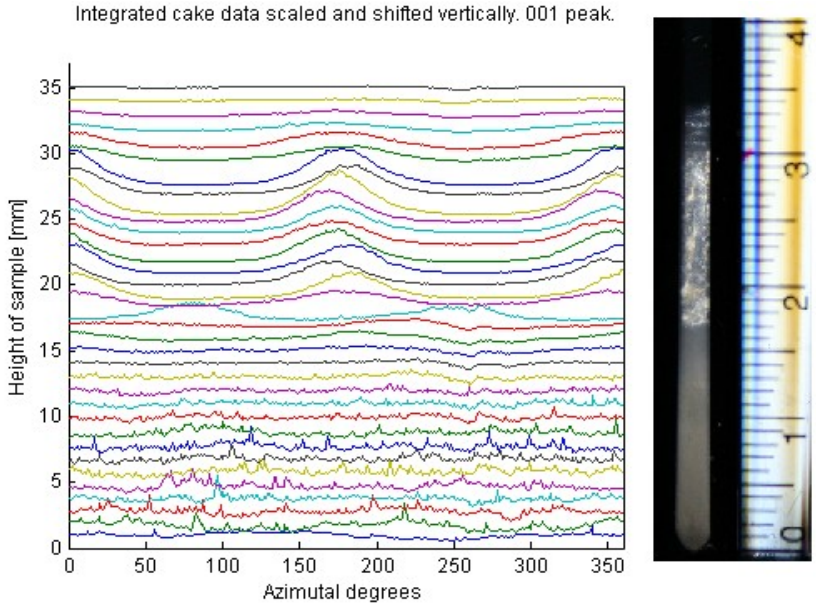

Figure 3.83: Azimuthal integration of the Bragg peaks from the bottom sediment to the isotropic top of a 2 mm capillary sample of 3 w/w% August 10^{-3} M. At 17 mm, right at the boundary of the isotropic and nematic phase, the anisotropic Bragg peak is opposite to the rest of the nematic phase. This means the particles in this region are lying down with their faces perpendicular to the walls. The settling time of the sample before the experiment was 5 weeks. Since the actual sample used in the experiment was destroyed, the picture to the right is just a representation of a similar sample with same clay and salt concentration. Experiments and analyses by Henrik Hemmen (NTNU).

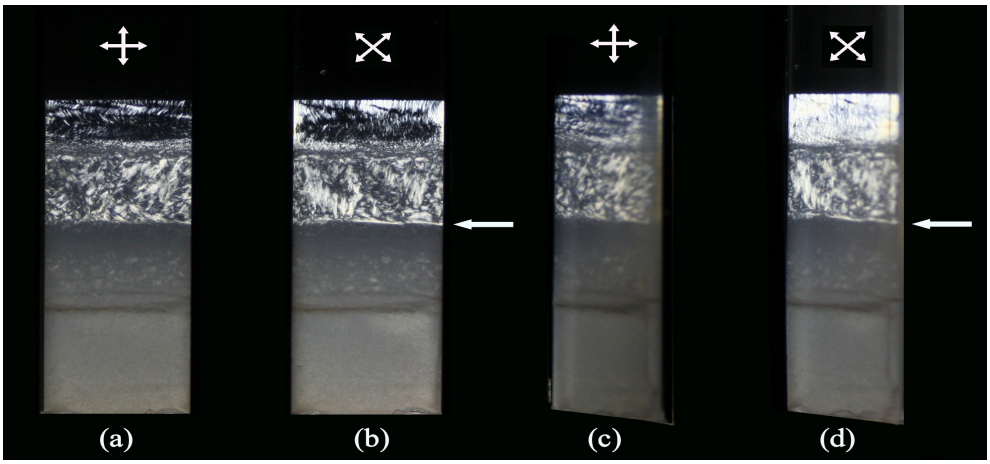

Figure 3.84: Detection of lying particles at the boundary between the isotropic and nematic phase in a suspension of 2 w/w% August 10^{-3} M. (a) The axes of the cross polarizers is oriented parallel and perpendicular to the edges of the sample tube. (b) A birefringent line at the isotropic-nematic boundary appears brightest when the axes of the cross polarizers are oriented 45° to the edges of the sample. This means the particles there are oriented with their director either parallel or perpendicular to the sample tubes. (c) The sample is rotated rotated 45°, but has the same cross-polarizing configuration as the first picture. No birefringent boundary line appears. (d) Both the sample and cross polarizers are rotated 45°. The birefringent line appears, which means the particles at the boundary are lying with their faces towards the bottom.

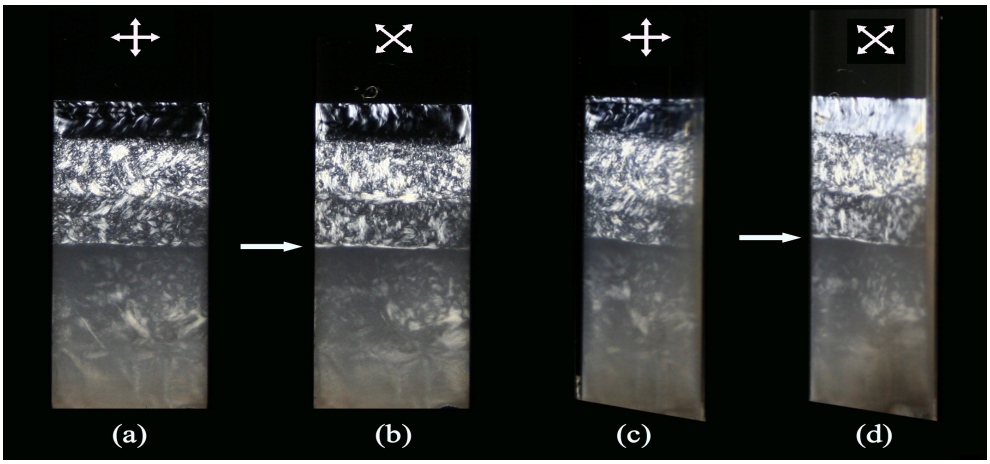

Figure 3.85: (a)-(d) The same situation as in Figure 3.84, but with a sample of 2 w/w% November 10^{-3} M. In this sample, 3 separate strata of nematic phases can be observed, where there also between the two middle strata is a slight tendency of a bright birefringent line ((b) and (d)). The upper nematic phase, consists of thread-like nematic domains and becomes particular white in (d) since the domains are oriented with an angle between 45° and 90°.

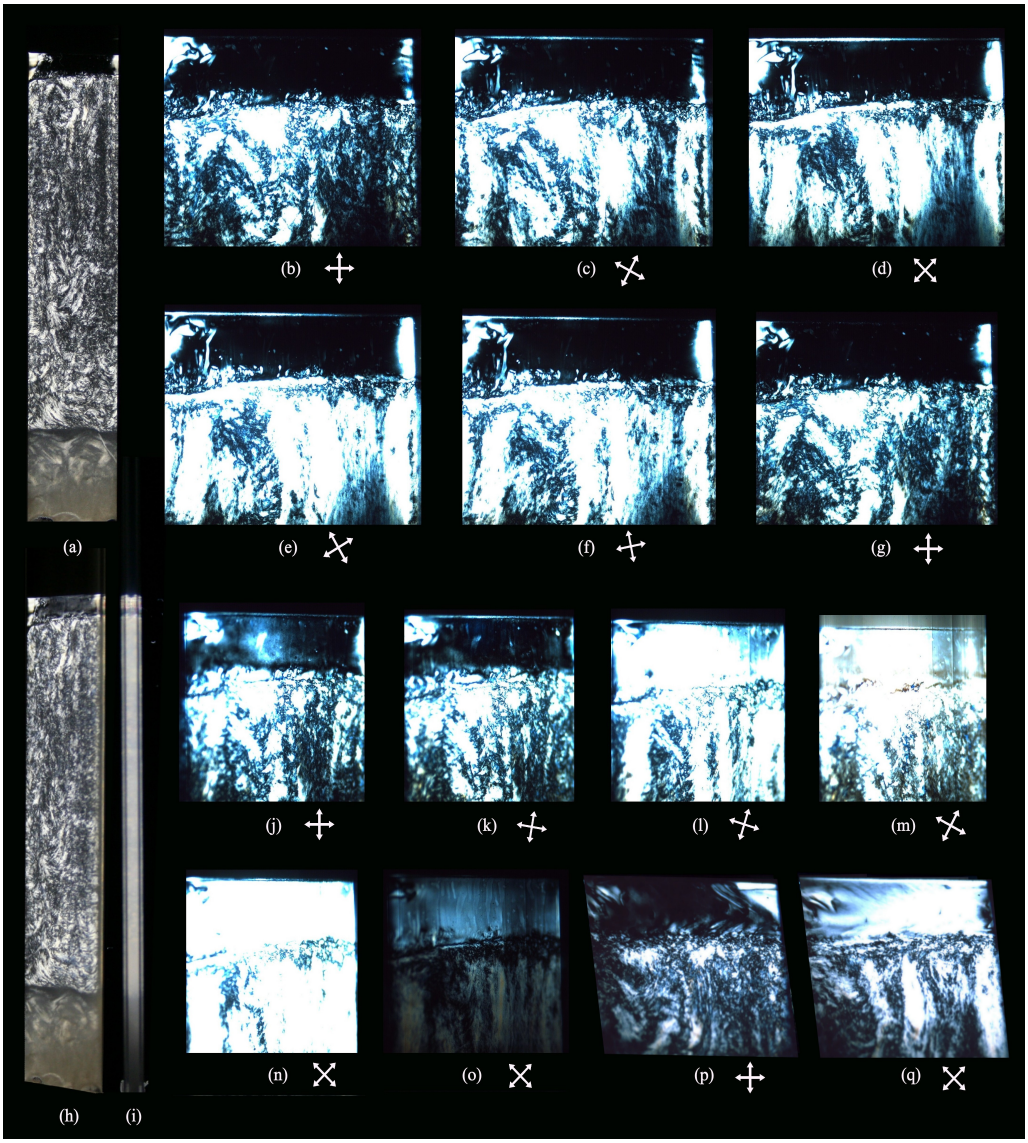

Figure 3.86: Different particle alignment in the nematic sol phase of a 3 w/w% uncrushed April 10^{-3} M suspension. The sample is initially half-filled and the pictures are taken 5 months after the preparation. (a) The whole sample, and (b) a close-up microscope picture of the nematic sol viewed between crossed polarizers with axes parallel to the edge of the sample tube. (c) The polarizers are rotated 30°, and the appearance of a thin birefringent layer atop of the homeotropic region, shows that the particles there are edge-wall oriented. (d) The birefringence of the layer is most intense at 45° polarizer rotation, indicating parallel or perpendicular director orientation. (e) 60°, (f) 80° and (g) 90° rotation. For picture (h)-(n) the sample is rotated 45°, except for (i) where it is viewed edge on. (m) The polarizers are not completely crossed, which promotes the appearance of a black stratum right under the birefringent layer. (o) The light exposure is decreased from (n). (p) and (q) The sample is tilted 45° down.

Also between different nematic phases and between the upper nematic and isotropic phases some samples have shown to have a different particle orientation. Figures 3.86 shows the changes that occur in the upper nematic phase during rotation of the sample and polarizers. When the sample is viewed from the front, most of the upper nematic phase appears black in any angle of the cross polarizers. When the sample is turned around 45° with the axes of the polarizers rotated 45°, the whole phase becomes birefringent. This means the particles in the black region are oriented with their faces against the walls, that is homeotropic alignment.

As seen in pictures (c)-(f) of Figure 3.86 a birefringent line appears at the transition to the upper isotropic phase when the polarizers make an angle to the axis of the sample tube. The line is brightest when the angle is 45°, which means the particles at the nematic-isotropic boundary are either standing or lying with their edges towards the walls. It has turned out to be difficult to decide which of these two alternatives is the correct one. If the particles are lying, the birefringent line should not appear when the sample is rotated.

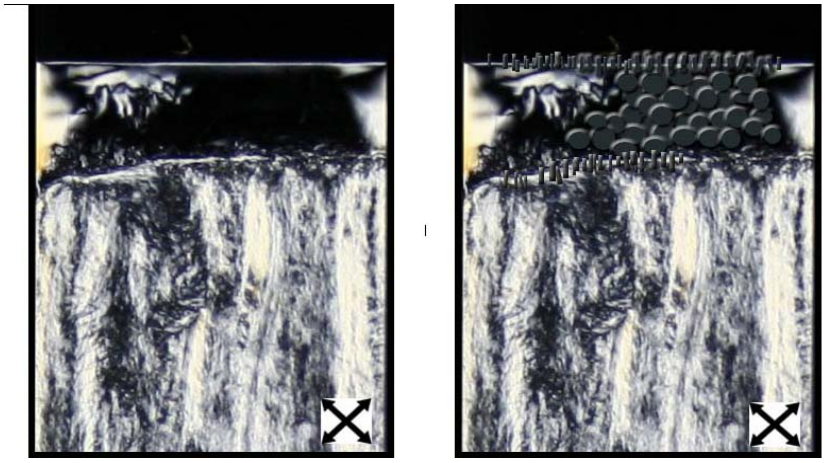

Figure 3.87: Illustration of how the particles are aligned in the upper part of the 3 w/w% uncrushed April sample 10^{-3} M.

Picture (j) in Figure 3.86 shows that a weak birefringent line indeed do appear when the sample tube is rotated approximately 45°. This should mean the particles are standing with horizontal director between the homeotropic alignment and the isotropic phase. This configuration is illustrated in Figure 3.87, where also the particles below the homeotropic region is proposed to have the same alignment as at the top[21]. The pictures in Figure 3.86 do still not give certain proof that the birefringent line corresponds to standing particles. It is possible to imagine the birefringence appearing because of the anisotropic surface shape of the Na-fluorohectorite particles.

[21]The evidence for this proposal is very weakly present from the pictures. The particles in the rest of the nematic gel, have a higher orientational distribution of being aligned with their normals along the axis of the sample tube.

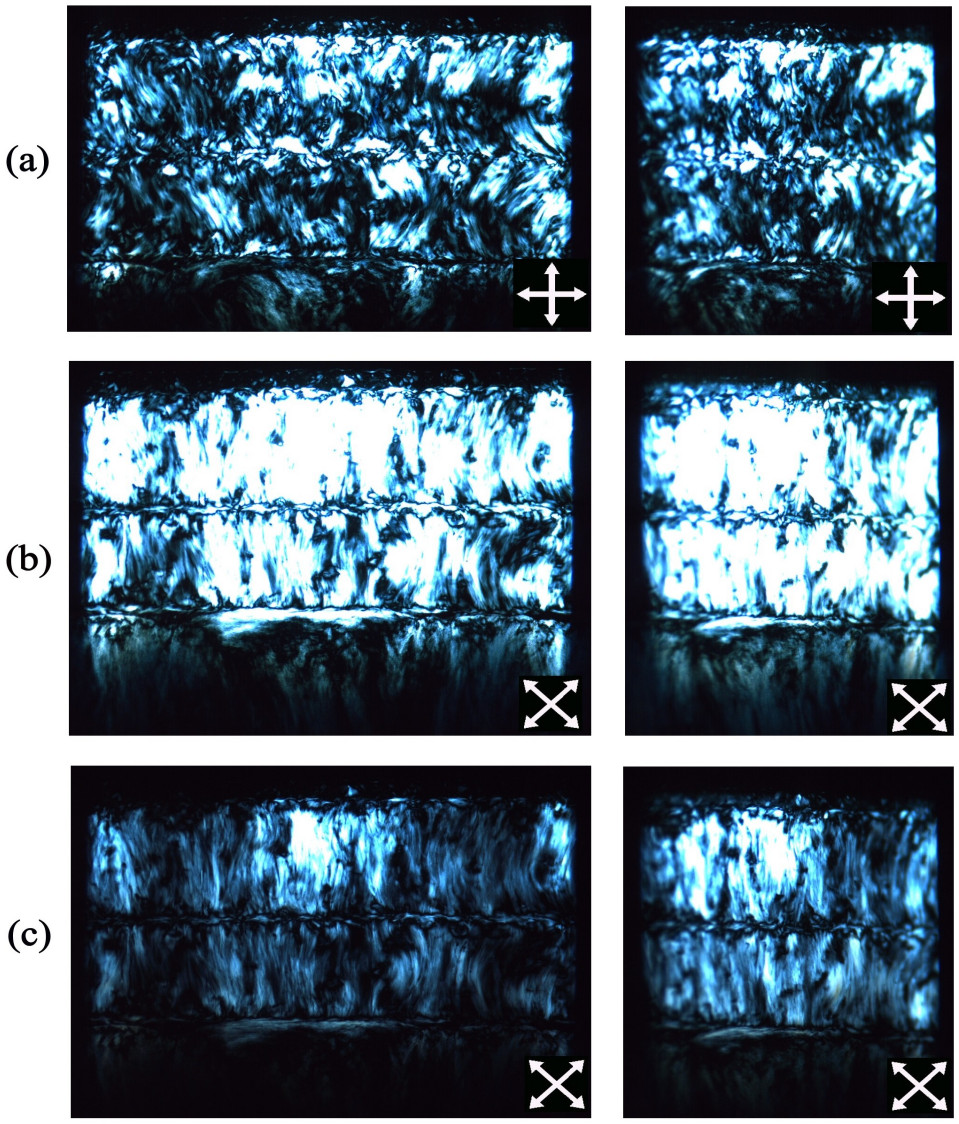

Figure 3.88: The upper nematic phase of 2 w/w% April 10^{-3} M. (a) The sample is viewed from front and 45° rotation with the axes of the polarizer and analyzer parallel to the edges of the sample tube. (b) The polarizers are rotated 45°. (c) Reduced exposure.

Figure 3.88 shows microscope pictures of the nematic sol phase of the 2 w/w% April 10^{-3} M sample which the time evolution is shown in Figure 3.4. The micrographs are taken 8 months after preparation, and the nematic sol has divided into two parts separated by a black and white interface. From the rotations of the sample and cross polarizers, it can be concluded that the particles at the "dividing line" and at the interface between the nematic gel and nematic sol are lying down. A similar dividing with lying particles is also seen for the nematic gel phase of the November sample in Figure 3.85. The

results of applying a magnetic field to this phase is shown in Section 3.8.

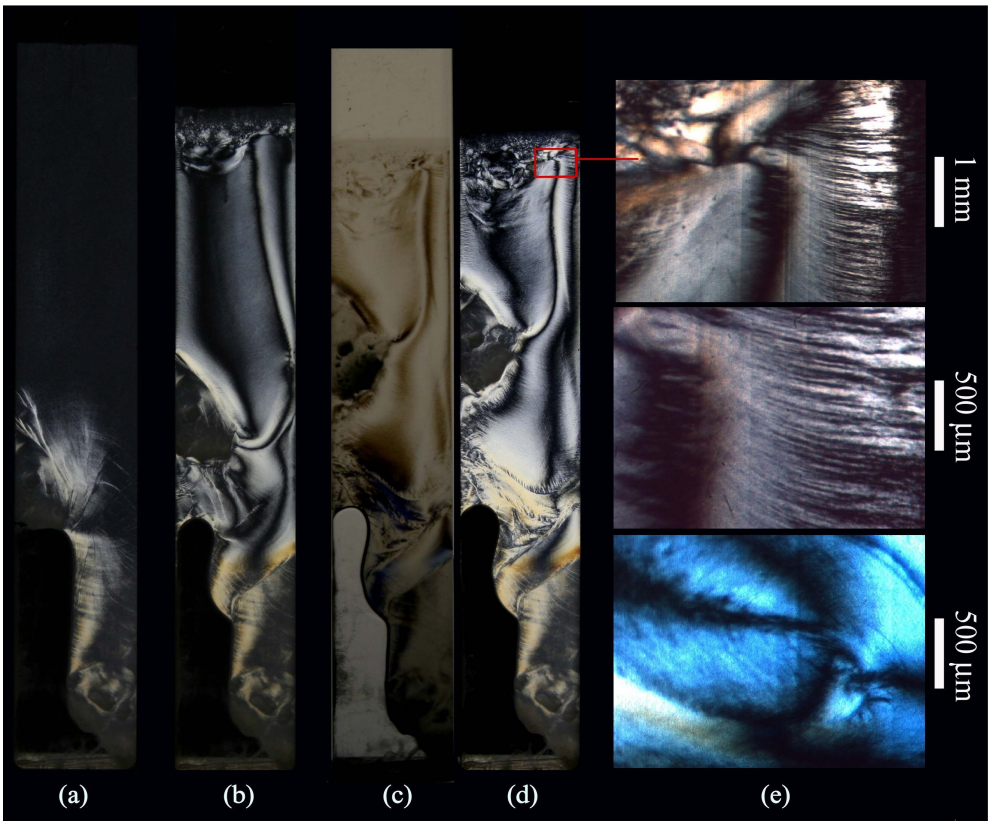

Figure 3.89: Pictures of a tube with 3 w/w % crushed April 10^{-3} M filled from a 5 ml vial that had already been settling for 4.5 months. A rather large air bobble has penetrated through the bottom and disturbed the settling process. (a) 5 weeks from preparation there is some white birefringence that has been pushed up by the air bobble. (b) 7 weeks after preparation. (c) and (d) are 8 weeks after preparation, where in (d) the polarizers are both in the same direction. This give the opposite distinction for the two pictures. The pictures in (e) are taken by optical microscopy with crossed polarizers. The two upper pictures are 10x and 20x magnification of the region marked in (d). The last picture shows a schlieren pattern that is formed in the upper left part of the sample.

3.12.3 Nematic Schlieren and Threaded Textures

In some of our samples the appearance of a special stripe pattern arise, of which the origin of formation is not yet understood. The two upper pictures in Figure 3.89 (e) show its characteristics of horizontal birefringent stripes between black grooves. The stripes have a typical thickness around 20 μm, but can spend over several millimeter in length. The pattern is only observed for suspensions of 3 w/w% crushed April at salt concentration 10^{-3} M. Lower or slightly higher clay and salt concentrations might probably also give the same pattern. The appearance of the structure varies much from each individual sample, where

there has proved to be a dependence of what have happened to the suspension both before and during settling. The pattern is found to especially appear at samples where the suspension has already undergone a period of settling before it was poured into the final sample tube[22].

An example of such a sample is shown in Figure 3.89, where the settling behaviour is revealed to be very different from similar samples where the suspension is filled into the sample tube very soon after dissolution. The fluctuations that is typical for ordinary samples of the April powder (Figure 3.3) do not take place in the same sense for samples injected with pre-settled suspension. Instead the whole suspension settles faster and leaves a larger region of the top isotropic phase.

Picture (a) in Figure 3.89 and picture (g) in Figure 3.13 show that a region of dense birefringence has formed one and two months after injection for two different samples. This birefringence forms and changes very slowly, and the appearance of such a sample may be almost identical within a period of one-two months. The only major noticeable change would be that the boundary to the upper isotropic phase has settled some closer to the bottom. When this settlement has reached a particular level, its compression of the suspension seems to be the provoking factor behind a drastic change of the particle orientation.

Picture (b) in Figure 3.89 shows how the sample is transformed into a nematic schlieren texture with dark brushes corresponding to either horizontal or vertical particle orientation. In a rather short period of some days, the microscopic structure of birefringent stripe and black grooves appear in the sample. Picture (d) shows the sample one week later, where the stripes is seen to go crosswise of the dark schlieren brushes.

The birefringent stripes becomes dark when they are oriented along the polarizer or analyzer axes, but it is not possible to tell whether they are composed of clay particles connected edge-to-edge, face-to-face or for that matter face-to-edge. When it comes to the black grooves, it does not seem to be any change in either brightness or position during rotation of the cross polarizers. This is shown in Figure 3.90, but it is best observed when the pictures change by overlapping. From this it would be reasonable to imagine the black grooves correspond to regions of isotropic orientation, giving nematic-isotropic coexistence in almost every height of the settled suspension. A possible coexistence of nematic and isotropic microdomains is also suggested to exist in suspensions of laponite and montmorillonite, where small-scale heterogeneities is reported to exist in the gel structure [37, 38].

Another possibility could be that there is homeotropic alignment in the black grooves and the particles crosswise of the stripes orient in a helical structure similar to chiral (cholesteric) nematic phases. A way to test this could be to rotate the sample and see if the black grooves moved either up or down, since that would change the optical position of the homeotropically aligned particles. Unfortunately this has shown to be not practical successful in our

[22]The Vitrotube was filled with suspension from a 5 ml vial that was fully re-shaken after it had been left standing to settle for some months.

samples, since the increase in optical path length through our 1 mm thick samples tubes changes the appearance of the pattern too much.

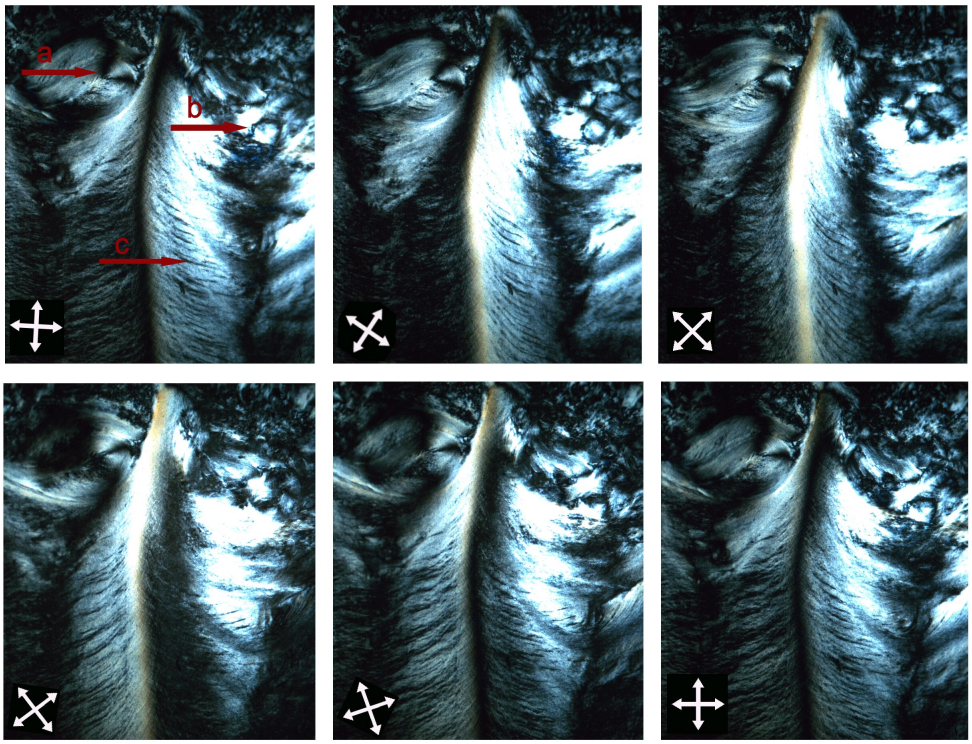

Figure 3.90: A sample of 3 w/w % April 10^{-3} M at different angles of the cross polarizers. From the upper left to the lower right picture, the polarizers are rotated 20°, 45°, 55°, 75° and 90° with respect to the edges of the sample tube. Arrow a shows a disclination with two brushes emanating from each other at 90°. In the first two pictures of the last row, the two more brushes may be seen in a very undefined manner. The brushes rotate in the same direction as the polarizers, and the strength can therefore be regarded as being +1. Arrow b shows a singularity where two dark brushes meet and rotate in the opposite direction as the cross polarizers. This corresponds to a disclination with strength -1/2. Arrow c marks the position of dark grooves located between birefringent stripes. As the polarizers are rotated, there is no apparent movements of the grooves.

The same textures as observed for samples with pre-settled suspension, may also appear in samples that are filled with suspension short time after its first mixture of clay and salt solution. The textures of these samples can be characterized to differ from the first case by having a less smooth appearance. The birefringent stripes may also be more pronounced and appear larger in size. An example of such a sample is shown in Figure 3.91, where it is compared to a similar pattern in a suspension of F-actin[23], obtained by J. Viamontes

[23]F-actin is long protein filaments formed from polymerization of monomeric actin (G-actin) and are the principal components of the thin filaments in skeletal muscles. They have

and J. X. Tang [178]. In their sample, the F-actin filaments spread with a characteristic curvature from the centre to the sidewalls of the sample tube. They obtained this defined pattern by spin inversion of the sample tube.

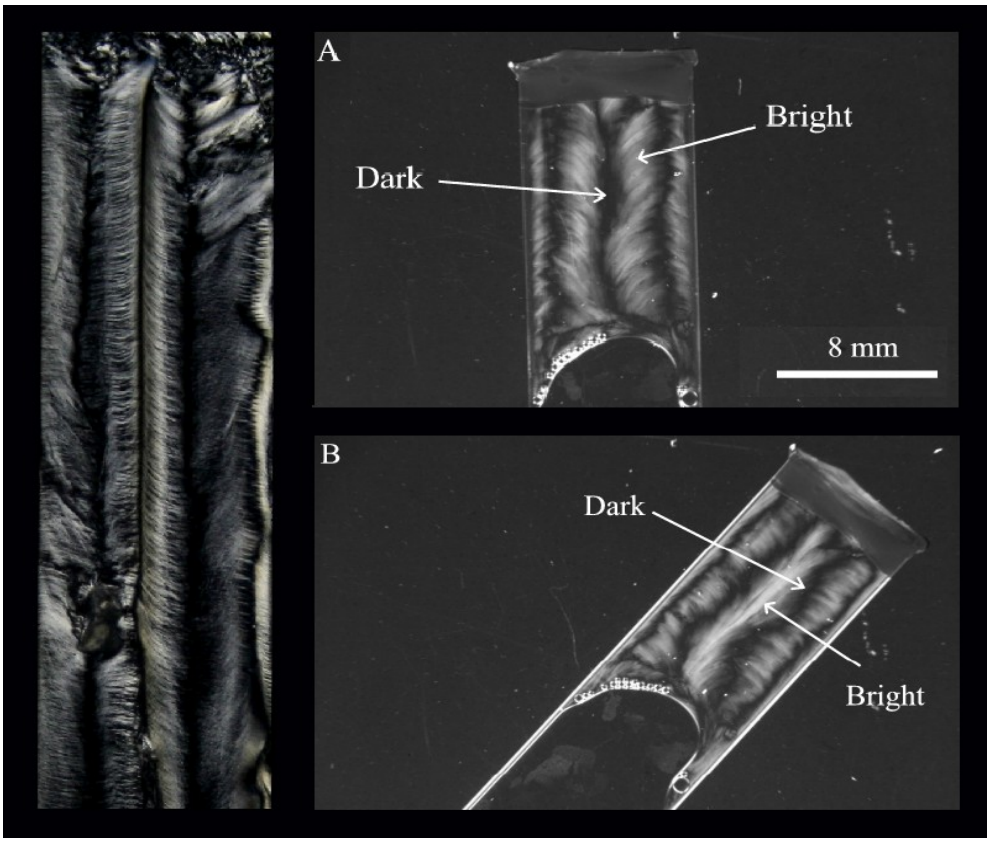

Figure 3.91: A sample of F-actin (left) adapted from reference [178] shows a similar pattern that forms in our samples of 3 w/w % April 10^{-3} M (right).

Our sample is not exposed to any kind of centrifugation, but some outer disturbances have still happened to the sample. When the sample was three months from preparation, it was moved to ESRF and then taken back some days later. It is impossible to tell how much the "shaking" it was exposed to during this movement affected the suspension.

Another disturbance which probably has had a more important influence to the formation of the structure, is penetration of air-bobbles. The longest and most straight black vertical line, centred in the middle of the sample in Figure 3.91, is caused by a rather large air bobble which float to the top. This movement seems to have oriented the particles or stripes along the direction of ascent, and consequently widened the space between the birefringent stripes and dark grooves.

a length of a few tens of micrometers and a diameter of approximately 7 nm.

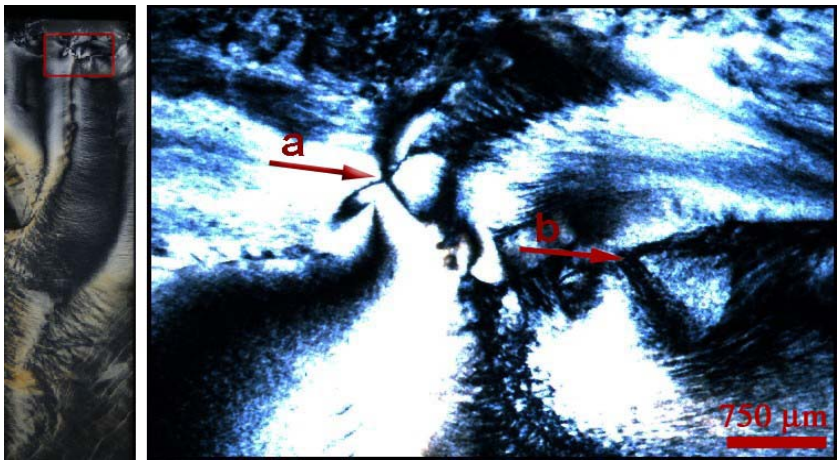

Figure 3.92: Defects in the region close to the isotropic phase for a sample which is filled with pre-settled suspension of 3 w/w % April 10^{-3} M. The pictures are taken 8 months after the time of injection. Arrow a shows a disclination of strength -1, and arrow b shows a disclination of strength +1.

For all the samples that have the schlieren pattern, disclination points are found with both two (strength 1/2) and four (strength 1) emanating brushes. The disclinations seem to appear most frequent in the upper part close to the isotropic phase. The strength of the disclinations is defined in Chapter 1.9.6, where the sign is determined by rotation of the cross polarizers. If the brushes rotate in the same way as the polarizers, the sign is positive. If they rotate in the opposite direction, the strength is negative. Figures 3.90 and 3.92 show disclinations of both strengths ± 1 and -1/2. The fact that this is observed when 1 mm thick sample tubes should be regarded as being rather large concerning observations of nematic schlieren pattern, it clearly demonstrates the large size of the Na-fluorohectorite particles.

Chapter 4

Concluding Remarks

4.1 Phase Behaviour in Gravitational Field

In this study, suspensions of Na-fluorohectorite have by settling in the gravitational field shown to exhibit a rich phase behaviour. Samples with preferable salt and clay concentration, phase separate into different strata of sediment, gels and sols. Birefringence and X-ray scattering experiments have shown that a clear separation of isotropic and nematic phases occurs in several of the studied samples. By carefully observing the settling of the suspensions over several months, great insight is obtained for the process of phase separation. The time evolution for the nematic ordering is revealed to undergo dynamics in form of fluctuations and movements of small birefringent domains. The understanding of the physics behind these dynamics is not successfully proposed from this work. Similar studies of the dynamical birefringent behaviour of the nematic (gel) ordering in suspensions of colloidal particles is not present in available literatures, and comparison to other systems has not been possible. The crushing property of the Na-Fht powder is observed to be of decisive importance to the dynamical behaviour of the birefringence in the suspensions. Future work, by AFM or TEM characterization of the particles in crushed and not crushed powder, would be helpful to the understanding for this dependence.

Short time after the flat sample tubes are poured with Na-Fht suspension, long vertical streaks sometime appear in the process of sedimentation. Any corroboration of the origin of the streaks is not determined, but the behaviour is apparently influenced from the combination of sample geometry and flow properties of the clay. Another, very different, streak phenomena is observed after some days of settling in a few samples. These streaks appear horizontally, separated by an equal distance. A relation to backward-propagating waves is proposed, but more extensive experiments is needed to gain more information about the phenomena.

The effect of varying the salt concentration of the Na-Fht suspensions is found to be in prediction to the DLVO theory of colloidal stability. For most samples, there is minor difference in phase behaviour between salt concentrations of 10^{-4} M and 10^{-3} M. The flocculation transition is found to be between

10^{-2} M and 2×10^{-2} M, which is similar to other studies on clay suspensions.

Attributable to the restriction of mainly using visual observations to characterize gelation in the suspension, a proper sol-gel/isotropic-nematic phase diagram is not accurately obtained. There is anyway a clear indication that suspensions of crushed powder seem to gel at lower clay concentrations than suspensions of higher clay concentrations. It is not clear if this behaviour should be attributed to different particle anisotropy, smaller particle sizes or a changed electrostatic charge distribution, which could be the effect of the crushing. The optical study also indicate that the gelation process is presently exhibited at lower salt concentrations. This phase behaviour is similar to other studies of Na-montmorillonite [33].

The clay density as varying with altitude is measured for two samples of crushed and not crushed Na-Fht powder. For crushed powder, the average concentration of the isotropic and nematic phase is found to be 14 mg/ml and 30 mg/ml respectively. For uncrushed powder, the corresponding concentrations are 9 mg/ml and 32 mg/ml. The gap between the isotropic and nematic phase is about 30% larger for the suspension of uncrushed powder than the crushed suspension. This may indicate the polydisperity is lower for suspensions of crushed powder. Compared to theoretical calculations [50] of the coexisting isotropic-nematic phases, the density values for our samples are at least a factor 5 lower than the predicted values. This large deviation to the theoretical values may be explained by the morphology of the particles [51], the influence of gravity, electrostatic effects and the fact that the Onsager formalism does not really apply to the gel phase. The relative proportion of the nematic phase is from 0.5 w/w% to 5 w/w% found to increase linearly with the overall clay concentration. This is similar to other studies which have observed a proper entropy-driven isotropic-nematic transition [41, 121]. The thermodynamic nature of the formation of the nematic order in our Na-Fht suspensions is not confirmed, but the birefringence is observed to develop within a separated non-birefringent stratum and from slow gravity settling from the above isotropic sol. The influence the gelation process might have to the nematic ordering in the Na-Fht suspensions is still to be described.

4.2 Influence of Magnetic Fields

Application of magnetic fields of high strengths to the nematic phase of Na-Fht suspensions, have from recent MRI studies [70] revealed to reorient the particles with their normals perpendicular to the field direction. In this work, magnetic field strengths until 1 Tesla have been applied to the different strata separated in the sample tubes. The measured effect of these magnetic fields have shown to be restricted to a specific stratum of nematic phase formed above the main nematic gel. This nematic phase is also more fluid than the nematic gel, and it is therefore characterized as a nematic sol. When a magnetic field is applied to the nematic sol, changes in the birefringence can be seen already after the first minutes. The feature of the changes depend of the Na-Fht powder batch used

in the suspension. The texture of the birefringence can become thread-like or almost monodomain white.

Some samples have seen to undergo a striking colour change when the magnetic field is applied for a very long time. Various first order yellow colours are detected, from where the retardation is found to vary from 300-400 nm. An effective birefringence is from this calculated to a value of $3.0\pm0.5\times10^{-4}$. By the relation of the birefringence to the nematic order parameter, it can be concluded that there is a time dependence between the magnetic field and the orientational ordering. Further experiments need to be done to find values of the magnetic susceptibility for the Na-Fht particles.

In the nematic sol phase of samples of 2 mm round capillaries, an inhomogeneous Fréedericksz transition has been induced, revealing typical transient periodic structures. This has been obtained by first orienting the particles in the nematic sol in one direction. By reorienting the magnetic field 90°, a periodic stripe pattern develops as the particles are being reoriented in the direction of the magnetic field. The first sign of the stripes appears just few minutes after the reorientation of the magnetic field. The stripe pattern is best visible from 45 minutes to 2 hours. The same inhomogeneous Fréedericksz transition is induced by van der Beek et el. using colloidal gibbsite platelets [142]. For both Na-Fht and gibbiste particles the anisotropy of the diamagnetic susceptibility is negative, something which gives a degeneracy in tilt-angles directions perpendicular to the director axis. In the experiment concerning the the gibbsite, this degeneracy is broken by rotating the sample in the magnetic field. This rotation has shown to not be necessary to induce the inhomogeneous Fréedericksz transition in our system of Na-Fht. Explanations to this can be the geometry of the sample tube, the biaxial shape of the Na-Fht particles or from the fact that our stripes pattern is simply observed in the same direction as the the magnetic field.

Various magnetic field strengths have been used to induce the Fréedericksz transition. The threshold value for the inhomogeneous Fréedericksz transition is found to be 0.5 Tesla. The theoretical quadratic dependence of the wavelength and magnetic, which is predicted from the linear stability analysis, has showed to be difficult to acquire due to large scattering in our experimental data.

4.3 Structural Particle Orientations

Synchrotron wide angle X-ray scattering was carried out on the purpose to investigate the effect magnetic fields may have on particle alignment. Because of experimental problem and the lack of good samples with nematic sol, the first attempt to do these measurements did not succeed. Instead two other unexpected results were obtained. From the position of the Bragg peaks, some samples were found to have different water-layer hydration states in different birefringent regions in the same sample. In the "ordinary" nematic phases for flat sample cells, one water-layer was found to be intercalated. The sediment

in flat samples, and all phases of capillaries tubes showed a Hendricks-Teller state of mixed intercalation. Two water-layers was found in a special region of birefringence, which had formed because of evaporation or shearing due to air-bubbles. Between cross polarizers, this region appears more birefringent and continuous than the other birefringence in the sample. Explanations to why clay particles in the vivid birefringent region had two water-layers is not completed. The close interface to the air, different salt concentration, smaller particles in the top better tend to intercalate water, are some proposed explanations to the findings.

For the first time, X-ray scattering was successfully carried out on flat sample tubes. As a surprise, the anisotropic orientation of the scattering pattern from these sample cells showed to be opposite to what have been previously observed for round sample tubes. For all the measurements, the position of the Bragg semi-rings showed that the particles are lying with normals in vertical direction. This did not turn out to be the case for the measurements of the 2 mm round capillaries, which had the expected vertical particle face alignment. Optical considerations also show that the phase behaviour in general depends on the sample holder. Further experimental and theoretical work, would be necessary to fully understand the role sample geometry and wall-effects have on the particle alignment.

The nematic sol phase, which develops by several weeks and months of settling, is for many samples shown to be compounded of a peculiar domain structure. These nematic domains have a visual width of 0.1-0.2 mm, and can vary up to 5 mm in height. The domains are very often seen as zigzag pattern, where the period of the steps tends to increase with the height. Optical microscopy shows that the domains consist of thinner birefringent threads with a typical thickness of 20 μm. The area between the domains and threads appears for the most dark between cross polarizers. From this it is suggested that the nematic sol is a coexisting region of both isotropic and nematic ordering. Smaller particles could form isotropic regions that are trapped between nematic domains of larger particles.

A similar coexistence of birefringent threads and dark grooves is also observed in the gel structure of samples of crushed Na-Fht powder. Shearing effects, due to air bubbles etc., appear to be the cause to some of the threaded textures. The patterns are particularly seen when the sample consists of presettled suspension. Schlieren textures with disclinations of strength 0.5 and 1 are also seen in these samples. The fact that we are able to observe Schlieren pattern when the sample tubes are 1 mm thick, indirectly reveals the large size of the Na-Fht particles.

With support from X-ray scattering measurements, there are at some samples observed to be a different particle alignment at the interface between the different strata. At the lower and upper interfaces of the nematic gel, a thin layer is revealed to consists of lying particles. This observation is consistent to other experiments and simulations [174, 176]. A particular birefringent experiment indicates that the particles at the interface between a homeotropically nematic sol and the upper isotropic phase are oriented with the normals hor-

izontally. Further investigations need to be carried out check the validity of this observation.

Bibliography

[1] Peter J. Collings. *Liquid Crystals: Nature's Delicate Phase of Matter.* Princeton University Press, 2nd edition, 2002. 1

[2] C. Tschierske. Non-conventional liquid crystals the importance of microsegregation for self-organisation. *J. Mater. Chem.*, 8:1485, 1998. 1

[3] D. Demus, J. W. Goodby, G. W. Gray, H. W. Spiess, and V. Vill. *Handbook of liquid crystals.* Wiley, Weinheim, 1998. 1

[4] J. C. P. Gabriel and P. Davidson. Mineral liquid crystals from self-assembly of anisotropic nanosystems. *Top. Curr. Chem.*, 226:119, 2003. 1

[5] A. S. Sonin. Inorganic lyotropic liquid crystals. *J. Mater. Chem.*, 8:2557, 1998. 1

[6] J. C. P. Gabriel and P. Davidson. New trends in colloidal liquid crystals based on mineral moieties. *Adv. Mater.*, 12:9, 2000. 1

[7] J. C. P. Gabriel and P. Davidson. Mineral liquid crystals. *Curr. Opin. Colloid Interface Sci.*, 9:377, 2005. 1, 3

[8] J. C. P. Gabriel and P. Davidson. Self-assemblies of anisotropic nanoparticles: Mineral liquid crystals. In M. P. Pileni, editor, *Nanocrystals forming mesoscopic structures*, chapter 7. Wiley-VCH Verlag GmbH Co. KGaA Weinheim, 2005. 1

[9] J. Sayettat, L. M. Bull, J. C. P. Gabriel, S. Jobic, F. Camerel, A. M. Marie, M. Fourmigué, P. Batail, R. Brec, and R. L. Inglebert. Complex fluids based on the flexible one-dimensional mineral polymers $[k(mps4)]_\infty$(m=ni, pd): Autofragmentation to concave, cyclic (pph4)3[(nips4)3]. *Angew. Chem. Int. Ed.*, 37:1711, 1998. 1

[10] H. Zocher. Über freiwillige strukturbildung in solen. (eine neue art anisotrop flüssiger medien.). *Z. Anorg. Allg. Chem*, 147:91, 1925. 1

[11] I. Langmuir. The role of attractive and repulsive forces in the formation of tactoids, thixotropic gels, protein crystals and coacervates. *J. Chem. Phys*, 6:873, 1938. 1

[12] D. van der Beek and H. N. W. Lekkerkerker. Nematic ordering *vs.* gelation in suspensions of charged platelets. *Europhys. Lett.*, 61:702, 2003. 2, 6

[13] H. Van Olphen. Rheological phenomena of clay sols in connection with the charge distribution on the micelles. *Discuss. Faraday Soc.*, 11:82, 1951. 2

[14] G. Broughton and L. Squires. The gelation of bentonite suspensions. *J. Phys. Chem.*, 40:1041, 1936. 2

[15] E. A. Hauser and C. E. Reed. Studies in thixotropy. ii. the thixotropic behavior structure of bentonite. *J. Phys. Chem.*, 41:911, 1937. 2, 86

[16] E. A. Hauser. Colloid chemistry of clays. *Chem. Rev.*, 37:287, 1945. 2

[17] K. Norrish. The swelling of montmorillonite. *Discuss. Faraday Soc.*, 18:120, 1954. 2

[18] A. Mourchid, A. Delville, J. Lambard, E. Lécolier, and P. Levitz. Phase diagram of colloidal dispersions of anisotropic charged particles: Equilibrium properties, structure, and rheology of laponite suspensions. *Langmuir*, 11:1942, 1995. 2, 5

[19] A. Mourchid, E. Lécolier, H. Van Damme, and P. Levitz. On viscoelastic, birefringent, and swelling properties of laponite clay suspensions: Revisited phase diagram. *Langmuir*, 14:4718, 1998. 2, 5, 6

[20] F. Pignon, J. M. Piau, and A. Magnin. Structure and pertinent length scale of a discotic clay gel. *Phys. Rev. Lett.*, 76:4857, 1997. 2

[21] F. Pignon, A. Magnin, and J. M. Piau. Butterfly light scattering pattern and rheology of a sheared thixotropic clay gel. *Phys. Rev. Lett.*, 79:4689, 1997. 2

[22] D. Bonn, H. Tanaka, G. Wegdam, H. Kellay, and J. Meunier. Aging of a colloidal 'wigner' glass. *Europhys. Lett.*, 45:52, 1998. 2

[23] D. Bonn, H. Kellay, H. Tanaka, G. Wegdam, and J. Meunier. Laponite: What is the difference between a gel and a glass? *Langmuir*, 15:7534, 1999. 2

[24] P. Levitz, E. Lécolier, A. Mourchid, A. Delville, and S. Lyonnard. Liquid-solid transition of laponite suspensions at very low ionic strength: Long-range electrostatic stabilisation of anisotropic colloids. *Europhys. Lett.*, 49:672, 2000. 2, 5

[25] A. Knaebel, M. Bellour, J-P. Munch, V. Viasnoff, F. Lequeux, and J. L. Harden. Aging behavior of laponite clay particle suspensions. *Europhys. Lett.*, 52:73, 2000. 2

[26] H. Tanaka, J. Meunier, and D. Bonn. Nonergodic states of charged colloidal suspensions: Repulsive and attractive glasses and gels. *Phys. Rev. E*, 69:031404, 2004. 2

[27] H. Tanaka, S. Jabbari-Farouji, J. Meunier, and D. Bonn. Kinetics of ergodic-to-nonergodic transitions in charged colloidal suspensions: Aging and gelation. *Phys. Rev. E*, 71:021402, 2005. 2

[28] D. R. Strachan, G. C. Kalur, and S. R. Raghavan. Size-dependent diffusion in an aging colloidal glass. *Phys. Rev. E*, 73:041509, 2006. 2

[29] F. Ianni, R. Di Leonardo, S. Gentilini, and G. Ruocco. Aging after shear rejuvenation in a soft glassy colloidal suspension: Evidence for two different regimes. *Phys. Rev. E*, 75:011408, 2007. 2

[30] L. Bellon, M. Gibert, and R. Hernández. Coupling between aging and convective motion in a colloidal glass of laponite. *Eur. Phys. J. B*, 55:101, 2007. 2

[31] M. Dijkstra, J. P. Hansen, and P. A. Madden. Gelation of a clay colloid suspension. *Phys. Rev. Lett.*, 75:2236, 1995. 2, 18

[32] M. Kroon, G. H. Wegdam, and R. Sprik. Dynamic light scattering studies on the sol-gel transition of a suspension of anisotropic colloidal particles. *Phys. Rev. E*, 54:6541, 1996. 2

[33] L. J. Michot, I. Bihannic, K. Porsch, S. Maddi, C. Baravian, J. Mougel, and P. Levitz. Phase diagrams of wyoming na-montmorillonite clay. influence of particle anisotropy. *Langmuir*, 20:10829, 2004. 2, 86, 152

[34] C. Martin, F. Pignon, J.-M. Piau, A. Magnin, P. Lindner, and B. Cabane. Dissociation of thixotropic clay gels. *Phys. Rev. E*, 66:021401, 2002. 2

[35] P. Mongondry, J. F. Tassin, and T. Nicolai. Revised state diagram of laponite dispersions. *J. Colloid Interface Sci.*, 283:397, 2005. 2

[36] B. Ruzicka, L. Zulian, and G. Ruocco. More on the phase diagram of laponite. *Langmuir*, 22:1106, 2006. 2

[37] I. Bihannic, L. J. Michot, B. S. Lartiges, D. Vantelon, J. Labille, F. Thomas, J. Susini, M. Salomé, and B. Fayard. First direct visualization of oriented mesostructures in clay gels by synchrotron-based x-ray fluorescence microscopy. *Langmuir*, 17:4144, 2001. 2, 147

[38] F. Cousin, V. Cabuil, and P. Levitz. Magnetic colloidal particles as probes for the determination of the structure of laponite suspensions. *Langmuir*, 18:1466, 2002. 2, 5, 147

[39] J. C. P. Gabriel, C. Sanchez, and P. Davidson. Observation of nematic liquid-crystal textures in aqueous gels of smectite clays. *J. Phys. Chem.*, 100:11139, 1996. 2, 4, 6, 80

[40] B. J. lemaire, P. Panine, J. C. P. Gabriel, and P. Davidson. The measurement by saxs of the nematic order parameter of laponite gels. *Europhys. Lett.*, 59:55, 2002. 2, 5, 6

[41] L. J. Michot, I. Bihannic, S. Maddi, S. S. Funari, C. Baravian, P. Levitz, and P. Davidson. Liquid-crystalline aqueous clay suspensions. *PNAS*, 103:16101, 2006. 2, 32, 80, 95, 152

[42] L. Onsager. The effects of shape on the interaction of colloidal particles. *Ann. N. Y. Acad. Sci.*, 51:627, 1949. 2, 44

[43] F. C. Bawden, N. W. Pirie, J. D. Bernal, and I. Fankuchen. Liquid crystalline substances from virus-infected plants. *Nature*, 138:1051, 1936. 2

[44] J. D. Bernal and I. Fankuchen. X-ray and crystallographic studies of plant virus preparations. *J. Gen. Physiol.*, 25:111, 1941. 2

[45] R. Eppenga and D. Frenkel. Monte carlo study of the isotropic-nematic transition in a fluid of thin hard disks. *Phys. Rev. Lett.*, 49:1089, 1982. 2, 46

[46] R. Eppenga and D. Frenkel. Monte carlo study of the isotropic and nematic phases of infinitely thin hard platelets. *Mol. Phys.*, 52:1303, 1984. 2, 25

[47] D. Frenkel. Onsagers spherocylinders revisited. *J. Phys. Chem.*, 91:4912, 1987. 2

[48] J. A. C. Veerman and D. Frenkel. Phase behavior of disklike hard-core mesogens. *Phys. Rev. A*, 45:5632, 1992. 2, 95

[49] P. Bolhuis and D. Frenkel. Tracing the phase boundaries of hard spherocylinders. *J. Chem. Phys.*, 106:666, 1997. 2

[50] M. A. Bates and D. Frenkel. Nematic-isotropic transition in polydisperse systems of infinitely thin hard platelets. *J. Chem. Phys.*, 110:6553, 1999. 2, 95, 152

[51] M. A. Bates. Influence of particle shape on the nematic-isotropic transition of colloidal platelet systems. *J. Chem. Phys.*, 111:1732, 1999. 2, 96, 152

[52] G. J. Vroege and H. N. W. Lekkerkerker. Phase transitions in lyotropic colloidal and polymer liquid crystals. *Rep. Prog. Phys.*, 55:1241, 1992. 2, 47

[53] P. A. Forsyth, Jr. S. Marcelja, D. J. Mitchell, and B. W. Ninham. Ordering in colloidal systems. *Adv. Colloid Interface Sci.*, 9:37, 1978. 2, 5

[54] W. W. Emerson. Liquid crystals of montmorillonite. *Nature*, 178:1248, 1956. 2

[55] H. Van Olphen. *An introduction to clay colloid chemistry.* Wiley-Interscience, New York, 2nd edition, 1977. 4

[56] B. Velde. *Introduction to clay minerals.* Chapman and Hall, London, 1998. 4

[57] A. Mourchid and P. Levitz. Long-term gelation of laponite aqueous dispersions. *Phys. Rev E*, 57:R4887, 1998. 5

[58] J. M. Saunders, J. W. Goodwin, R. M. Richardson, and B. Vincent. A small-angle x-ray scattering study of the structure of aqueous laponite dispersions. *J. Phys. Chem. B*, 103:9211, 1999. 5, 6

[59] W. Maier and A. Saupe. *Z. Naturforsch. A*, 13:564, 1958. 5, 44

[60] J. D. F. Ramsay and P. Lindner. Small-angle neutron scattering investigations of the structure of thixotropic dispersions of smectite clay colloids. *J. Chem. Soc., Faraday Trans.*, 89:4207, 1993. 6

[61] J. D. F. Ramsay, S. W. Swanton, and J. Bunce. Swelling and dispersion of smectite clay colloids: Determination of structure by neutron diffraction and small-angle neutron scattering. *J. Chem. Soc. Faraday Trans.*, 86:3919, 1990. 6

[62] C. Martin, F. Pignon, A. Magnin, M. Meireles, V. Lelière, P. Lindner, and B. Cabane. Osmotic compression and expansion of highly ordered clay dispersions. *Langmuir*, 22:4065, 2006. 6

[63] E. DiMasi, J. O. Fossum, T. Gog, and C. Venkataraman. Orientational order in gravity dispersed clay colloids: A synchrotron x-ray scattering study of na fluorohectorite suspensions. *Phys. Rev. E*, 64:061704, 2001. 6, 115

[64] J. O. Fossum, E. Gudding, D. d. M. Fonseca, Y. Meheust, E. DiMasi, T. Gog, and C. Venkataraman. Observations of orientational ordering in aqueous suspensions of a nano-layered silicate. *Energy*, 30:873, 2005. 6, 115

[65] P. Porion, M. Al Mukhtar, S. Meyer, A. M. Faugère, J. R. C. van der Maarel, and A. Delville. Nematic ordering of suspensions of charged anisotropic colloids detected by ^{23}na nuclear magnetic resonance. *J. Phys. Chem. B*, 105:10505, 2001. 6

[66] P. Porion, M. Al Mukhtar, A. M. Faugère, R. J. M. Pellenq, S. Meyer, and A. Delville. Water self-diffusion within nematic dispersions of nanocomposites: A multiscale analysis of ^{1}h pulsed gradient spin-echo nmr measurements. *J. Phys. Chem. B*, 107:4012, 2003. 6

[67] P. Porion, Stéphane Rodts, M. Al-Mukhtar, A. M. Faugère, and A. Delville. Anisotropy of the solvent self-diffusion tensor as a probe of nematic ordering within dispersions of nanocomposites. *Phys. Rev. Lett.*, 87:208302, 2001. 6

[68] P. Porion, M. Al-Mukhtar, A. M. Faugère, and A. Delville. ^{23}na nuclear magnetic resonance and 1h pulsed gradient spin-echo detection of the critical concentration corresponding to the isotrope/nematic transition within aqueous dispersions of charged anisotropic nanoparticles. *J. Phys. Chem. B*, 108:10825, 2004. 6

[69] P. Porion, A. M. Faugère, and A. Delville. Analysis of the degree of nematic ordering within dense aqueous dispersions of charged anisotropic colloids by ^{23}na nmr spectroscopy. *J. Phys. Chem. B*, 109:20145, 2005. 6

[70] E. N. de Azevedo, M. Engelsberg, J. O. Fossum, and R. E. de Souza. Anisotropic water diffusion in nematic self-assemblies of clay nanoplatelets suspended in water. *Langmuir*, 23:5100, 2007. 6, 26, 27, 28, 97, 109, 115, 152

[71] M. Schmidt, M. Dijkstra, and J.-P. Hansen. Competition between sedimentation and phase coexistence of colloidal dispersions under gravity. *J. Phys.: Condens. Matter*, 16:S4185, 2004. 6

[72] C. P. Royall, R. vanRoij, and A. van Blaaderen. Extended sedimentation profiles in charged colloids: the gravitational length, entropy, and electrostatics. *J. Phys.: Condens. Matter*, 17:2315, 2005. 6

[73] M. Rasa, B. H. Erné, B. Zoetekouw, R. van Roij, and A. P. Philipse. Macroscopic electric field and osmotic pressure in ultracentrifugal sedimentationdiffusion equilibria of charged colloids. *J. Phys.: Condens. Matter*, 17:2293, 2005. 6

[74] L. Bellier-Castella and H. Xu. Sedimentation profiles of polydisperse fluids. *J. Phys.: Condens. Matter*, 15:5417, 2003. 6

[75] W. Zhu, D. Sun, S. Liu, N. Wang, J. Zhang, and L. Luan. Multiphase coexistence in colloidal dispersions of positively charged layered double hydroxides. *Colloids and Surfaces A*. 6

[76] V. A. Baulin. Self-assembled aggregates in the gravitational field: Growth and nematic order. *J. Chem. Phys.*, 119:2874, 2003. 6

[77] Z. Dogic, A. P. Philipse, S. Fraden, and J. K. G. Dhont. Concentration-dependent sedimentation of colloidal rods. *J. Chem. Phys.*, 113:8368, 2000. 6

[78] V. A. Baulin and A. R. Khokhlov. Nematic ordering of rigid rods in a gravitational field. *Phys. Rev. E*, 60:2973, 1999. 6

[79] A. V. Petukhov, D. van der Beek, R. P. A. Dullens, I. P. Dolbnya, G. J. Vroege, and H. N. W. Lekkerkerker. Observation of a hexatic columnar liquid crystal of polydisperse colloidal disks. *Phys. Rev. Lett.*, 95:077801, 2005. 6, 25

[80] D. van der Beek, T. Schilling, and H. N. W. Lekkerkerker. Gravity-induced liquid crystal phase transitions of colloidal platelets. *J. Chem. Phys.*, 121:5423, 2004. 6

[81] J. E. G. J. Wijnhoven, D. D. vant Zand, D. van der Beek, and H. N. W. Lekkerkerker. Sedimentation and phase transitions of colloidal gibbsite platelets. *Langmuir*, 21:10422, 2005. 6

[82] J. Zhang, L. Luan, W. Zhu, S. Liu, and D. Sun. Phase behavior of aqueous suspensions of mg$_2$al layered double hydroxide: The competition among nematic ordering, sedimentation, and gelation. *Langmuir*, 23:5331, 2007. 6

[83] A. P. Philipse and G. H. Koenderink. Sedimentationdiffusion profiles and layered sedimentation of charged colloids at low ionic strength. *Adv. Colloid Interface Sci.*, 100-102:613, 2003. 6

[84] A. P. Philipse. Remarks on the donnan condenser in the sedimentation-diffusion equilibrium of charged colloids. *J. Phys.: Condens. Matter*, 16:S4051, 2004. 6

[85] R. van Roij. Defying gravity with entropy and electrostatics: sedimentation of charged colloids. *J. Phys.: Condens. Matter*, 15:S3569, 2003. 6

[86] D. M. Fonseca, Y. Méheust, J. O. Fossum, K. D. Knudsen, K. J. Måløy, and K. P. S. Parmar. Phase behavior of platelet-shaped nanosilicate colloids in saline solutions a small-angle x-ray scattering study. *J. Appl. Cryst.*, 40:292, 2007. 6

[87] J. O. Fossum. Physical phenomena in clays. *Physica A*, 270:270, 1999. 7

[88] http://en.wikipedia.org/wiki/colloid. 7

[89] edited by P. Bernier et al. S. A. Solin. *Chemical Physics of Intercalation II, page 161.* Plenum Press, New York, 1993. 10

[90] G. W. Brindley and G. Pedro. Report of the aipea nomenclature committee. *AIPEA Newsletter*, No. 7:8–13, 1972. 11

[91] P. D. Kaviratna, Thomas J. Pinnavaia, and P. A. Schroeder. Dielectric properties of smectite clays. *J. Phys. Chem. Solids*, 57:1897, 1996. 12

[92] J. Israelachvili. *Intermolecular Surface Forces.* Academic Press, Inc., London, 1992. 17

[93] P. J. Flory. Introductory lecture. *Faraday Discuss. Chem. Soc.*, 57:7, 1974. 18

[94] B. J. Lemaire, P. Panine, J. C. P. Gabriel, and P. Davidson. The measurement by saxs of the nematic order parameter of laponite gels. *Europhys. Lett.*, 59:55, 2002. 21

[95] P. J. Collings and M. Hird. *Introduction to Liquid Crystals Chemistry and Physics*. Taylor Francis, 1997. 21

[96] P. Bolhuis and D. Frenkel. Tracing the phase boundaries of hard spherocylinders. *J. Chem. Phys.*, 106:666, 1997. 22

[97] D. van der Beek. *Liquid crystal phase behaviour of colloidal platelets in external fields*. Ph.d. thesis, Universiteit Utrecht, Utrecht, 2005. 24, 26

[98] D. van der Beek and H. N. W. Lekkerkerker. Liquid crystal phases of charged colloidal platelets. *Langmuir*, 20:8582, 2004. 25, 96

[99] J. Kerr. A new relation between electricity and light: dielectrified media birefringent. *Phil. Mag.*, 50:337, 1875. 26

[100] Q. Majoran. Sur la biréfringence magnétique. *C. R. Acad. Sci.*, 135:159, 1902. 26

[101] Q. Majoran. Sur le dichroïsme magnétique. *C. R. Acad. Sci.*, 135:235, 1902. 26

[102] Q. Majoran. Su due nuovi fenomeni magneto-ottici osservati normalmente alle linee di forza. *Rend. Accad. Lincei*, 11-1:374, 1902. 26

[103] Q. Majoran. Sul metode e sulle sostanze da adoperarsi, per osservare la birefrangenza magnetica. *Rend. Accad. Lincei*, 11-1:463, 1902. 26

[104] Q. Majoran. Sulla birifrangenza magnetica e su altri fenomeni che l'accompagnano. *Rend. Accad. Lincei*, 11-1:531, 1902. 26

[105] Q. Majoran. Sulle rotazioni bimagnetiche del piano di polarizazione della luce. *Rend. Accad. Lincei*, 11-2:90, 1902. 26

[106] Q. Majoran. Sulla rapidità con cui si manifesta la birifrangenza magnetica. *Rend. Accad. Lincei*, 11-2:139, 1902. 26

[107] A. Cotton and H. Mouton. Sur le phénomène de majorana. *C. R. Acad. Sci.*, 141:317, 1905. 26

[108] A. Cotton and H. Mouton. Sur la biréfringence magnétique. nouveaux liquides actifs. *C. R. Acad. Sci.*, 141:349, 1905. 26

[109] A. Cotton and H. Mouton. Nouvelles propriétés magnéto-optiques des solutions colloïdales d'hydroxyde de fer. *C. R. Acad. Sci.*, 142:203, 1906. 26

[110] A. Cotton and H. Mouton. Sur les proriétés magnéto-optiques des colloides et des liqueurs hétérogènes. *Ann. de Chim. et de Phys.*, 11:145, 1907. 26

[111] A. Cotton and H. Mouton. Sur les proriétés magnéto-optiques des colloides et des liqueurs hétérogènes-deuxième partie. *Ann. de Chim. et de Phys.*, 11:289, 1907. 26

[112] A. Cotton and H. Mouton. Nouvelle propriété optique (biréfringence magnétique) de certains liquides organiques non colloïdaux. *C. R. Acad. Sci.*, 145:229, 1907. 26

[113] F. Kimura, Tsunehisa Kimura, M. Tamura, A. Hirai, M. Ikuno, and F. Horii. Magnetic alignment of the chiral nematic phase of a cellulose microfibril suspension. *Langmuir*, 21:2034, 2005. 26

[114] T. Kimura, , and M. Yoshino. Three-dimensional crystal alignment using a time-dependent elliptic magnetic field. *Langmuir*, 21:4805, 2005. 26

[115] T. B. Cardon, P. C. Dave, and G. A. Lorigan. Magnetically aligned phospholipid bilayers with large q ratios stabilize magnetic alignment with high order in the gel and lα phases. *Langmuir*, 21:4291, 2005. 26

[116] B. J. Lemaire, J. Ferré P. Davidson, J. P. Jamet, P. Panine, I. Dozov, and J. P. Jolivet. Outstanding magnetic properties of nematic suspensions of goethite (α-feooh) nanorods. *Phys. Rev. Lett.*, 88:125507, 2002. 26

[117] B. J. Lemaire, P. Davidson, Jacques Ferre, P. Panine I. Dozov D. Stoenescuc J. P. Jamet, D. Petermann, and J. P. Jolivet. The complex phase behaviour of suspensions of goethite (α-feooh) nanorods in a magnetic field. *Faraday Discuss.*, 128:271, 2005. 26

[118] B. J. Lemaire, P. Davidson, P. Panine, and J. P. Jolivet. Magnetic-field-induced nematic-columnar phase transition in aqueous suspensions of goethite (α-feooh) nanorods. *Phys. Rev. Lett.*, 93:267801, 2004. 26

[119] D. van der Beek, A. V. Petukhov, P. Davidson, J. Ferré, J. P. Jamet, H. H. Wensink, G. J. Vroege, W. Bras, and H. N. W. Lekkerkerker. Magnetic-field-induced orientational order in the isotropic phase of hard colloidal platelets. *Phys. Rev. E*, 73:041402, 2006. 26

[120] Gert Strobl. *Condensed Matter Physics, Crystals, Liquid, Liquid Crystals, and Polymers.* Springer-Verlag Berlin Heidelberg New York, 2004. 26, 37

[121] F. M. van der Kooij and H. N. W. Lekkerkerker. Formation of nematic liquid crystals in suspensions of hard colloidal platelets. *J. Phys. Chem. B*, 102:7829, 1998. 28, 95, 96, 152

[122] F. C. Frank. I. liquid crystals. on the theory of liquid crystals. *Disc. Faraday Soc.*, 25:19, 1958. 29

[123] V. Fréedericksz and V. Zolina. Forces causing the orientation of an anisotropic liquid. *Trans. Faraday Soc.*, 29:919, 1933. 31

[124] R. Williams. Domains in liquid crystals. *J. Chem. Phys.*, 39:384, 1963. 32

[125] S. Chandrasekhar. *Hydrodynamic and Hydromagnetic Instability.* Oxford Univeristy Press, London, 1961. 32, 34

[126] Y. W. Hui, M. R. Kuzma, M. San Miquel, and M. M. Labes. Periodic structures induced by director reorientation in the lyotropic nematic phase of disodium cromoglycatewater. *J. Chem. Phys.*, 83:288, 1985. 32

[127] A. J. Hurd, S. Fraden, F. Lonberg, and R. B. Meyer. *J. Phys. (Paris)*, 46:905, 1985. 32

[128] N. Schwenk. Ph.d. thesis, Max-Planck-Institut für Polymerforschung, Mainz, 1991. 32

[129] M. R. Kuzma. Nonequilibrium periodic structures induced by rotating and static fields in a lyotropic nematic liquid crystal. *Phys. Rev. Lett.*, 57:349, 1986. 32, 34, 112

[130] F. Lonberg and R. B. Meyer. New ground state for the splay-fréedericksz transition in a polymer nematic liquid crystal. *Phys. Rev. Lett.*, 55:718, 1985. 32

[131] E. F. Carr. Domains due to magnetic fields in bulk samples of a nematic liquid crystal. *Mol. Cryst. Liq. Cryst*, 34:159, 1977. 32

[132] J. Charvolin and Y. Hendrikx. *J. Phys. (Paris) Lett.*, 41:L597, 1980. 32

[133] L. J. Yu and A. Saupe. Liquid crystalline phases of the sodium decylsulfate/decanol/water system. nematic-nematic and cholesteric-cholesteric phase transitions. *J. Am. Chem. Soc.*, 102:4879, 1980. 32

[134] H. Lee and M. M. Labes. Lyotropic cholesteric and nematic phases of disodium cromoglycate in magnetic fields. *Mol. Cryst. Liq. Cryst*, 84:137, 1982. 32

[135] F. Lonberg, S. Fraden, A. J. Hurd, and R. B. Meyer. Field-induced transient periodic structures in nematic liquid crystals: The twist-fréedericksz transition. *Phys. Rev. Lett.*, 52:1903, 1984. 32

[136] S. Fraden, A. J. Hurd, R. B. Meyer, M. Cahoon, and D. L. D. Caspar. *J. Phys. (Paris) Colloq.*, 46:C3–85, 1985. 32

[137] D. V. Rose and M. R. Kuzma. *Mol. Cryst. Liq. Cryst., Lett. Sect.*, 4:L39, 1986. 32

[138] Jr. C. R. Fincher. Field-induced textures and elastic constants of nematic polymers. *Macromolecules*, 19:2431, 1986. 32

[139] A. F. Martins, P. Esnault, and F. Volono. Measurement of the viscoelastic coefficients of main-chain nematic polymers by an nmr technique. *Phys. Rev. Lett.*, 57:1745, 1986. 32

[140] J. P. McClymer and M. M. Labes. The dynamics of the formation of a periodic deformation in a lyotropic liquid crystal. *Mol. Cryst. Liq. Cryst.*, 144:275, 1987. 32

[141] X. Commeinhes, P. Davidson, C. Bourgaux, and J. Livage. Orientation of liquid-crystalline suspensions of vanadium pentoxide ribbons by a magnetic field. *Adv. Mater.*, 9:900, 1997. 32

[142] D. van der Beek, P. Davidson, H. H. Wensink, G. J. Vroege, and H. N. W. Lekkerkerker. Influence of a magnetic field on the nematic phase of hard colloidal platelets. *Phys. Rev. E*, 77:031708, 2008. 32, 34, 112, 153

[143] H. Haken. *Synergetics: An Introduction.* Springer-Verlag, New York, 1978. 33

[144] G. Nicolis and I. Prigogine. *Self-Organization in Non-equilibrium Systems.* Wiley, New-York, 1977. 33

[145] E. Guyon, R. Meyer, and J. Salan. Domain structure in the nematic freedericksz transition. *Mol. Cryst. Liq. Cryst*, 54:261, 1979. 34

[146] S. Fraden and R. B. Meyer. Comment on 'nonequilibrium periodic structures induced by rotating and static fields in a lyotropic nematic liquid crystal'. *Phys. Rev. Lett.*, 57:3122, 1986. 34

[147] M. Grigutsch, N. Klöpper, H. Schmiedel, and R. Stannarius. Transient structures in the twist fréedericksz transition of low-molecular-weight nematic liquid crystals. *Phys. Rev. E*, 49:5452, 1994. 34

[148] G. Srajer, S. Fraden, and R. B. Meyer. Field-induced nonequilibrium periodic structures in nematic liquid crystals: Nonlinear study of the twist frederiks transition. *Phys. Rev. A*, 39:4828, 1989. 35

[149] F. Sagues, F. Arias, and M. San Miguel. Nonlinear effects in the dynamics of transient pattern formation in nematics. *Phys. Rev. A*, 37:3601, 1988. 35

[150] T. Scharf. *Polarized Light in Liquid Crystals and Polymers.* John Wiley Sons, Inc, 2007. 42, 103

[151] G. Guidone Peroli, G. Hillig, A. Saupe, and E. G. Virga. Orientational capillary pressure on a nematic point defect. *Phys. Rev. E*, 58:3259, 1998. 42

[152] J. P. Straley. The gas of long rods as a model for lyotropic liquid crystals. *Mol. Cryst. Liq. Cryst.*, 22:333, 1973. 46

[153] L. Harnau, D. Costa, and J. P. Hansen. A solvable interaction site model for lamellar colloids. *Europhys. Lett.*, 53:729, 2001. 47

[154] K. S. Schweizer and J. G. Curro. Integral equation theories of the structure, thermodynamics, and phase transitions of polymer fluids. *Adv. Chem. Phys.*, 98:1, 1996. 47

[155] D. G. Rowan and J. P. Hansen. Salt-induced ordering in lamellar colloids. *Langmuir*, 18:2063, 2002. 47, 80

[156] P. A. Buining. *Preparation and properties of dispersion of colloidal Boehmite rods*. Ph.d. thesis, Universiteit Utrecht, Utrecht, 1992. 47

[157] H. N. W. Lekkerkerker and G. J. Vroege. Lyotropic colloidal and macromolecular liquid crystals. *Philos. Trans. R. Soc. London A*, 344:419, 1993. 47

[158] http://www.vitrocom.com/home.htm. 50

[159] J. M. Bennett. In M. Bass, E. W. van Stryland, D. R. Williams, and W. L. Wolfe, editors, *Handbook of Optics*, volume 1. McGraw-Hill, New York, 1995. 52

[160] http://en.wikipedia.org/wiki/traffic_flow. 66

[161] S. Abend and G. Lagaly. Sol-gel transition of sodium montmorillonite dispersions. *Applied Clay Science*, 16:201, 2000. 80

[162] K. D. Knudsen, J. O. Fossum, G. Helgesen, and V. Bergaplass. Pore characteristics and water absorption in a synthetic smectite clay. *J. Appl. Cryst.*, 36:587, 2003. 94

[163] L. J. Michot, I. Bihannic, S. Maddi, C. Baravian, P. Levitz, and P. Davidson. Sol/gel and isotropic/nematic transitions in aqueous suspensions of natural nontronite clay. influence of particle anisotropy. 1. features of the i/n transition. *Langmuir*, 24:3127, 2008. 95

[164] F. M. van der Kooij and H. N. W. Lekkerkerker. Liquid-crystal phases formed in mixed suspensions of rod- and platelike colloids. *Langmuir*, 16:10144, 2000. 97

[165] A. Delville, J. Grandjean, and P. Laszlo. Order acquisition by clay platelets in a magnetic field. nmr study of the structure and microdynamics of the adsorbed water layer. *J. Phys. Chem.*, 95:1383, 1991. 97

[166] C. Uyeda. Diamagnetic anisotropies of oxide minerals. *Phys. Chem. Miner.*, 20:77, 1993. 97

[167] C. Uyeda, T. Takeuchi, A. Yamagishi, and M. Date. Diamagnetic orientaion of clay mineral grains. *J. Phys. Soc. Jpn.*, 60:3234, 1991. 97

[168] C. Uyeda, T. Takeuchi, A. Yamagishi, and M. Date. Diamagnetic orientation of layered silicates. *Physica B*, 177:519, 1992. 97

[169] C. Uyeda, A. Tsuchiyama, T. Yamanaka, and M. Date. Field-induced oscillation and rotation of diamagnetic oxide crystals. *Phys. Chem. Miner.*, 20:82, 1993. 97

[170] T. Takahashi, T. Ohkubo, and Y. Ikeda. Montmorillonite alignment induced by magnetic field: Evidence based on the diffusion anisotropy of water molecules. *J. Colloid Interface Sci.*, 299:198, 2006. 97

[171] http://www.brocku.ca/earthsciences/people/gfinn/optical/polylit1.jpg. 103

[172] G. J. da Silva, J. O. Fossum, E. DiMasi, K. J. Måløy, and S. B. Lutnæs. Synchrotron x-ray scattering studies of water intercalation in a layered synthetic silicate. *Phys. Rev. E*, 66:011303, 2002. 116

[173] G. J. da Silva, J. O. Fossum, E. DiMasi, K. J. Måløy, and S. B. Lutnæs. Dynamics of water intercalation fronts in a nano-layered synthetic silicate: A synchrotron x-ray scattering study. *Physica B: Condensed Matter*, 370:90, 2005. 116

[174] D. van der Beek, H. Reich, P. van der Schoot, M. Dijkstra, T. Schilling, R. Vink, M. Schmidt, R. van Roij, and H. Lekkerkerker. Isotropic-nematic interface and wetting in suspensions of colloidal platelets. *Phys. Rev. Lett.*, 97:087801, 2006. 116, 140, 154

[175] R. Zwanzig. First-order phase transition in a gas of long thin rods. *J. Chem. Phys.*, 39:1714, 1963. 140

[176] M. Bier, L. Harnau, and S. Dietrich. Bulk and interfacial properties of binary hard-platelet fluids. *Phys. Rev. E*, 69:021506, 2004. 140, 154

[177] M. Bier, L. Harnau, and S. Dietrich. Free isotropic-nematic interfaces in fluids of charged platelike colloids. *J. Chem. Phys.*, 123:114906, 2005. 140

[178] Jorge Viamontes and Jay X. Tang. Nematic liquid crystalline formation of f-actin displays features of a continuous transition. *Mat. Res. Soc. Symp. Proc.*, 711:FF4.9.1, 2002. 149

[179] http://en.wikipedia.org/wiki/birefringence. 187

Appendix A

Videos

Table A.1: Videos showing the dynamical behaviour of some selected samples. The file names display the clay concentration, powder type and salt concentration.

#	File name	Running time (min.sek)	Recording time	Notes
1	0.5%_april_10^4.mpg	1.31	75 days	The video of Figure 3.2.
2	1%_august_10^4.mpg	0.09	11 days	
3	1%_august_5x10^4.mpg	0.33	60 days	
4	1%_august_5x10^3.mpg	0.31	70 days	
5	1%_crushed_august_10^3.mpg	0.37	35 days	
6	1%_april_10^3.wmv	0.18	4 days	Shows magnet and shearing effects.
7	2%_august_5x10^4.mpg	0.53	53 days	
8	2%_august_10^3.avi	3.31	55 days	High frame (picture) rate, sample in Figure 3.2.
9	2%_august_10^3se.wmv	3.31	55 days	Special edition showing COMPLEX banner and web addresses.
10	2%_august_5x10^2.avi	0.11	3 days	Effective dynamics in only 3 days.
11	2%_crushedAugust_10^3.mpg	0.25	36 days	
12	2%_april_10^4.mpg	0.40	20 days	Shows backward propagating waves?
13	2%_april_10^3.mpg	0.31	35 days	
14	3%_august_5x10^4.avi	0.26	30 days	
15	3%_august_10^3.avi	0.37	50 days	Large file, not consistent with the suspensions on presented pictures.
16	3%_crushed_august_10^3.mpg	1.46	50 days	Times at the end are missing, but the period ends at 50 days.
17	stripepattern.mpg	0.30	10 hours	Videos of Fréedericksz transition.

Appendix B

SAXS

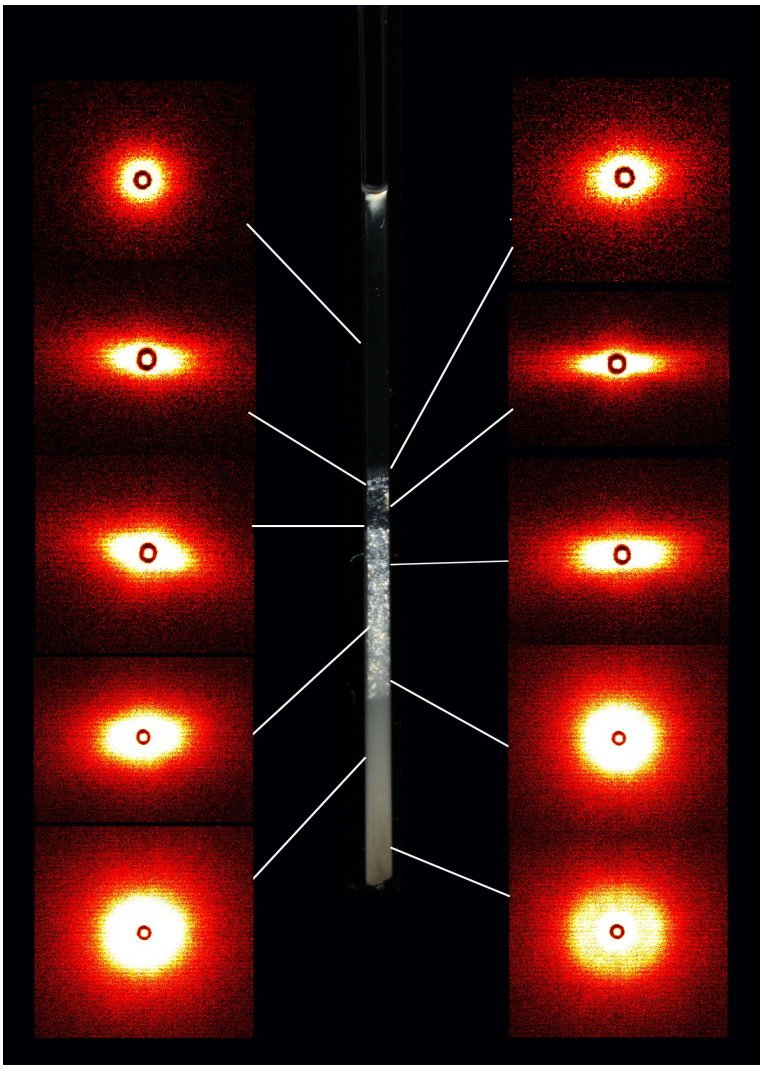

Figure B.1: Small angle X-ray scattering of various heights of a 3 w/w% November 10^{-3} M capillary sample.

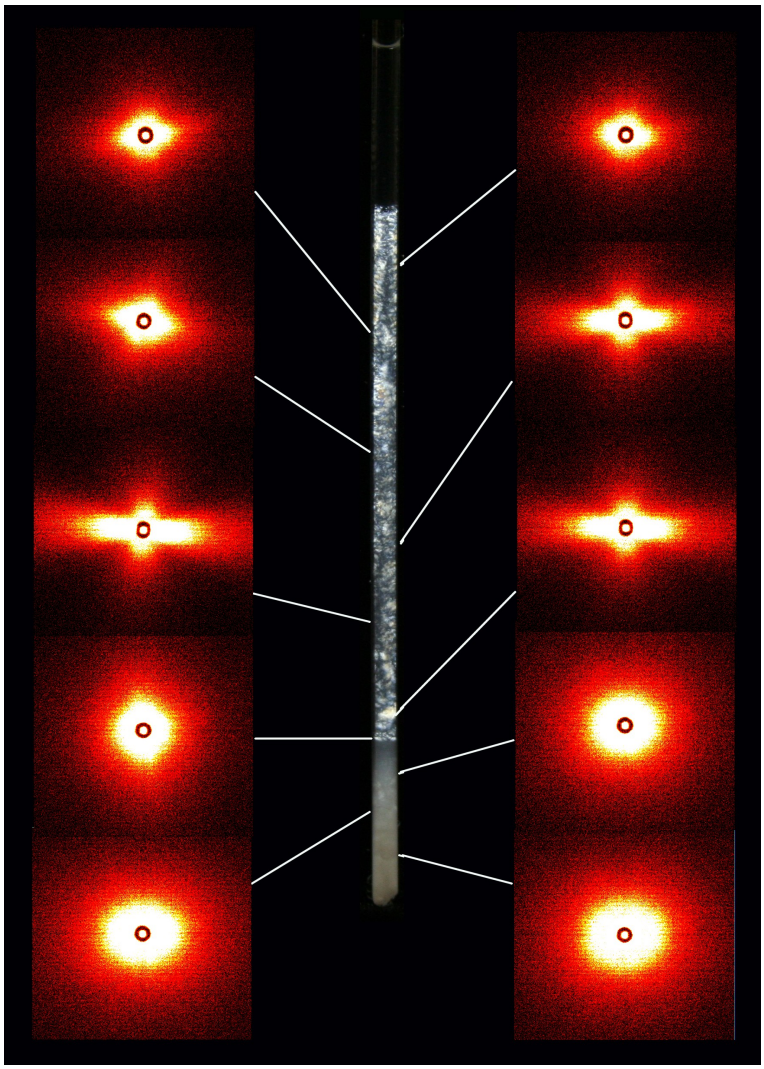

Figure B.2: Small angle X-ray scattering of various heights of a 3 w/w% uncrushed April 10^{-3} M capillary sample.

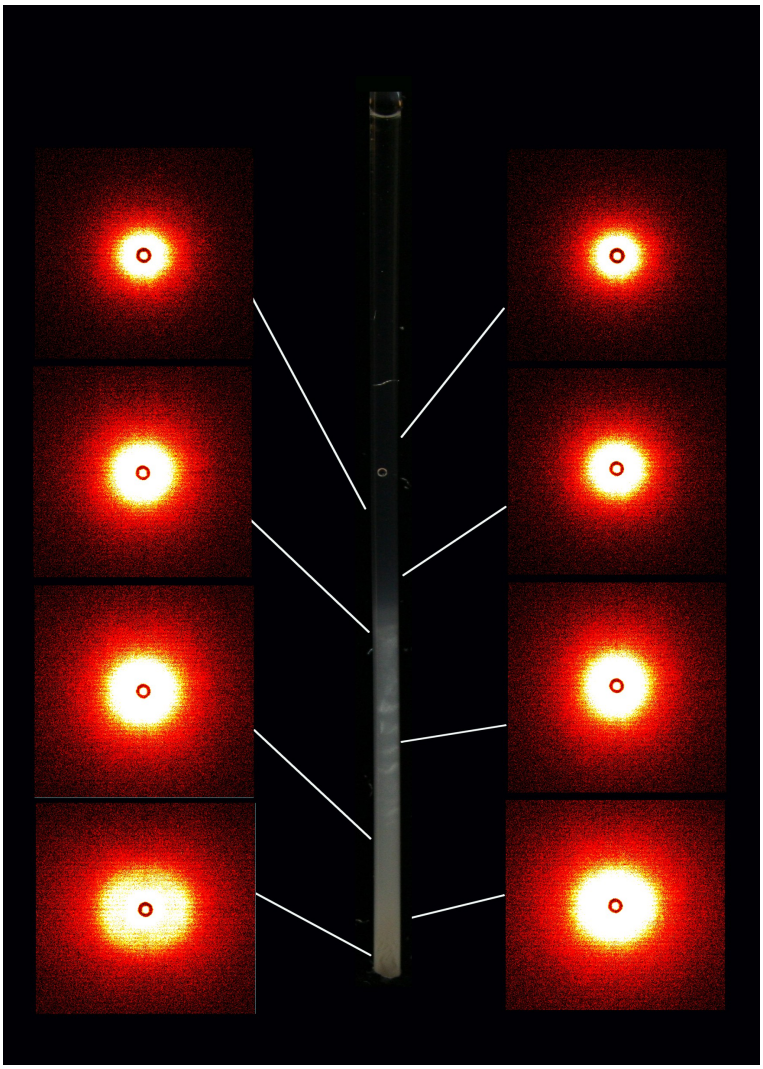

Figure B.3: Small angle X-ray scattering of various heights of a 3 w/w% crushed August 10^{-3} M capillary sample.

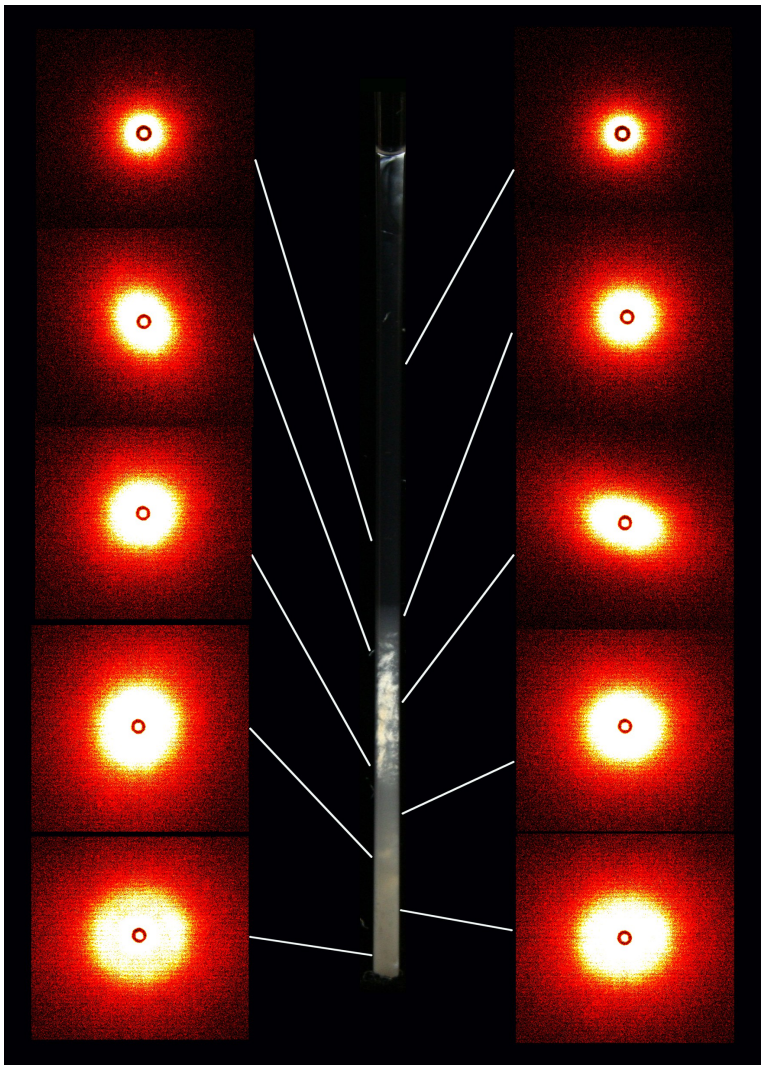

Figure B.4: Small angle X-ray scattering of various heights of a 3 w/w% milling machine crushed August 10^{-3} M capillary sample.

Appendix C

Drawings

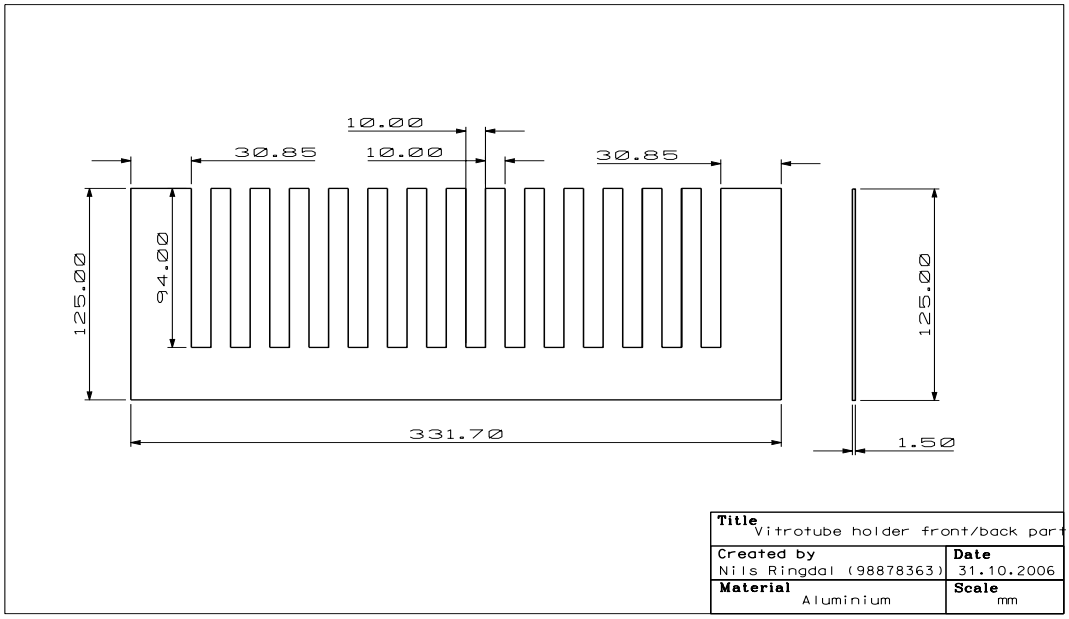

Figure C.1: The part that makes up the front and back of the sample rack. In one rack two pieces are made and attached by screws to the middle part.

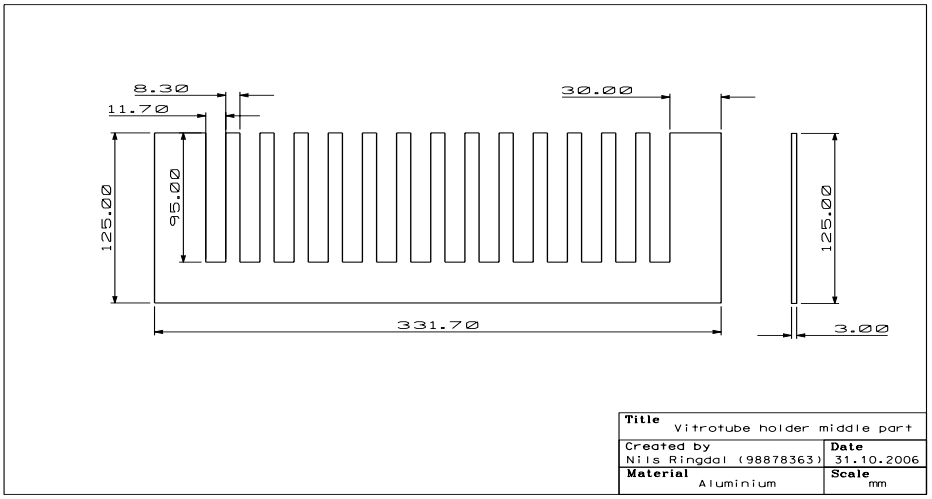

Figure C.2: The middle part of the Vitrotube rack. Because the Vitrotubes become a bit wider when they are sealed with parafilm, the openings are made slightly larger than the 10 mm width of the Vitrotube.

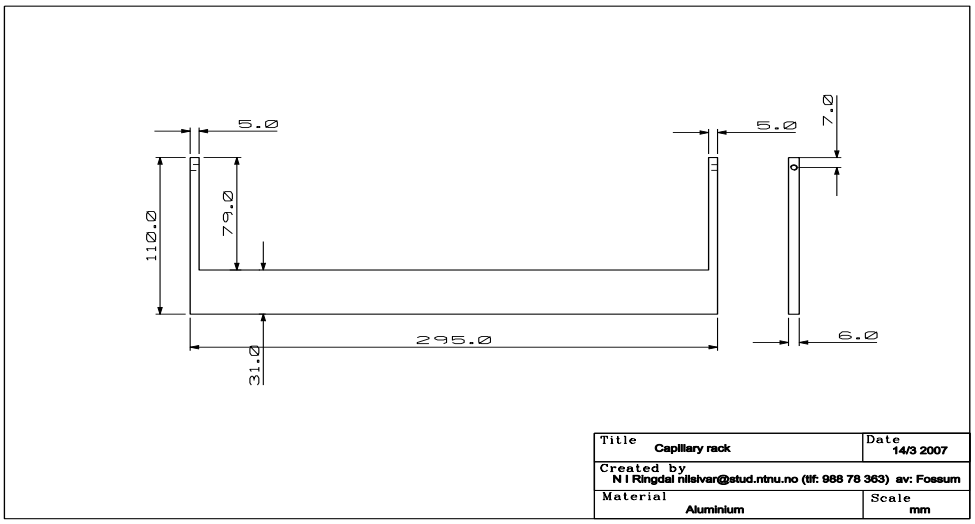

Figure C.3: Sample rack which is designed to contain Mark tubes.

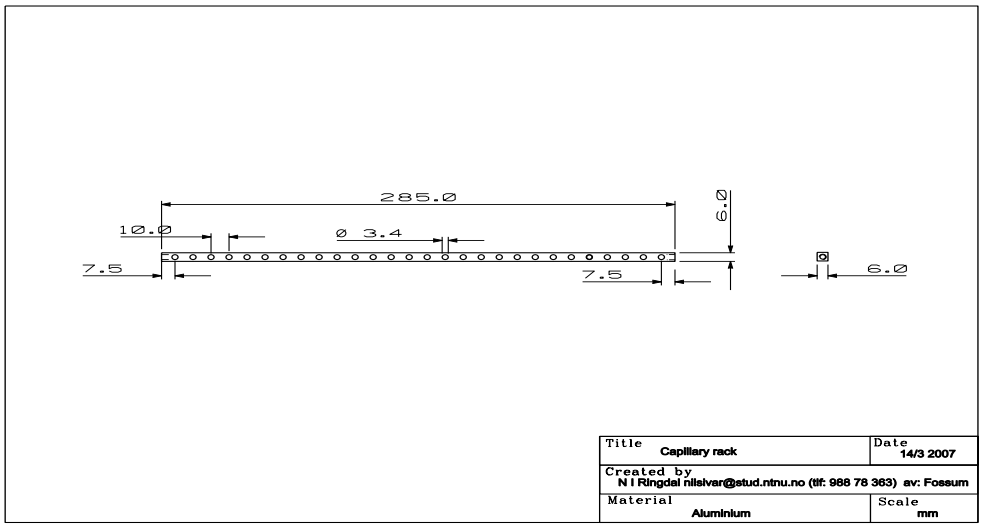

Figure C.4: The top part of the capillary rack in Figure C.3.

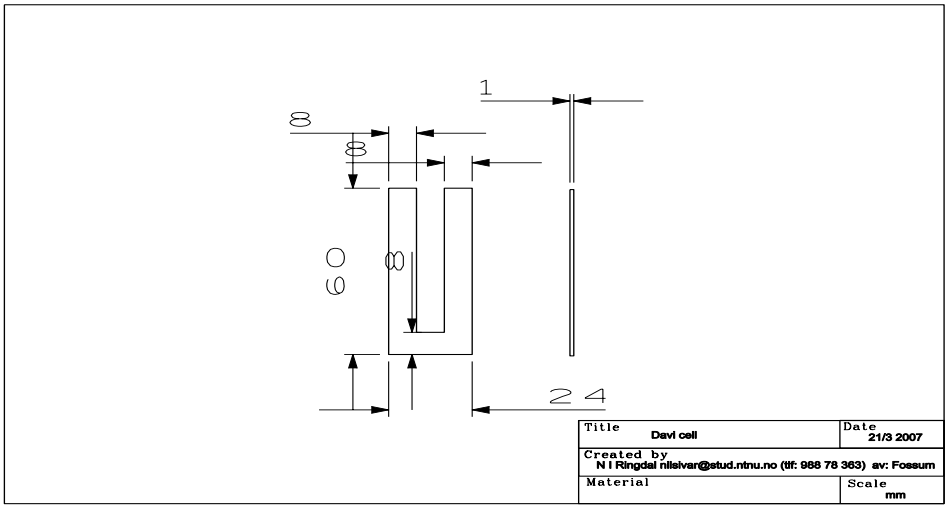

Figure C.5: The plastic POM structure of the Davi cell. The final cell is made by gluing microscope glass slides on both sides.

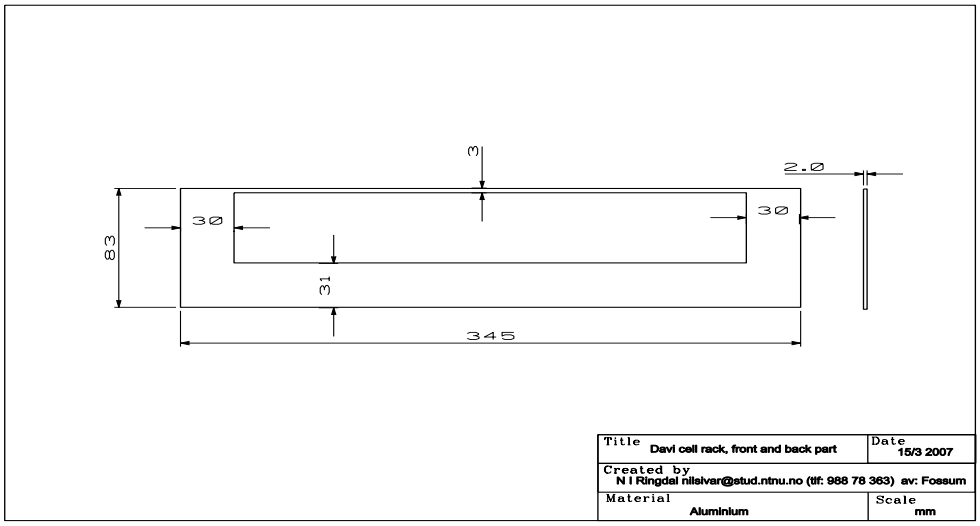

Figure C.6: The front/back parts of a rack designed to contain Davi cell samples. Can also be used for other flat capillaries.

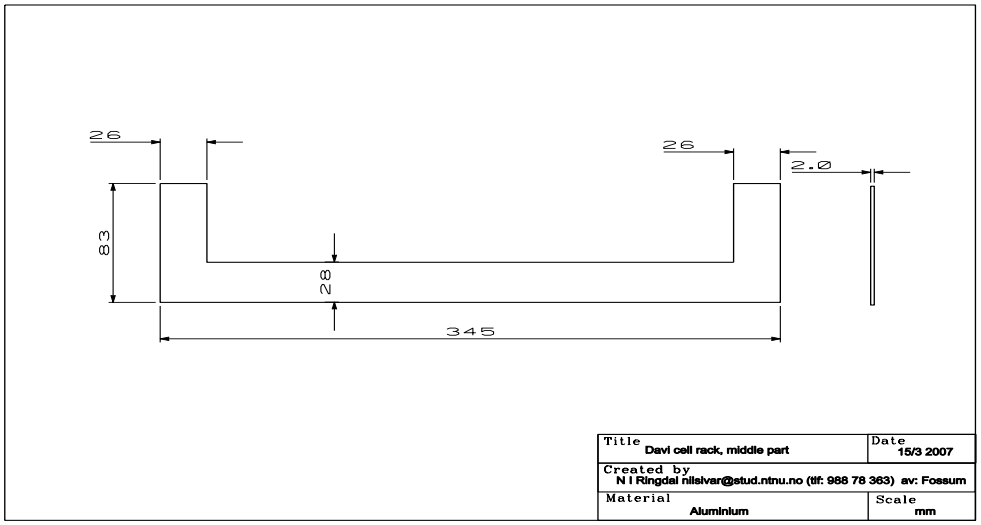

Figure C.7: The middle part of the Davi cell rack.

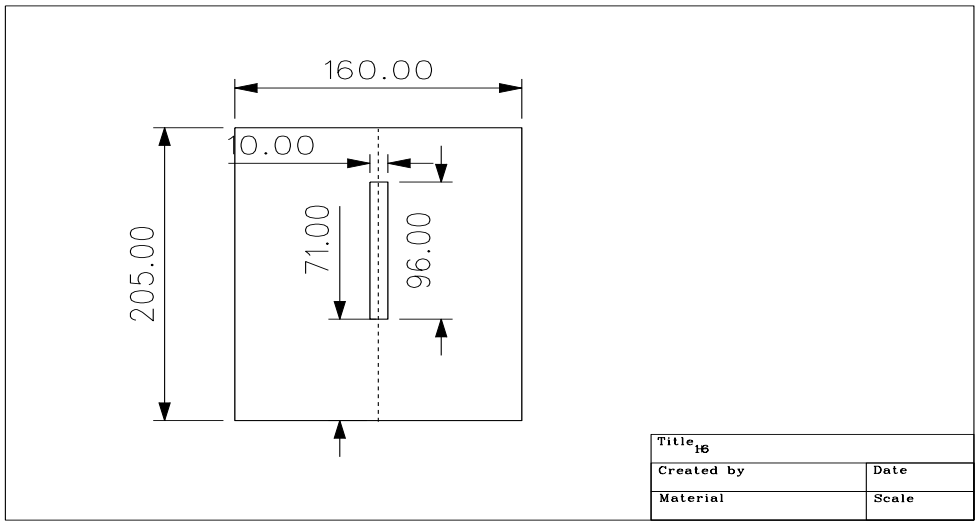

Figure C.8: This slit screen is placed between the camera and the samples to shut out light.

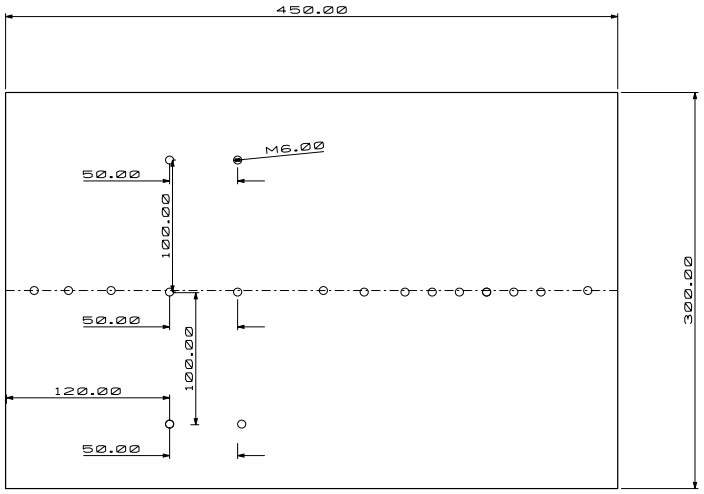

Figure C.9: This makes up the board for the camera, stage and polarizers.

C.1 Rack

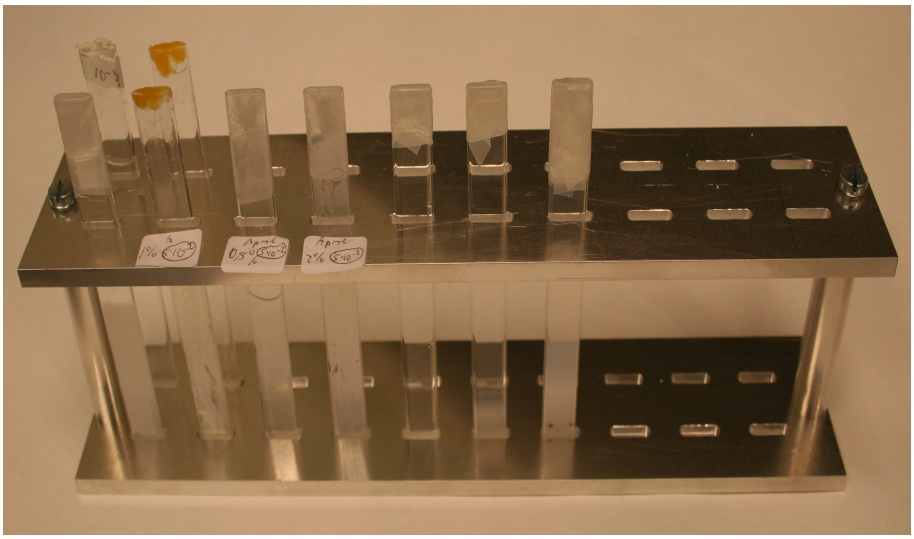

Figure C.10: A special designed rack for the Vitrotubes.

Appendix D

Matlab Script for Measuring Image Intensity Variations

D.1 Settling from Isotropic Sol

```
0001 function isotropicSettling
0002
0003 Image = rgb2gray(imread('rImage_4013.JPG'));
0004
0005 IsotropicSol = 0; %This matrix shall contain the pixelvalues of
0006                   %the black isotropic.
0007 Pixel_height = 800; %The height of the isotropic upper sol in pixels.
0008 Start_left = 1690; %The pixel value from the left end of the image.
0009 End_right = 1990; %The pixel value that ends the image.
0010 numberOfIntervals = Pixel_height/50
0011
0012 for k = Start_left:End_right; %From Imtool(Image) this specifies
0013                               %the width of the isotropic sol.
0014     for i = 1:Pixel_height; %Read from the top (1) to the start
0015                             %of the nematic phase (Pixel_height)
0016         IsotropicSol(i,k) = double(Image(i,k)); %Set IsotropicSol
0017                                                 %equal double grI
0018     end
0019 end
0020
0021 %Correcting for white pixel impurities (dust, scratch, bubbles etc.).
0022 for k = Start_left:End_right;
0023     for i = 16:Pixel_height-0; %Set the height 50 px since the
0024                                %region close to the nematic phase
0025                                %will naturally be whiter.
0026         if IsotropicSol(i,k) > 4 %If the pixel value is higher than 5,
0027                                  %it is most likely an impurity.
0028             IsotropicSol(i,k) = IsotropicSol(i-15,k); %Use the pixel
```

```
0029                                    %value that is 10 pixels higher.
0030         end
0031     end
0032 end
0033
0034 VerticalPixels = 0;
0035 for i = 1:Pixel_height;
0036     VerticalPixels(i) = 0;
0037 end
0038
0039 %VerticalPixels is the sum of the pixel values of the iotropic width.
0040 for k = Start_left:End_right;
0041     for i = 1:Pixel_height;
0042         VerticalPixels(i) = VerticalPixels(i) + IsotropicSol(i,k);
0043     end
0044 end
0045
0046 %Devide the isotropic phase into equal regions of pixel height 50.
0047 interval = 0;
0048 for i = 1:39;
0049     interval(i) = 0;
0050 end
0051
0052 pixelStart = 1;
0053 pixelEnd = 50;
0054 for i=1:numberOfIntervals;
0055     for j = pixelStart:pixelEnd;
0056         interval(i) = interval(i) + VerticalPixels(j);
0057     end
0058     pixelStart = pixelEnd + 1;
0059     pixelEnd = pixelEnd + 50;
0060 end
0061
0062 %Average intensity
0063 for i = 1:numberOfIntervals;
0064     interval(i) = interval(i)/(50*(End_right-Start_left));
0065 end
0066 intervalkorrigert = 0;
0067 for i = 1:numberOfIntervals;
0068     intervalkorrigert(i) = interval(i);
0069 end
0070
0071 %One interval length corresponds to 1.5 mm.
0072 endOfLength = numberOfIntervals*1.5
0073 x = [1.5:1.5:endOfLength];
0074
```

```
0075 plot(x,intervalkorrigert,'k.')
0076 xlabel('\bf Height from top (mm)')
0077 ylabel('\bf Intensity (Average pixel value)')
0078
```

D.2 Changes in Intensity over Time

```
0001 function intensity
0002
0003 %The script gives the change of intensity of a series of
0004 %several pictures taken for a given period of time.
0005 %Save the script in a folder consisting of pictures
0006 %that are more or less the same.
0007
0008 x = dir;
0009 numofpic =  length(x)
0010 i=9;
0011
0012 x(9).name
0013
0014 intensityd1 = 0
0015
0016 o=1;
0017 p=1;
0018 intens = 0;
0019 for o=1:19;
0020     for p=1:12;
0021         intens(o,p) = 3;
0022     end
0023 end
0024
0025 totaltime = 0;
0026 tq=1;
0027 for tq=1:numofpic;
0028     totaltime(tq) = tq;
0029 end
0030
0031 totalTimeHour = 0;
0032 tqr=1;
0033 for tqr=1:numofpic;
0034     totaltime(tqr) = tqr;
0035 end
0036
0037 totalTimeDays = 0;
0038 tqrw=1;
```

```
0039 for tqrw=1:numofpic;
0040     totaltime(tqrw) = tqrw;
0041 end
0042
0043 Image = imread(x(9).name);
0044 gr = rgb2gray(Image);
0045 b = double(gr);
0046
0047 info = imfinfo(x(9).name);
0048 dateOfFirstImage = info.FileModDate;
0049
0050 for i=9:numofpic;
0051     Image = imread(x(i).name);
0052      gr = rgb2gray(Image);
0053      b = double(gr);
0054
0055      x(i).name
0056
0057      pixel_height_start = 2147;
0058      a=1;
0059      for a=1:19;
0060          pixel_row_start = 1600; %1675
0061          pixel_row_end = 2050;  %2027
0062          height = pixel_height_start - 107;
0063          intensityd1 = 0;
0064
0065          while pixel_height_start > height;
0066
0067             for pixel_row_start = pixel_row_start:pixel_row_end;
0068             intensityd1 = b(pixel_height_start,pixel_row_start) + intensityd1;
0069             end
0070             pixel_height_start = pixel_height_start-1;
0071          end
0072
0073      intens(a,i) = intensityd1;
0074
0075      end
0076
0077 info = imfinfo(x(i).name)
0078 date = info.FileModDate
0079
0080 minsec = str2double(date(19:20))/60;
0081
0082 minmin = str2double(date(16:17));
0083
0084 minhou = str2double(date(13:14))*60;
```

```
0085
0086 minmon = 0;
0087 if date(4:6) == 'Jan'
0088     minmon = 0;
0089 elseif date(4:6) == 'Feb'
0090     minmon = 44640;
0091 elseif date(4:6) == 'Mar'
0092     minmon = 84960;
0093 elseif date(4:6) == 'Apr'
0094     minmon = 129600;
0095 elseif date(4:6) == 'May'
0096     minmon = 172800;
0097 elseif date(4:6) == 'Jun'
0098     minmon = 217440;
0099 elseif date(4:6) == 'Jul'
0100     minmon = 260640;
0101 elseif date(4:6) == 'Aug'
0102     minmon = 305280;
0103 elseif date(4:6) == 'Sep'
0104     minmon = 349920;
0105 elseif date(4:6) == 'Oct'
0106     minmon = 393120;
0107 elseif date(4:6) == 'Nov'
0108     minmon = 437760;
0109 elseif date(4:6) == 'Des'
0110     minmon = 480960;
0111 elseif date(4:6) == 'Jan2'
0112     minmon = 525600;
0113 else
0114     minmon = 4;
0115 end
0116
0117 minmon;
0118
0119 minday = (str2double(date(1:2))-1)*24*60;
0120
0121 totalTimeOfFirstImage = totaltime(9);
0122 totaltime(i) = (minsec + minmin + minhou + minmon + minday) - totalTimeOfFirstImag
0123 totalTimeHour(i) = totaltime(i)/60;
0124 totalTimeDays(i) = totalTimeHour(i)/24;
0125 totalTimeHours = totalTimeHour(i)
0126 end
0127
0128 intensityd1;
0129
0130     plot(totaltime(9:numofpic),intens(1,9:numofpic),'*')
```

Appendix E

Electromagnetic waves in an anisotropic material

Birefringence can be generally defined by considering a dielectric permittivity and a refractive index that are tensors. Consider a plane wave propagating in an anisotropic medium, with a relative permittivity tensor ϵ, where the refractive index $\mathbf{n}$, is defined by $\mathbf{n}\cdot\mathbf{n} = \epsilon$ [179]. If the wave has an electric vector of the form:

$$\mathbf{E} = \mathbf{E_0} e^{i(\mathbf{k}\cdot\mathbf{r}-\omega t)} \tag{E.1}$$

where $\mathbf{r}$ is the position vector and t is time, then the wave vector $\mathbf{k}$ and the angular frequency ω must satisfy Maxwell's equations in the medium, leading to the equations:

$$-\nabla \times \nabla \times \mathbf{E} = \frac{1}{c^2}\epsilon \cdot \frac{\delta^2 \mathbf{E}}{\delta t^2} \tag{E.2}$$

$$\nabla \cdot \epsilon \cdot \mathbf{E} = 0 \tag{E.3}$$

where c is the speed of light in a vacuum. Substituting Equation (E.1) in Equations (E.2) and (E.3) give the conditions:

$$|\mathbf{k}|^2 \mathbf{E_0} - (\mathbf{k}\cdot\mathbf{E_0})\mathbf{k} = \frac{\boldsymbol{\omega^2}}{\mathbf{c^2}}\epsilon \cdot \mathbf{E_0} \tag{E.4}$$

$$\mathbf{k} \cdot \epsilon \cdot \mathbf{E_0} = 0 \tag{E.5}$$

To find the allowed values of $\mathbf{k}$, $\mathbf{E}_0$ can be eliminated from Equation (E.4). One way to do this is to write Equation (E.4) in Cartesian coordinates, where the x, y and z axes are chosen in the directions of the eigenvectors of ϵ, so that

$$\epsilon = \begin{bmatrix} n_x^2 & 0 & 0 \\ 0 & n_y^2 & 0 \\ 0 & 0 & n_z^2 \end{bmatrix} \tag{E.6}$$

Hence Equation (E.4) becomes

$$\left(-k_y^2 - k_z^2 + \frac{\omega^2 n_x^2}{c^2}\right) E_x + k_x k_y E_y + k_x k_z E_z = 0 \tag{E.7}$$

$$k_x k_y E_x + \left(-k_x^2 - k_z^2 + \frac{\omega^2 n_y^2}{c^2}\right) E_y + k_y k_z E_z = 0 \tag{E.8}$$

$$k_x k_z E_x + k_y k_z E_y + \left(-k_x^2 - k_y^2 + \frac{\omega^2 n_z^2}{c^2}\right) E_z = 0 \tag{E.9}$$

where E_x, E_y, E_z, k_x, k_y and k_z are the components of $\mathbf{E_0}$ and $\mathbf{k}$. This is a set of linear equations in E_x, E_y, E_z, and they have a solution if their determinant is zero:

$$det \begin{bmatrix} \left(-k_y^2 - k_z^2 + \frac{\omega^2 n_x^2}{c^2}\right) & k_x k_y & k_x k_z \\ k_x k_y & \left(-k_x^2 - k_y^2 + \frac{\omega^2 n_y^2}{c^2}\right) & k_y k_z \\ k_x k_z & k_y k_z & \left(-k_x^2 - k_y^2 + \frac{\omega^2 n_z^2}{c^2}\right) \end{bmatrix} = 0 \tag{E.10}$$

Multiplying out Equation (E.10), and rearranging the terms, gives

$$\frac{\omega^4}{c^4} - \frac{\omega^2}{c^2}\left(\frac{k_x^2 + k_y^2}{n_z^2} + \frac{k_x^2 + k_z^2}{n_y^2} + \frac{k_y^2 + k_z^2}{n_x^2}\right) + \left(\frac{k_x^2}{n_y^2 n_z^2} + \frac{k_y^2}{n_x^2 n_z^2} + \frac{k_y^2}{n_x^2 n_y^2}\right)\left(k_x^2 + k_y^2 + k_z^2\right) = 0 \tag{E.11}$$

In the case of a uniaxial material, where $n_x = n_y = n_\perp$ and $n_z = n_{||}$, Equation (E.11) can be factorised into

$$\left(\frac{k_x^2}{n_\perp^2} + \frac{k_y^2}{n_\perp^2} + \frac{k_z^2}{n_\perp^2} - \frac{\omega^2}{c^2}\right)\left(\frac{k_x^2}{n_{||}^2} + \frac{k_y^2}{n_{||}^2} + \frac{k_z^2}{n_\perp^2} - \frac{\omega^2}{c^2}\right) = 0 \tag{E.12}$$

Each of the factors in Equation (E.12) defines a surface in the space of vectors $\mathbf{k}$ the surface of wave normals. The first factor defines a sphere and the second defines an ellipsoid. Therefore, for each direction of the wave normal, two wave vectors $\mathbf{k}$ are allowed. Values of $\mathbf{k}$ on the sphere correspond to the ordinary rays while values on the ellipsoid correspond to the extraordinary rays. For a biaxial material, Equation (E.11) cannot be factorised in the same way, and describes a more complicated pair of wave-normal surfaces. Birefringence is often measured for rays propagating along one of the optical axes (or measured in a two-dimensional material). In this case, $\mathbf{n}$ has two eigenvalues which can be labelled n_1 and n_2. $\mathbf{n}$ can be diagonalised by:

$$n = \mathcal{R}(\chi) \begin{bmatrix} n_1 & 0 \\ 0 & n_2 \end{bmatrix} \mathcal{R}(\chi)^T \tag{E.13}$$

where $\mathcal{R}(\chi)$ is the rotation matrix through an angle (χ). Rather than specifying the complete tensor $\mathbf{n}$, the magnitude of the birefringence may be specified by Δn and extinction angle (χ), where $\Delta n = n_1$ - n_2.

Appendix F

Paper

An almost finished version of an articles which is being sent to Langmuir for publication.

The results of the paper is taken from this thesis, but some of the figures are modified and the text a bit changed. Figures 4 and 5 correspond to Figures 3.10 and 3.77 in the thesis, but samples of 5 w/w% and 6 w/w% clay are now added. Figure 7 is Figure 3.14, where the pictures of the samples without polarizers are removed. In the paper we have named the different Na-Fht powder types by batches, where batch B1 is November powder, batch B2 is crushed April powder and batch B3 is August powder.

Birefringent Textures in the Nematic Phase of Na-Fluorohectorite Synthetic Clay.

N.I. Ringdal, J.O. Fossum, D. d.M. Fonseca, A. Gmira*

Department of Physics, Norwegian University of Science and Technology, Hoegskoleringen 5, N-7491, Trondheim, Norway.

*jon.fossum@ntnu.no

RECEIVED DATE (xx.xxx 2008)

TITLE RUNNING HEAD: Schlieren Patterns in Na-Fluorohectorite.

ABSTRACT : *We have studied stable strata of gravity define phase separation in ionic [NaCl] suspensions of synthetic Na-Fluorohectorite clay. We have observed and reported how the strata depend on clay concentration as well as on salt [NaCl] contents of the suspension. The mass distribution in the isotropic and in the nematic phase, at the isotropic – nematic as well as the and the density variation at the isotropic – nematic interface indicate that existing models, and assumptions in existing simulations do not account for the present system behavior. We suggest that this could be due to the polydispersity as well as to the irregular shape of the present Na-Fluorohectorite particles, as well as to effects of the double layer, which could result in an overlap of, and even possibly a competition between, nematic ordering and gelation, in our system.*

*The dependence on ionic [NaCl] strength display three main regimes irrespective of clay concentration. At low inoinc strength (~10^{-4} M – ~5*10^{-3} M) the Debye screening length is longer than the van der Waals force range. In this regime, the particles repel each other electrostatically, and entropy driven nematic ordering, in the Onsager sense, may occur, although gelation effects may also play an integral role. One may thus use the term "repulsive nematic" for this regime. For*

*ionic strengths above about 5*10^{-3} M, we believe that the van der Waals force come into play, and that gelation is important, and we may use the term "attractive nematic" for this regime. For ionic strengths above ~10^{-2} M the clay particles flocculate, due to the dominant van der Waals force, and thus no nematic ordering.*

We have studied the nematic phase in detail in between crossed polarizers, and we have found textures showing nematic Schlieren patterns and by rotating polarizers as well as samples, and we have seen examples of disclinations of strengths -1 and -1/2. These patters can be observed directly by eye, reflecting the the large size of the Na-fluorohectorite particles, and thus domain sizes in this system.

KEYWORDS: Nematics, Clays, Birefringence, Schlieren Patterns, Disclination Defects.

1. Introduction

The formation of liquid-crystalline order in colloidal dispersions of anisotropic mineral nanoparticles has recently seen an increased research activity [1][2][3]. From the early investigations of vanadium pentoxide (V_2O_2) [4] and tobacco mosaic virus (TMV) [5] [6], suspensions of various rod-like nanoparticles [7] are found to exibit a spontaneous transition from an isotropic (I) phase to a nematic (N) phase in good agreement with statistical mechanical theories. In the 1940s, Lars Onsager [8] modeled this phase transition considering the competition between the orientational and the packing entropies of the colloidal system, thus concluding that at a sufficiently high enough particle concentration, the packing entropy dominates and it becomes favorable for the particles to order in nematic alignment. Onsager showed that interaction between the particles is not necessary for orientational ordering, but the shape anisotropy of the particles alone is enough to drive the I-N phase transition. As Onsager proposed, and as later confirmed by computer simulations [9] [10], nematic ordering can occur for plate-like particles that are fairly anisometric. This possibility was first studied experimentally by Langmuir in 1938 [11], who reported observations of an I-N phase transition in sols of natural clay particles, although conclusive evidence for a true thermodynamically stable I-N tranaition was lacking.

An obstacle against using clay as model to study nematic ordering of colloidal system is the clays tendency to gel when dispersed in solution. The gel structure and its formation, which are responsible for many of the clays practical applications, have from the 30-50s [12][13][14][15][16] until today been substantially studied [17][18][19][20][21][22][23][24][25][26][27][28][29][30][31][32] [33][34][35] [36][37]. A transition from a sol to a gel may take place at very low clay concentrations. In recent years, the presence of orientational order in clay gels have been documented by optical measurements [38][18] showing visual nematic textures. Neutron- [39][40][41] and X-ray - scattering [42][43][44][45] as well as Magnetic Resonance Imaging (MRI) experiments [46] [47][48][49][50][51] have all revealed structural correlations with nematic order. Since the gel phase may not be at thermodynamic equilibrium, the nematic ordering in the gels cannot be explained by the Onsager theory alone.

There is today no theory for the process of orientational ordering in the gel structure. There has been suggestions that the sol-gel transition may be directly related to the I-N transition [17][18][52][53], but this possibility has been contradicted in experiments by Michot et al. [32]. They showed that the concentration for the sol-gel transition of suspensions of size selected Wyoming Na-montmorillonite increases linearly with particle anisotropy. This is opposite to what could be expected for the corresponding evolution of the I-N transition, since large aspect ratio for the particles shifts the I-N transition towards lower volume fractions. Other studies concerning systems of charged colloidal platelets as Mg_2Al LDH [54] and gibbsite [55][56] also suggest that the liquid crystal phase transition, and gelation, are separate and even could be competitive processes. In these last two systems, the I-N phase transition has been observed to take place at a lower concentration than the sol-gel transition [57][58][54]. The thermodynamic stability of the nematic ordering could therefore be achieved and further compared to the Onsager model. For clay plateletes, an I-N transition, was recently obtained in suspensions of natural nontronite [59][60]. Experimental systems of colloidal clay suspensions should be expected to differ from the Onsager model, since factors like particle morphology, electrostatic and van der Waals forces [61], gravitational force [62][63][64] and Brownian motion [65][66] may be of importance to the phase behavior.

In the present manuscript, we describe the phase behavior the synthetic 2:1 phyllosilicate (smectite) clay Na-fluorohectorite (Na-Fht) suspended in aqueous NaCl solutions of concentrations ranging from 10^{-4} M to 10^{-2} M. In the gravitational field, a suspension of Na-Fht may be effectively separated into different strata of gels, sols and sediments. In one of the phases, particle orientation of nematic order is found as evidenced by previous X-ray scattering [32][43][67] and MRI [51] studies. Here, we present the birefringent nature of the nematic ordering, the role of different salt concentration and study how the clay concentration varies in the gravity dispersed suspension. We also report on observations of topological defects in the nematic phase. It is known that many of the topological defects which are commonly present in molecular liquid crystals, may also form in mineral liquid crystals. Schlieren textures and different disclinations have been observed in nematic clay gels of bentonite and laponite [38] and in the nematic phase of other systems of nanoplatelets [67, 58, 75], similar to our present observations.

2. Experimental details

2.1 Materials

Synthetic fluorohectorite clay was purchased in powder from Corning Inc., New York. The chemical formula of Na-Fht is $Na_{0.6}Mg_{2.4}Li_{0.6}Si_4O_{10}F_2$, for which two inverted silicate tetrahedral layers share their apical oxygens with one octahedral layer. As shown in Figure 1, the individual Na-Fht particles are composed of around 80-100 silicate lamellae [43] that stack by sharing Na^+ ions between their basal plane. Each 2:1 silicate lamellae is around 1 nm thick, with a charge of 1.2 e^-/unit cell. This charge is relatively large compared to other smectite clays, such as synthetic laponite (0.4 e^-/unit cell) and natural montmorillonite (0.6 e^-/unit cell) [68]. The large surface charge makes the particle stacks remain intact when suspended in water, in contrast to laponite and montmorillonite [42]. From AFM imaging (Figure 1), the polydisperity in particle size is quite large with highly variable particle morphology. The effective diameter of the platelets can vary from a few hundred nanometer up to about 20 microns.

70 g of fluorohectorite as purchased from Corning Inc. was added to 1000 ml distilled and deionized water, where it was dissolved and stirred by shaking for 2 days using an incubator at 300 rpm. Sodium ions were added as 60 g NaCl (0.5 M), which corresponds to about 10 times the known

surface charge per unit cell. The suspension was further shaken at 300 rpm for 2 weeks. Cl^- ions were removed by dialyzis process, where the Cl^- content was checked regularly using a standard silver nitrate procedure. Na-Fluorohectorite powder was obtained by drying the resultant solution at 105 C° for about 3 days. A mortar with pestle was used before the Na-Fht powder was further pulverized using a milling machine (IKA A11 basic).

Three different batches of Na-Fht were studied in the present experiments, we call them B1, B2 and B3 respectively. All three batches were prepared as described above. Due to some differences in the time sequences spent at the different preparation steps, and due to differences in crushing and milling procedures, there may be differences between the particle sizes of the three batches, so that the particles of batch B1 and B2 are similar, whereas the B3 particles are expected to be smaller than both B1 and B2 type particles.

2.2 Experimental Methods

Two kinds of rectangular sample tubes were used for optical studies of the phase behavior of the suspensions: Vitrotube 4410-100 from VitroCom, is 10 cm long, 1 cm wide and 1 mm thick, a cell made of polyoxymethylene plastic (pom) and micro glass slides have inner dimensions 24*60*1 mm. This cell has glass walls of thickness 0.2 mm. Cylindrically shaped thin walled capillary tubes were also used in some of the studies: Hilgenberg Mark-tubes, of 2mm, and 1 mm respectively. The sample cells used are shown in Figure 2, and in Figure 3, we show the experimental setup used for the reported experiments, thus studying phase behavior of the samples, carefully measured by means of crossed polarizers and a PC-controlled camera.

3. Results

3.1 Results: Clay Concentration

In Figure 4, we show suspended B1 samples with Na-Fht concentrations of 0.5, 1, 2, 3, 4, 5 or 6 weight% clay respectively and at 10^{-3} M [NaCl]. The image in Figure 1 is typical for our samples, and irrespective of powder type or ionic strength, the phase behaviour is very much similar for most of the different clay concentrations.

The main difference between different powders is in the height level and relative fraction of the separated phases in the sample tubes. For the samples with the lowest clay concentration, the relative amount of birefringence is in general lower for the same induced phase than for those of higher concentration.

The contribution of the sediment to the sample height increases as what could be expected when the clay concentration is increased. Above the sediment, a density profile is induced where the formation of an interface between the isotropic gel and nematic gel takes place. This behaviour is common to all of the samples in this concentration range.

The 6 w/w% sample has not phase separated into different phases similar to the others. After the suspension is injected into the sample tube, slow sedimentation occurs for about a week until it stops due to gelation. Some birefringence is observed for this sample as well, but there is no clear distinction between separate phases.

For the 2 w/w%, the nematic phase can be divided into two regions with a upper part being more birefringent than the lower part. It is not clear why this special effect occur for the 2 w/w% sample, but it could be due to a earlier gelation of the lower part. Figure 5 is a graphical representation of Figure 4.

3.2 Results: Mass Distribution

In order to map out density differences between the various phases, and how much the density varies within each phase, the clay concentration was measured for two similar samples of 3 w/w% B2 and B3 respectively, both at 10^{-3} M [NaCl], from the liquid at the top to the sediment at the bottom. Suspensions were made in 5 containers of 50 ml each, all with height 7.5 cm and diameter 2.9 cm. The samples were left to settle for 2 months (B2) and 2.5 months (B3) respectively, before the measurements. At this time the samples had separated into different static strata from top to bottom. The measurements were carried out by pipetting out 250 microlitres bu inserting the pipette from the top of the container. In total; 177 sampled measurements were done for the M3 sample and 163 sampled measurements for the M2 sample. Since it was too difficult to pipette the sediment part of the samples into the pipette, the remaining sediment at the bottom of each sample was dried and weighed to be 0.285 gram for the M3 sample (8.5 mm) and 0.561 gram for the M2 sample (14 mm).

Figure 6 shows the clay concentration as function of relative height, where zero is chosen at the edge of the nematic phase. The volume fraction is found by dividing the clay concentration by the mass density of Na-Fht, which is 2.0 g/cm3 where it is taken into account that two water layers are incorporated in between the clay platelets [69].

3.3 Results: Salt Concentration

The salt concentration is known to play a major role of the phase behaviour of the aqueous Na-fluorohectorite solutions [42] [43], because of the particles surface charge. Figure 7 shows a series of 3 w/w% B1samples with an increasing salt concentration from 10^{-4} M to $5*10^{-2}$ M [NaCl]. Other examples, made from other powder batches, all show the same trend, irrespective of powder type and clay concentration. At low salt concentrations, the phase separation is the same with the formation of nematic phases between an isotropic gel and a upper dilute isotropic sol. As the ionic strength is increased, the relative height of nematic phase decreases along with an increase of the upper isotropic sol. In general, the relative height of the isotropic gel also clearly decreases with ionic strength from 10^{-4} M to 10^{-3} M [NaCl]. This is not as pronounced as for other batches, for the B1 powder in Figure 7, where just a very slight decrease can be seen over the same salt concentration range. As the ionic strength is further increased, the height of the isotropic gel and the nematic phase suddenly get a larger drop when the salt concentration is increased from $2.5*10^{-3}$ M to $5*10^{-3}$ M [NaCl]. A further increase to $7.5*10^{-3}$ M [NaCl] makes very little change to any of these heights, but the next increase to $1*10^{-2}$ M [NaCl] gets a new pronounced drop for both the nematic and the isotropic gel. Above $1*10^{-2}$ M [NaCl], there seems to be a gravity settled equilibrium distribution of the particles above the sediment.

4. Discussion

4.1 Discussion: Clay Concentration

Irrespective of powder type or ionic strength, the phase behavior is very much similar for most of the different clay concentrations. In all the samples there are some birefringent spots with low intensity that can be seen at the interface between the sediment and the gel. As the border to the nematic phase is lowered, a slight increase in this birefringence is observed. This may be due to a

density increase, as greater pressure is induced by the weight of the nematic phase and the isotropic gel itself.

This is also the case for other batch powders than B1. The phase separation is very similar to suspensions made from batch B2 powder, and differs only in some specifics. Of the most pronounced differences compared to the B2 samples, is a finer grained and more homogeneous appearance of the birefringence in the nematic gel for all concentrations. This is probably due to the more extensive crushing process of the B1 powder. Figure 5 is a graphical representation of the relative height nematic phase of the samples in Figure 4. From 1 w/w% to 5 w/w%, there is a linear increase of the nematic gel as the clay concentration is increased. At clay concentrations above 5 w/w%, the whole sample gels before any phase separation occur.

4.2 Discussion: Mass Distribution

The concentration step between the clay concentration at the nematic and isotropic phase is slightly different for the M2 and M3 based suspensions: The clay densities at the phase boundaries the M2 sample is about 0.031 g/cm^3 for the nematic phase and 0.010 g/cm^3 at the isotropic phase. For the M3 sample it is 0.029 g/cm^3 and 0.015 g/cm^3 at the nematic and isotropic phase respectively. This difference between the two batches may be explained by the suggestion that the B3 batch is finely crushed and therefore might have a lower polydispersity.

Because of sedimentation and gelation it is not possible to obtain samples where isotropic or nematic phase constitute the whole volume of the sample. Figure 5 shows that the relative amount of the nematic gel increases linearly from 1 to 5 w/w% before gelation takes place at about 6 w/w%. Such a linear increase is similar to other systems reported in the literature, such as gibbsite [58] and nontronite [59][60], when the volume fraction is gradually increased in those systems. Those systems have been reported to display a true thermodynamic isotropic-nematic phase transition, where attractive forces are not of importance for the nematic ordering.

For gibbsite and nontronite, experimental values for the densities of the coexisting isotropic and nematic phases are in reasonable agreement with theoretical computer simulations [70] (for infinitely thin platelets), where dimensionless number densities, i.e. the number density n = N/V multiplied by the diameter D cubed, at zero polydispersity are found to be $n_{iso}D^3 \sim 3.7$ and $n_{nem}D^3 \sim 4.0$. These

simulations [70] are done for infinitely thin platelets, but platelets with a finite thickness do not give any major difference $n_{iso}D^3 \sim 3.8$ and $n_{nem}D^3 \sim 3.9$ when the diameter to thickness ratio is 10 [71]. If the polydispersity is 25%, which could well be the case for our system, the densities are $n_{iso}D^3 \sim 3.5$ and $n_{nem}D^3 \sim 5.0$ respectively [70].

Since the sedimentation process in our Na-fluorohectorite suspensions may fractionate the particles, the size (or shape) of the particles in the isotropic phase may be different from the particles in the nematic phase. The values in Figure 6 for the volume fractions at the isotropic and nematic phase might still be used to give an estimate for number densities to compare to theoretical and other experimental [55][57] results. The relation between volume fraction ϕ and nD^3 is for round platelets of diameter D and thickness t is [57]:

$$\phi = n\frac{\pi}{4}D^2 t = \frac{\pi}{4}\frac{t}{D}nD^3 \tag{1}$$

When polydispersity in taken into account, Equation (1) is replaced by [57]:

$$\phi = \frac{1+\sigma_D^2}{1+3\sigma_D^2}\frac{\pi}{4}\frac{\langle t\rangle}{\langle D\rangle}n\langle D^3\rangle \tag{2}$$

where σ_D is the standard deviation representing the polydispersity of the diameter [57]. Rewriting gives

$$n\langle D^3\rangle = \phi\frac{4}{\pi}\frac{1+3\sigma_D^2}{1+\sigma_D^2}\frac{\langle D\rangle}{\langle t\rangle} \tag{3}$$

An exact value for the polydispersity of our suspensions of Na-fluorohectorite is not known, but AFM pictures (Figure 1) have revealed that the polydispersity is quite high. To estimate quantities, the use of an approximated average particle diameter of 2 μm, which corresponds to a circle of same facial area, give the coexisting densities $n_{iso}D^3 \sim 0.4$ and $n_{nem}D^3 \sim 0.8$, when the polydispersity is chosen as high as possible and 100 nm is used for the thickness of the particles. The large difference between the isotropic and nematic densities, may be indicative of large polydispersity. These estimated values are about a factor 10 smaller than predicted values of the cited computer

simulations [57]. Since the Na-Fht particles are very irregular in shape, neither equation 3 nor the cited simulations seem to represent our clay system.

Further computer simulations by Bates [72] have showed that the coexisting densities for the nematic-isotropic transition is dependent on the shape of the particles. The study showed that the transition densities for triangular particles (which may be a better approximated shape for Na-fluorohectorite than a round object), are almost one order of magnitude lower than particles of circular shape. The simulation data [72] do not account for lath-shape biaxial particles with large differences between the facial dimensions, something which is representative for the Na-Fht particles.

It difficult to be estimate how much influence attractive and repulsive forces might have for the ordering of nematic and isotropic orientation in our suspensions. The high particle charge of the Na-Fct particles, means that they are not hard-body objects. Attempts to estimate effective diameter and effective thickness from the Debye screening length do not give better agreement with the predictive simulation data.

Also, the different Na-Fct particles within the suspension may interact, separate and behave differently from each other epending on particle size. Particles of large size (3-10 μm), may form nematic ordering in coexistence with an isotropic phase of smaller particles (< 1 μm).

4.3 Discussion: Salt Concentration

Since the theoretical understanding of the salt-induced ordering of charged colloidal particles of large particle size is not yet fully established, the phase behavior present in this section are qualitatively discussed within DLVO [61] and Onsager theories [8]. By studying the pictures of the samples without polarizers in Figure 7, there seems to be a density increase in all the phases which is expected due to less repulsion. For any clay concentration or powder type, the Na-Fht suspensions coagulate at a salt concentration of about $5*10^{-2}$ M, and for higher ionic strengths, the suspensions undergoes fast coagulation and very little sediments settle at the bottom.

In Figure 7, a flocculation transition is found to take place between an ionic strength of $1*10^{-2}$ M and $2.5*10^{-2}$ M [NaCl]. Such a flocculation transition is similar to data found for Wyoming

montmorillonite, published by Abend and Lagaly [73], where the transition line shows a negative slope as the clay concentration is increased, which is also probably the case for Na-Fht since slightly slower coagulation occur for the lowest clay concentration. Experiments carried out by Michot et.al [59] on sodium nontronite, also show a flocculation transition at ionic strength 10^{-2} M. However, the phase diagram of this clay type has a positive flocculation slope at low volume fractions, and thereafter displaying a negative sol-gel transition as the volume fraction is further increased.

Compared to other clay minerals, the flocculation transition for Na-Fht is lower than for bentonite and higher than for laponite [38]. When theDebye screening length values are taken with the total potential energy curve of the DLVO interaction, a secondary minimum at a screening length of 5 nm may correspond to the sudden behavior change that take place for the B1 suspensions at $2.5*10^{-3}$ M. A flocculation transition at $2.5*10^{-2}$ M then corresponds to a screening length of about 2 nm, for which the interaction is “taken over” by van der Waals attraction. The energy barrier is then surmounted, and the colloidal clay suspension is referred to as being unstable.

From salt concentration 10^{-4} M to 10^{-3} M, the Debye screening length decreases from about 30 to 10 nanometer. As the screening length is roughly proportional to the electric double layer, the particle dimensions swell as the salt concentration is decreased. In aqueous salt solution, the thickness of the particles is increased by an extra height of two times the screening length. From the Onsager theory of the interplay between excluded volume entropy and orientational entropy, a change in the particle dimensions should reduce the critical concentration of particles at the isotropic-nematic transition. It is however difficult to estimate how much influence this growth in effective particle size could have for the observations of the increased nematic ordering with decreasing ionic strength in the Na-Fht suspensions. From simulation experiments by Rowan and Hansen [74], it is suggested that the swelling effect is negligible for large particles, and that the phase behavior may be explained solely on electrostatic grounds. In suspensions of very large Na-Fct particles, the phase diagram is then dominated by long-range electrostatics. However, the strong influence of polydispersity in the size of the Na-Fht particles should possibly be taken into account in the explanation of the phase behaviour. Since the smallest particles remain in the upper isotropic sol

after gravity has been acting on the suspension, the significance of the double layer expansion in particle size could have most influence for this phase.

The increase in the relative amount of nematic phase for the low salt concentrations, could come from particles in the upper isotropic sol where nematic orientation has become favourable. The extra height of the nematic phase for low salt concentration, can also be thought of being driven by repulsion alone.

4.4 Discussion: Schlieren Patterns, Textures and Defects

In a normal unaligned nematic phase the director usually points in different directions at different points within the sample. Since the regions where the director orients parallel, perpendicular or along the normal of the polarizer, appear dark, and all other directions appear bright when viewed between crossed polarizers, a nematic phase often consists of both bright and dark areas. In many nematic textures, the brightness often changes abruptly, which indicate that the director also changes abruptly at those places. It is impossible to define the direction of the director at the point of an abrupt change, so such a point represents a defect in the liquid crystalline order. Theoretically, these defects could be points, lines or sheets where the director discontinuously changes in passing through one of the defects. Point defects tend to occur in restricted geometries and at surfaces. For example, point defects sometimes occur in spherical droplets of liquid crystals, around droplets of isotropic liquid in a liquid crystal, and in thin capillary tubes [76]. Sheet defects tend to spread out so that the change in orientational order is continuous over a slab containing the sheet rather than discontinuous at a set of two-dimensional points defining a sheet. Such structures are called walls.

Line defects are the most common in liquid crystals and have been given the special name disclination, i.e. a "discontinuity" in the "inclination" of the director. Viewed between crossed polarizers, disclinations are often visible as a characteristic pattern with dark branches converging at perpendicular angles. These dark branches are usually named brushes and the pattern is referred to as a Schlieren texture. Many different disclinations are possible, and they can be specified in terms of a description of the change in the director direction around the point where the director field is not

defined. A mathematical description of this is done by defining a polar angle, ϕ, and the director direction, Ψ, in the director configuration in the plane perpendicular to the direction of the line:

$$\Psi = m\phi + \phi_0 = \pi/2 \quad (4)$$

The parameter m is referred to as the strength of the disclination and equals a multiple of ±1/2. For negative strengths, the director rotates clockwise in traversing along the same counter-clockwise path of ϕ. For positive strengths the director rotates counter-clockwise. The strength is a measure of how much the director is rotated when ϕ is increased by 2ϕ. If the strength is ±1/2, the director rotates 180 π for one full loop around the disclination point. For a disclination of strength ±1, the director rotates 360π for a similar full loop.

Figure 8 shows the director structure of different disclinations with various strengths and constant ϕ_0. The corresponding appearance of Schlieren brushes when the nematic distortion is also illustrated. These brushes appear black, since the director in these places is either parallel or perpendicular to one of the crossed polarizer axes. The rest of the liquid crystal is bright. Thus there will be two dark bands merging from opposite sides of disclinations of strength ±1/2, and four dark bands emanating from disclinations of strength ±1. The sign of the strength can be determined by a simultaneous rotation of the two polarizers. If they are rotated counter-clockwise, the dark bands will rotate clockwise for disclinations of negative strengths and counter-clockwise for disclinations of positive strengths. By combining the number of brushes with rotation of the crossed polarizers, the type of disclination can easily be identified.

In Figure 9, we show birefringence from a sample of 3 w/w % B3 10^{-3} M [NaCl] at different angles of the crossed polarizers, including a disclination defect [76] with two brushes emanating from each other at 90°. In the first two pictures of the last row, the two more brushes may be seen. The brushes rotate in the same direction as the polarizers, and the strength can therefore be regarded as being +1. Arrow b shows a singularity where two dark brushes meet and rotate in the opposite direction with respect to the crossed polarizers. This corresponds to a disclination with strength -1/2. Arrow c marks the position of dark grooves located between birefringent stripes. The birefringent stripes

become dark when they are oriented along the polarizer or analyzer axes, but it is not possible to tell whether they are composed of clay particles connected edge-to-edge, face-to-face or for that matter face-to-edge. The black grooves, do not seem to change in either brightness or position during rotation of the crossed polarizers. This is shown in Figure 9, but it is best observed when the pictures change by overlapping. From this it would be reasonable to imagine the black grooves correspond to regions of isotropic orientation, giving nematic-isotropic coexistence in almost every height of the settled suspension. Another possibility could be that there is homeotropic alignment in the black grooves and the particles crosswise of the stripes orient in a helical structure similar to chiral (cholesteric) nematic phases. A way to test this could be to rotate the sample and see if the black grooves moved either up or down, since that would change the optical position of the homeotropically aligned particles. Unfortunately this has shown to be not practical successful in our samples, since the increase in optical path length through our 1 mm thick samples tubes changes the appearance of the pattern too much.

In Figure 10, we show defects in the nematic region close to the isotropic phase for a sample which is filled with pre-settled suspension of 3 w/w % B3 powder at 10^{-3} M [NaCl]. The pictures are taken 8 months after the time of injection. Arrow a shows a disclination of strength -1, and arrow b shows a disclination of strength +1. For all the samples that display Schlieren patterns, disclination points are found with both two (strength 1/2) and four (strength 1) emanating brushes. The disclinations seem to appear most frequent in the upper part close to the isotropic phase. The strength of the disclinations is defined in section, where the sign is determined by rotation of the cross-polarizers. If the brushes rotate in the same way as the polarizers, the sign is positive. If they rotate in the opposite direction, the strength is negative. Figures 9 and 10 show disclinations of both strengths -1 and -1/2. The fact that such nematic Schlieren patterns are observed, using 1 mm thick sample tubes, reflects the large size of the Na-fluorohectorite particles.

5. Conclusions

We have studied stable strata of gravity define phase separation in ionic [NaCl] suspensions of synthetic Na-Fluorohectorite clay. We have observed and reported how the strata depend on clay concentration as well as on salt [NaCl] contents of the suspension. The mass distribution in the

isotropic and in the nematic phase, at the isotropic – nematic as well as the and the density variation at the isotropic – nematic interface indicate that existing models, and assumptions in existing simulations do not account for the present system behavior. We suggest that this could be due to the polydispersity as well as to the irregular shape of the present Na-Fluorohectorite particles, as well as to effects of the double layer, which could result in an overlap of, and even possibly a competition between, nematic ordering and gelation, in our system.

The dependence on ionic [NaCl] strength display three main regimes irrespective of clay concentration. At low inoinc strength (~10^{-4} M – ~$5*10^{-3}$ M) the Debye screening length is longer than the van der Waals force range. In this regime, the particles repel each other electrostatically, and entropy driven nematic ordering, in the Onsager sense, may occur, although gelation effects may also play an integral role. One may thus use the term “repulsive nematic” for this regime. For ionic strengths above about $5*10^{-3}$ M, we believe that the van der Waals force come into play, and that gelation is important, and we may use the term “attractive nematic” for this regime. For ionic strengths above ~10^{-2} M the clay particles flocculate, due to the dominant van der Waals force, and thus no nematic ordering.

We have studied the nematic pahse in detail in between crossed polarizers, and we have found textures showing nematic Schlieren patterns and by rotating polarizers as well as samples, and we have seen examples of disclinations of strengths -1 and -1/2. These patters can be observed directly by eye, reflecting the the large size of the Na-fluorohectorite particles, and thus domain sizes in this system.

Looking in detail at our images, we always spot a narrow nematic like regime just at the interface of the isotropic-nematic transition. This will be the subject of future studies, already underway, along with studies of the dynamics of this phase separation in gravity, also underway. We have previously shown that these phase are sensitive to magnetic fields [51], and this we will also study in more detail in the future both in terms of nematic textures and alo by means of other techniques like X-ray scattering and MRI. Beyond our own expertise and capabilities, we also hope that the discrepancies we report between our density measurements, and existing models and simulations, could initiate theoretical or simulation work by other groups.

ACKNOWLEDGMENT We akcnowledge the Reserarch Council of Norway for funding throught the Nanaomat and Frinat Programs.

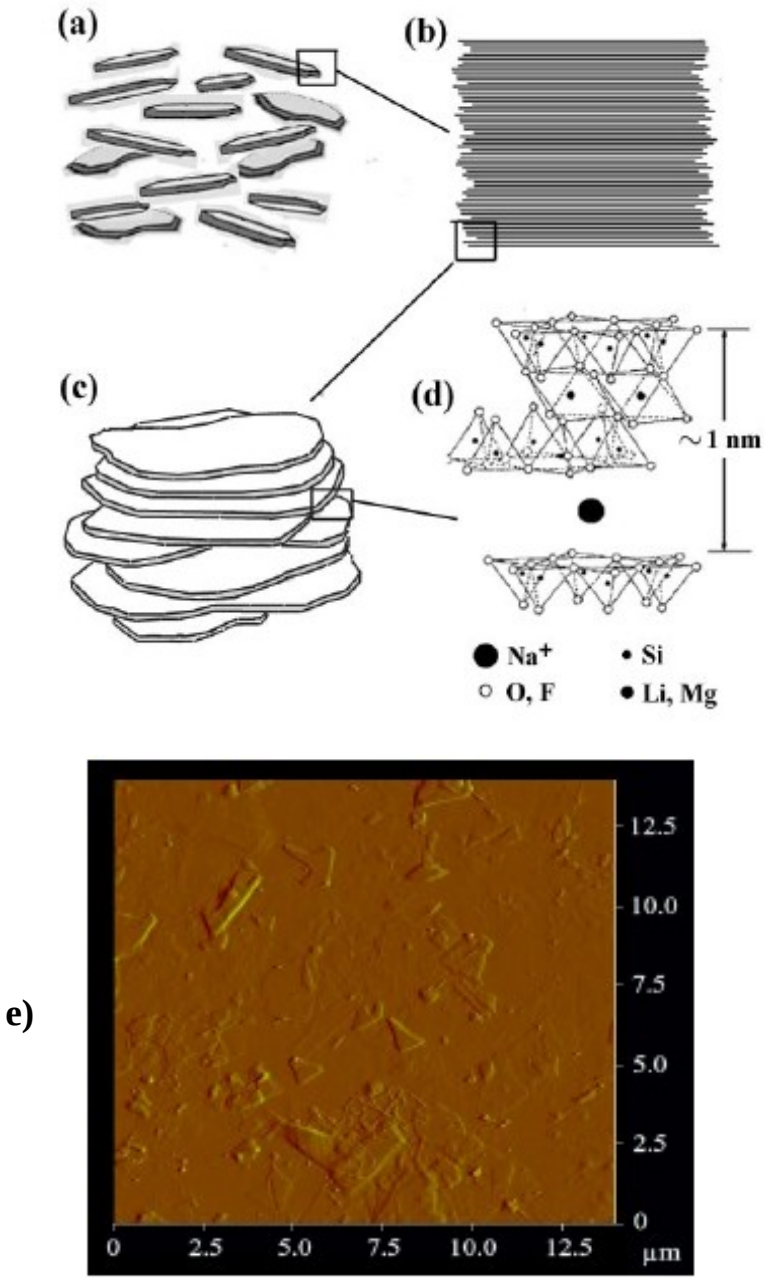

Figure 1. (a) Representation of Na-Fluorohectorite particles in nematic order. (b) Cross-section of a single clay particle, which consists of about 100 crystallized stacked lamellae. (c) The micron scale lamellas are layered with a thickness of around 1 nm. (d) Generic structure of the fluorohectorite, where the intercalated cation is Na+ for Na-Fht. (e) Atomic Force Microscope (AFM) image of Na-fluorohecorite particles extracted from the nematic phase and deposited on a freshly cleaved mica surface.

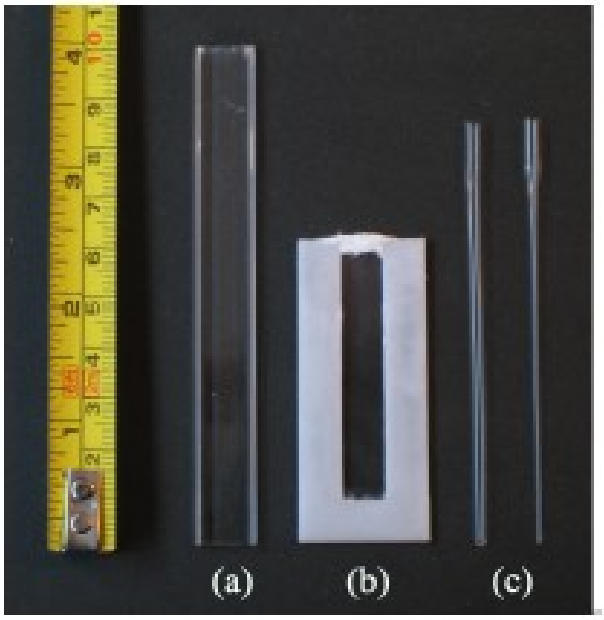

Figure 2. The different sample tubes used in the experiments. (a) Vitrotube 4410-100 from VitroCom (b) Rectangular cell 0 made from pom plastic and microglass slides (c) Hilgenberg Mark-tubes, left: 2mm, right: 1 mm.

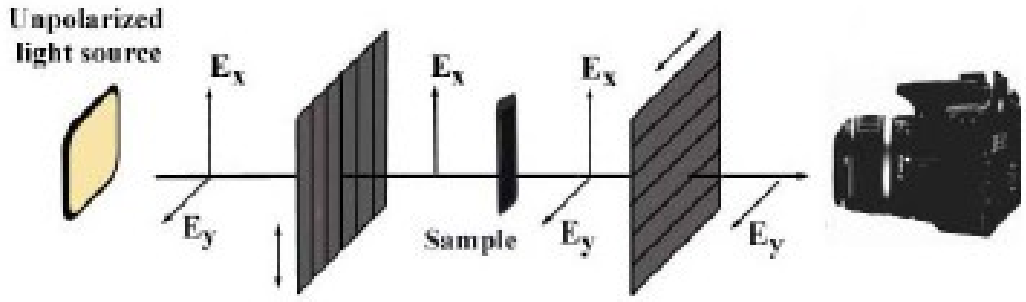

Figure 3. Our simple experimental setup for studiyng the long time sedimentation and phase behavior of the samples, carefully measured by crossed polarizers and a PC-controlled camera.

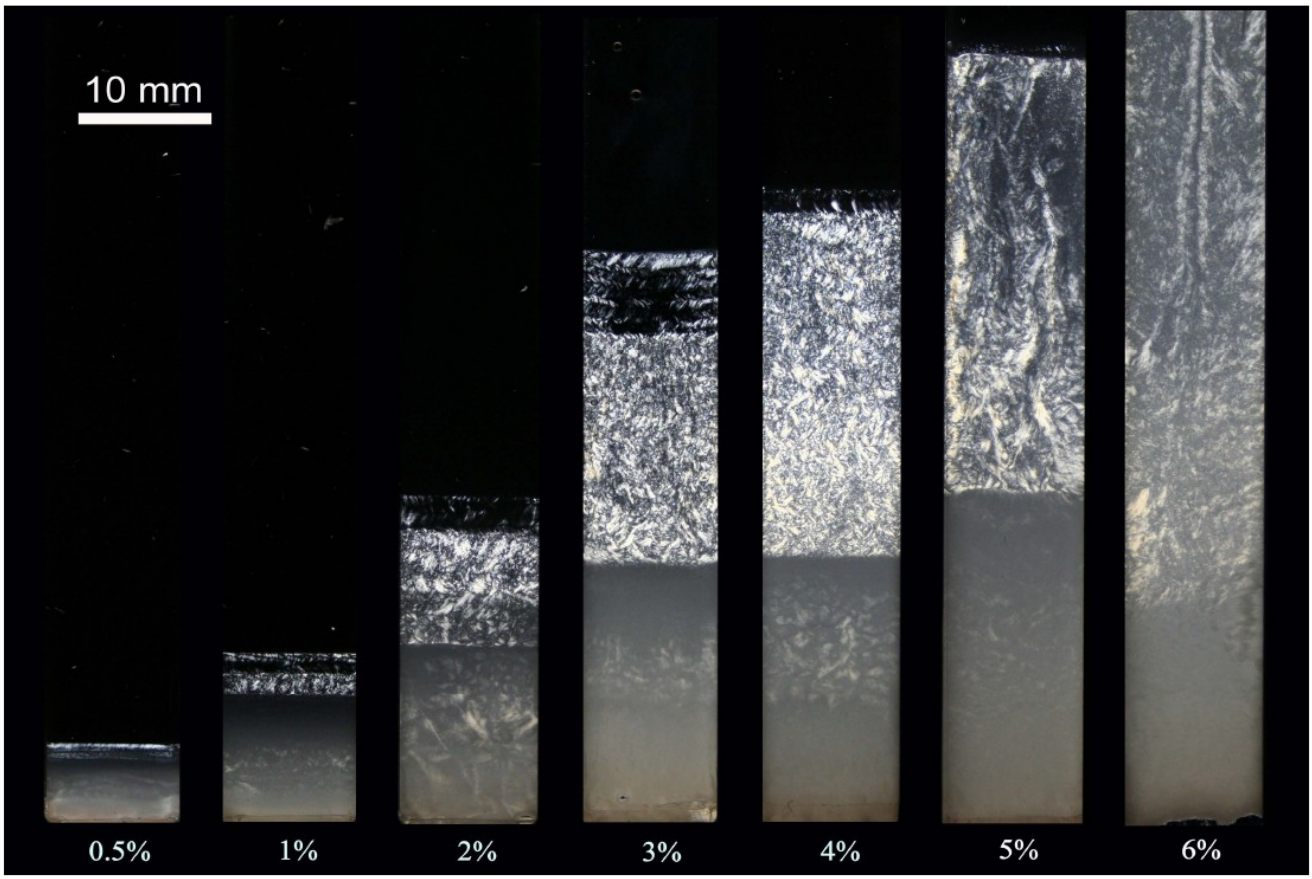

Figure 4. Suspended B1 samples with Na-fluorohectorite concentrations of 0.5, 1, 2, 3, 4, 5 and 6 weight% clay respectively, and all at 10-3 M [NaCl]. The time after preparation for the photographs are 1 months for 0.5 %, 2.5 months for 1%, 3 months for 3% and 5%, 4 months for 6% and 4.5 months for 2% and 4%. The picture of the 3% sample represents the stabilized settling state, where no further dynamics or changes of the phases are observed. The sample therefore looks the same after 4.5 months, and can be directly compared to the 2% and 4% samples.

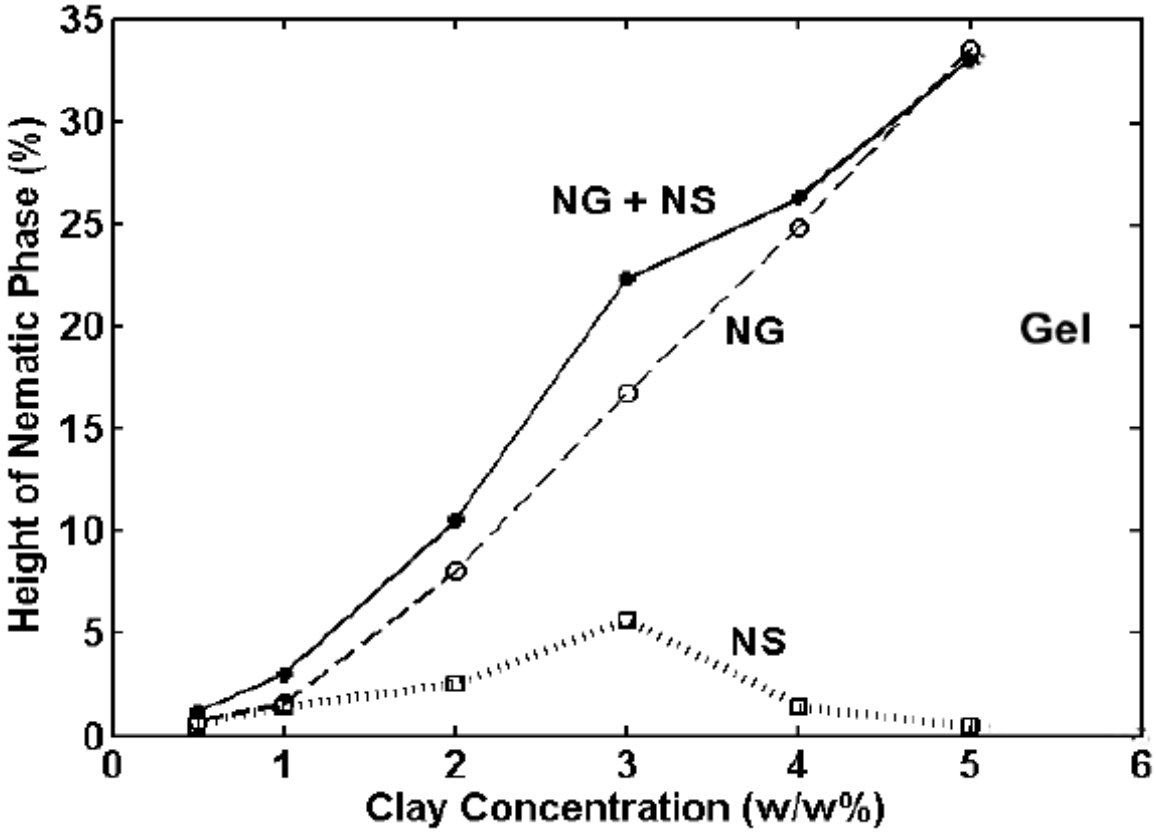

Figure 5. The height (volume) fraction of the nematic phase of the B1 powder at ionic strength 10^{-3} M [NaCl] as the clay concentration is increased from 0.5 to 4 w/w%. The top height of the sample is almost 10 cm, and the fraction % is equal to the relative height of the nematic phase in centimetres.

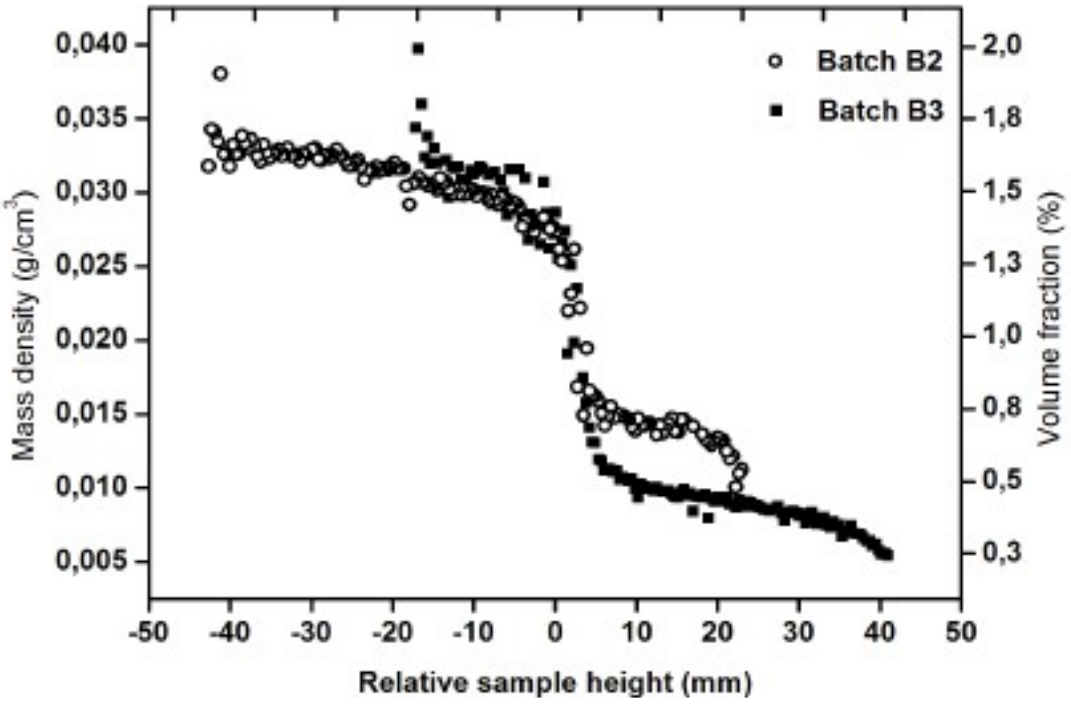

Figure 6. Clay concentration as function of relative sample height for a 3% B3 sample at 10^{-3} M [NaCl] and for a 3% B2 also at 10^{-3} M [NaCl] . We have chosen a (zero) reference point at right above the sediment, where the density is about 0.2 g/cm^3.

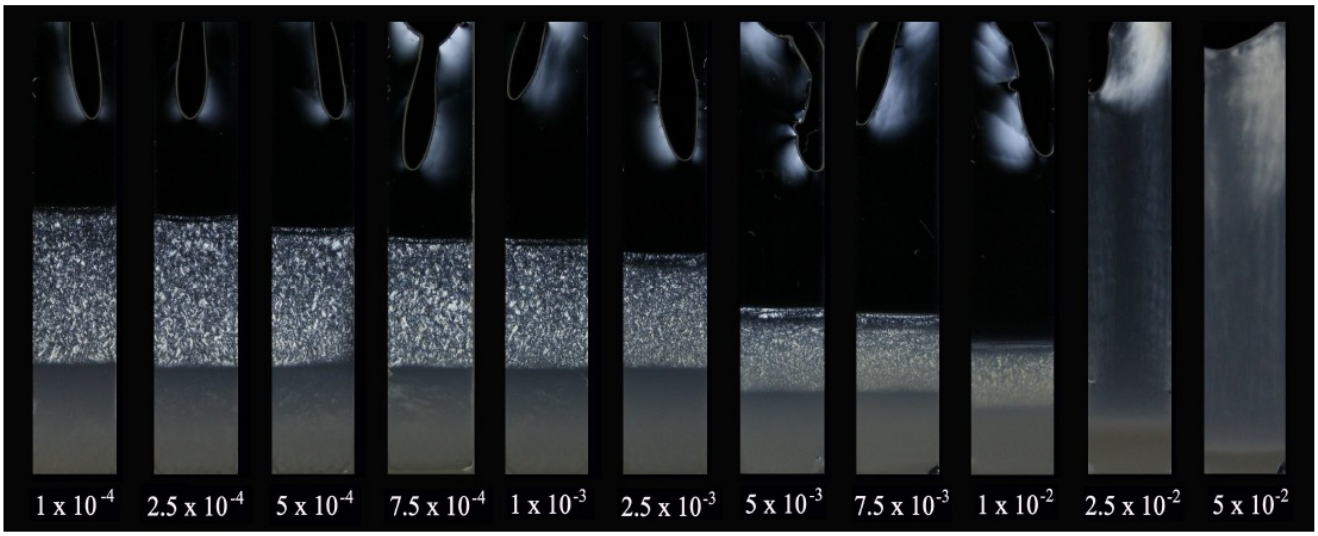

Figure 7. 3 w/w% B1 samples at [NaCl] salt concentration ranging from 10^{-4} M to $2.5*10^{-2}$ M. The samples are prepared in cells of the type shown in Figure 2, where the formations at the top part is due to artificial sample damage. For each salt concentration; the picture to the right is with the samples placed in between crossed polarizers, while the picture to the left is without polarizers. The relative height of the nematic phase decreases with ionic strength as the electrostatic interaction is more effectively screened. The transition between the repulsive and attractive forces, happens at a ionic strength between 10^{-2} M and $2.5*10^{-2}$ M. The images shown here are typical and reproducible in between samples prepared from different powder batches.

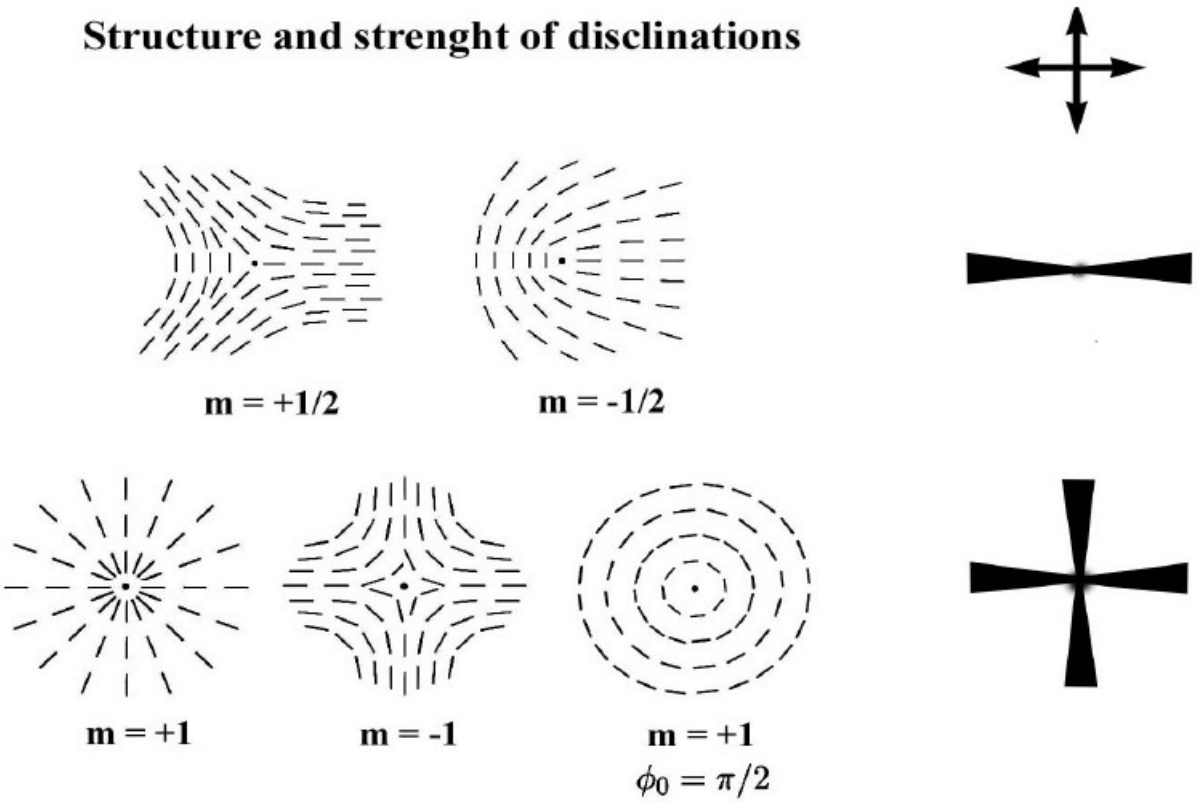

Figure 8. The structure and strengths of five disclinations as described by equation (4). The respective appearances of the structures when viewed between crossed-polarizers are shown to the right. Except for the last four-brush Schlieren structure, all cases have initial director direction $\phi_0 = 0$.

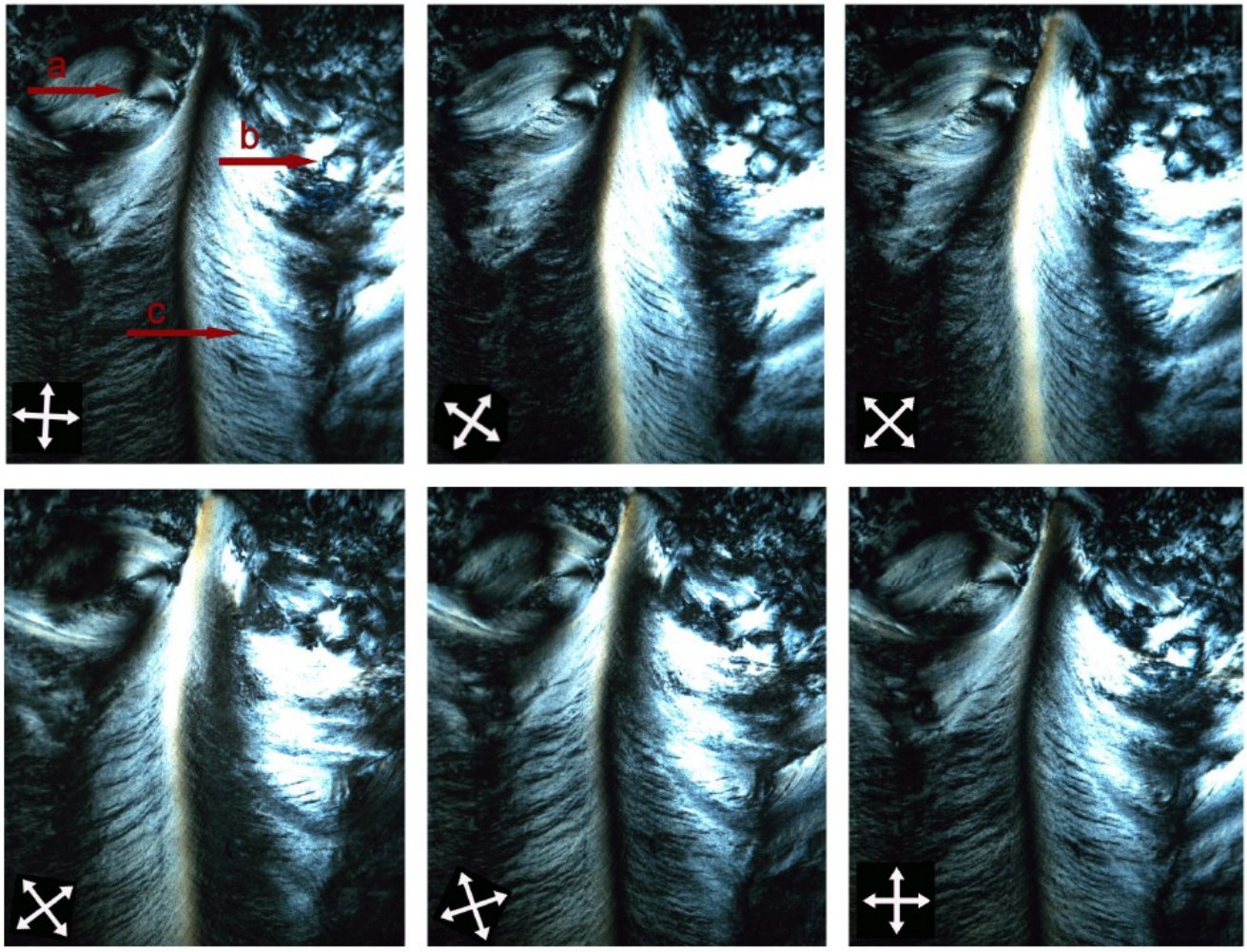

Figure 9. Observed birefringence from a sample of 3 w/w % B3 10^{-3} M [NaCl] at different angles of the crossed polarizers. From the upper left to the lower right picture, the polarizers are rotated succesively to 20 °, 45°, 55°, 75° and 90° with respect to the edges of the sample tube. Arrow **a** shows a disclination with two brushes emanating from each other at 90°. In the first two pictures of the last row, the two more brushes may be seen. The brushes rotate in the same direction as the polarizers, and the strength can therefore be regarded as being +1. Arrow **b** shows a singularity where two dark brushes meet and rotate in the opposite direction with respect to the crossed polarizers. This corresponds to the **a** disclination with strength -1/2. Arrow **c** marks the position of dark grooves located between birefringent stripes. As the polarizers are rotated, there is no apparent movements of the grooves.

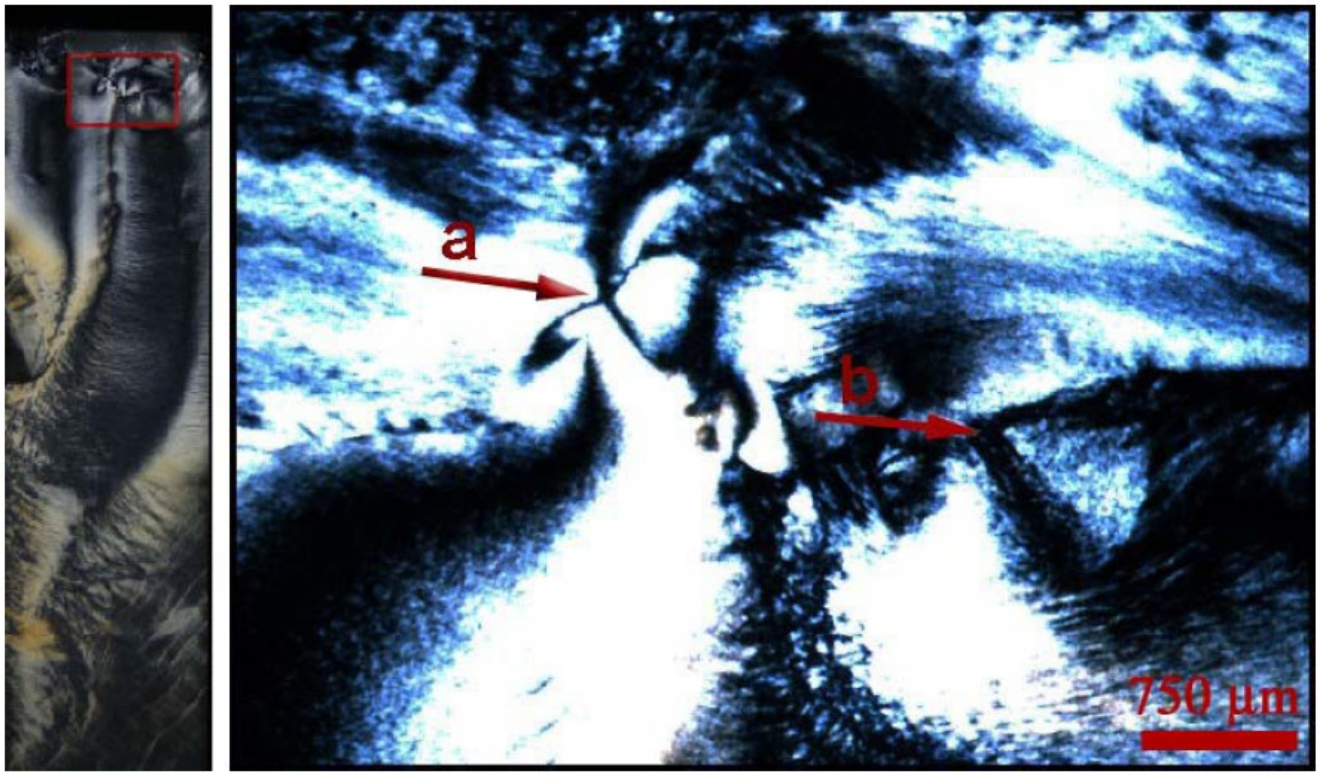

Figure 10. Defects in the nematic region close to the isotropic phase for a sample which is filled with pre-settled suspension of 3 w/w % B3 powder at 10^{-3} M [NaCl]. The pictures are taken 8 months after the time of injection. Arrow **a** shows a disclination of strength -1, and arrow **b** shows a disclination of strength +1.

REFERENCES

[1] Sonin, A. S. J. Mater. Chem. **1998**, 8, 2557

[2] Gabriel, J. C. P.; Davidson, P. Top. Curr. Chem. **2003**, 226, 119

[3] Gabriel, J. C. P. ; Davidson, P. Curr. Opin. Colloid Interface Sci. **2005**, 9, 377

[4] Zocher, H. Z. Anorg. Allg. Chem **1925**, 147, 91

[5] Bawden, F. C., Pirie, N. W., Bernal, J. D., and Fankuchen, I. Nature **1936**, 138, 1051

[6] Bernal, J. D.; Fankuchen, I. J. Gen. Physiol. **1941**, 25, 111

[7] Zhang, Z. X.; van Duijneveldta, J. S. J. Chem. Phys. **2006**, 124, 154910

[8] Onsager, L. Ann. N. Y. Acad. Sci. **1949**, 51, 627

[9] Eppenga, R.; Frenkel, D. Mol. Phys. **1984**, 52, 1303

[10] Veerman, J. A. C.; Frenkel, D. Phys. Rev. A **1992**, 45, 5632

[11] Langmuir, I. J. Chem. Phys **1938**, 6, 873

[12] Olphen, H. V. Discuss. Faraday Soc. **1951**, 11, 82

[13] Broughton, G.; Squires, L. J. Phys. Chem. **1936**, 40, 1041

[14] Hauser, E. A.; Reed, C. E. J. Phys. Chem. **1937**, 41, 911

[15] Hauser, E. A. Chem. Rev. **1945**, 40, 287

[16] Norrish, K. Discuss. Faraday Soc. **1954**, 18, 120

[17] Mourchid, A.; Delville, A.; Lambard; J.; L'ecolier; E., Levitz, P. Langmuir **1995**, 11, 1942

[18] Mourchid, A.; L'ecolier; E., Damme, H. V.; Levitz, P. Langmuir **1998**, 14, 4718

[19] Pignon, F.; Piau, J. M.; Magnin, A. Phys. Rev. Lett. **1997**, 76, 4857

[20] Pignon, F.; Magnin, A.; Piau, J. M. Phys. Rev. Lett. **1997**, 79, 4689

[21] Bonn, D.; Tanaka, H.; Wegdam, G.; Kellay, H.; Meunier, J. Europhys. Lett. **1998**, 45, 52

[22] Bonn, D.; Kellay, H.; Tanaka, H.; Wegdam, G.; Meunier, J. Langmuir **1999**, 15, 7534

[23] Levitz, P.; L'ecolier, E.; Mourchid, A.; Delville, A.; Lyonnard, S. Europhys. Lett. **2000**, 49, 672

[24] Knaebel, A.; Bellour, M.; Munch, J.-P.; Viasnoff, V.; Lequeux, F.;Harden, J. L. Europhys. Lett. **2000**, 52, 73

[25] Tanaka, H.; Meunier, J.; Bonn, D. Phys. Rev. E 69 **2004**, 031404

[26] Tanaka, H.; Jabbari-Farouji, S.; Meunier, J.; Bonn, D. Phys. Rev. E **2005**, 71, 021402

[27] Strachan, D. R.; Kalur, G. C.; Raghavan, S. R. Phys. Rev. E **2006**, 73, 041509

[28] Ianni, F.; Leonardo, R. D.; Gentilini, S.; Ruocco, G. Phys. Rev. E **2007**, 75, 011408

[29] Bellon, L.; Gibert, M.; Hernandez, R. Eur. Phys. J. B **2007**, 55, 101

[30] Dijkstra, M.; Hansen, J. P.; Madden, P. A. Phys. Rev. Lett. **1995**, 75, 2236

[31] Kroon, M.; Wegdam, G. H.; Sprik, R. Phys. Rev. E **1996**, 54, 6541

[32] Michot, L. J.; Bihannic, I.; Porsch, K.; Maddi, S.; Baravian, C.; Mougel, J.; Levitz, P. Langmuir **2004**, 20, 10829

[33] Martin, C.; Pignon, F.; Piau, J.-M.; Magnin, A.; Lindner, P.; Cabane, B. Phys. Rev. E **2002**, 66, 021401

[34] Mongondry, P.; Tassin, J. F.; Nicolai, T. J. Colloid Interface Sci. **2005**, 283, 397

[35] Ruzicka, B.; Zulian, L.; Ruocco, G. Langmuir **2006**, 22, 1106

[36] Bihannic, I.; Michot, L. J.; Lartiges, B. S.; Vantelon, D.; Labille, J.; Thomas, F.; Susini, J.; Salome, M.; Fayard, B. Langmuir **2001**, 17, 4144

[37] Cousin, F.; Cabuil, V.; Levitz, P. Langmuir **2002**, 18, 1466

[38] Gabriel, J. C. P. ; Sanchez, C. ; Davidson, P. J. Phys. Chem. **1996**, 100, 11139

[39] Ramsay, J. D. F.; Lindner, P. J. Chem. Soc., Faraday Trans. **1993**, 89, 4207

[40] Ramsay, J. D. F.; Swanton, S. W.; Bunce, J. J. Chem. Soc. Faraday Trans. **1990**, 86, 3919

[41] Martin, C.; Pignon, F.; Magnin, A.; Meireles, M.; Leliere, V.; Lindner, P.; Cabane, B. Langmuir **2006**, 22, 4065

[42] DiMasi, E.; Fossum, J. O.; Gog, T.; Venkataraman, C. Phys. Rev. E **2001**, 64, 061704

[43] Fossum, J. O.; Gudding, E.; d. M. Fonseca, D.; Meheust, Y.; DiMasi, E.: Gog, T.; Venkataraman, C. Energy **2005**, 30, 873

[44] Lemaire, B. J.; Panine, P. ; Gabriel, J. C. P. ; Davidson, P. Europhys. Lett. **2002**, 59, 55

[45] Saunders, J. M.; Goodwin, J. W.; Richardson, R. M.; and Vincent, B. J. Phys. Chem. B **1999**, 103, 9211

[46] Porion, P.; Mukhtar, M. A.; Meyer, S.; Faugere, A. M.; van der Maarel, J. R. C.; Delville, A. J. Phys. Chem. B **2001**, 105, 10505

[47] Porion, P.; Mukhtar, M. A.; Faugere, A. M. ; Pellenq, R. J. M.; Meyer, S. ; Delville, A. J. Phys. Chem. B **2003**, 107, 4012

[48] Porion, P.; Rodts, S.; Al-Mukhtar, M.; Faugere, A. M.; Delville, A. Phys. Rev. Lett. **2001**, 87, 208302

[49] Porion, P.; Al-Mukhtar, M.; Faugere, A. M.; Delville, A. J. Phys. Chem. B **2004**,108, 10825

[50] Porion, P.; Faugere, A. M.; Delville, A. J. Phys. Chem. B **2005**, 109, 20145

[51] de Azevedo, E. N.; Engelsberg, M.; Fossum, J. O.; de Souza, R. E. Langmuir **2007**, 23, 5100

[52] Kroon, M.; Vos, W. L.; Wegdam, G. H. Phys. Rev. E **1998**, 57, 1962

[53] Bhatia, S., Barker, J., and Mourchid, A. Langmuir **2003**, 19, 532

[54] Zhang, J.; Luan, L.; Zhu, W.; Liu, S.; Sun, D. Langmuir **2007**, 23, 5331

[55] van der Beek, D.; Lekkerkerker, H. N. W. Europhys. Lett. **2003**, 61, 702

[56] Mourad, M.; Wijnhoven, J.; van't Zand, D.; van der Beek, D.; Lekkerkerker, H. Phil. Trans. R. Soc. A **2006**, 364, 2807

[57] van der Kooij, F. M.; Lekkerkerker, H. N. W. J. Phys. Chem. B **1998**, 102, 7829

[58] van der Beek, D.; Lekkerkerker, H. N. W. Langmuir **2004**, 20, 8582

[59] Michot, L. J.; Bihannic, I.; Maddi, S.; Funari, S. S.; Baravian, C.; Levitz, P.; Davidson, P. PNAS **2006**, 103, 16101

[60] Michot, L. J.; Bihannic, I.; Maddi, S.; Baravian, C.; Levitz, P.; Davidson, P. Langmuir **2008**, 24, 3127

[61] Israelachvili, J. Intermolecular Surface Forces. Academic Press, Inc., London, **1992**

[62] Schmidt, M.; Dijkstra, M.; Hansen, J.-P. J. Phys.: Condens. Matter **2004**, 16, S4185

[63] Baulin, V. A. J. Chem. Phys. **2003**, 119, 2874

[64] Dogic, Z.; Philipse, A. P.; Fraden, S.; Dhont, J. K. G. J. Chem. Phys. **2000**, 113, 8368

[65] Gonzalez, A. E. Phys. Rev. Lett. 86, 1243

[66] Gonzalez, A. E. Eur. Phys. J. E 13, 165

[67] Fonseca, D. d.M. ; Meheust, Y. ; Fossum, J. O. ; Knudsen, K. D. ; Maly, K. J. ; Parmar, K. P. S. J.Appl. Cryst. **2007**, 40, 292

[68] Kaviratna, P. D.; Pinnavaia, T. J.; Schroeder, P. A. J. Phys. Chem. Solids **1996**, 57, 1897

[69] Knudsen, K.D.; Fossum, J.O.; Helgesen, G.; Bergaplass, V. J.Appl.Cryst. **2003**, 36, 587

[70] Bates, M. A.; Frenkel, D. J. Chem. Phys. **1999**, 110, 6553

[71] Veerman, J. A. C.; Frenkel, D. Phys. Rev. A **1992**, 45, 5632

[72] Bates, M. A. J. Chem. Phys. **1999**, 111, 1732

[73] Abend, S.; Lagaly, XX, Applied Clay Science **2000**, 16, 201

[74] Rowan, D. G.; Hansen, J. P. Langmuir **2002**, 18 , 2063

[75] van der Beek, D.; Davidson, P.; Wensink, H. H.; Vroege, G. J.; Lekkerkerker, H. N. W. Phys. Rev. E **2008**, 77, 031708

[76] Peroli, G. G.; Hillig, G.; Saupe, A.; Virga, E. G. Phys. Rev. E **1998**, 58, 3259